Development of a High Power RF Measurement System

By

Nilaped Russamee

A Thesis Submitted in Fulfilment of the Requirements for the Degree of Doctor of Philosophy of Cardiff University

Division of Electrical and Electronic Engineering
School of Engineering
Cardiff University
United Kingdom

November, 2012

DECLARATIONS

This work has not previously been in substance for any degree and is not concurrently submitted in candidature for any degree.

Signed…….(candidate)
Date…….

STATEMENT 1

This thesis is being submitted in partial fulfilment of the requirements for the degree of PhD.

Signed…….(candidate)
Date…….

STATEMENT 2

This thesis is the result of my own independent work/investigation, except where otherwise stated. Other sources are acknowledged by footnotes giving explicit references.

Signed…….(candidate)
Date…….

STATEMENT 3

I hereby give consent for my thesis, if accepted, to be available for photocopying and for inter-library loan, and for the title and summary to be made available to outside organisations.

Signed…….(candidate)

Date…….

Acknowledgements

Firstly, I would like to thank my supervisor, Professor Paul Tasker, for giving me the opportunity to further my study in Cardiff University. I have gained invaluable knowledge in RF measurement systems in Cardiff University. I also would like to thank my second supervisor, Professor Johannes Benedikt, for his academic advice, research ideas, and kind encouragement. I am also grateful to Dr. Jonathan Lees for his assistance and technical advice. He gave me a lot of research ideas.

I am also grateful to a number of my colleague in the Centre for High Frequency Engineering at Cardiff University for their friendship and the warm atmosphere which they provided. I would also like to thank Simon Woodington and Tudor Williams who advised me in the ADS simulation. I would like to thank Chris Roff for his help in the first year in Cardiff. I would also like to thank Aamir Sheikh for his help in the calibration of the measurement system.

I would like to thank my Thai friends in Cardiff for their friendship and the happy times that we shared when we went around together. I am extremely thanked to Sutatsanee Tansalinkarn and Pawadee Tavorrachote for her delicious food, entertainment, social advice, and friendship.

I would like to give my special thanks to U-Sa Russamee, my wife, for her support and impartial encouragement. She is always available when I need help.

Lastly, and most importantly, I would like to thank my parents, my brother, and my sister for their huge support and encouragement.

Nilaped Russamee
Cardiff, 2012

Summary

This research project has developed a high power RF Measurement system in the Centre for High Frequency Engineering, Cardiff University. There are two main contributions of this thesis. The first contribution is the implementation of step attenuators in the RF high power measurement system, incorporated with the approach of using the S-parameter model for correction measured waveform in measurement software processing. The step attenuator is situated between the broadband directional couplers (which obtains the incident and reflected signal from the DUT) and signal receivers (such as a sampling oscilloscope or MTA). The aim of this implementation is to extend the dynamic range of the measurement system and to develop a technique for reducing the recalibration process while the measurement system needs more attenuation in the signal condition part of the measurement system. These benefits allow the quick and convenient characterisation of the DUT under large signal excited environment. The second contribution is the further development of the Harmonic Bypass Structure (HBS), which is used instead of the step attenuator. The advantage of a HBS is that it can overcome the harmonic distortion drawback of the step attenuator approach. This drawback is caused by choosing improper high attenuation which is unsuitable for the measured signal condition. There is, therefore, a trade-off between the fundamental and harmonic frequencies. The advantage of an HBS is that it is capable of selecting the frequency band to attenuate while other frequencies can pass through to the receiver. In the meantime, the S-parameter model and modified measurement software are well suited similar to the step attenuator approach.

Contents

List of Illustrations

List of Tables

List of Acronyms Used in this Thesis

CW – Continuous Wave

CAD – Computer Aided Design

DAC – Digital to Analogue Converter

DUT – Device Under Test

FET – Field Effect Transistor

FFT – Fast Fourier Transform

GaN – Gallium Nitride

GPIB – General Purpose Instrument Bus

GUI – Graphic User Interface

HBS – Harmonic Bypass Structure

IFFT – Inverse Fast Fourier Transform

LO – Local Oscillator

LSNA – Large Signal Network Analyzer

MTA – Microwave Transition Analyzer

NVNA – Nonlinear Vector Network Analyzer

PA – Power Amplifier

RF – Radio Frequency

VNA – Vector Network Analyser

Chapter 1

Introduction

Chapter 1: Introduction

1.1 Introduction

There are two categories of microwave and Radio Frequency (RF) measurement, the first is signal measurement and the second is network measurement. Signal measurement obtains the characteristic of waves and waveforms (e.g. frequency and phase). Network measurement obtains the relative terminal and signal transfer characteristics of devices and systems (e.g. impedance, gain power, and reflection coefficient). Some microwave and RF applications use both signal and network measurement, which overlap each other.

Microwave and RF measurement can be categorised into linear and nonlinear measurement. These categories suggest the importance of the behaviour of devices or a circuit system. For example, in the characterisation of a PA the nonlinear behaviour of a PA has been obtained from the output power at 1dB Gain compression, the Third Order Intercept Point, and Inter-Modulation Distortion (IMD).

Over the years, a large number of microwave and RF measurement instruments have been developed and built, including power sensors for power measurements, waveguide bridges for impedance measurement, and microwave cavities for wavelength measurements. For example, the introduction of the principle of super-heterodyne conversion revolutionised microwave and RF measurement during the early part of the twentieth century. The principle of super-heterodyne conversion is that it converts each microwave signal frequency component to an Intermediate Frequency (IF), from where the signal can be more easily detected. Meanwhile, Vector Network Analysers (VNA) were developed for practical use in the 1960s. A VNA uses the principle of super-heterodyne conversion in combination with the use of S-parameters. A VNA has a number of benefits for the characterisation of linear devices and systems. More recent

active research into microwave and RF measurement techniques has led to the development of the next generation of instruments for nonlinear measurement, including the Large-Signal Network Analyser (LSNA); however, the architecture and measurement techniques used in an LSNA are still being actively developed. This research project aims to extend the ability and efficiency of the instruments used for measuring the nonlinear devices and systems in a real excitation environment.

1.2 Research Aims

Time-domain load-pull measurement systems have been shown to provide access to the voltage and current waveforms present at the input and output terminals of a device, which represents an extremely powerful tool in modern PA design [1]. For example, these tools allow the observation of key device characteristics, such as: the knee-walk-out phenomena that is associated with GaN devices; device memory investigations; dynamic load-line and transfer characteristic behaviour; model creation and verification; and, the ability to actively synthesise complex harmonic impedance environments. However, a number of dynamic-range problems present themselves when these systems are used in high-power applications. Firstly, high-power measurements involve the modification of the 'conventional' low-power microwave test-set in order to accommodate significant forward and reverse power levels. Meanwhile, the broadband nature of the measurement system, coupled with the difficulty and expense in achieving significant very broad-band power amplifiers, forces the calibration to be conducted at much lower power levels.

One solution to this dynamic range problem is to use highly repeatable programmable step attenuators within the calibrated path. This approach, if properly implemented, overcomes most of the difficulties presented by large signal calibration and can be used to generally increase the measurement dynamic range. It also introduces additional flexibility into microwave measurement at high power levels, which is especially useful

(for example) when measuring very high gain devices where a significant power difference can exist between the input and output of a device.

A number of measurement systems have been developed at Cardiff University over recent years that are all based upon a common theme of waveform measurement and engineering through active harmonic load-pull [1]. The most recent of these systems include modulated envelope and IF load-pull systems, and a high-power harmonic load-pull system employing broad-band impedance transformers that is capable of operating at fundamental power levels in excess of 100W over a bandwidth of 1 GHz to 12.5 GHz. This system has been demonstrated through the extensive characterisation of various 100W LDMOS devices, enabling measurement and characterisation under optimum harmonic load conditions [2].

The increasing need to actively load-pull and measure very high power, high gain devices presents new and challenging demands for load-pull measurement systems. One example is the need to achieve and manipulate the necessary dynamic range for accurate high and low-power measurement without affecting overall measurement accuracy.

It is usually the case, and indeed a necessity, that the microwave test-set architecture once calibrated remains physically unchanged for the measurement phase. The obvious and current approach of using fixed, broad-band attenuators effectively fixes the measurement dynamic range. This results in a problem where the system is unable to measure small signals when large attenuation values are used. Similarly, the calibrated system cannot measure large signals when using small attenuation values.

Another related problem surrounds the final stage, or what will be termed here, the ‘large-signal’ calibration of these systems, which involves attaching one of the small-signal calibrated measurement ports directly to a calibrated power meter. This ‘absolute’ power calibration step involves using a ‘thru’ connection as the DUT and then driving the system with sufficient power in order to obtain a measurable relationship between coupled and thru signal levels from the attenuated directional couplers and the

calibrated port. However, for high-power measurements, this can easily result in the coupled power being up to 60 dB smaller than the thru power; hence, there is a significant risk of overdriving the calibrated receiver being used as the power meter. The proposed solution involves the introduction of highly characterised, highly repeatable, high-quality step attenuators inserted within the calibration path. These attenuators are situated between the directional couplers and the calibrated receiver, with the measured attenuator S-parameter data used to correct measured voltage travelling waves in advance of software processing within the measurement system itself. However, a drawback occurs when step attenuators are used in high attenuation because the harmonic contents are significant distorted. The proposed solution involves the use of a Harmonic Bypass Structure (HBS), which is inserted instead of step attenuator within the calibration path. This structure overcomes the distortion of the harmonic content that is caused by step attenuators. An HBS improves the previous proposed solution.

1.3 Thesis Structure

This section will describe the thesis structure. There are eight chapters, including this introduction chapter that has described the purposes of this research and outlined the structure of this thesis.

The second chapter will give an overview of the high power RF measurement system.

The third chapter describes the modification of the measurement software for high power RF measurement system, which was implemented in Cardiff University. This chapter opens by describing the concept of the modification of measurement system, it then gives an overview of the research work. The S-parameter model is an important part of this high power RF measurement system. The formulation of the S-parameter model was devised. It was found that there are two models, namely: the full S-

parameter model and the simple S-parameter model. The full S-parameter model includes the influence of the varied impedance environments surrounding the step attenuator while the simple S-parameter model assumes that impedance is constant throughout the operational range. Therefore, in this demonstration the simple S-parameter model is formed on S21 alone. This chapter then describes how the S-parameter data is prepared and it discusses the reflection coefficient procedure. This procedure generates an accurate and suitable format of S-parameter data. The next section describes the implementation of the S-parameter model into the measurement software, which allows the measurement software to correct the travelling wave a0, b0, a3, and b3. The operation of the modified measurement software will be briefly explained. Finally, the verification of the simple S-parameter in a practical measurement system will be discussed. This verification has proved the acceptable accuracy of the measurement system.

The fourth chapter describes the demonstration of the extended dynamic range of the measurement system using step attenuators. It starts with the characterisation of the step attenuator, with the aim of collecting the step attenuator's S-parameter data and analysing its repeatability. After the implementation of the step attenuator into the measurement system, the demonstration was set to prove the extended dynamic range by using the step attenuator approach. A CW power sweep was performed in a thru 7mm standard and a GaN 50 W transistor device with the aim of investigating the power output comparison in respect to varied step attenuator states.

The S-parameter characterisation of the HBS is described in the fifth chapter; this will include the conceptual design, an explanation of how to build an HBS, and the simulation of an HBS which will observe its behaviour and its S-parameters. It is important to know the S-parameter of the HBS so that the S-parameter model can be implemented into the high power RF measurement system. However, during this process some limitations were found, which are described in this fifth chapter. This chapter will also describe the HBS S-parameter simulation model, which can be used if this structure has to provide the measurement system above its limitation.

The sixth chapter describes the demonstration of the extended dynamic range in RF measurement system by using the HBS, which has been implemented instead of a step attenuator. The HBS has been found to provide the extension the dynamic range in the measurement system while overcoming the harmonic distortion issue. Similarly, the S-parameter model was used to compensate the measured signal in the HBS approach. This chapter discusses several aspects of the measurement configuration, including the software configuration, the calibration method TRM- short (Thru, Reflect-short, Match) and the measurement procedure.

The seventh chapter describes the improvement provided an HBS, which is its ability to pass through the harmonic content without distortion while extending the dynamic range. The demonstration implemented the HBS in an RF measurement system at the input measurement plane. A GaN transistor device was placed as a DUT on the measurement system to incorporate the 2^{nd} harmonic frequency source at the input side. The demonstration has shown that the source harmonic can move around the Smith chart by comparing between HBS at the 0 dB and 10 dB states. The demonstration has shown good results.

Finally, the eighth chapter concludes this thesis and makes a number of suggestions for further research, including the use of a fully automated independent step attenuator control switch, a new improved HBS, and an implementation of the HBS approach in a multi-tone measurement system.

References

[1] J. Benedikt, R. Gaddi, P. J. Tasker, and M. Goss, "High Power Time-Domain Measurement system with Active Harmonic Load-Pull for High-Efficiency Base-Station Amplier Design," IEEE Trans. On Microwave Theory and Technique, vol. 48, pp. 2617-2624, 2000.

[2] D.J. Williams, "Non-Linear Measurement System and Techniques for RF Power Amplifier Design," Cardiff University, PhD thesis 2003.

[3] R. Ludwig and P. Bretchko, RF Circuit Design Theory and Applications. Upper saddle River NJ, USA: Prentice Hall, 2000.

[4] A. Chenakin, "2-22 GHz Continuously Variable Attenuator Has Low IMD and Float Response," High Frequency Electronics, pp. 16-20, July 2006.

[5] J. Benedikt, "Evaluation and Measurement Enhancement of the High Frequency Measurement System at the University of Wales College Cardiff," Cardiff University, Cardiff, Thesis 2000.

[6] V. Camarchia, V. Teppati, S. Corbellini, and M. Pirola, "Microwave Measurements Part II Non-linear measurements," IEEE instrumentation & Measurement Magazine, vol. 10, no. 3, pp. 34-39, June 2007.

[7] V. Teppati, A. Ferrero, V. Camarchia, A. Neri, and M. Pirola, "Microwave Measurements Part III Advanced non-linear measurements," IEEE Instrumentation & Measurement Magazine, vol. 11, no. 6, pp. 17-22, December 2008.

[8] F.H. Raab et al., "Power amplifiers and transmitters for RF and microwave," IEEE Transactions on Microwave Theory and Techniques, vol. 50, no. 3, pp. 814-826, 2002.

[9] K.A. Remley, "Practical Applications of Nonlinear Measurements," in Microwave Measurement Conference, 2009 73rd ARFTG, Boston, MA, June 2009, pp. 1-15,Nist.gov.[Online]."http://www.nist.gov/eeel/electromagnetics/rf_fields/

upload/ R16_ARFTG73_Remley.pdf.

[10] G.H. Bryant, Principles of Microwave Measurements. London, United kingdom: Peter Peregrinus Ltd, 1993.

[11] J. F. Sevic, "Theory of High-Power Load-Pull Characterization for RF and Microwave Transistors," in RF AND MICROWAVE CIRCUITS, MEASUREMENTS, AND MODELING, M. Golio and J. Golio, Eds. NewYork, .S.A: CRC press, 2008, ch. 7.

Chapter 2

RF Measurement Systems: An Overview

Chapter 2 - RF Measurement Systems: An Overview

2.1 Introduction

The development of measurement methods and instruments is a challenging aspect of the study of Radio Frequency (RF) and microwave engineering. It is well known that the traditional methods of measuring the voltage and current of network circuits is not practical for RF and microwave circuit networks; for example, the voltage meter is no longer able to measure voltage and current due to the high frequencies that are now used. Wavelengths at high frequency are smaller than the physical size of lump electronic components or devices. Voltage and current magnitudes are changing rapidly as electronic components are being developed and, therefore, it is hard for conventional electronic measurement equipment to work properly in this new environment.

Historically, extremely active research has been conducted into the use of RF and microwaves. A number of new techniques and tools have been introduced that allow engineers to characterise, design, and implement new circuit networks for new applications in an effective and sophisticated way.

One of the most active areas of RF and microwave is the design and characterisation of Power Amplifiers (PAs) for communication applications; for example, designing PAs for use in a base-station in a mobile network. The Large Signal Network Analyser (LSNA) is an important tool that allows researchers and design engineers to measure, model, and simulate PAs more conveniently and with a significantly reduced design time. These tools also help process engineers to work with circuit designers and system level engineers based on measurement tools and methods. This will increase productivity in the design flow [1].

This chapter will give an overview of the development of RF and microwave measurement systems, including the development of major instruments such as the

VNA (Vector Network Analyser) and the LSNA. The VNA was developed to measure the linear behaviour of DUT while the LSNA was developed to measure the non linear behaviour of the DUT.

2.2 A Background of the Development of Microwave and RF Measurement Systems

The magnitude and phase of the transmission and reflection wave are basic parameters that are essential in the development of microwave and RF measurement systems. At first, the slotted line, power detector, and phase bridges were key technologies to obtain these parameters. Consequently, these instruments allow the engineer and researcher to characterise or to model microwave and RF devices.

The introduction of the S-parameter measurement technique in the 1950s and the rapid growth of semiconductor technology and devices led to the introduction of the network analyser, which can be distinguished into two categories: the first is the Scalar network analyser and the second is the Vector Network Analyser (VNA). These instruments have been built on either sub-sampling or mixer down-conversion microwave signal into Intermediate Frequencies (IF) techniques, where it can detect the magnitude and phase of the measured signal. Although the scalar network analyser can provide only the magnitude of forward and reflected wave, it does not determine the phase difference between forward and reflected waves. Meanwhile, unlike the scalar network analyser, the VNA has the ability to determine the phase difference of these measured waves.

A VNA has a number of advantages for the characterisation and modelling of linear system devices; however, it is a strictly linear system because the VNA does not provide the phase information of the harmonic that is usually generated by non-linear devices or systems. The characterisation of a non-linear system needs more information than the relative measurement that is given by a VNA; therefore, a new measurement instrument

must provide a separate measure of the incident and reflected wave, the absolute magnitude, and the phase coherence between the different spectral components of measured waves. Consequently, a new instrument that is able to characterise and model a nonlinear system was needed.

The next development was to extend the ability of the VAN to measure DUT in nonlinear behaviour. This has been actively developed since 1988 to 1990 when Urs Lott [2] introduced the method of calibrating harmonic phase reference by using a millimetre-wave Schottky diode. New microwave nonlinear measurement systems have since been proposed by many groups, such as: Demmler Tasker, and Schlechtweg, who developed a Microwave Transition Analyser (MTA); Gunter Kompa and Friedbert van Raay, who developed a sampling oscilloscope; and, Agilent-NMDG group and the ELEC/VUB department of the Vrije Universiteit Brussel, who developed MTA-technology and included full control of the frequency down conversion mechanism.

2.3 Linear Measurement and Non-linear Measurement

RF measurement can be performed successfully if the user knows the behaviour of the DUT. When the DUT is excited by the external signal source, the output can be either a linear or non-linear response. Figure 2.1 below shows the basic response of linear and nonlinear systems. The linear system interacts with the signal input only by generating the same input frequency as the magnitude and phase change at the output. Unlike the linear system, the nonlinear system produces the additional frequencies at the output, which can be called the harmonics.

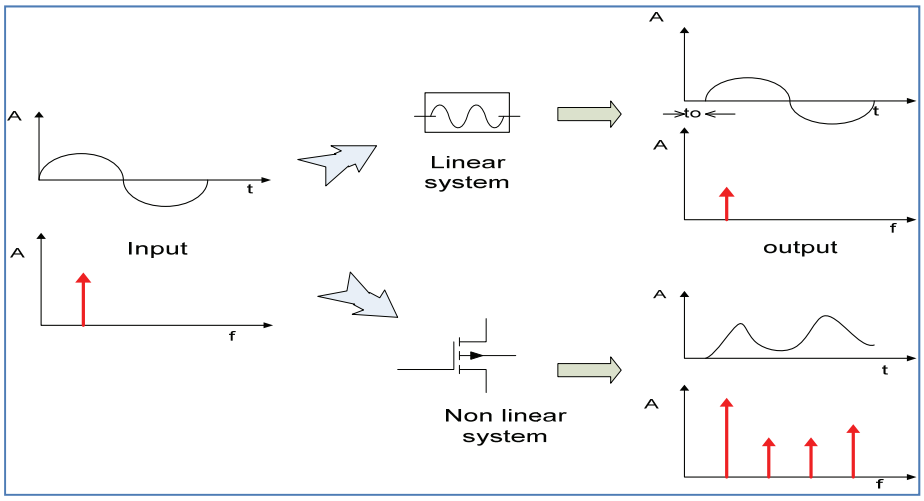

Figure2.1: Linear and non-linear behaviour.

In an RF measurement system, the small signal S-parameter is the most popular of the linear measurement systems and it can be achieved by using a VNA. The use of S-parameter is well known by many users of RF and microwave measurement while many users are still unfamiliar with non-linear measurement. In fact, this kind of measurement can be achieved by measured by comparing the magnitude and phase difference between measured waveforms. This allows the user to obtain the measured waveform in the time or frequency domain. Although the configuration and calibration of an RF non-linear measurement system is quite complicated, the exploration of a non-linear system has gained from this benefit.

2.4 Vector Network Analyser (VNA)

A VNA is a core part of the measurement instrumentation that is in modern RF and microwave laboratories. The VNA has been developed to measure the ratio of incident and reflection signal waveforms. In other words, it is designed to measure the S-parameter of the DUT. The principle of VNA measurement is to use a sub-sampling or mixer down-conversion technique that down-converts the forward and reflected wave

from microwave frequency to IF, which is then passed to IF detection and phase lock. Finally, these analogue signals are converted into a digital signal, which is then displayed on a screen monitor or sent to a computer for processing. In addition, the forward or reflected wave is collected from microwave test set by low-loss broadband directional couplers.

2.4.1 VNA Calibration

Although there is no doubt that imperfections exist in all measurement systems or measurement instruments, including the famous VNA RF and microwave measurement instrument, VNA calibration removes many of these measurement system errors. These systems error in [3] can categorise measurement errors into three types, which are: random errors, drift errors, and systematic errors. Random errors change over time and they generally come from instrument noise, such as sampler noise or the IF noise floor. Random errors cannot be removed from the measurement system but they can be minimised; for example, by using a sufficient power source or by narrowing IF bandwidth. Meanwhile, drift errors are caused by temperature variation after the calibration state. Drift errors can be reduced by doing an addition calibration or by keeping the temperature stable. Finally, systematic errors are caused by an imperfectly implemented measurement system and they do not vary with the time function. Systematic errors can be modelled and be cancelled by the calibration process. Systematic errors can be classified by error modelling, such as in a mismatch and leakage signals in the test setup, isolation characteristics between the reference and test signal parts, and system frequency response.

To generate the error model, calibration standards are used to measure the two ports. These calibration techniques were developed for removing these imperfections. Systematic errors can be modelled with a signal flow graph, as illustrated below in Figure 2.2.

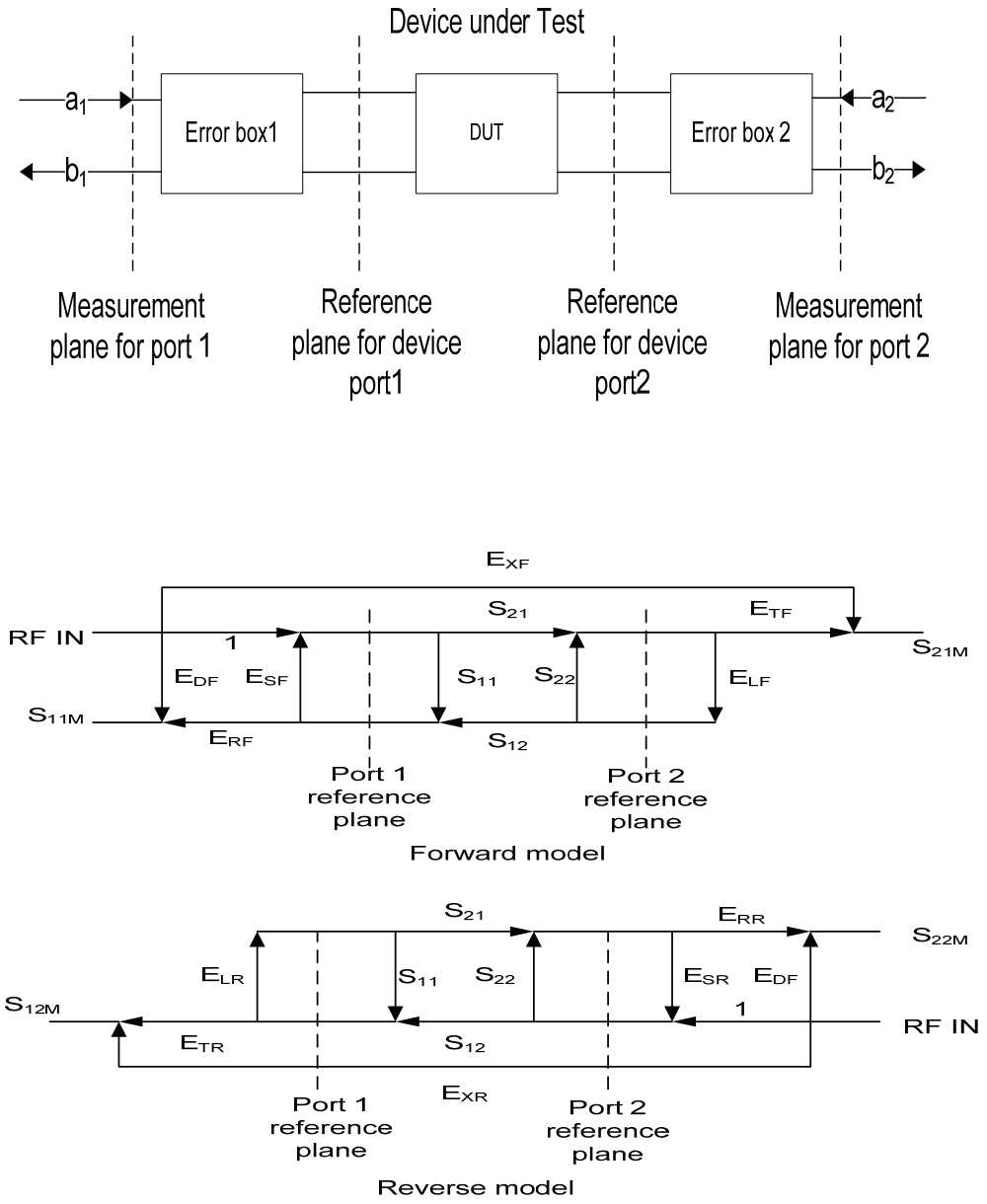

Figure 2.2: Block diagram of a network analyser measurement of a two port device and a two-port error correction model.

Where $\mathbf{E_{DF}}$=Fwd Directivity

$\mathbf{E_{SF}}$=Fwd Source Match

$\mathbf{E_{RF}}$= Fwd Reflection Tracking

$\mathbf{E_{LF}}$ =Fwd Load Match

$\mathbf{E_{TF}}$=Fwd Transmission Tracking

$\mathbf{E_{XF}}$ =Fwd Isolation

$\mathbf{E_{DR}}$= Rev Directivity

$\mathbf{E_{SR}}$=Rev Source Match

$\mathbf{E_{RR}}$= Rev Reflection Tracking $\mathbf{E_{LR}}$ =Rev Load Match

$\mathbf{E_{TR}}$=Rev Transmission Tracking $\mathbf{E_{XR}}$ =Rev Isolation.

A number of calibration methods have been developed to remove measurement errors; for example, Short Open Load Thru (SOLT), Thru Reflection Line (TRL), and Line Reflect Match (LRM).A brief description of each of these VNA calibration methods is [4] given in the table below:

Description of the most widely adopted calibration techniques for VNAs			
Calibration Type	**SOLT**	**TRL**	**LRM**
Required standards	Short open load thru	Thru reflection line	Line reflect match.
available environment	Waveguide coaxial on wafer.	Coaxial on-wafer. Does not require a complete set of fully known calibration standard.	Coaxial on-wafer. Mainly for on-wafer measurements where the probe movement is difficult.
Description	Most widely adopted for two-port VNA. Standards available in every environment.	Only the knowledge of the line reference impedance is needed.	Fully known one-port matched load instead of the line of the TRL algorithm.
Major Constraints	Perfect knowledge of all standards needed. Measurements during calibration. Requires a direct port connection.	Working bandwidth limited below the resonant frequency of the line where it is undistinguishable from the thru connection. Multiline methods can overcome this problem [5]	Quality of the match standard is extremely important.

Table 2.1: VNA calibration methods.

2.5 Large Signal Network Analyser (LSNA)

When it was first developed the Large Signal Network Analyser (LSNA) was known by six different names, they were: Nonlinear Network Analyser (NLNA) , Nonlinear Vectorial Network Analyser (NVNA), Vectorial Nonlinear Network Analyser (VNLNA), Nonlinear Network Analyser System (NNAS), Nonlinear Network Measurement System (NNMS) and Large-Signal Network Analyser (LSNA) [6]. However, the two most common names are LSNA and NVNA [4]. The main distinction between NVNA and LSNA are the method of down-converting the RF signal to an IF spectrum. While the LSNA uses a sampling down-conversion technique, the NVNA is based on the heterodyne principle, which uses mixers for the down-conversion process. In this thesis, the LSNA is used to represent this entire class of instruments.

The LSNA provides an advantage for RF and microwave measurement because it enables the measurement of DUT under realistic conditions, such as high power and large signal operating conditions. In addition, these measurements allow the user access to the instantaneous current and /or voltage waveforms at the terminals of the DUT.

The LSNA is one of several non-linear waveform measurement systems. These systems are different in terms of configuration, calibration method, and extra environment (such as load pull system capability and high power enable). Kate Remley [7] reviews some non-linear waveform measurement architectures, a summary of which is given below in Figure 2.3:

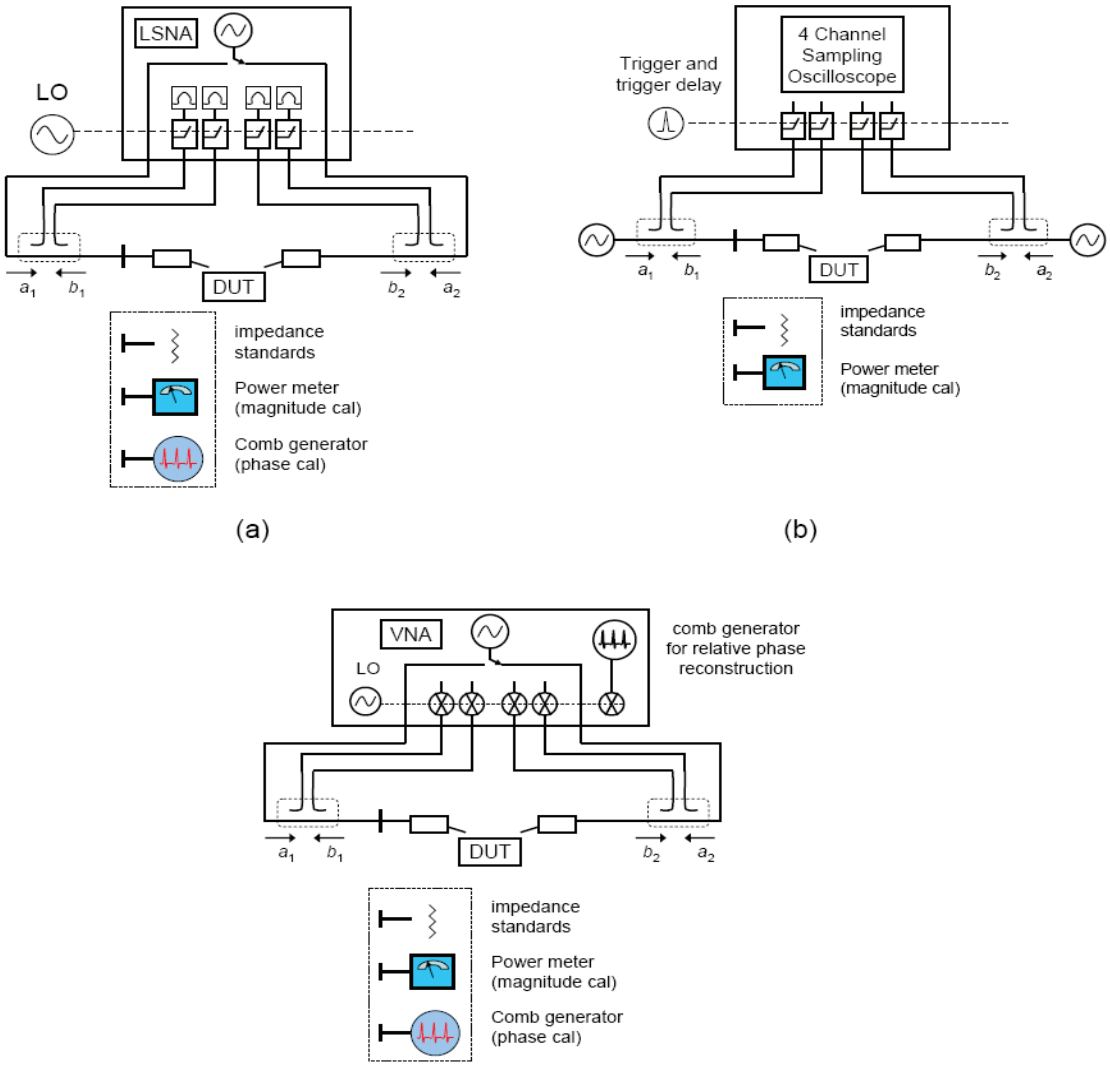

Figure 2.3: Three architectures for non-linear measurement systems.

Figure 2.3 illustrates the three architectures that are used in non-linear measurement systems. The first, [7] (a), was presented by Van den Broeck [8]; this system provides the relative phases between the fundamental and harmonics by sampling down-conversion. The second, (b), was presented by T. Williams [9]; this system provides the magnitude and phase information of the waveform at the input and output ports of a device by a multi-channel equivalent-time sampling oscilloscope. The last non-linear measurement system, (c), was presented by P. Blockley [10]; this system provides the

reconstruction of relative phases of the measured signal by using an additional comb generator.

2.5.1 Hardware Configuration

A typical LSNA configuration consists of modules or components, as shown in Figure 2.4 below:

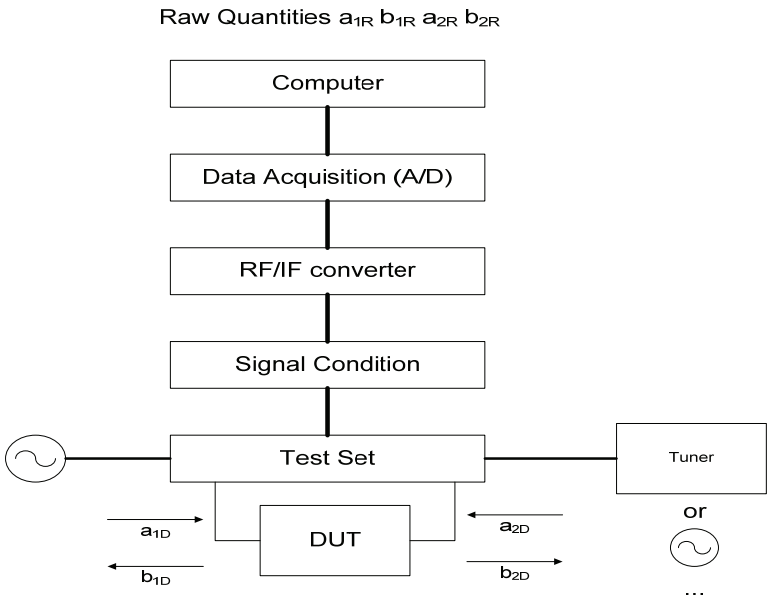

Figure 2.4: LSNA architecture from [1].

Although the exact configuration of an LSNA may vary, the basic hardware components consist of a test set, a signal condition, an RF/IF converter, data acquisition (A/D), and a computer. The test set is the main piece of hardware that connects the DUT to the LSNA. The test set provides the necessary hardware components that the DUT uses to read the excited environments. It should have bias tees for the DUT, a signal generator, and a source- load pull connected to it. In addition, the test set can obtain the separate incident and reflected wave from DUT that routes to the signal condition part. The signal condition hardware provides the limits of the incident or reflected waves as specified by the LSNA. Variable gain attenuators can control the measured wave in intervals of dynamic range before it proceeds to the down-conversion from RF signal to IF. The down-conversion is usually based on the harmonic sampling principle. Harmonic sampling is a process that compresses a wide-band spectrum into a relatively small band. By choosing the relation carefully between the sampling rate and the spectral tones, a reconstruction of the original spectrum can be successful in case of a sparse spectrum with spectral components that are separated by large distances and each of them having a small bandwidths[24]. Next, the IF signal is converted to a digital signal, which is then it is sent to a computer for software processing and display.

2.5.2 Mathematical Background

The LSNA measures the waveform of the voltage and current, or incident and reflected travelling waves, at the ports of the DUT; this is unlike a traditional VNA which measures the two-port S-parameters of the DUT [4]. The LSNA technology is based on a unique combination of two mathematical transformations, which are: firstly, the transformations between travelling voltage wave formalism and a voltage-current representation; and secondly, the transformation between the time domain and the frequency domain [11].

2.5.2.1 Physical Quantities:

Voltage/current and travelling voltage waves [1]:

$$A = \frac{V+ZcI}{2}, B = \frac{V-ZcI}{2} \quad \leftrightarrow \quad V = A + B, I = \frac{A-B}{Zc} \tag{1}$$

Zc is the characteristic impedance associated with the wave formalism. By convention, most of todays instrumentation uses a *Zc* equal to 50Ω.

2.5.2.2 Representation domain

The LSNA can display the measured signals in the frequency domain, time domain or envelope domain.

Time and frequency domain representation of a periodic continuous wave:

$$x(t) = Re(\sum_{b=0}^{H} X_h e^{-2\pi hft}) \quad \leftrightarrow \quad X_h = \frac{2}{T}\int_0^T X(t)e^{-j2\pi hft}\,dt \tag{2}$$

With f=fundamental frequency and h=harmonic index.

Time and frequency domain representation of a periodic signal with a modulation frequency f_m:

$$x(t) = Re\left(\sum_{h=0}^{H}\sum_{m=-M}^{+M} X_{hm} e^{-j2\pi(hf_c+mf_m)t}\right) \leftrightarrow X_{hm}$$
$$= \lim_{t\to\infty}\frac{1}{T}\int_{-T}^{T} x(t)e^{-j2\pi(hf_c+mf_m)t}dt \tag{3}$$

With f_c= carrier frequency, h=harmonic index, m=modulation index.

Another way to represent the above signal [4]

$$x(t) = Re\left\{\sum_{h=0}^{H}\sum_{m=-M}^{+M} X_{hm} e^{-j2\pi(hf_c+mf_m)t}\right\}$$

$$= \mathrm{Re}\left\{\sum_{\mathrm{h=0}}^{\mathrm{H}}\left[\sum X_{hm} e^{-j2\pi(mf_m)t}\right]e^{-j2\pi(hf_c)t}\right\} \tag{4}$$

where the term in square brackets is a slowly time-varying complex function representing the envelope of the signal. In cases when the baseband terms and the higher harmonics can be ignored, we express the signal completely in the envelope domain [4].

$$X_h(t) = \sum_{m=-M}^{M} X_{1m}\, e^{-j2\pi m f_m t} \tag{5}$$

With f_m=modulation frequency, m=modulation index.

2.5.3 LSNA Calibration

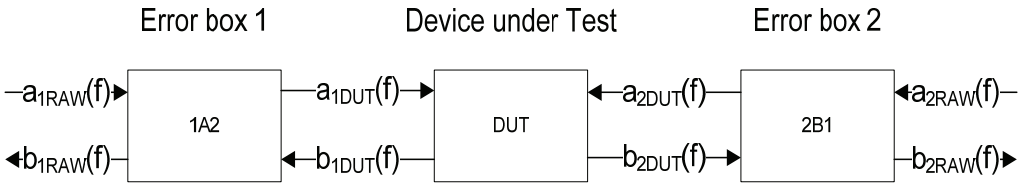

Figure 2.5: Error model of LSNA.

The linear error model can be described by the following matrix equation:

$$\begin{bmatrix} a^n_{1DUT} \\ b^n_{1DUT} \\ a^n_{1DUT} \\ b^n_{DUT} \end{bmatrix} = K^n \begin{bmatrix} 1 & \beta^n_1 & 0 & 0 \\ \gamma^n_1 & \delta^n_1 & 0 & 0 \\ 0 & 0 & \alpha^n_2 & \beta^n_2 \\ 0 & 0 & \gamma^n_2 & \delta^n_2 \end{bmatrix} \begin{bmatrix} a^n_{1RAW} \\ b^n_{1RAW} \\ a^n_{2RAW} \\ b^n_{2RAW} \end{bmatrix}$$

Where n is the frequency index and the 4x4 matrix is the equivalent of the S-parameters of the A and B blocks; $K^{(n)}$ provides the link between frequencies in both magnitude and phase[4] These parameters can be fulfilled by a calibration process, which can be done in three steps: firstly, an S-parameter calibration (relative calibration); secondly, a power calibration (absolute calibration); and finally, a phase calibration (absolute calibration).

The S-parameter calibration can be obtained by a standard method and applied to the VNA. The following calibration methods were available; Short-Open-Load-Thru (SOLT), Thru-Reflect-Load (TRL), or Thru-Reflect-Match (TRM). The S-parameter calibration is a relative calibration, which can describe only the ratio the measurement waves. Consequently, the absolute of magnitude and phase are required, which are given by the power and phase calibration. Power calibration is done by attaching a power meter into the measurement system. The measurement systems can then determine the absolute power flowing into the DUT. This allows the system to obtain the absolute amplitude of the measured wave. The final step is phase calibration, which gives the phase relationships between the harmonics present in the measured spectra. The phase calibration uses a known stable phase relationship between frequencies. When the three calibrations have been completed the error model can be established for the LSNA. From [7] , Kate Remley shows an example of the phase calibration on LSNA.

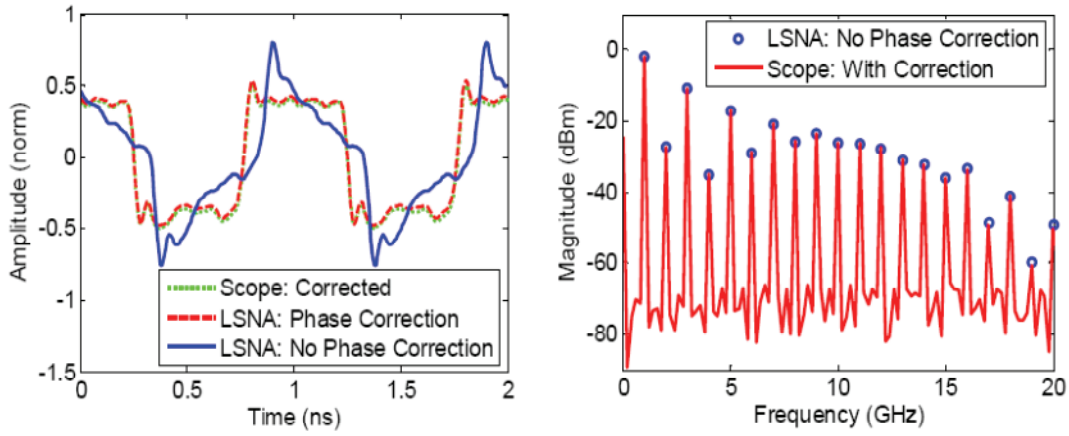

Figure 2.6: the measurement of a 1 GHz square wave.

The measurement of a 1 GHz square wave shows: (a) Time domain representation comparing LSNA measurement made with and without phase calibration. The corrected measurements nearly overlay on this scale. In (b), we see that the spectrum is not affected by the lack of a phase calibration, even though (a) clearly shows higher peak waveform values [7].

2.5.4 LSNA Applications

The LSNA was a significant development in the non-linear measurement of RF and microwave instruments. LSNAs are widely used in RF and microwave research. Table 2.2 below gives a brief overview of LSNA applications [4]:

Applications	
1. Semiconductor Device Development	This measurement system provides the terminal voltage and current of device. These parameters exploit the limit of the device's performance. These limits can be related to device breakdown, dispersion caused by trapping, or thermal effects.
2. Semiconductor Device Model Extraction and Verification	This LSNA has well-established measurement reference planes, which provides accurate measurements that can be directly compared to a device, RF simulation. It allows the user to do extensive exercises with a variety of RF signals/stimuli, these signals include: small- and large-signal, single-and multi-tone, continuous and pulsed, and matched and mismatched operation.
3. Amplifier Circuit Analysis	This LSNA provides both scalar and phase information. It can show the important parameters to analyse the amplifier circuit, such as: AM/AM distortion, AM/PM distortion, and Vector IM distortion. An LSNA with the addition of a load-pull system can characterise the amplifier circuit in both a nominal 50 Ω environments or in a mismatched environment. It also simplifies testing with active injection, where an RF signal is applied simultaneously at the input and output of the DUT.
4. Device/Circuit Behavioural Modelling:	A data set can be easily collected to fit or train phenomenological or behavioural models due to the wide variety of signals available for LSNA measurement (i.e. the fitting of a functional form to a circuit's response to realistic signals at realistic operation conditions). The model can be created more easily in higher level system simulations.

Table 2.2: A brief overview of LSNA applications.

2.6 An Overview of the Cardiff RF Waveform Measurement System

A number of RF measurement systems have been developed in the high frequency engineering centre at Cardiff University. The general configuration of the Cardiff RF waveform measurement system is illustrated below in Figure 2.7. This measurement system was reported by David Williams [12], which was original reported in [13]. The Cardiff RF waveform measurement system has been developed around the MTA sampling scope, which is capable of measuring a single-tone signal between 0.5 GHz and 40 GHz. The two channel MTA is set to operate as a four channel receiver, which measures all four incident and reflected waveforms, by using the high frequency coaxial switches A and B. Both the incident and reflected signal are captured by the two broadband directional couplers that are installed as the input and output of the DUT. There are two bias-tees, which are used for providing the required biasing to the DUT.

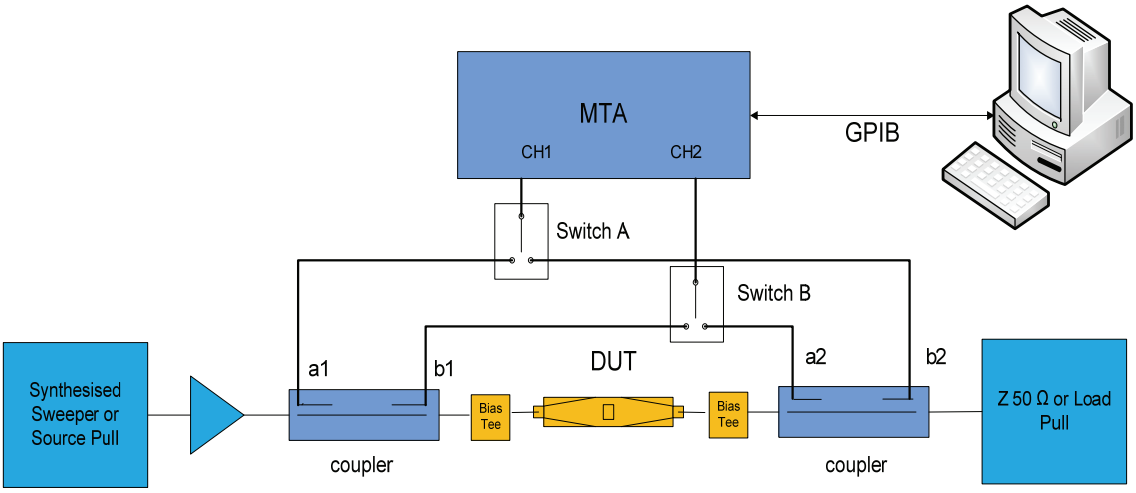

Figure 2.7: A block diagram of MTA based large signal measurement.

2.6.1 The Setup Present at Cardiff University

The calibration of the measurement system at Cardiff has achieved by three steps, which are: S-parameter calibration, power meter calibration, and phase calibration. This calibration is completed like a general LSNA. This measurement system is fully automated. It has a significant, advanced capability to conduct waveform engineering with the extension of source and harmonic load pull. Although this measurement system has also modified the configuration for two-tone measurement, it is not able to determine the DUT in multi-tone excitations environment.

In another interesting aspect, this measurement system has extended the power handling capability for characterisation of a base station PA up to least 30W [14,15]. In order to meet this power level, Benedikt [14,16] has developed test-set components for this measurement system. A high power bias tee is illustrated in Figure 2.8, which gives power levels up to 100 W CW, and DC currents of up to 10A. The bias tee is composed of two 90^{o} hybrids connected in a back to back configuration.

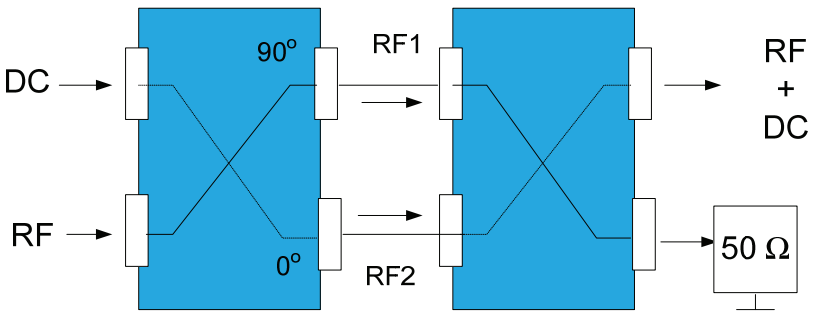

Figure 2.8: Bias tee 90o back –to-back operated over a 1-18 GHz at power levels up to 100 W CW with DC currents up to 10 A [14].

At the same time, an active harmonic load pull for high power use has also been developed. Although the measurement has achieved the characterisation of a high power PA device, the measure has a disadvantage in that it requires a high power active harmonic load pull, which causes increasing differences between the measurement system characteristic impedance (50Ω) and the PA device optimum impedance (sub 2Ω) [17,18]. Aboush et al. suggest a technique whereby the broadband impedance transformers are implemented in the measurement reference ports, as shown in Figure 2.9. This set-up can claim a remarkable reduction in required active harmonic load pull from 688 W down to only 120 W.

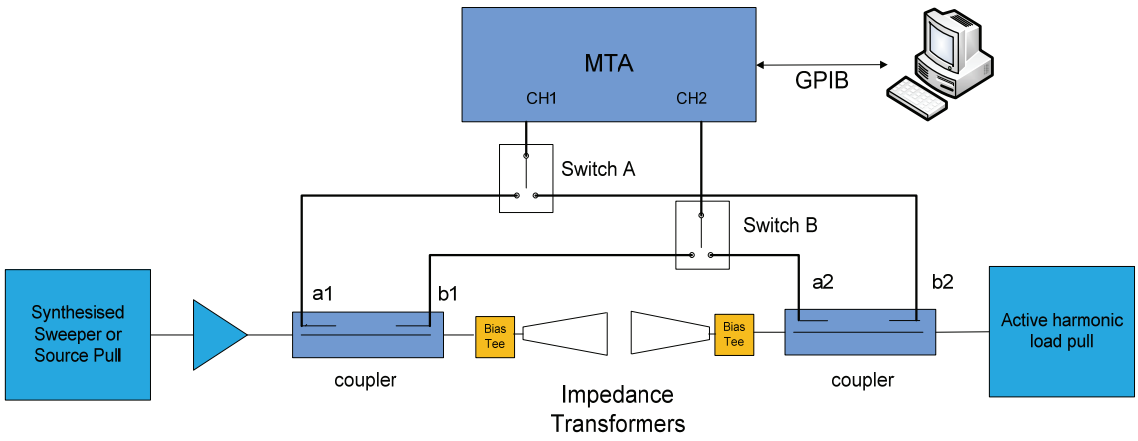

Figure 2.9: RF waveform measurement, including the impedance transformer and Active load-pull [17].

The other development is the enhancement of the Cardiff measurement system into excited modulated signal characterisation environments. The architecture configuration that is shown in Figure 2.10 is a subsequent development of this [9,19,20,21,22,23]. The measurement system is replaced by an MTA receiver with a four channel sampling oscilloscope, which incorporates source pull, load pull, IF source pull, IF load pull, active harmonic load pull and active envelope load pull. This can extend the system capability for both CW and multi-tone excitations. It can also be used to characterise devices in a wide range of applications; for example, in the characterisation of CDMA and W-CDMA power amplifiers.

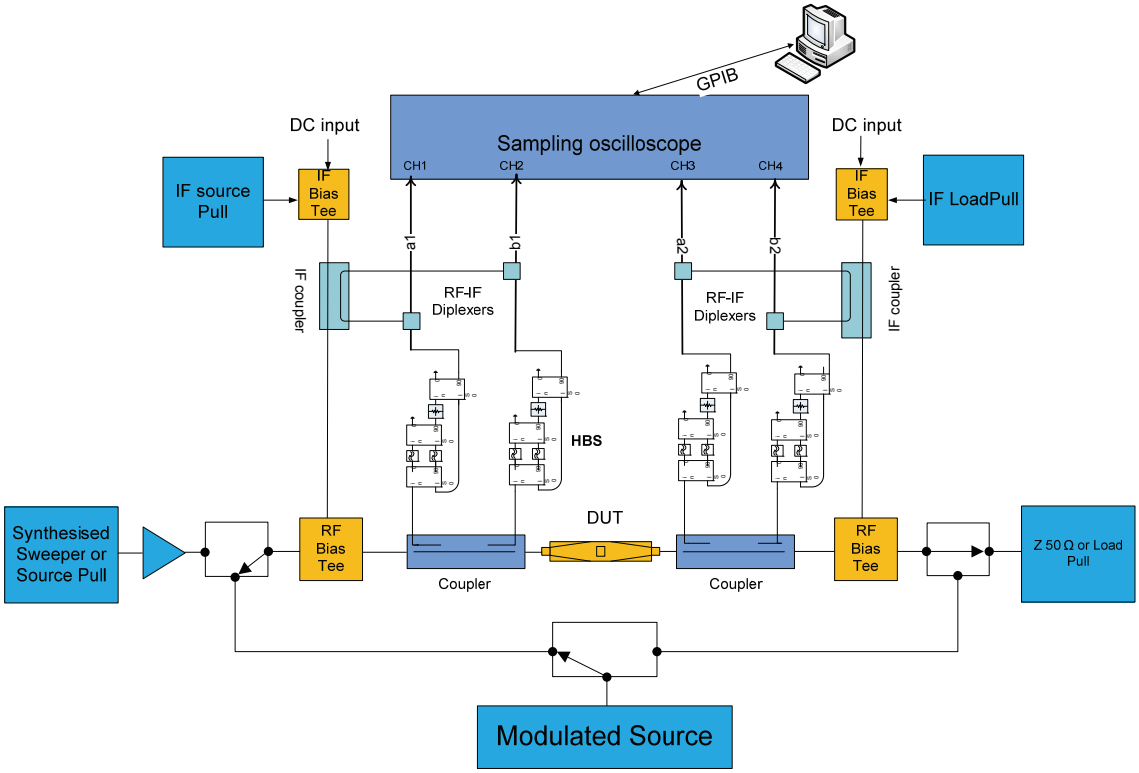

Figure 2.10: A block diagram of a sampling oscilloscope based multi-tone large signal measurement setup.

2.7 Conclusion

This chapter has described some of the basic theories used in RF measurement system. It has also reviewed some RF measurement instruments, such as the VNA and LSNA. These RF measurement systems enable the user to characterise the DUT in terms of both linear and non-linear measurement. The review of Cardiff waveforms measurement system has shown that is an advanced RF measurement system that has recently been developed.

References

[1] F. Verbeyst and E. Vandamme, "Large-Signal Network Analysis. Overview of the measurement capabilities of a Large-Signal Network Analyzer," in *ARFTG Conference Digest-Fall, 58th*, San Diego, CA, USA, Nov. 2001, pp. 1 - 14.

[2] U. Lott, "Measurement of Magnitude and Phase of Harmonics Generated in Nonlinear Microwave Two-Ports," *IEEE Transactions on microwave theory and techniques*, vol. 37, no. 10, pp. 1506-1511, October 1989.

[3] Agilent, Agilent AN 1287-3 Applying Error Correction to Network Analyzer Measurements, 2002, Application Note.

[4] J.M. Gering, "Large Signal Network Analysis/waveform measurement," in *RF and Microwave circuits, measurements, and modeling*, M. Golio and J. Golio, Eds. New York, US: CRC Press, 2008, ch. 11, pp. 1 -17.

[5] Marks and B. Roger, "A multiline method of network analyzer calibration," *Microwave Theory and Techniques, IEEE Transactions on*, vol. 39, no. 7, pp. 1205-1215, July 1991.

[6] A. Barel, "History of Nonlinear Microwave Measurements," Vrije Universiteit Brussel(Dept. ELEC), 2002.

[7] K.A. Remley, "Practical Applications of Nonlinear Measurements," in *Microwave Measurement Conference, 2009 73rd ARFTG*, Boston, MA, June 2009, pp. 1-15, Nist.gov. [Online]. http://www.nist.gov/eeel/electromagnetics/rf_fields/upload/R16_ARFTG73_Remley.pdf.

[8] T. Van den Broeck and J. Verspecht, "Calibrated vectorial nonlinear-network analyzers," *IEEE MTT-S Int. Microwave Symp. Dig*, vol. 2, pp. 1069-1072, May 1994.

[9] T. Williams, J. Benedikt, and P.J. Tasker, "Fully functional 'real time' non-linear

device characterization system incorporation active load control," *36th European Microwave connf. Dig.*, pp. 1610-1613, Sept. 2006.

[10] P. Blockley, D. Gunyan, and J.B. Scott, "Mixer-based, vector-corrected, vector signal/network analyzer offering 300kHZ-20GHz bandwidth and traceable phase response," *IEEE MTT-S Int. Microwave Symp. Dig*, pp. 1497-1500, June 2005.

[11] J. Verspecht, "Large-Signal Network Analysis," *IEEE microwave magazine*, vol. 6, no. 4, pp. 82-92, December 2005.

[12] D.J. Williams, "Non-Linear Measurement System and Techniques for RF Power Amplifier Design," Cardiff University, PhD thesis 2003.

[13] M. Demmler, P. J. Tasker, and M. Schlectweg, "A Vector Corrected High power on-Wafer Measurement System with a Frequency Range for the Higher Harmonics up to 40 GHz," in *24th European Microwave Conference*, Cannes, France, 1994, pp. 1367-1372.

[14] J. Benedikt and P.J. Tasker, "High-power time-domain measurement bench for power amplifier development," in *ARFTG Conference Digest, Fall 2002. 60th*, 5-6 Dec. 2002, pp. 107-110.

[15] J. Benedikt, R. Gaddi, P. J. Tasker, and M. Goss, "High Power Time-Domain Measurement system with Active Harmonic Load-Pull for High-Efficiency Base-Station Amplier Design," *IEEE Trans. On Microwave Theory and Technique*, vol. 48, pp. 2617-2624, 2000.

[16] J. Benedikt, Novel high frequency power amplifier design system, 2002, Thesis, Cardiff University.

[17] Z. Aboush et al., "High power active harmonic load-pull system for characterization of high power 100-watt transistors," in *Microwave Conference, 2005 European*, 4-6 Oct. 2005, p. 4 pp.

[18] Z. Aboush, J. Lees, J. Benedikt, and P.J. Tasker, "Active Harmonic Load-Pull System for Characterizing Highly Mismatched High Power Transistors," in *Microwave Symposium Digest, 2005 IEEE MTT-S International*, 12-17 June 2005, p. 4 pp.

[19] P.J. Tasker, "Practical Waveform Engineering," *IEEE microwave magazine*, vol. 10, no. 7, pp. 65-76, December 2009.

[20] P.J. Tasker, "RF Waveform Measurement and Engineering," in *Compound Semiconductor Integrated Circuit Symposium, 2009. CISC 2009. Annual IEEE*, Greensboro, NC, 11-14 Oct. 2009, pp. 1-4.

[21] M. S. Hashmi, S. J. Hashim, T. Williams, J. Benedikt, and P. J. Tasker, "A Broadband Control Electronics for Envelope Load Pull System," in *Signals, Systems and Electronics, 2007. ISSSE '07. International Symposium on*, 2007, pp. 197-200.

[22] T. Williams, J. Benedikt, and P. J. Tasker, "Experimental Evaluation of an Active Envelope Load Pull Architecture for High Speed Device Characterization," in *Microwave Symposium Digest, 2005 IEEE MTT-S International*, 12-17 June 2005, pp. 1509-1511.

[23] T. Williams, J Benedikt, and P. J. Tasker, "Application of a Novel Active Envelope Load Pull Architecture in Large Signal Device Characterization," in *Microwave Conference, 2005 European*, 4-6 Oct. 2005, p. 4 pp.

[24] C. Nader, W. Van Moer, K. Barbe, N. Bjorsell, and P. Handel, "Harmonic Sampling and Reconstruction of Wideband Undersampled Waveforms: Breaking the Code," *Microwave Theory and Techniques, IEEE Transactions on* , vol. 59, no. 11, pp. 2961 - 2969, 2011.

[25] W. Van Moer and L. Gomme, "NVNA Versus LSNA: Enemies or Friends?," *IEEE Microwave magazine*, pp. 97-103, Feb 2010.

[26] D.M. Pozar, *Microwave engineering*, 3rd ed. New York, USA: John Wiley & Son,INC., 2005.

[27] M. Pirola, V. Teppati, and V. Camarchia, "Microwave Measurements Part I : Linear Measurements," *IEEE Instrumentation & Measurement Magazine*, vol. 10, no. 2, pp. 14-19, April 2007.

[28] V. Camarchia, V. Teppati, S. Corbellini, and M. Pirola, "Microwave Measurements Part II Non-linear measurements," *IEEE instrumentation & Measurement Magazine*, vol. 10, no. 3, pp. 34-39, June 2007.

[29] V. Teppati, A. Ferrero, V. Camarchia, A. Neri, and M. Pirola, "Microwave Measurements Part III Advanced non-linear measurements," *IEEE Instrumentation & Measurement Magazine*, vol. 11, no. 6, pp. 17-22, December 2008.

[30] F.H. Raab et al., "Power amplifiers and transmitters for RF and microwave," *IEEE Transactions on Microwave Theory and Techniques*, vol. 50, no. 3, pp. 814-826, 2002.

[31] K. Kurokawa, "Power waves and the Scattering Matrix," *IEEE Transactions on Microwave Theory and Techniques*, vol. MTT-13, no. 2, pp. 194-202, March 1965.

[32] G.H. Bryant, *Principles of Microwave Measurements*. London, United kingdom: Peter Peregrinus Ltd, 1993.

[33] M. Sippila, K. Lehtinen, and V. Porra, "High-frequency periodic time domain waveform measurement system," *IEEE Trans. Microwave theory Tech.*, vol. 36, no. 10, pp. 1397-1405, Otc. 1988.

[34] P. Roblin, "Application of Large signal Network Analyzer Measurements to Model Verification and Device Modeling," in *Wireless and Microwave Technology Conference*, WAMICON'09, 20-21 April 2009, pp. 1-5.

[35] J.R. Wilkerson, K.G. Gard, and M.B. Steer, "Automated Broadband High-Dynamic-Range Nonlinear Distortion Measurement System," *IEEE Transactions on microwave theory and techniques*, vol. 58, no. 5, pp. 1273-1282, May 2010.

[36] W. Van Moer and Y. Rolain, "An Improved Broadband Conversion Scheme for the Large-Signal Network Analyzer," *IEEE Transactions on instrumentation and measurement*, vol. 58, no. 2, pp. 483-487, Feb 2009.

[37] V. Teppati, S. Pinarello, A. Ferrero, and J.-E. Mueller, "An unconventional VNA-based time-domain waveform load-pull test bench," in *Proceedings of Asia-Pacific Microwave Conference*, 2010, pp. 1893-1896.

[38] M. Isaksson and E. Zenteno, "A Synthetic Vector Network Analyzing Measurement System," *IEEE transactions on instrumentation and measurement*, vol. 60, no. 6, pp. 2154-2161, June 2011.

[39] C. Baylis, R.J. Marks, J. Martin, H. Miller, and M. Moldovan, "Going Nonlinear," *IEEE microwave magazine*, vol. 12, no. 2, pp. 55-64, April 2011.

[40] M.A. Chahine et al., "Time-Domain Characterization Using LSNA of A Broad band cross mudulation in CDMA communication systems," in *Advances in Computational Tools for Engineering Applications, 2009. ACTEA '09. International Conference on* , Zouk Mosbeh, 15-17 July 2009, pp. 133-136.

[41] R. Stancliff and J. Dunsmore, "The Evolution of RF/Microwave Network Analyzer," *Agilent Measurment*, pp. 1-6, January 2007.

[42] Anritsu Company, "Non-linear Effects and the Use of Network Analyzer Time Domain," in *Microwave Measurement Conference, 2009 73rd ARFTG*, 12-12 June 2009, pp. 1-5.

[43] Youngseo Ko et al., "Multi-Harmonic Broadband Measurements using an Large Signal Network Analyzer," in *Microwave Measurements Conference (ARFTG),*

2010 75th ARFTG, 2010, pp. 1-6.

[44] Doug, Rytting, "ARFTG 50 Year Network Analyzer History," in *Microwave Symposium Digest, 2008 IEEE MTT-S International*, Atlanta, GA, 15-20 June 2008, pp. 11-18.

Chapter 3
Implementing an S-parameter Model in High Power RF Measurement Software

Chapter 3 - Implementing an S-parameter model in High Power RF Measurement Software

3.1 Introduction

The proposed solution to the problem of extending a system's dynamic range through the use of a step attenuator required the modification of the software code that was used in the advanced software processing application. These modifications enabled the measurement system to obtain more accurate S-parameter data by correcting the travelling voltage wave. This approach also helps the user to avoid lengthy re-calibration in order to obtain the extended system dynamic range.

This chapter describes in detail the work involved in modifying the measurement software for use in a high power RF measurement system, which was implemented in the School of Engineering at Cardiff University. The first section will describe the concept of the modification of measurement system and will give an overview of the research work. The S-parameter model is an important part of this implementation, and so it was vital that the formulation of the S-parameter model was devised first. There are two models that are available for use: the full S-parameter model and the simple S-parameter model. The full S-parameter model assumes a different impedance between the step attenuator and the surrounding impedance environment that is also constant. In contrast, the simple S-parameter model assumes that impedance is constant throughout the operation range and, therefore, simplifying of the simple S-parameter model is formed on S21 alone. The preparation of the S-parameter data and reflection coefficient procedure will be discussed in the next section. This procedure is used to generate accurate and suitably formatted S-parameter data. Next to be discussed will be the implementation of the S-parameter model into the measurement software which allows the measurement software to correct the travelling wave a0, b0, a3, and b3 by an S-parameter model. The operation of the modified measurement software will then be briefly explained. Finally, the verification of the simple S-parameter model, which has

proved the acceptable accuracy of the measurement in a practical measurement system, is going to be discussed.

3.2 Overview of High Power RF Waveform Measurement System Development

The high power RF waveform measurement system developed in this research has three main aspects: hardware configuration, software modification, and the measurement and calibration procedure. An outline of the work is shown in Figure 3.1. Firstly, hardware configuration tasks employ the insertion of step attenuator or Harmonic Bypass Structure (HBS) in to the measurement system. The hardware configuration handles the electrical and electronic control work (e.g. wiring the cable and installing the power supply for the step attenuators). Secondly, software modification involves the task of conducting an S-parameter characterisation of the step attenuator and HBS, preparing the S-parameter model for the measurement system, and modifying the measurement software code to compensate measurement data. Finally, the measurement and calibration procedure task provides a verification of the measurement system by verifying its calibration using a thru standard or through nonlinear device measurements. Thirdly, and finally, the high power RF waveform measurement system needs to be measured and calibrated. Figure 3.2 shows a concept idea for extending dynamic range using the step attenuators. The diagram describes the extension of the dynamic range while using the step attenuator together with the compensation of the step attenuator S-parameter model.

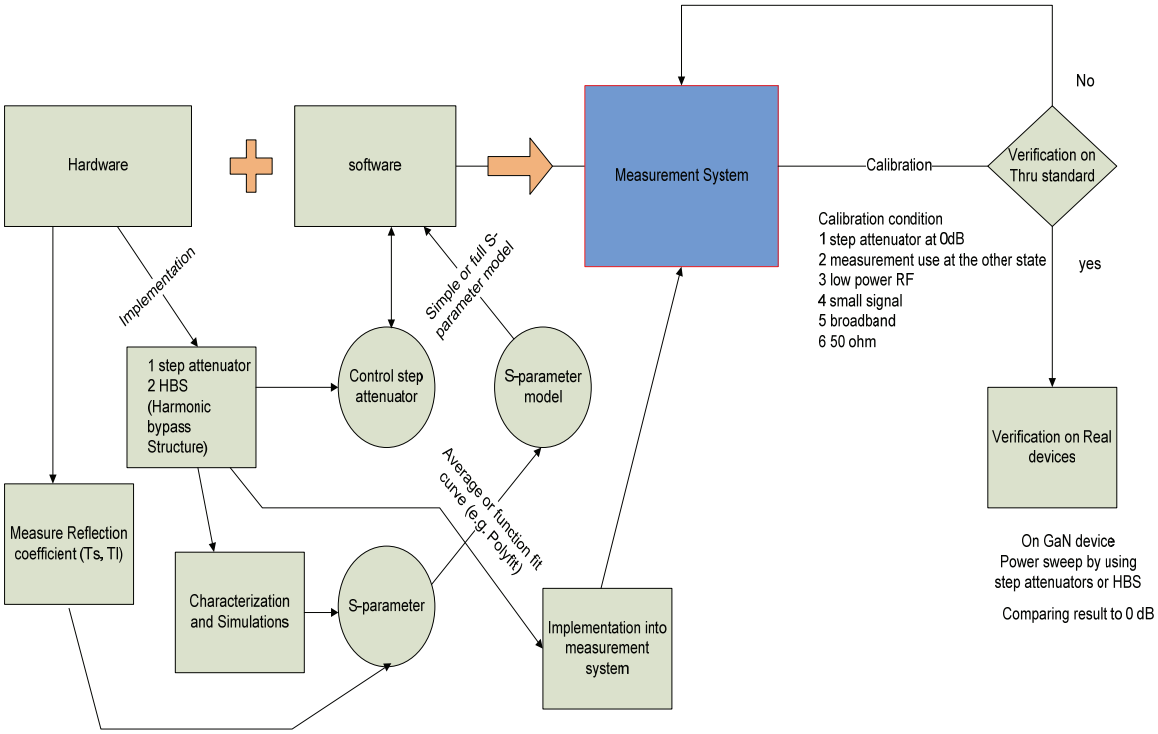

Figure 3.1: Overview of the tasks for the development of the high power RF measurement system.

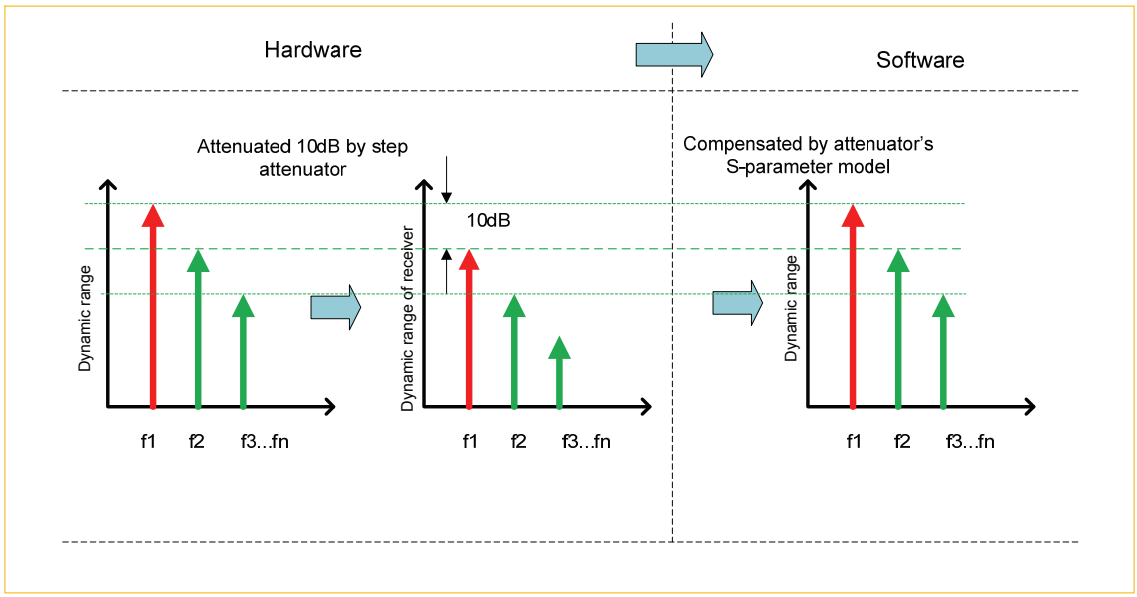

Figure 3.2: A concept for extending dynamic range using the step attenuators.

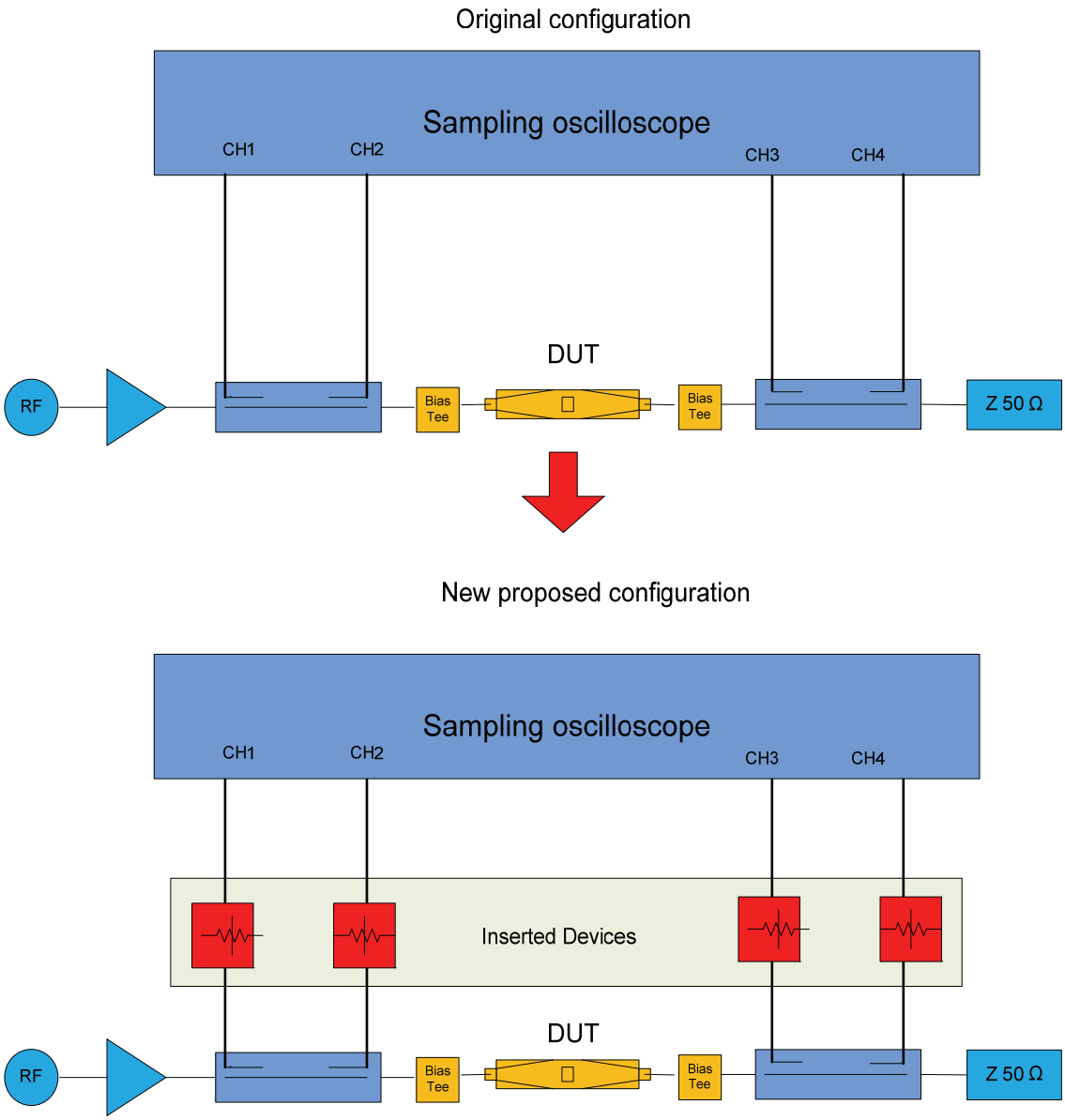

Figure 3.3: Schematic of proposed measurement system.

Figure 3.3 shows the hardware modification at work. The modified measurement system is provided with an extra inserted device: either step attenuators or an HBS. These devices play an important role in moving dynamic range of the measurement system for the fundamental frequency towards higher power levels by keeping the detected signals at the receiver's input within its specified linear range. The crucial specification of the step attenuator and HBS is the attenuation factor.

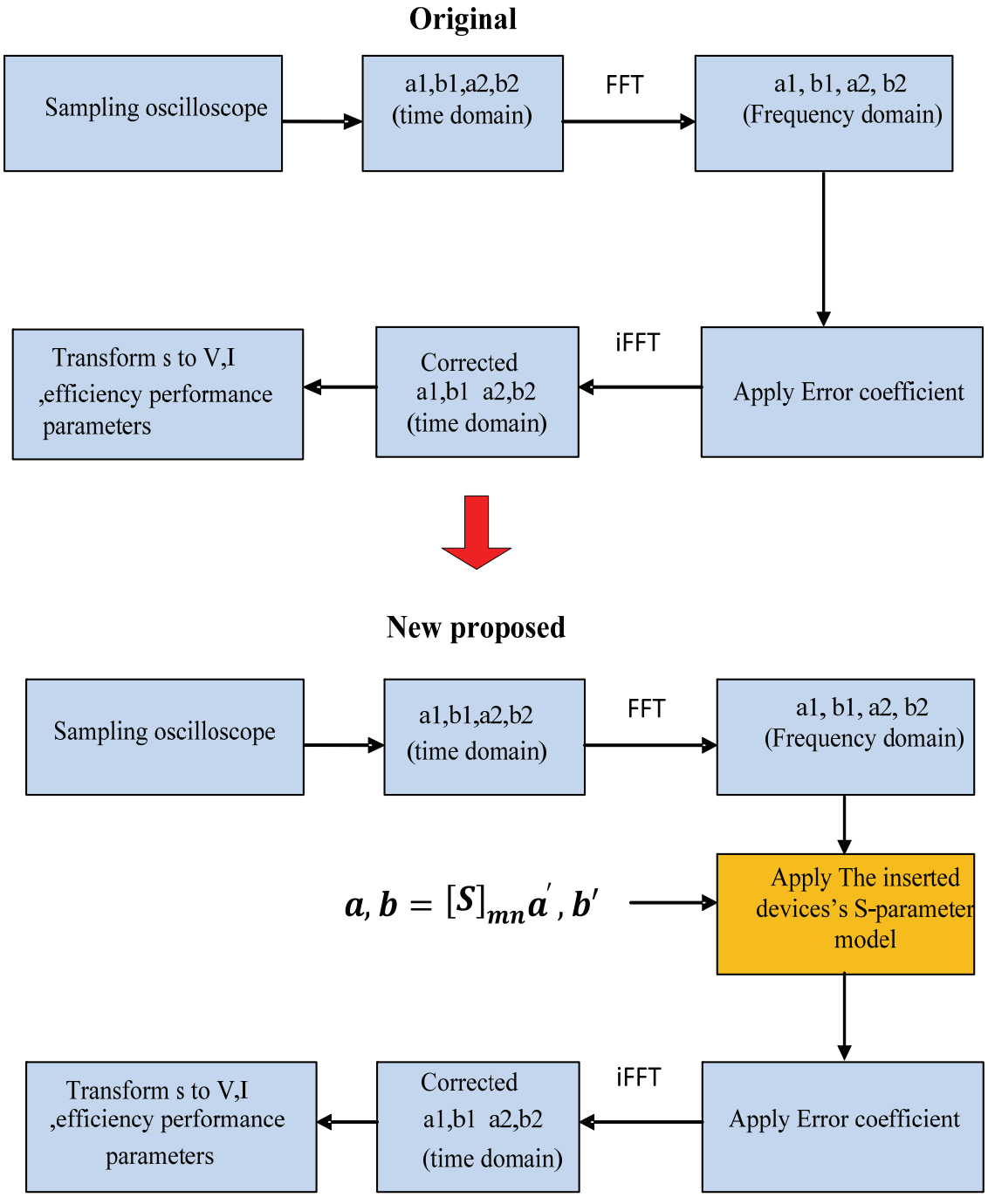

Figure 3.4: A flow chart of the proposed software correction approach.

Figure 3.4 shows a flow chart of the new software correction approach. The additional module is the S-parameter model of the inserted device, which is placed in calibration path. The S-parameter model corrects the measured travelling waves a1, b1, a2, and b2 when the measurement system is operating outside of the state for which it has been calibrate, e.g. when the measurement system is calibrated with the step attenuator state to 0 dB. If the measurement system measures the travelling waves with the step attenuator set to a value other than 0dB then the S-parameter model is used to correct these travelling waves to be detected, i.e. a1, b1, a2, and b2.

3.3 S-parameter Model Formation

3.3.1 S-parameter Overview

The concept of S-parameter was introduced by Korokawa [1]. It was derived from the incident and reflected power wave a_i and b_i, which are defined by:

$$a_i = \frac{V_i i + Z_i I_i}{2\sqrt[2]{|Re(Z_i)|}} \qquad b_i = \frac{V_i i + Z_i^* I_i}{2\sqrt[2]{|Re(Z_i)|}} \qquad (1)$$

Where V_i and I_i are the voltage and current flowing into the i^{th} port of a junction and Z_i is the impedance looking out from the i^{th} port.

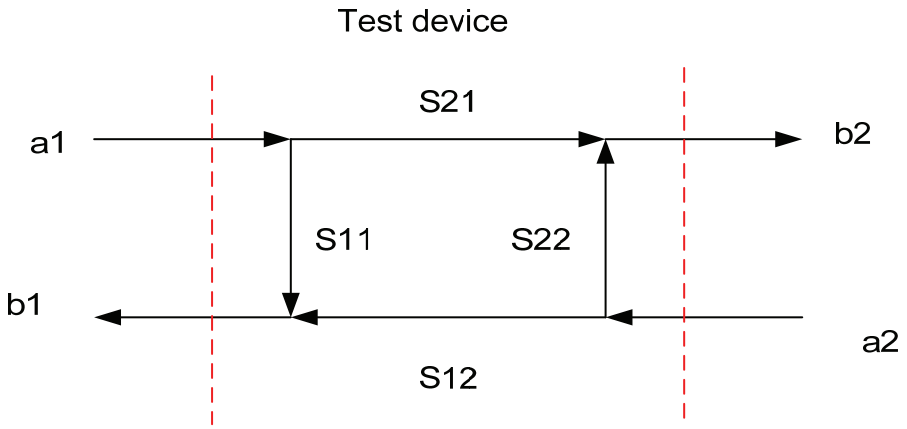

Figure 3.5: Defined S-parameter.

Figure 3.5 is the generally used to define the S-parameter matrix for a two port network. They can be expressed in a matrix equation as:

$$\begin{bmatrix} b1 \\ b2 \end{bmatrix} = \begin{bmatrix} S11\ S12 \\ S21\ S22 \end{bmatrix} \begin{bmatrix} a1 \\ a2 \end{bmatrix} \quad (2)$$

They can be written as individual the terms S11, S12, S21 and S22 as below [2]:

$$S11 = \left.\frac{b1}{a1}\right|_{a2=0} \equiv \text{reflected power wave at port 1 /incident power wave at port 1} \quad (3)$$

$$S21 = \left.\frac{b2}{a1}\right|_{a2=0} \equiv \text{transmitted power wave at port 2 /incident power wave at port 1} \quad (4)$$

$$S22 = \left.\frac{b2}{a2}\right|_{a1=0} \equiv \text{reflected power wave at port 2 /incident power wave at port 2} \quad (5)$$

$$S12 = \left.\frac{b1}{a2}\right|_{a1=0} \equiv \text{transmitted power wave at port 1 /incident power wave at port 2} \quad (6)$$

S-parameters are well known for use in the characterisation of RF and microwave circuits, where they are used instead of the more traditional parameters such as “H”, “Y” or “Z” parameters that are more often used to characterise low frequency network circuits but which become impractical for use in high frequency network circuits. The advantages of using S-parameters are that they are easy to use and measure because they are only terminated by characteristic impedance while measuring S-parameters. S-

parameters do not need an open and short technique that can oscillate at the high frequency, which could possibly damage the network circuit.

3.3.2 Full S-parameter Model

The full S-parameter model was defined to represent the behaviour of inserted devices in the measurement system. In this research project, the inserted device could be either a step attenuator or a Harmonic Bypass Structure (HBS) (more details of HBS are given in Chapters 5 and 6).

Figure 3.6 depicts the implementation of step attenuators in the measurement system. Four step attenuators were employed between the receiver (i.e. sampling oscilloscope) and the directional coupler. As a result, the travelling waves a1, b1, a2 and b2 that were captured through the directional coupler are controlled by each of the step attenuators. This configuration is well known to the VNA user and it can extend the dynamic range of the VNA toward higher power levels. Many configurations of attenuator for characterisation of high power device are described in [3]. Basically, the calibration is performed with the reference plane at the DUT, with the attenuators in the calibration path. In this research project, step attenuators are used instead of fixed attenuators. Calibration is performed including the attenuator effect only in the defined calibration state (e.g. at step attenuator value of 0dB), the other state is compensated for by using the step attenuator's full S-parameter model. Therefore, this project needs to devise an S-parameter model of the step attenuator that can be applied while it is in the measurement system.

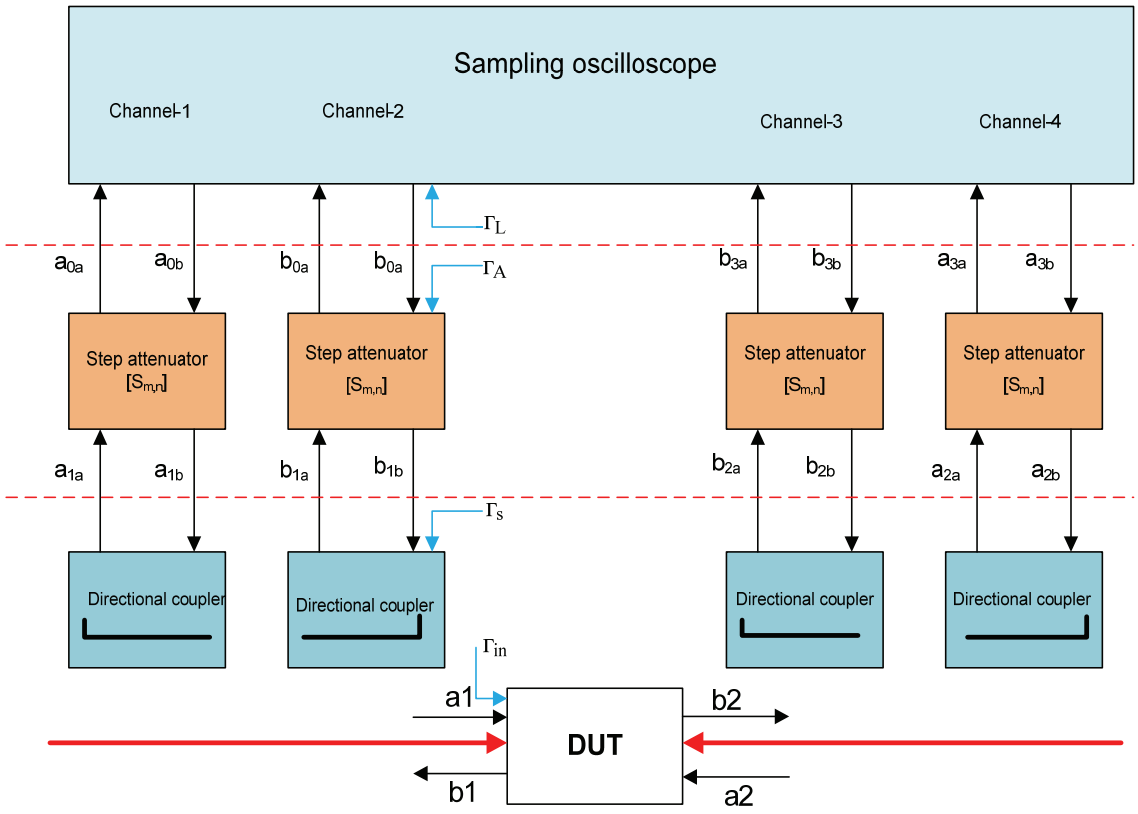

Figure 3.6: Schematic of the implementation of step attenuators in the measurement system.

This section will derive the formulation of the step attenuator's full S-parameter model for an inserted device. The assumed environment of the S-parameter model is shown in Figure 3.6. The travelling waves a1, b1, b2 and a2 of DUT are coupled by a directional coupler into the receiver sampling oscilloscope's 4 channels. The $\Gamma_{in,}$ $\Gamma_{S,}$ Γ_A and Γ_L are the reflection coefficient from the DUT, directional coupler, step attenuator, and receiver sampling oscilloscope, respectively. There are four step attenuators inserted between the directional and receiver sampling oscilloscope, their configurations are identical and, therefore, the formation of the S-parameter model is devised from the step attenuator on channel 1 of the sampling oscilloscope. The a_{0a}, a_{0b}, a_{1a} and a_{1b} are two ports of the S-parameter of the step attenuator; these parameters present the incident travelling wave a1 of DUT. The assumption of the impedance of the step attenuator is 50Ω; however, in

practice the impedance can vary over the operating range. In other words, the matching network is not perfectly matched because there is a slight reflected wave from the load or a reflected wave from the input network. Therefore, both Γ_L and Γ_S have been included in the S-parameter model in order to make it more accurate.

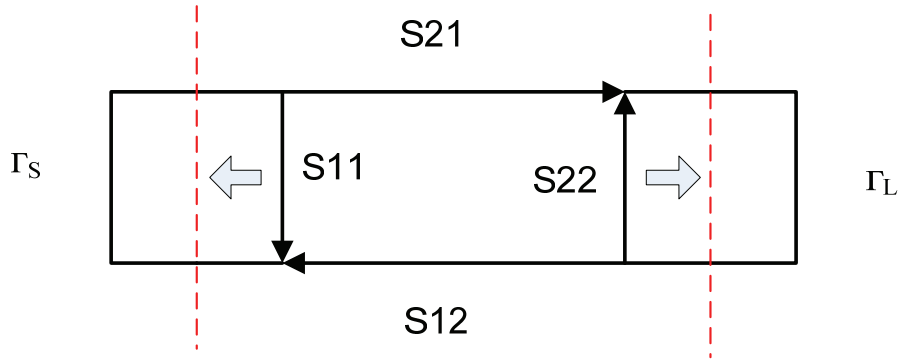

Figure 3.7: Flow graph used for the modelling of the step attenuator.

Figure 3.7 shows the step attenuator model in the S-parameter, including the reflection coefficient Γ_S and Γ_L. This flow graph can be represented in terms of signal flow (as in Figure 3.8) which is convenient to devise the model equations, where a1 is a travelling wave from DUT captured by the directional coupler and a0 is a travelling wave received by the receiver sampling oscilloscope.

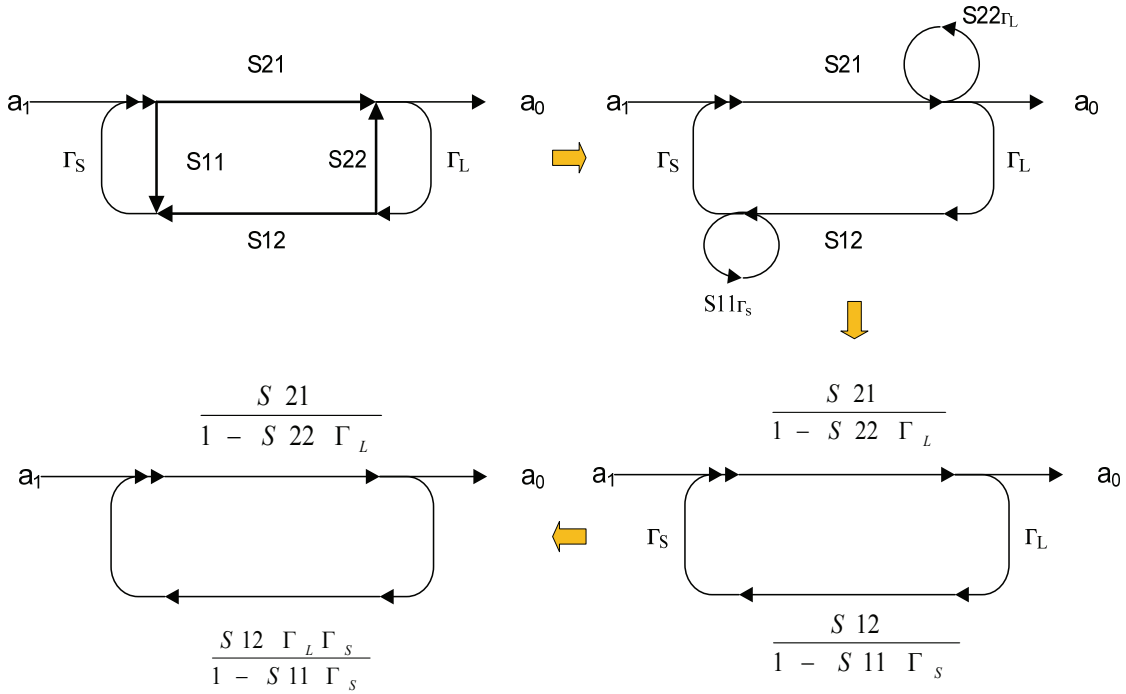

Figure 3.8: Simplified signal flow of step attenuator.

Figure 3.8 shows the simplified signal flow in the step attenuator model. The following equations have been derived from the signal flow chart:

$$a_0 = \frac{\frac{S21}{1-S22\Gamma_L}}{1-\frac{\Gamma_S\Gamma_L S12S21}{(1-S11\Gamma_S)(1-S22\Gamma_L)}}a_1$$

$$a_0 = \frac{S21}{(1-S22\Gamma_L)-\frac{\Gamma_S\Gamma_L S12S21}{(1-S11\Gamma_S)}}\,a_1 \qquad (7)$$

$$a_1 = \left[\frac{1-S22\Gamma_L}{S21}-\frac{\Gamma_S\Gamma_L S12S21}{S21(1-S11\Gamma_S)}\right]a_0$$

Equation (7) can be rewritten for travelling wave a1, b1, a2 and b2, as show in Equations 8 to 11:

$$a_1 = \left[\frac{1-S22_m\Gamma_{L1}}{S21_m} - \frac{\Gamma_{S1}\Gamma_{L1}S12_mS21_m}{S21_m(1-S11_m\Gamma_{S1})}\right] a_0 \quad (8)$$

$$b_1 = \left[\frac{1-S22_m\Gamma_{L2}}{S21_m} - \frac{\Gamma_{S2}\Gamma_{L2}S12_mS21_m}{S21_m(1-S11_m\Gamma_{S2})}\right] b_0 \quad (9)$$

$$a_2 = \left[\frac{1-S22_m\Gamma_{L3}}{S21_m} - \frac{\Gamma_{S3}\Gamma_{L3}S12_mS21_m}{S21_m(1-S11_m\Gamma_{S3})}\right] a_3 \quad (10)$$

$$b_2 = \left[\frac{1-S22_m\Gamma_{L4}}{S21_m} - \frac{\Gamma_{S4}\Gamma_{L4}S12_mS21_m}{S21_m(1-S11_m\Gamma_{S4})}\right] b_3 \quad (11)$$

Where S_m are the 2 port S-parameters of the step attenuator; Γ_{SX} is the reflection coefficient from the directional coupler; Γ_{LX} is the reflection coefficient from the sampling oscilloscope; with the subscripts x and m referring to the port channel and step attenuator state, respectively.

All S-parameters in Equations 8 to 11 include both of the actual Γ_L and Γ_S, which can be measured in a practical measurement system (see section 3.4).

3.3.3 Simple S-parameter Model

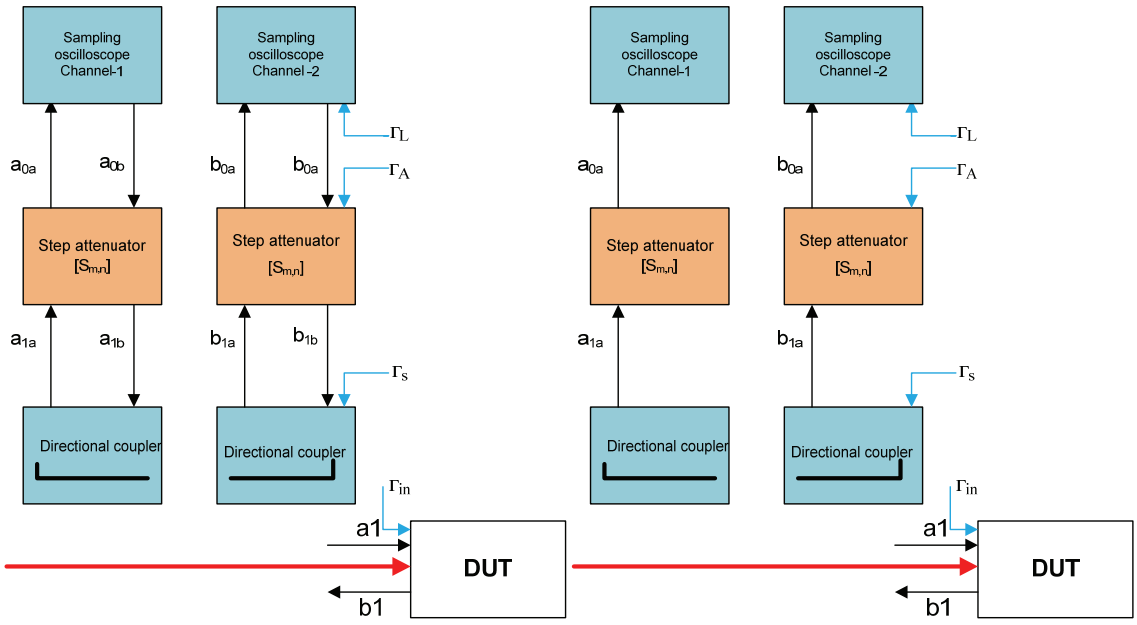

Figure 3.9: Schematic of the implementation of the step attenuator for a simple S-parameter model.

The simple S-parameter model assumes a match at the ports of the attenuators. It is based on the assumption that the impedance surrounding the step attenuator is constant and equal to50Ω throughout its range of operation. Therefore, the reflection coefficients are Γ_L=0 and Γ_S=0 which exit from the receiver and the directional coupler, respectively; or in other words, Γ_L and Γ_S remain equal to 50Ω for all step attenuator states and for all passive values of Γ_{in}. The result, which can be seen in Figure 3.9, is that the refection wave a_{0b}, a_{1b}, b_{0a}, and b_{1b} have been removed. The full S-parameter model can then be transferred to the simple S-parameter model by putting Γ_L=0 and Γ_S=0 into Equation 8. The result is found that the first term $S22_m\Gamma_{L1}$ and the second term $\frac{\Gamma_{S1}\Gamma_{L1}S12_mS21_m}{S21_m(1-S11_m\Gamma_{S1})}$ are equal to zero. Consequently, the simple S-parameter model can be rewritten in terms of S21 alone. As shown below, they can be rewritten for four travelling waves: a1, a2, b1, and b2:

$$a_1 = \left[\frac{1}{S21_m}\right] a_0 \qquad b_1 = \left[\frac{1}{S21_m}\right] b_0$$
$$a_2 = \left[\frac{1}{S21_m}\right] a_3 \qquad b_2 = \left[\frac{1}{S21_m}\right] b_3 \tag{12}$$

It is important to note that the assumptions that allow this simplified approach to be used need to be considered carefully. This approach can only be used if the coupling factor of the directional coupler is high enough (in this case it is 35 dB) otherwise the full S-parameter model will have to be used instead as it is dealing with full S-parameters and reflection coefficients of both the directional coupler and receiver.

The advantage of the simple S-parameter is that it is simplified only in terms of S21; the other S-parameters S11, S12 and S22 of the step attenuator are not necessary to measure or characterise and the reflection coefficient Γ_L and Γ_S can also be neglected. This helps save time while doing the step attenuator S-parameter measurement.

3.4 S-parameter Model Procedure

The implementation of Equations 8 to 11 can be achieved by measuring: the full 2 port S-parameters of the step attenuators, the four reflection coefficients of the oscilloscope, and the four reflection coefficients of the directional couplers at both input and output of the DUT. Measurement of the S-parameter of an inserted device is required for the formulation of the S-parameter model. The RF or microwave device manufacturer provides a device data sheet together with an S-parameter data sheet; however, in reality these S-parameter data sheets are not suitable to be reliably used in terms of format and resolution frequency.

The following section will explain how the step attenuator's and HBS's S-parameter data were collected and then transferred to a suitable electronic file format for use by the measurement software.

In the initial S-parameter model procedure the step attenuator or HBS was disconnected from the measurement system, it was measured instead by the external VNA or PNA-X Microwave Network Analyser (the configurations are shown in Figure 3.10). In the case of the HBS, the PNA-X configuration is better for use than the VNA due to the highly dynamic HBS characteristics. It must be present in the high resolution frequency grid.

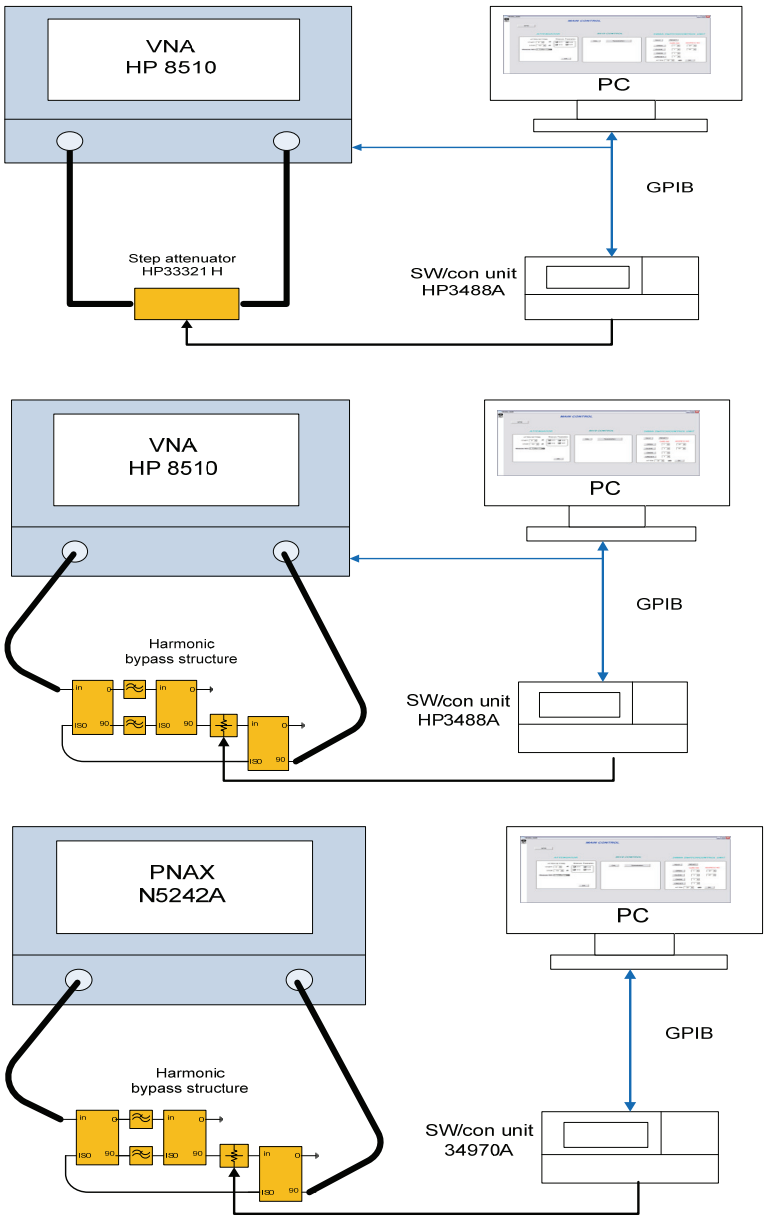

Figure 3.10: Measurement configurations for S-parameter characterisation of step attenuator or HBS. PNA-X was used to characterize the HBS's S-parameters when a dense frequency grid was required.

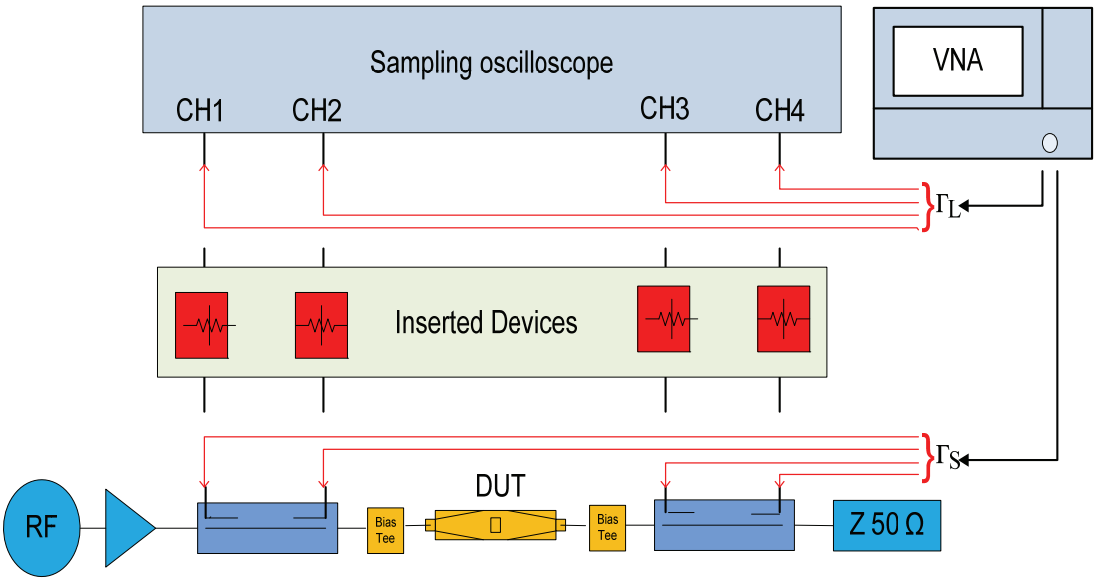

Figure 3.11: System configuration for measurement of the reflection coefficients r_L and r_S.

Similarly, Figure 3.11 shows the system configuration for the measurement of the reflection coefficients Γ_L and Γ_S from the sampling oscilloscope and directional couplers. Essentially the reflection coefficient can be measured in terms of S11 or S22.

The inserted devices are the step attenuator or HBS. The measuring of the reflection coefficient Γ_L and Γ_S was followed by the calibration of the VNA or PNA-X, this was done using the traditional TRL calibration method with a 3.5 mm calibration kit. The electronic calibration module was found to be more convenient in practice because it is a standard calibration tool for use in the modern VNA, and it is a tool which can help users save time and reduce calibration errors.

The IGOR environment software enables PC control of the switch control unit and VNA throughout the GPIB port. IGOR software is a scripting language environment similar to the high level programming languages (for example C or Perl). It also provides built-

in features and functions which can be incorporated into the user written software. In this research project, the measured S-parameter data were processed and stored in an IGOR binary wave data file (extension .ibw) according to the flowchart shown in Figure 3.12.

The next step is the implementation of a full S-parameter model in the measurement system, which is needed to prepare compatible data. The measurement software was also developed using the IGOR software environment. The raw travelling wave a0, b0, a3 and b3 that was processed in the measurement software was stored as IGOR wave variables. These waves define the format in the complex data type R+jX (where R is the real part and X is the imaginary part of the complex number). Therefore, when preparing the S-parameter data model it was found necessary to store the data in a complex form. Consequently the mathematical operations between raw travelling waves and the full S-parameter model have been easily achieved.

In the next step, the measured S-parameter data was processed using a statistical method based on the curve fitting that is provided as a built-in function of the IGOR programming software tool. The aim was to provide realisable and accurate S-parameter data. Figure 3.13 shows the flow chart of the S-parameter data processing operation. In the initial state the N-number of measured S-parameter data (that is in R+jX form) are loaded into the IGOR wave variables. The data are then separated into their real and imaginary parts. To provide data format from VNA the S-parameter data is averaged in both real and imaginary parts. The N samples of the real S-parameter data should be averaged separately from the N samples imaginary S-parameter. Next, the R and X parts are transferred to R+jX form. At this state, the S-parameter data is ready to be transferred into the measurement software.

In addition, if the user needs to do a better smooth fit curve for the S-parameter characteristic then they can carry out the other curve fitting functions (e.g. polynomial curve fitting). The polar format of the S-parameter data is suitable for doing polynomial curve fitting, they can fit the curve in terms of magnitude and phase. The final result the

S-parameter data is transferred to the rectangular form. This process has been similarly applied to Γ_L and Γ_S data.

In the final step the S-parameters data set and Γ_L and Γ_S data was saved in the IGOR binary file format so that it can be easily loaded into the measurement software. The data can now be used to form the full S-parameter model. Table 3.1 shows the assigned name for the S-parameter and Γ_L and Γ_S.

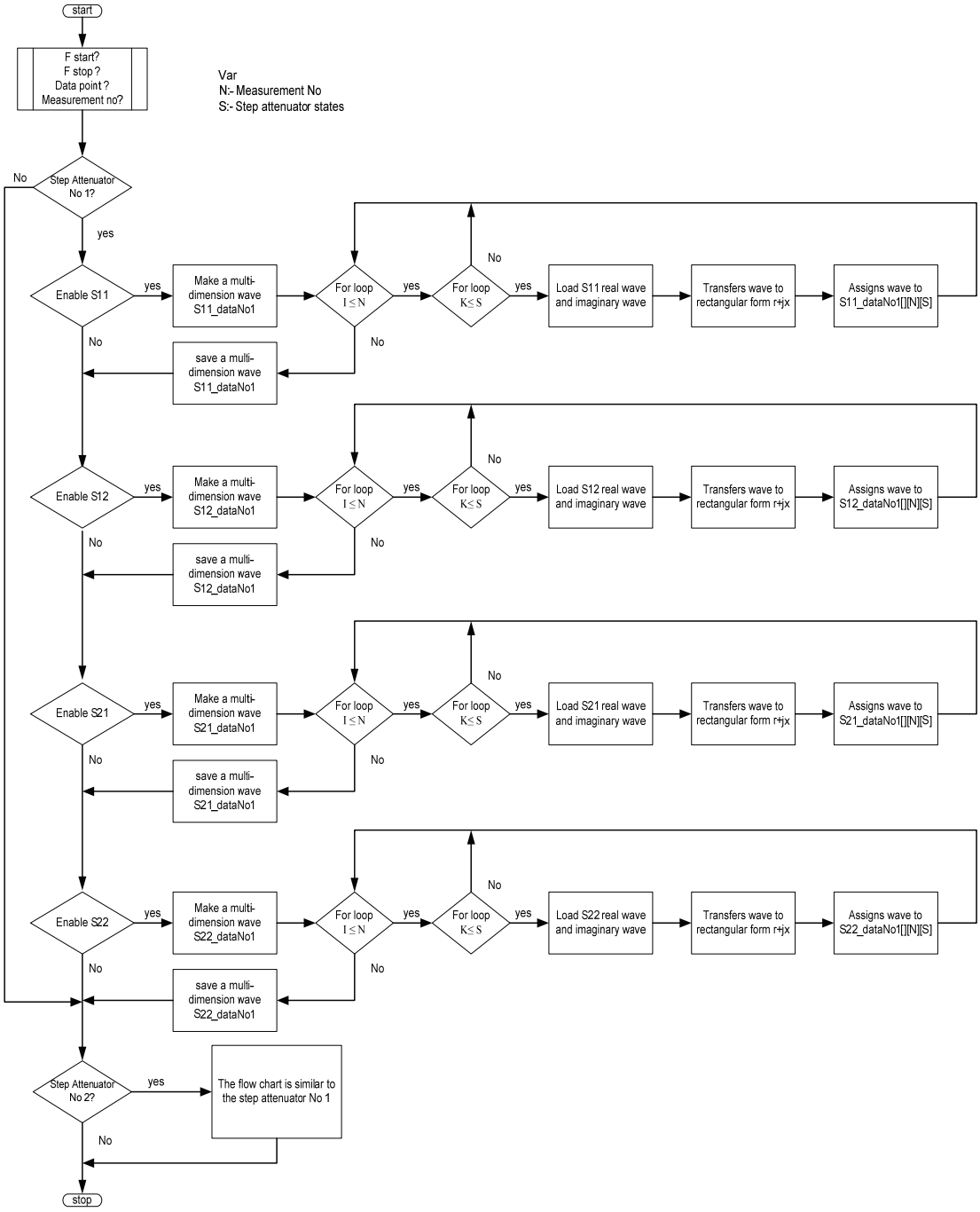

Figure 3.12: S-parameter data processing flowchart of the repeated S-parameter measurement (it collects the S-parameter data into a file which is then used in the IGOR software environment).

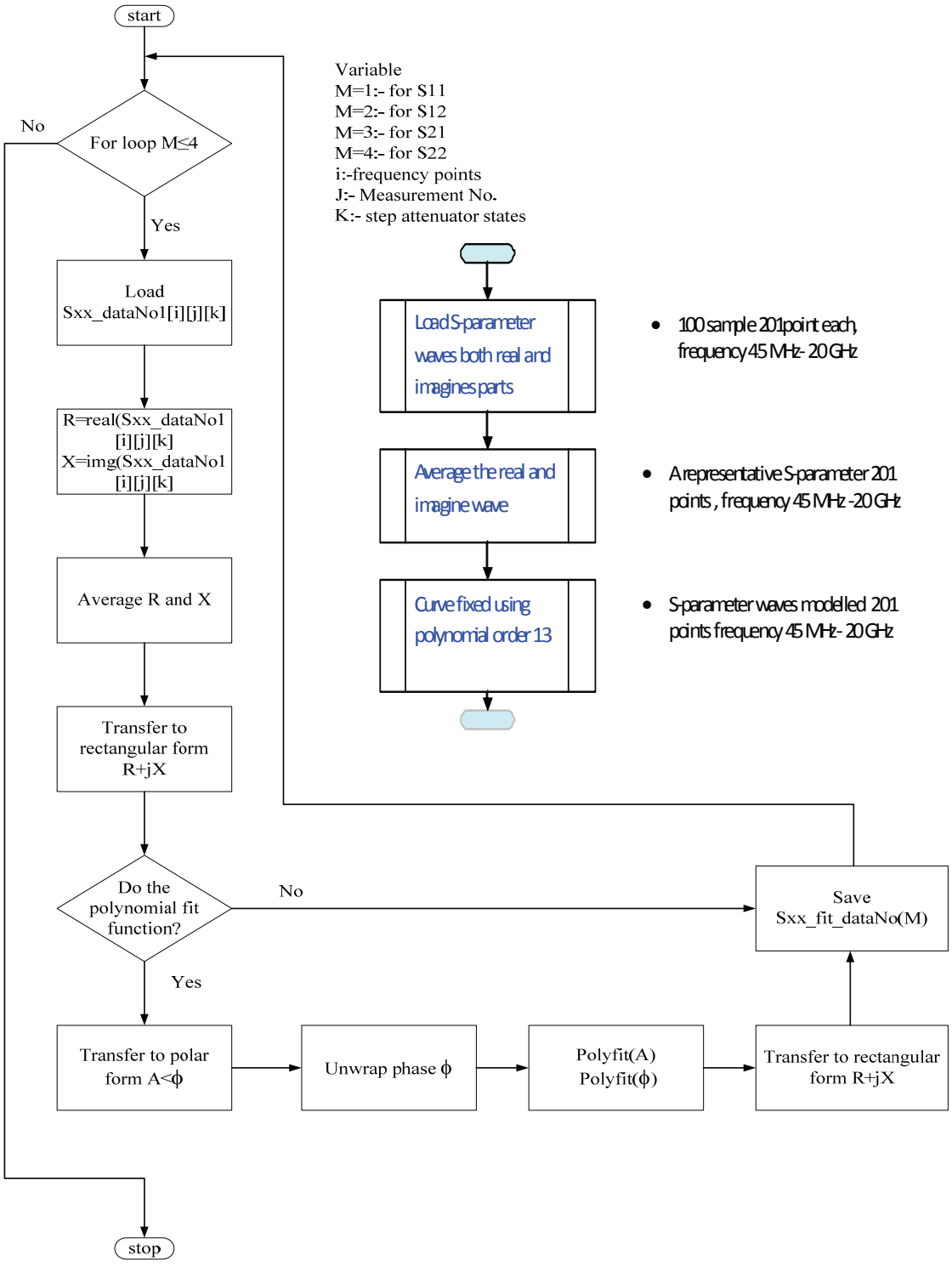

Figure 3.13: Modelled S-parameter flowchart for N measurement data. The synthesis of the S-parameter model uses either the average function or polynomial fit function.

Files name (.ibw)	Step attenuator serial No	Wave dimension	Assigned data
Sxx_fit_dataNo1 S21_fit_dataNo1 S21_fit_dataNo1 S22_fit_dataNo1	2804A22474	[m,9] m = frequency points	[m,0]= frequency [m,1] –[m,9] = S parameter for step attenuator state 0 to 70 dB respectively.
S11_fit_dataNo2 S21_fit_dataNo2 S21_fit_dataNo2 S22_fit_dataNo2	2523A06839		
S11_fit_dataNo3 S21_fit_dataNo3 S21_fit_dataNo3 S22_fit_dataNo3	3837M00671		
S11_fit_dataNo4 S21_fit_dataNo4 S21_fit_dataNo4 S22_fit_dataNo4	1436A00651		
GammaTS_data		[m,5]	[m,0] =frequency [m,1]-[m,5] = rs for CH1,2,3 and 4 respectively
GammaTL_data		[m,5]	[m,0] =frequency [m,1]-[m,5] = Γ_L from directional couplers a1,b1, b2,a2 respectively

Table 3.1: Designed electronic format type (.ibw) which store the S-parameter and the reflection coefficients.*

3.5 The Implementation of an S-parameter Model in Measurement Software

3.5.1 Cardiff High Power RF Measurement Software: An Overview

There are two software packages currently in use in the Cardiff High Power RF measurement system. They are both categorised by operation function into calibration software and measurement software. Both of these software packages have been developed using a software development environment called IGOR, which is available from WaveMetrics. IGOR provides built-in crucial features and functions (e.g. data processing, mathematical operation, visualisation etc.) that are suitable for engineering or scientific work. IGOR allows an external plug-in to be integrated into its packages, including the GPIB communication card that is in common use in engineering work and which enables the PC to control peripheral instruments. It is important that measurement software is able to carry out the data procession (e.g. Fast Fourier Transforms (FFT)) and that it can control the main instrument (e.g. oscilloscope).

The original software code of the Cardiff High power RF measurement software was developed by David Williams [4]. Figures 3.14 and 3.15 show the calibration software and measurement software code structure. The calibration software enables the measurement system to generate the error coefficients of its system. It also enables the measurement system to measure S-parameters. The measurement software provides more ability than the calibration software; for example, controlling the DC bias power supply, load pull, and source pull. The measurement software provides waveform engineering capability which is crucial for the characterisation DUT (e.g. power transistors). However, the measurement software needs the error coefficient data which is provided by the calibration software. The error coefficients are imported into the measurement software from the calibration file handling process box (as can been seen from Figure 3.15), which links to the data processing process box that allows the

measurement system to correct the raw travelling waves a1, b1, b3and a3. The data processing process function is shown in figure 3.4 on the original flow chart.

In this research project, the data processing box has been modified in order to implement the full S-parameter model. The new design functions are embedded between the operation of the FFT of the raw travelling wave and the applied error coefficient function.

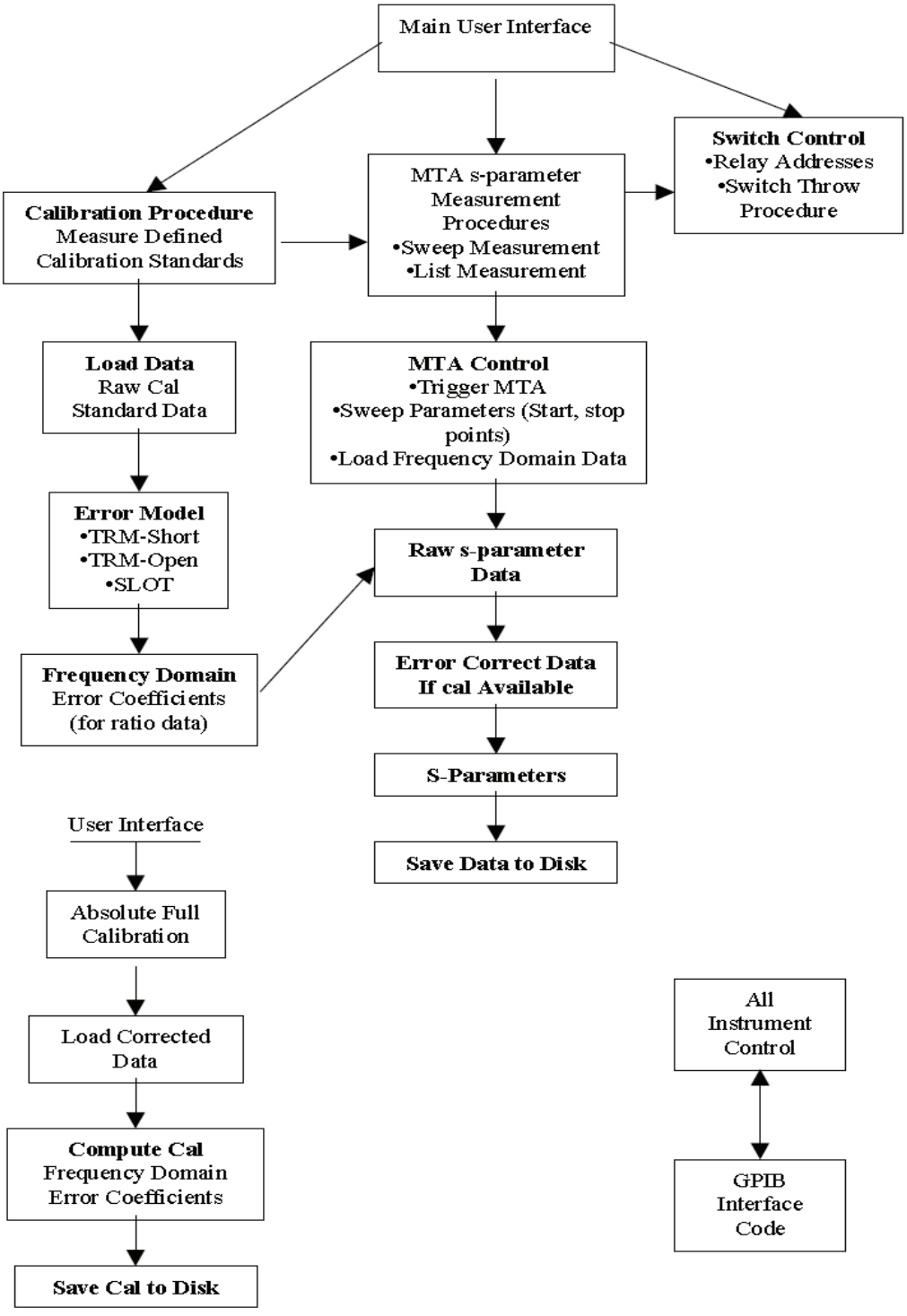

Figure 3.14: Calibration software code structure from [4].

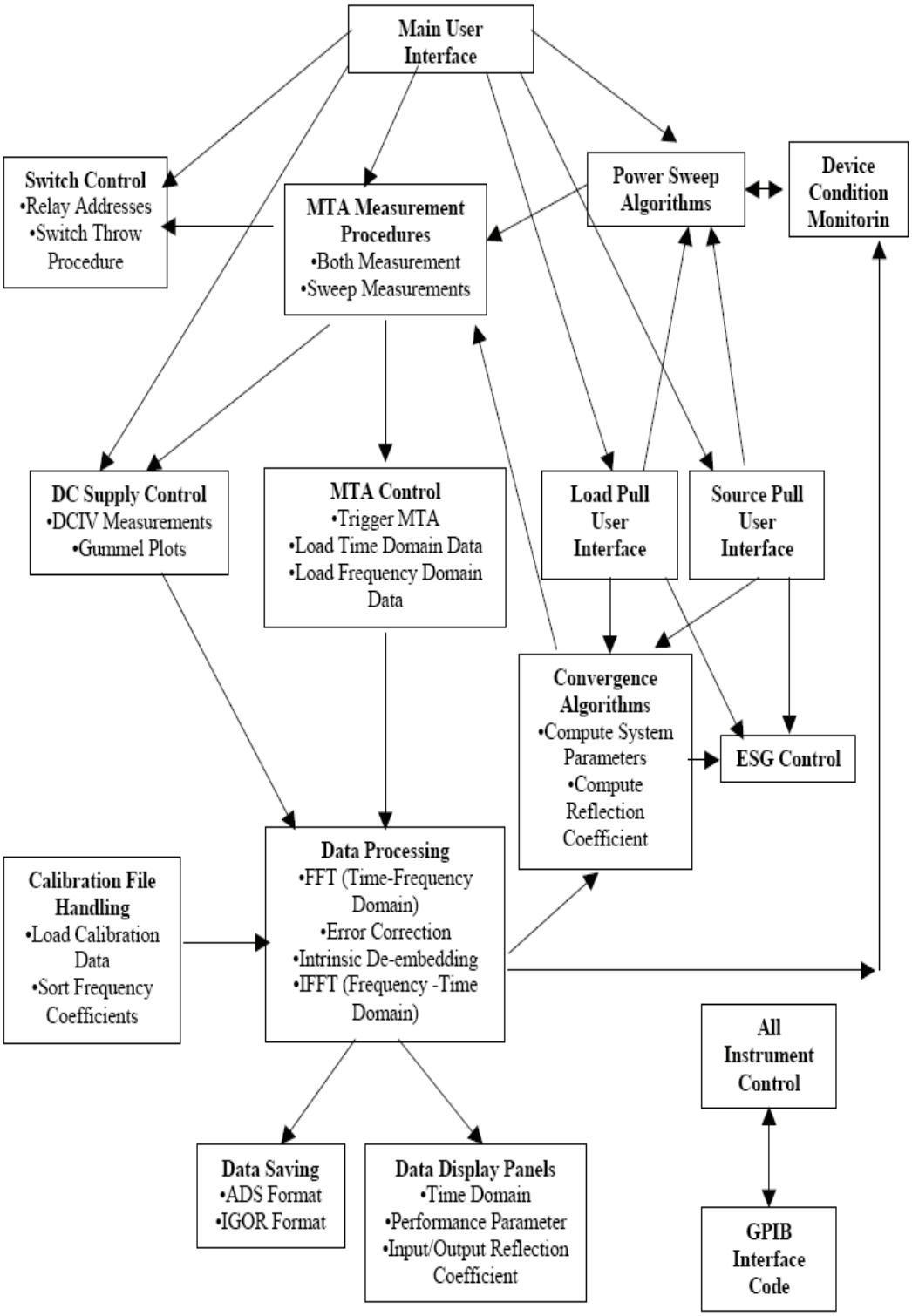

Figure 3.15: Waveform software code structure from [4].

3.5.2 Measurement Software and Correction Procedure

3.5.2.1 Correction for the Step Attenuator's Full S-parameter Model

The step attenuator's full S-parameter model is a function of its state, and they are unique to each attenuator. The accuracy of the measurement system depends on the accurate S-parameter model according to its state, frequency, and correct arrangement position; for example, the corrected travelling wave a0 would be wrong if the S-parameter model is generated from the attenuator set for the b0 wave, even if the attenuator is operating in the same state.

As show in Figure 3.4, the correction of the travelling waves have been achieved after they have been applied to the step attenuator's full S-parameter model (as formed in Equations 8 to 11). However, in an actual measurement setting (and as the calibration would have been conducted with the step attenuator in some defined reference state) the relative S-parameter must be used instead of the absolute S-parameter. From Equations 8 to 11 this can re-write as below:

$$a_1 = a_0 * \frac{S_{set}}{S_{cal}} \qquad b_1 = b_0 * \frac{S_{set}}{S_{cal}}$$

$$a_2 = a_3 * \frac{S_{set}}{S_{cal}} \qquad b_2 = b_3 * \frac{S_{set}}{S_{cal}} \tag{13}$$

Where S_{set} is the full S-parameter model of the step attenuator at measurement state, and S_{cal} is the full S-parameter model of the step attenuator at calibration state, then S_{set} and S_{cal} is defined as shown below:

$$S_{set} = \left[\frac{1-S22_m\Gamma_{L1}}{S21_m} - \frac{\Gamma_{S1}\Gamma_{L1}S12_mS21_m}{S21_m(1-S11_m\Gamma_{S1})}\right] \tag{14}$$

The subscript m refers to the step attenuator at measurement state:

$$S_{cal} = \left[\frac{1-S22_m\Gamma_{L1}}{S21_m} - \frac{\Gamma_{S1}\Gamma_{L1}S12_mS21_m}{S21_m(1-S11_m\Gamma_{S1})}\right] \quad (15)$$

The subscript m refers to the step attenuator in a calibration state. The equations above represent the actual implementation in the measurement software.

3.5.2.2 IGOR Procedure

The IGOR procedure file Convaratten.ipf has been developed to enable the correction of the raw travelling wave using the S-parameter model. It contains both the functions and the procedure scribes, which allow the measurement software to control the step attenuators, generate the S-parameter model, and to compensate the raw travelling waves. There is a GUI (Graphical User Interface) that makes it convenient to select and control the step attenuator. This GUI also allows the measurement software to enable or disable the S-parameter model correction.

Convaratten.ipf has been employed into the measurement software; however, there are a few code scribes which have been modified into the old measurement software, among them are the a calling function line scribes in loaddata11() and loaddata21() functions. This line calls the function CorrectdataAtten() which is an extremely important part of the modifying software because it provides the correction travelling wave.

The basic operation of the modified measurement software is described in the following outline:

- The measurement software will load the calibration file handing into the measurement software environment. The functions in the Convaratten.ipf procedure file will load the calibration state of step attenuator and control the step attenuator to the default state (usually at 0dB). Convaratten.ipf will also load the S-parameter data, Γ_L and Γ_S. file into the measurement software (as show in Table 3.1).

- The user selects the appropriate attenuation. This process will define the step attenuator state at the measurement point. The PC sends a command through the GPIB to the operation step attenuators.

- The user starts measuring the DUT parameter. If both buttons have been pressed then the measured travelling waves have been processed in the data processing box. At this state of correction the measurement software will call the CorrectDataAtten() function to correct the travelling wave due to the attenuation. After which, the travelling wave will transfer to the desired parameter (e.g. voltage and current waveforms, and gain parameter).

The entire procedure above is illustrated in Figure 3.16.

Figure 3.17 show the flowchart of function CorrectdataAtten(). This function enables the measurement software to correct the raw travelling wave. The function initially starts the imported the global variable a0, b0, a3 and b3. These variables are provided by function Loaddata11() and loaddata22(). Next the CorrectdataAtten () calls the other function to generate Sset and Scal model that is required to be applied to the raw travelling wave. By using the equation (13), the travelling wave is corrected by the S-parameter model. Finally, the CorrectdataAtten() function returns the variables a0, b0 , a3 and b3 and then they are applied to the error coefficient by the measurement software.

Figure 3.18 shows the flowchart for computing the S_{set} and S_{cal}, which represent the S-parameter model at measurement and calibration state. The function starts by determining the fundamental frequency, the harmonic of measurement software, and the step attenuator state. These variables are important to generate the right S-parameter model. The frequency list has been generated in the second process box, which contains the dc, fundamental and harmonics. The S-parameters and reflection coefficient have been interpolated according to the frequency list in the next two process boxes. As a result, the S-parameter model as show in Equations 14 and 15 has been calculated.

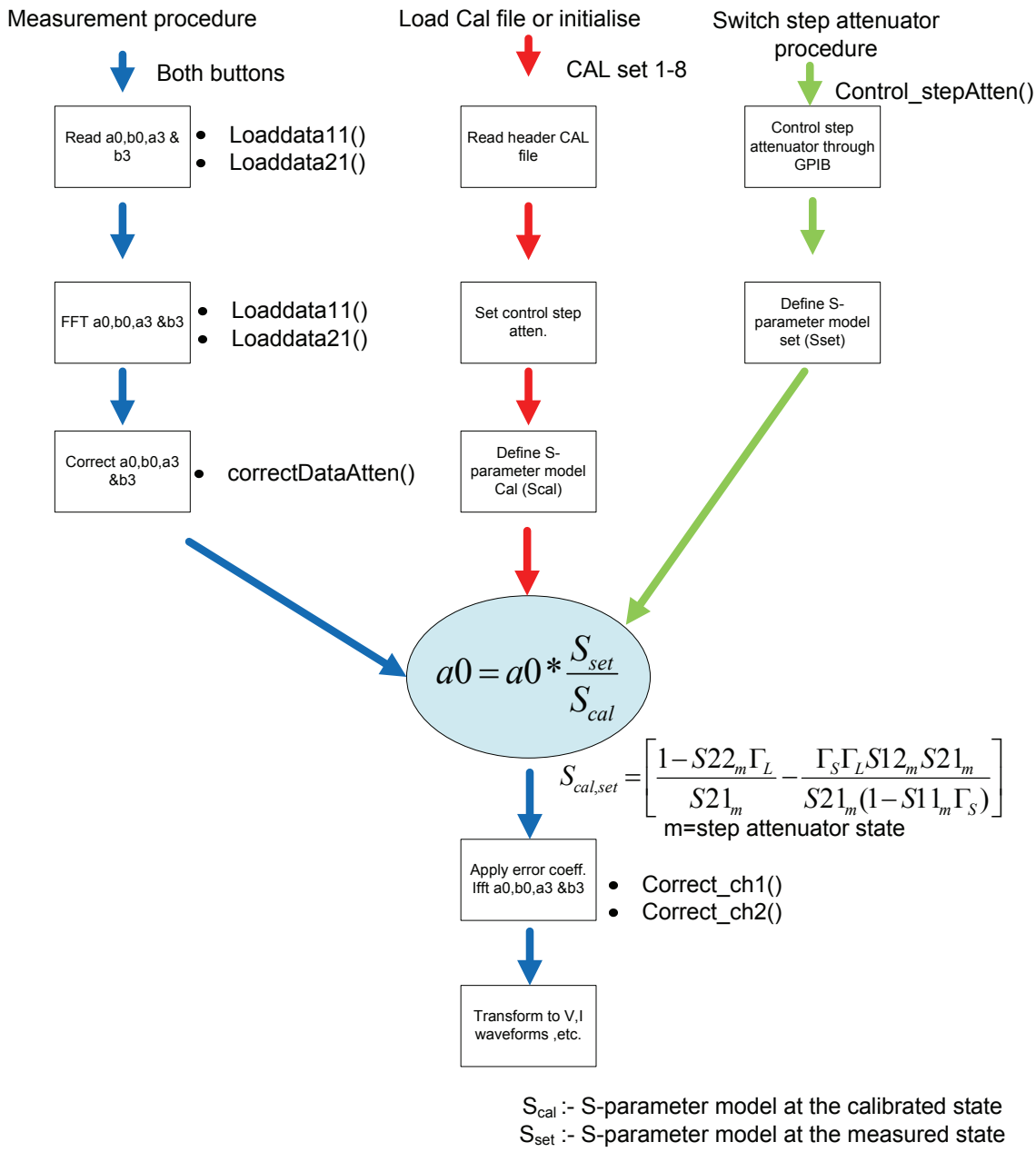

Figure 3.16: Flow chart for the correction of the travelling waves a0, b0, a3, and b3.

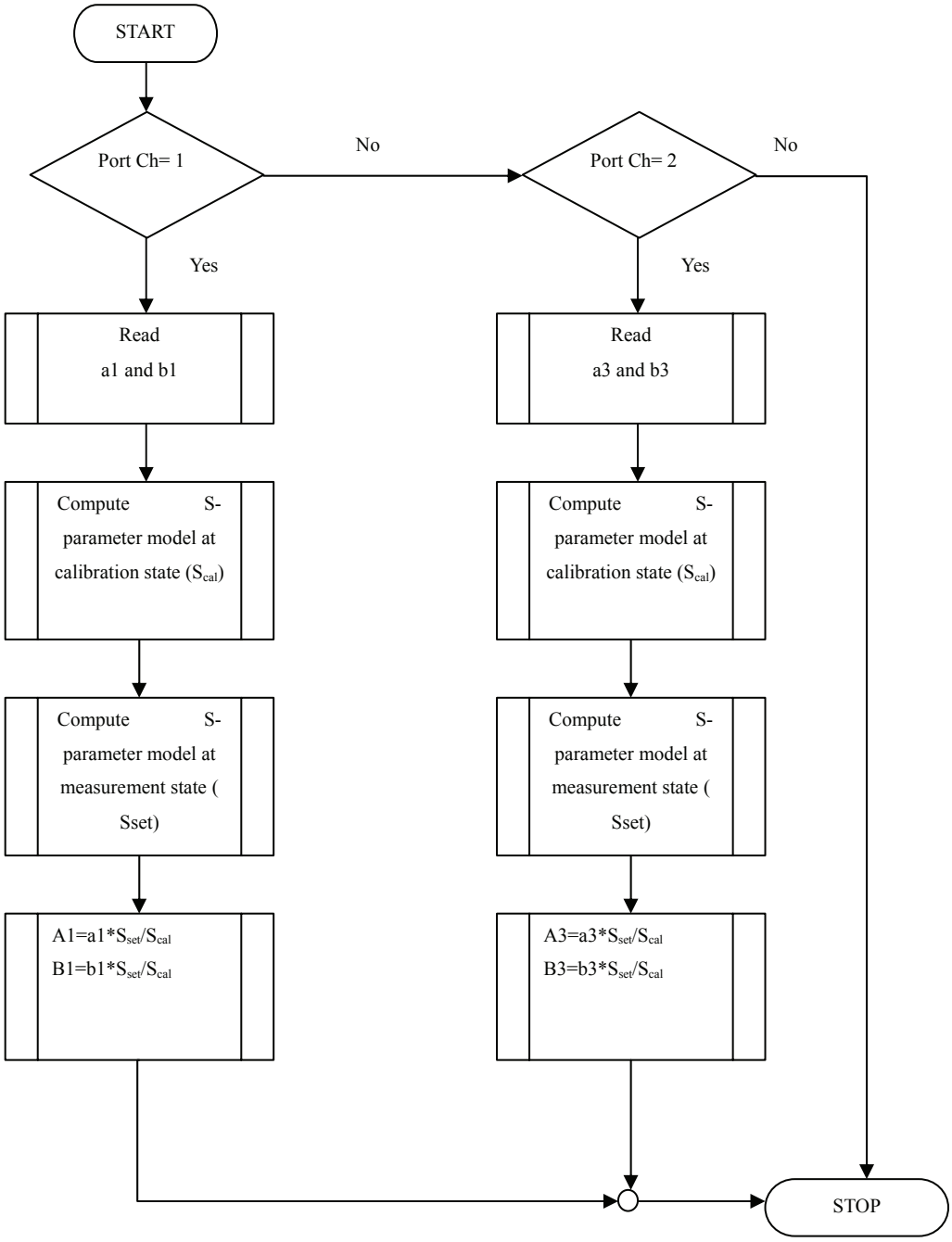

Figure 3.17: Flowchart for the IGOR function CorrectDataAtten().

Figure 3.18: Flowchart for computing the S_{cal} and S_{set}.

3.6 Verification of the Simple S-parameter Model in a Waveform Measurement System

The implementation of a simple S-parameter model in an actual measurement system has been conducted in the early stages of this research project. The verification measurement was performed in the thru standard 3.5mm. The results show that it is possible to employ measured attenuator S-parameters to generate models with which to accurately correct the measured voltage of travelling waves in advance of software processing within the measurement system itself. Two correction methods have been explored, with similar results: the first using simple averaging of measured s21; and the second employing a polynomial fit to the averaged data. The results indicate that the various attenuation states are highly repeatable, with measured s21 magnitude and phase varying by no more than 0.03dB and 0.2° (1SD) respectively over a switching sequence of at least 100 cycles per state, and over frequency range of 0 to12GHz. The full detail of verification can be seen in Appendix C.

3.7 Conclusion

This chapter has discussed the implementation of an S-parameter model into the high power RF measurement software. The step attenuator's S-parameter data was measured by the VNA or PNA-X with the incorporated software environments. This allowed the user to do statistical data processing, which increases the reliability and accuracy of the S-parameter data. Subsequently the S-parameter model that describes the representation behaviour of the step attenuators was devised. These models were used in the measurement software in order to correct the travelling voltage wave. Verification of the simple S-parameter model in an actual measurement system has been achieved and the results show that the accuracy of measurement is acceptable.

References

[1] K. Kurokawa, "Power waves and the Scattering Matrix," *IEEE Transactions on Microwave Theory and Techniques*, vol. MTT-13, no. 2, pp. 194-202, March 1965.

[2] Agilent, S-parameter Techniques for faster, more accurate Network design, 1997, Test & Measurement Application Note AN 95-1 S-parameter Techniques.

[3] Agilent, Agilent AN1287-6 Using Network Analyzer to Characterize High-Power components, 2003, Application note.

[4] D.J. Williams, "Non-Linear Measurement System and Techniques for RF Power Amplifier Design," Cardiff University, PhD thesis 2003.

[5] K.A. Remley, "Practical Applications of Nonlinear Measurements," in *Microwave Measurement Conference, 2009 73rd ARFTG*, Boston, MA, June 2009, pp. 1-15, Nist.gov. [Online]. http://www.nist.gov/eeel/electromagnetics/rf_fields/upload/R16_ARFTG73_Remley.pdf.

[6] Agilent, 3488A switch/control Unit operating ,Configuration Manual, 1995, USA.

[7] Agilent, 8510C Network Analyzer Key word dictionary, 2001, rev3, USA.

[8] Agilent, Agilent AN 1287-3 Applying Error Correction to Network Analyzer Measurements, 2002, Application Note.

[9] Agilent, Agilent Technologies 33320A/B/G/H 33321 A/B/D/G/H/K 33322A/B/G/H 33323K Step attenuator for OEM & System Use dc to 26.5GHz, 1990, Technical data sheet.

[10] Agilent, Specifying Calibration Standards for the Agilent 8510 Network Analyzer, 2004, Application Note 8510-5B.

[11] WaveMetrics Inc, *IGOR Pro Version 6.0 manual*, 1st ed. Lake Oswego, USA: WaveMetric Inc, 2007.

[12] D.M. Pozar, *Microwave engineering*, 3rd ed. New York, USA: John Wiley & Son,INC., 2005.

[13] J. Benedikt, "Evaluation and Measurement Enhancement of the High Frequency Measurement System at the University of Wales College Cardiff," Cardiff University, Cardiff, Thesis 2000.

CHAPTER 4

Improving Dynamic Range
Using Programmable Step Attenuators.

CHAPTER 4 - Improving Dynamic Range Using Programmable Step Attenuators.

4.1 Introduction

This chapter describes the demonstration of an extended dynamic range measurement system using step attenuators. It starts with the characterisation of a step attenuator, which aims to collect the step attenuator's S-parameter data and to analyse its repeatability. After implementing the step attenuator into the measurement system, a demonstration was set up to prove the possibility of extending dynamic range using a step attenuator approach. A CW power sweep was performed in both a 7mm standard and a GaN 50 W transistor device with the aim of investigating the power output comparison in respect to a number of step attenuator states. Finally, the results of the demonstration will be discussed.

4.2 S-Parameters Characterisation of Step Attenuators

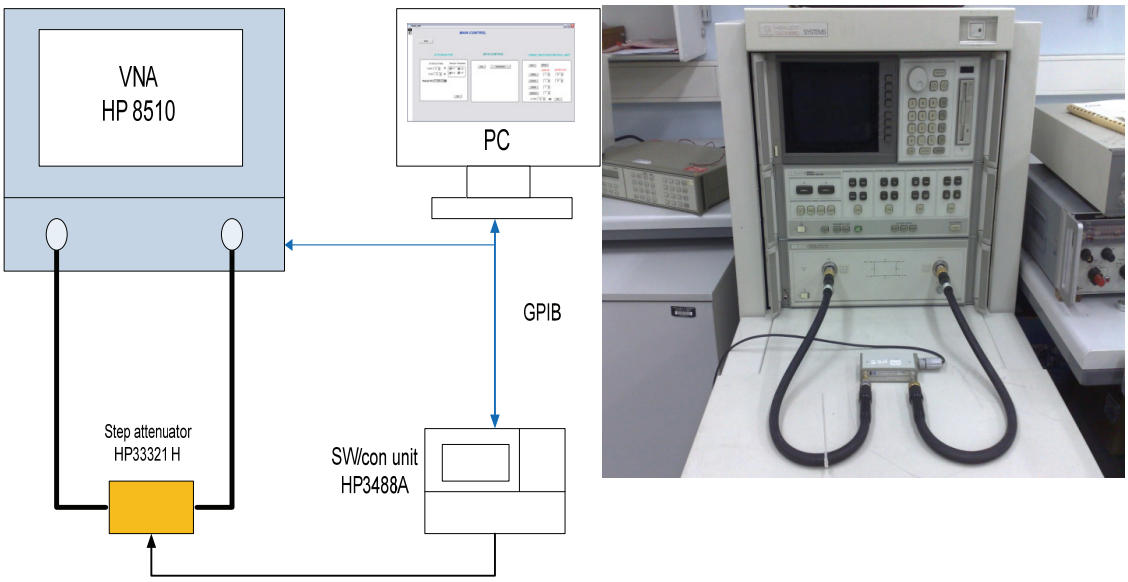

Figure 4.1: An automated measurement configuration for measuring the S-parameters of step attenuators.

There are two important objectives for the characterisation of an step attenuator. Firstly, to investigate S-parameter data, especially when the step attenuator has changed its state (the result is expected to show that the change should increase or decrease according to its state, as described in the S-parameter data sheet); and secondly, to collect the S-parameter data, which is then used to develop the step attenuator S-parameter model that is used in the measurement system.

Figure 4.1 shows an automated S-parameter measurement configuration, which was set-up for the characterisation of the step attenuators. The measurement configuration consists of a VNA HP8510, a switch controller unit HP3488A, a PC computer installed with the IGOR software environment, and a step attenuator HP33321H.

The characterisation initially started from the calibration of HP8510 using a measurement frequency range from 45MHz to 20 GHz, spreading over 201 frequency points. The measurement that was performed on the step attenuator state started from 0 dB to 70 dB, it then transits the original state of 0 dB and repeats the same measurement for 100 cycles. The S-parameter data was imported into the IGOR software, from where it was exported to ADS for plotting (the resulting graph can be seen in Figure 4.2). Although four step attenuators were characterised in total, the results show the results from only one step attenuator because the results of all four are similar.

From the results, it is obvious that the S-parameters are found to be in line with the specification and the accuracy of the step attenuator. For example, when the step attenuator state was 10 dB both S12 and S21 were also 10dB, so S12 and S21 were found to be a function of frequency (i.e. increasing the frequency caused a greater insertion loss). Similarly, an investigation of the reflection of the step attenuator shows that the S11 and S22 were a function of frequency; however, they provide good impedance matching at a low frequency (e.g. it reached below -30 dB and -20 dB at a frequency range 45MHz to 6 GHz and at frequency 6 GHz to 20 GHz respectively). Although the reflection with the step attenuator state, the overall S22 and S11 were below -20 dB over the whole frequency range, which still shows good matching.

It was found that the different reflection curves came from the combination of an attenuation card and a thru line within step attenuator unit; therefore, to access the influence of the reflection of the step attenuator the whole S-parameter set was used in the demonstration measurement system (as shown in Figure 4.2).

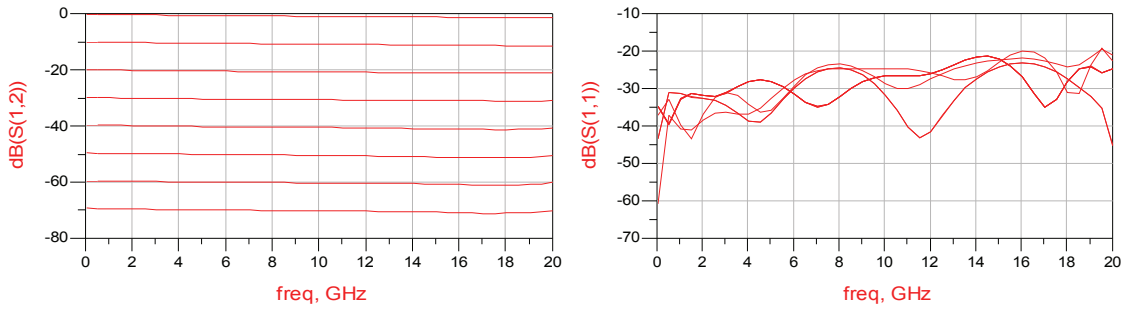

(a) *(b)*

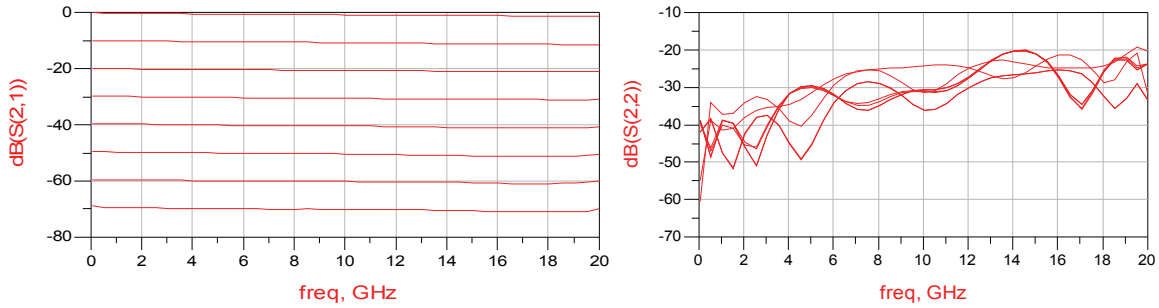

(c) *(d)*

Figure 4.2: S-parameters of the step attenuator for states ranging from 0 to 70 dB in 10dB steps: (a) S12 (b) S11 (c) S21 (d) S22.

4.3 Access Repeatability of the Step Attenuator

Repeatability of the step attenuator plays an important role in this research project. If the repeatability of the step attenuator cannot reach the requirements then it is impossible to get either an accurate or a precise measurement while the step attenuator is switching to other states. Therefore, one of the first and most important steps of this research project is to verify step attenuator repeatability.

The general specification of step attenuator HP33321H is shown in [Appendix B]. HP33321H provides an operating frequency range from DC to 18 GHz, an attenuation range 0dB to70 dB with 10dB/steps, insertion loss at 0dB (0.4dB+0.07 dB/GHz), a maximum SWR of 1.35 to 8GHz-1.5 to12.4 GHz-1.7 to 10 GHz, and a repeatability life of typically 0.01dB for up to 5 million cycles per section. The HP33321 attenuator module has three attenuation stages (10dB, 20dB, and 40dB) which are connected in cascade. Each section has a precision thin-film attenuation card, a lossless thru line, and a ganged pair of contacts that switch the attenuation card in or out. This combination results in high accuracy and exceptional repeatability [1].

To verify the step attenuator specification the automated measurement system has been arranged as illustrated in Figure 4.1. The HP8510 was calibrated to measure a frequency range from 45MHz to 20 GHz, spreading over 201 frequency points. The measurement that was performed on the step attenuator state started from 0 dB to 70 dB, it then transits the original state of 0 dB, the same measurement was repeated for 100 cycles. The S-parameter data was finally imported into the IGOR software for data processing.

The repeatability of the measurements were analysed, the results are shown in Figures 4.3 to 4.8. In the practical measurement system, the step attenuator states that were going to be used were only on 0 dB to 20 dB. Consequently, the results and discussion have focused on the step attenuator state from 0 to 20 dB. The frequency of interest

starts from 0 to 12 GHz, which covers up to 5th harmonic if the application fundamental frequency is 2.100 GHz. Magnitude and phase repeatability have been achieved at 0.02 dB and 0.02 dB, respectively, at the defined range at which the step attenuator will be used. This shows good repeatability and is suitable for use in the measurement system.

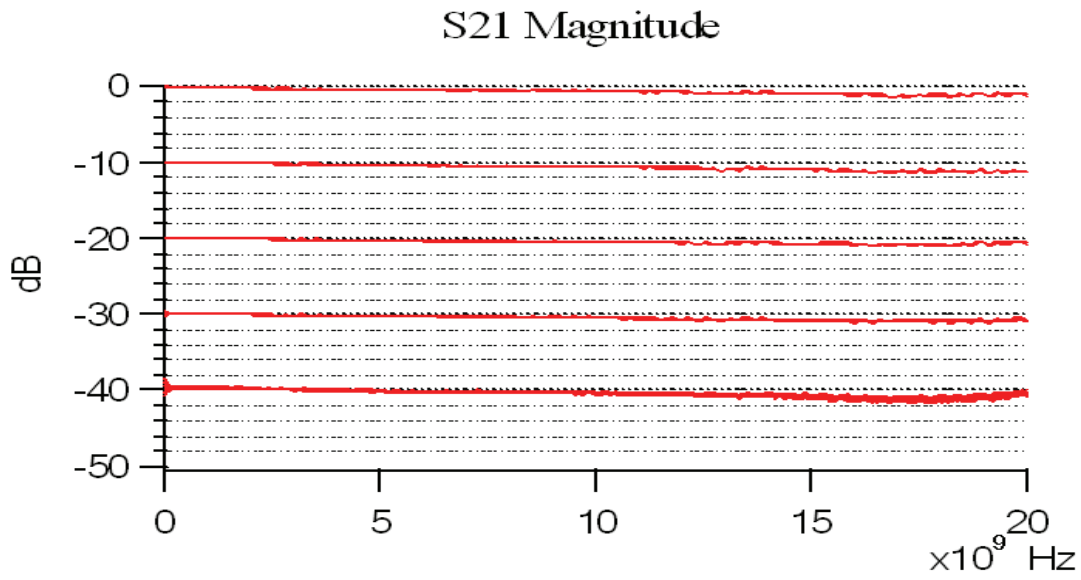

Figure 4.3: S21 Magnitude for a 45 MHz-20GHz frequency range, for states 0dB to 40 dB.

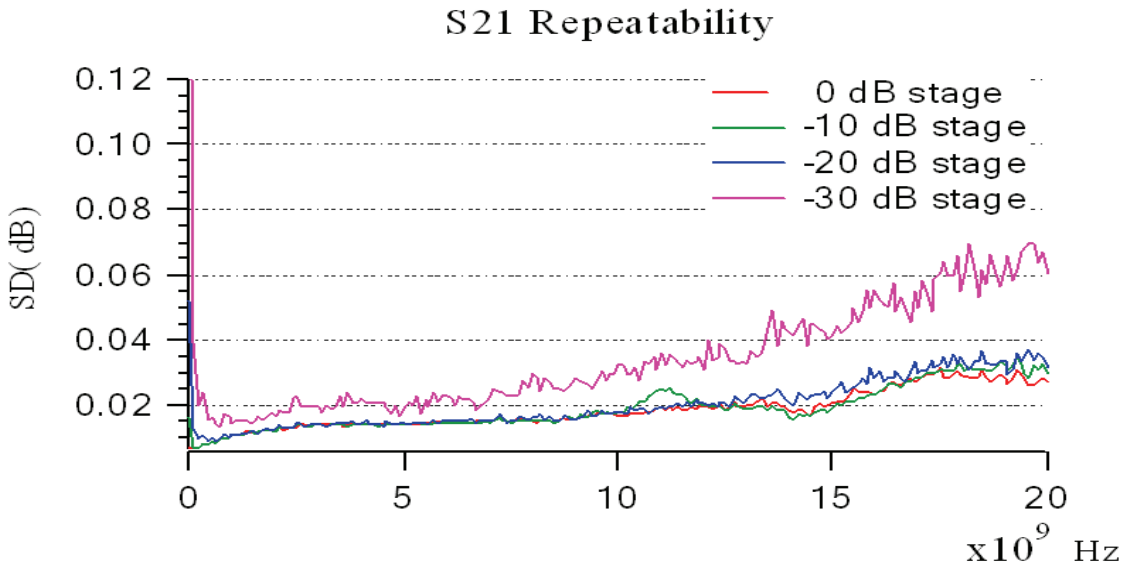

Figure 4.4: Standard deviation of magnitude vs. frequency, for states 0dB to 30 dB over a frequency range 45MHz-20GHz.

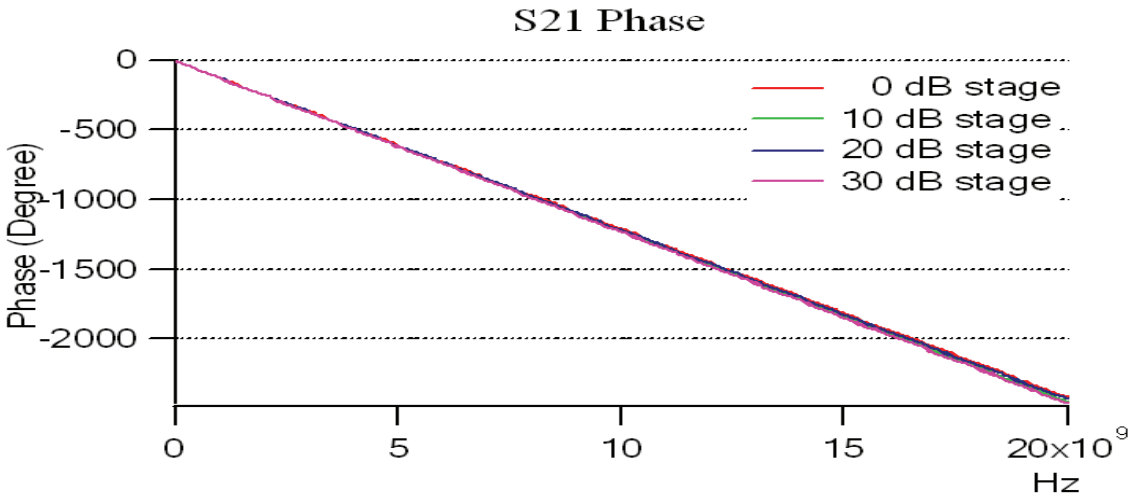

Figure 4.5: S21 Phase for states 0dB to 30dB over a frequency range 45 MHz-20GHz.

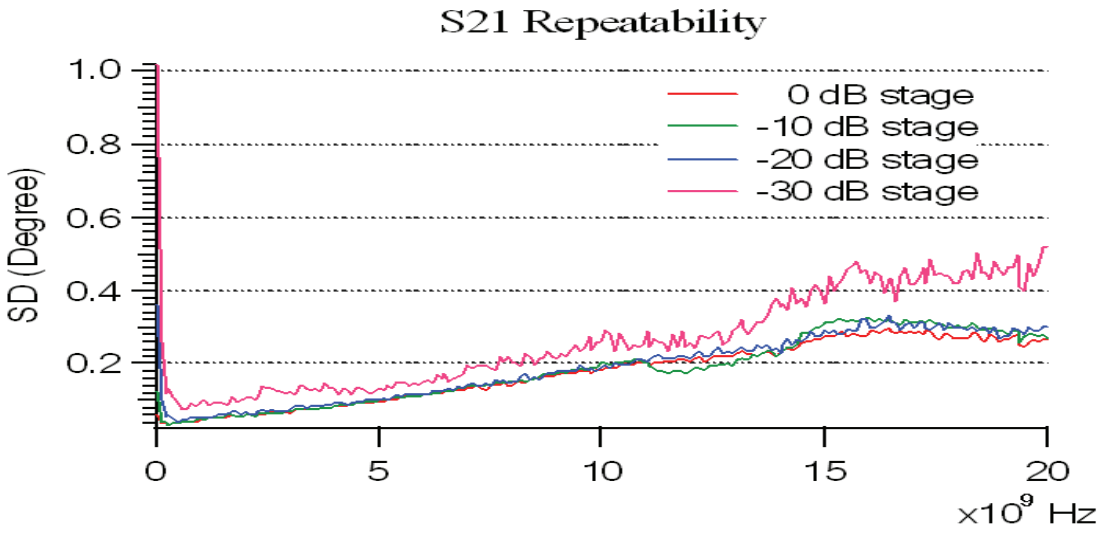

Figure 4.6: Standard deviation of phase for states 0dB to 30 dB over a frequency range 45 MHz- 20GHz.

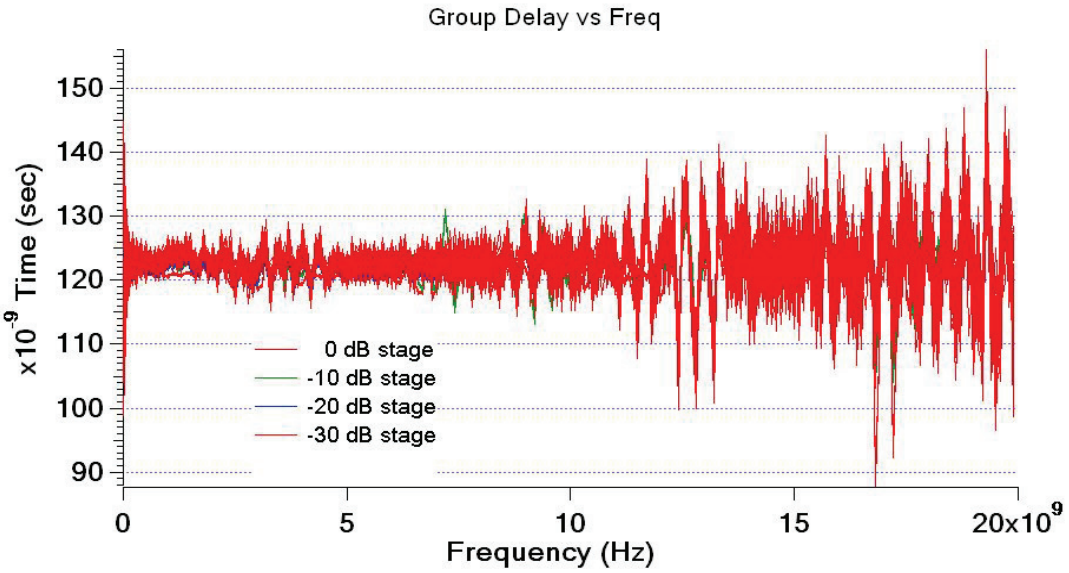

Figure 4.7: Group delay for states 0dB to 20dB over a frequency range 45 MHz-20GHz.

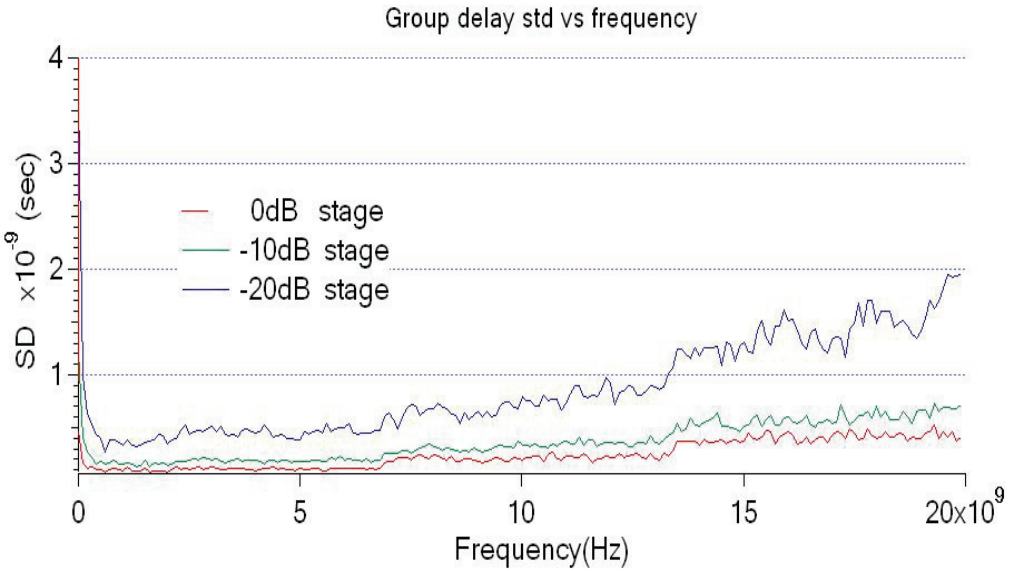

Figure 4.8: Standard deviation of the group delay for states 0dB to 20 dB over a frequency range 45 MHz-20GHz.

4.4 A Demonstration of High Power RF Measurement Systems

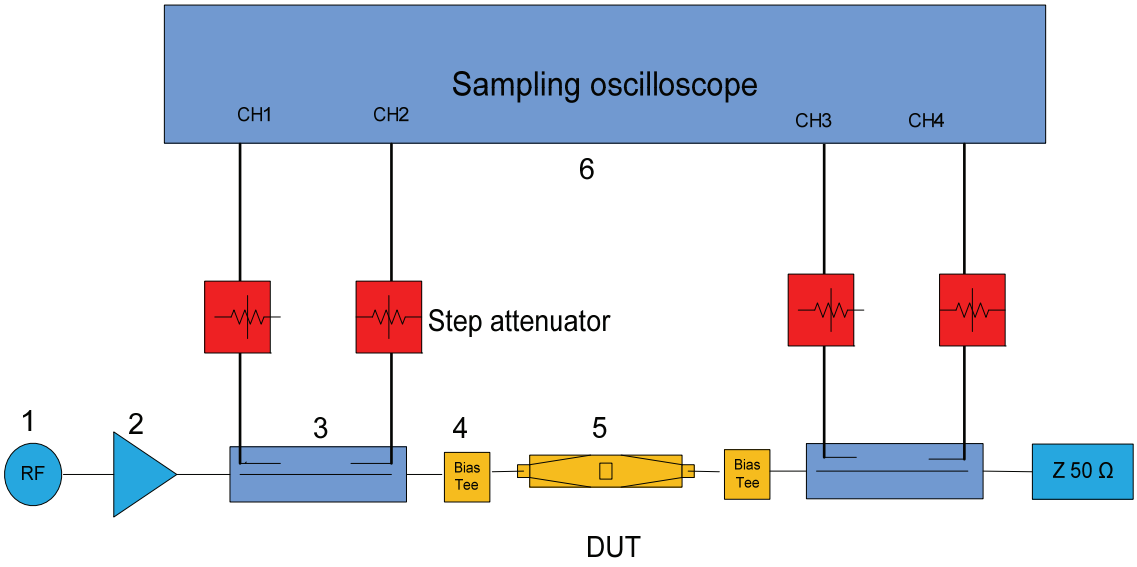

Figure 4.9: A simplified schematic diagram utilising the step attenuators within the measurement system.

4.4.1 System Configuration

A high power RF measurement system based on the 4 channel sampling oscilloscope (as described in [2]) was used in this demonstration. Figure 4.9 illustrates the simplified measurement system. This modified RF measurement system used four step attenuators instead of fixed attenuators, which are located between the direction coupler and the sampling oscilloscope. Two different power levels of step attenuator were installed. There was a 1W HP 33321H at the input plan of DUT, and a 2W HP33321H option 890 at the output plan of DUT. Although their power handing capabilities are different, they both provide the same functionality and characteristics. This modification deals with the measured incident and reflected travelling wave from the DUT at the input and output of the measurement plan. The other instruments and devices are:

(1) An Agilent 83623B that is used as an RF sweeper which provides a frequency range from 10MHz to 20GHz, and which has a maximum output 20dBm. This sweeper was used as a CW source of this measurement system.

(2) A narrow band power amplifier with an operational band coverage of 2.110-2.170 GHz, providing a gain of up to 40 dB at a maximum output power of 51dBm. This amplifier is used to amplify the signal power from the RF sweeper.

(3) A directional coupler, which is a 4 port directional coupler that is able to capture the incident and reflected signal separately providing a coupling factor of 35dB with broadband frequency.

(4) A bias tee, which is made of two 90º hybrids joined together as a back to back configuration that provides the external DC power supply to DUT.

(5) A DUT, which is an extensive transistor device GaN model NPTB00050 providing maximum average output power at 3dB gain compression, typically 50 W optimised for broadband operation from dc to 4.0 GHz (for more detail see Appendix B). The GaN transistor was mouthed in a test fixture with a 50 Ω line matching transformer. The test fixture incorporates a temperature regulator, which consists of a cooling, and heating system with a USB computer interface, the regulator is controlled by NI Labview application software. The demonstration can take an advantage of this test fixture because it can neglect temperature as a factor of the transistor device.

(6) A sampling oscilloscope, which was a Tektronix CSA8000 with 80E02 sampling module.

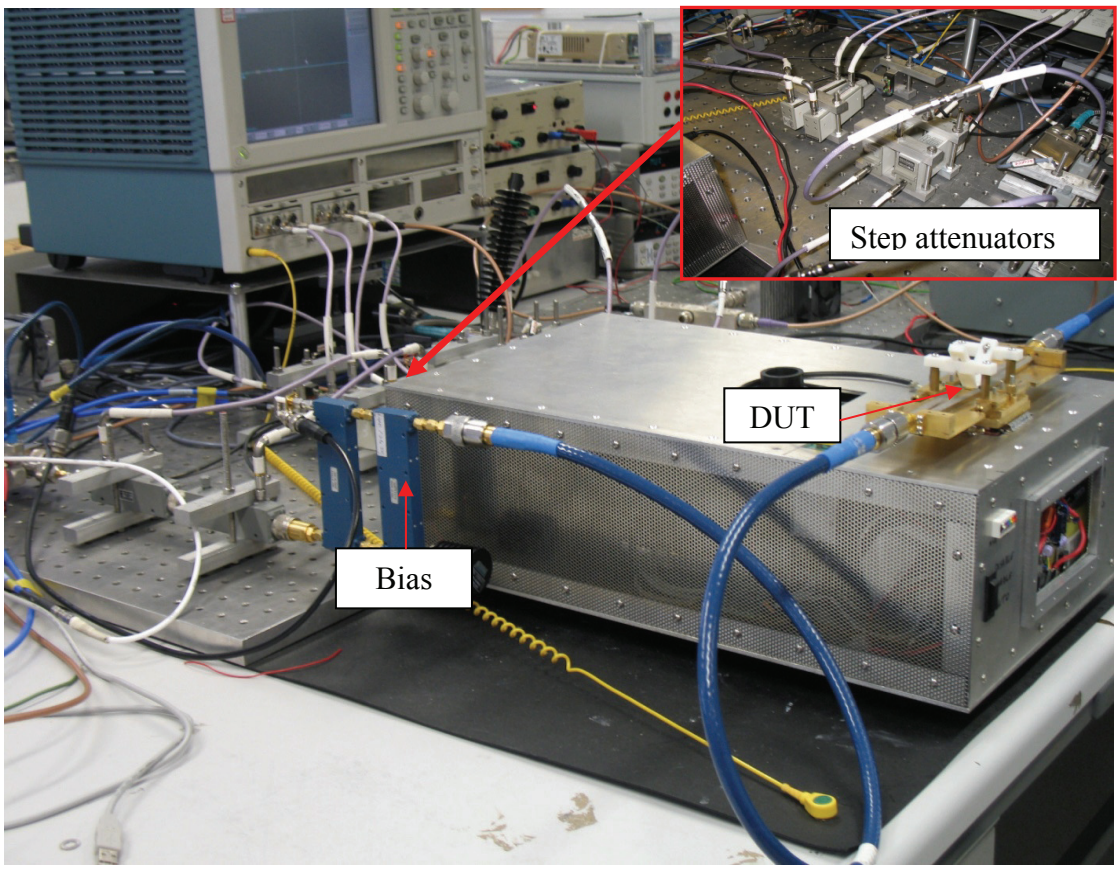

Figure 4.10: The practical realisation of a measurement system that employs the step attenuators.

4.4.2 Measurement Software Configuration

The step attenuator's S-parameters were implemented in the measurement software using the extensive utility tool that is included in the IGOR software environment. As described in Chapter 3, the S-parameter model is designed to deal with the measured travelling wave a1, b1, a2, and b2 that are captured from the DUT. The full S-parameter model was developed in the previous chapter with the aim of including the impedance mismatch issue. Basically, they are represented in the reflection coefficient Γ_S and Γ_L, which are found by looking into the directional coupler and a sampling oscilloscope, respectively.

When modelling the S-parameter model, the step attenuator's S-parameter data was measured by the VNA HP8510 with a frequency band 0.45-20 GHz 201 data point. These S-parameter models were created using the Polynomial data fit function approach (as described in Chapter 3). Furthermore, in order to minimise the errors caused by the S-parameter model, the S-parameter measurement has carefully considered its use of connectors, VNA calibration, and so on. Special care has been taken to carefully define the unique S-parameter of the step attenuator because it can introduce serious errors into the measurement system.

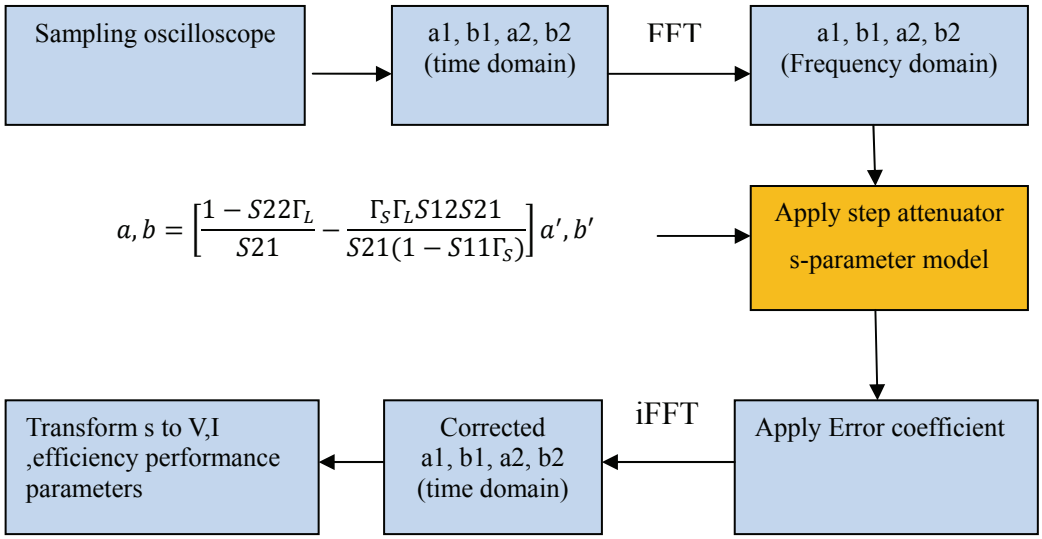

Figure 4.11: A simplified schematic diagram of measurement software configuration for the step attenuator.

4.4.3 System Calibration

It is possible to get an error comparison on the measurement system if the definition of the step attenuator calibration state differs from the actual physical step attenuator state. For example, if the calibration software defines the calibration state at the step

attenuator as 0dB even though the physical step attenuator is at 10dB, thereby introducing errors in terms of 10 to 20 dB depending on which step attenuator state is used. It is crucial to be able to define the exact match of the step attenuation state. The modification of the measurement software does not involve the calibration procedure including error coefficients, the only requirement is the defined calibration state of the step attenuator (basically it is defined at the step attenuator 0 dB). This information is particularly important to the correction of travelling wave a and b, before they are applied by the error coefficient.

The calibration procedure could be performed as usual using the TRM-short (Thru, Reflect, Match) calibration procedure because the measurement system employed a step attenuator instead of a fix attenuator. During calibration, the measurement system treated the step attenuators as a fix attenuator. The TRM-short calibration procedure is described in [2]. The TRM calibration procedures were developed to overcome the reproducibility problems associated with the high frequency on-wafer SLOT calibration procedures. The calibration was started by a small signal S-parameter calibration, which provides an error coefficient for travelling waves. In addition, absolute calibration was performed to provide the absolute power and phase of the travelling waves.

In this system calibration procedure was performed using small signal S-parameter calibration on TRM- short APC 7mm using the Agilent standard with the frequency grid 2.1-7.7 GHz 0.7 GHz step resolution. This frequency bandwidth covers the fundamental 2.1 GHz, and goes up to 3rd harmonic. The sampling oscilloscope was set on average 1024 and data point sampling 1024. Calibration at low frequencies used the SOLT with the Agilent 3.5 standard cal kit. For the absolute calibration, the power setting was 5.0 dBm, with the aim of reaching the power output at nearly 3 dB at sampling oscilloscope ch2. Figure 4.12 illustrates the S-parameter measurement on Thru 7 mm standard after finishing the S-parameter calibration. The calibration has achieved a good result with both the vector-corrected S11 and S22 below -50 dB, S21 and S12 are clearly 0dB.

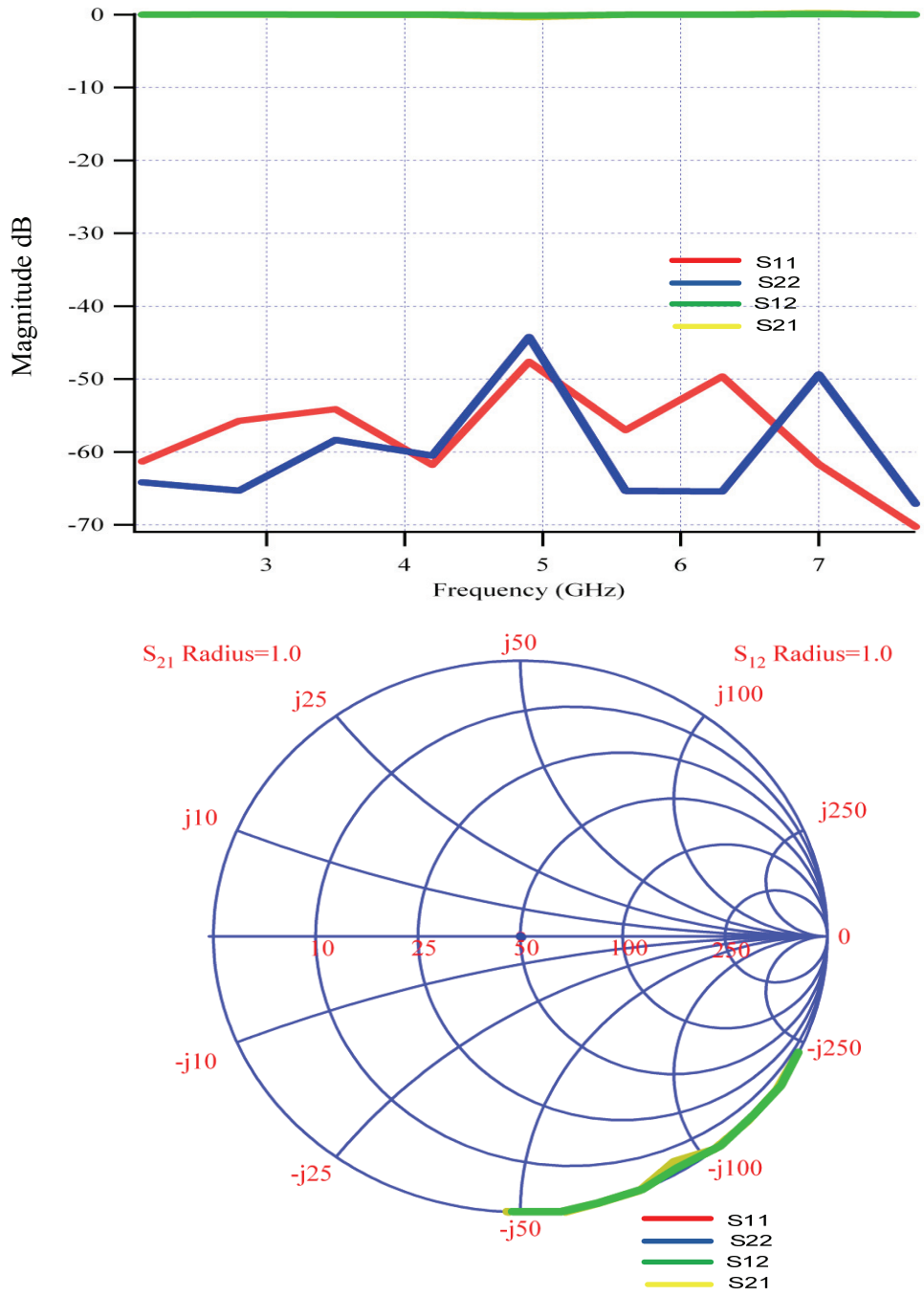

Figure 4.12: Log chart and Smith chart of S-parameter measurements on a thru 7mm standard verifying the small signal S-parameter calibration of the step attenuator.

4.4.4 Measurement Procedure for utilising the step attenuator approach

The demonstration was divided into two parts. The first was conducted on passive devices. Initially the single tone CW power sweep was performed on the DUT thru 7 mm standard with frequency 2.1 GHz, 4.2 GHz, and 6.3 GHz, which is required to stimulate the response of the fundamental and harmonic frequencies. Consequently, the investigation of the power spectrum of each individual frequency was performed without being impacted by the other frequencies. This is a useful technique to determine the S-parameter model correction error. To reach the maximum dynamic range for the power sweep at frequency 2.1GHz, a power sweep was performed throughout the power amplifier range (from -50 dBm to 40 dBm) with the condition of step attenuator 0dB states. However, when the step attenuator was at 10 dB and 20 dB the power sweep still kept the maximum at 40 dBm because doing so avoids oscilloscope damage if the step attenuators transit back to 0 dB states. The power sweep was performed on a range from -50 dBm to 20 dBm at the two frequencies of 4.2 GHz and 6.3 GHz because no suitable amplifier was available at the time.

The second part of the demonstration was conducted on active devices that validate the measurement system in a practical environment. Initially the measurement was performed on the DUT GaN transistor device by exiting the constant single tone CW power with a fixed bias condition. The step attenuator at the output plane of DUT was switched in sequence over its states from 0dB, 10dB, and 30 dB, and then transiting to the original state. These allow the measurement system to repeatedly measure the voltage and current waveform at each step attenuator state. In a further demonstration, a CW power sweep was performed with power setting ranges from -25 dBm to 30 dBm. An investigation of the power spectrum of both fundamental and harmonic were performed in order to compare the error correction achieved by the step attenuator S-parameter model. The effect of a system noise floor was also determined. To avoid the influence of temperature variation on the GaN transistor device the temperature control unit of the test fixture was operated with the temperature set at 40^{o}C.

4.4.5 Demonstration Results

It is important to note that the measurement system has been calibrated at the step attenuator state 0dB, and it is valid throughout the calibrated frequency band 2.1-7.7 GHz. Since step attenuators transit to other states (e.g. 10 dB or 20 dB) the measurement system is out of the calibrated state; however, corrected measurement waveforms can be achieved by applying the step attenuator S-parameter model. Therefore, the discussion result compared measurement results between a calibrated state at step attenuator 0dB and other states. The measurement setup is shown in figure 4.9 with the DUT being either the 7mm thru standard or a GaN device.

4.4.5.1 Verification of Results Using a 7mm thru Standard

Figure 4.13 illustrates the CW power sweep result on thru 7mm standard with a frequency of 2.1GHz, varying the step attenuator state from 0 dB to 20 dB at a power sweep range of -50 dBm to 40 dBm. At a step attenuator state of 0dB, the power spectrum increased linearly from input over a power range of -50 to 40dBm and the result is that the power output is identical with the input. When the step attenuator was switched to 10dB, although the power spectrum increases linearly with an output power of -40 dBm to 40 dBm between an increased power output range of between -50 dBm to -40 dBm, linearity is approximate and there are some dips. When the step attenuator was set at 20 dB, a linearity response occurs between the power outputs of -30 dBm to 40 dBm. While between a power input range of -50 dBm to -40 dBm, the power output response starts from -42 dBm it then dips and its increase is then approximately linear. The observation in Figure 4.14 shows the power output comparison between the step attenuator at 0dB, 10 dB and 20 dB. The results show that the power spectrum correction of the step attenuator at 10 dB and 20 dB are in an acceptable error band of 0.01 dB starting from power outputs at -40 dBm and -38 dBm, respectively.

Figure 4.15 illustrates the CW power sweep results on thru 7mm standard with a frequency of 4.2GHz with varying step attenuator states from 0dB to 20 dB and a power sweep range of -50 dBm to 20 dBm. Similarly, when the step attenuator was set at 0dB the power spectrum increased linearly from the input power range -50 dBm to 20 dBm. When the step attenuator was set at 10 dB, the linearity starts from -40 dBm but below that point, the power output curve is diverted from a possible linear curve. When the step attenuator was set at 20 dB the power output was not detected in a period of input power sweep between -50 dB to -38 dBm but after that it increased in a bended curve from -38 dBm and it approach the other curves at the power input of about -20 dBm. Figure 4.16 shows the power output comparison at the frequency 4.2 GHz. These results are similar to those with a power sweep frequency of 2.1 GHz in that the power spectrum correction of step attenuator 10 dB and 20 dB are in an acceptable error band of 0.01 dB starting from power outputs of -32 dBm and -20 dBm, respectively.

The last CW power sweep on thru 7mm standard (shown in figure 4.17) was conducted with a power input range of -50 dBm to 20dBm at a frequency of 6.3 GHz. In this case, when the step attenuator was set at 0dB the power output spectrum increased linearly across the power sweep ranges. After the step attenuator was changed to 10 dB the power output was constant at -50 dBm until the power sweep input reached -40dBm, it then increased linearly. When the step attenuator was set at 20 dB the power output was constant at -40 dBm as the power sweep input was set at -50 dBm to -40dBm, after which it increased linearly close to the other curves of approximately -30 dBm. From Figure 4.18 it can be determined that the correct use of the step attenuator was between 10 dB and 20 dB starting from power outputs of -40 dBm and -30 dBm, respectively.

The results clearly show that at the lower power sweep input range of -50 dB to -40 dBm the correction of the step attenuator S-parameter model is not valid. The reasons for this lack of validity are that the step attenuator has pushed the power sweep levels into the system noise floor of the receiver and as a result, the measurement software applies the step attenuator S-parameter model on the noise floor, hence amplifies it

mathematically to a higher power level. For example, in the case of Figure 4.17, when the step attenuator is set at 10dB, the power output sweep gain is at 10dB from the noise floor to constant level -50 dBm and if the step attenuator is at 20 dB then the power output sweep gains 20 dB from the noise floor to constant level -40dBm. Thus, the correction signal is valid whether the signals can be separated from the noise floor or not.

In summary, the CW power sweep results show that the correction of the step attenuator S-parameter model is valid. The error of correction exits if the S-parameter correction is applied into the system noise floor. Moreover, the S-parameter model correction can lift the noise floor to the higher power level and, therefore, as the system noise floor is -60 dB, the step attenuator at 10 dB and 20dB is functional at a power input of -50 dBm and -40dBm, respectively.

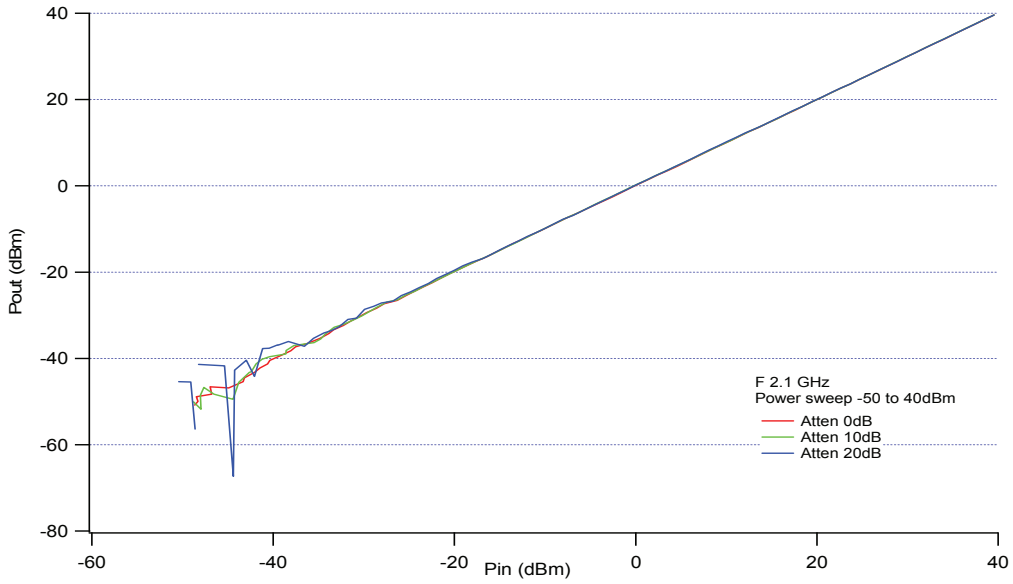

Figure 4.13: CW power sweep from -50 to 40 dBm for a frequency of 2.1 GHz using the 7mm thru standard. The result shows the comparison at the DUT output on for the step attenuator states 0, 10 and 20 dB.

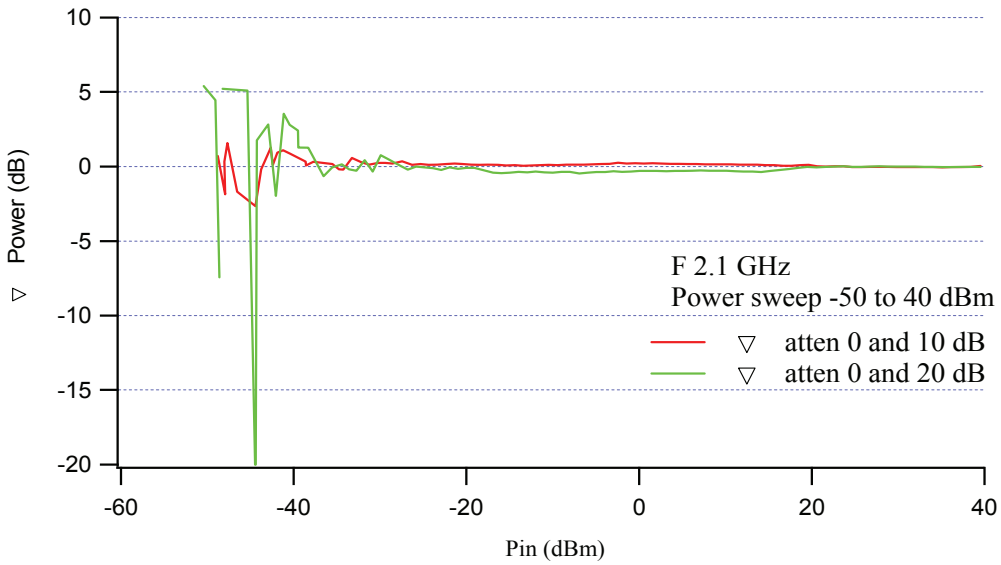

Figure 4.14: CW power sweep from -50 to 40 dBm for a frequency of 2.1 GHz using the 7mm thru standard. The result shows error comparison in term of ∇Output power between the step attenuator states 0 and 10 dB, and between the step attenuator states 0 and 20dB.

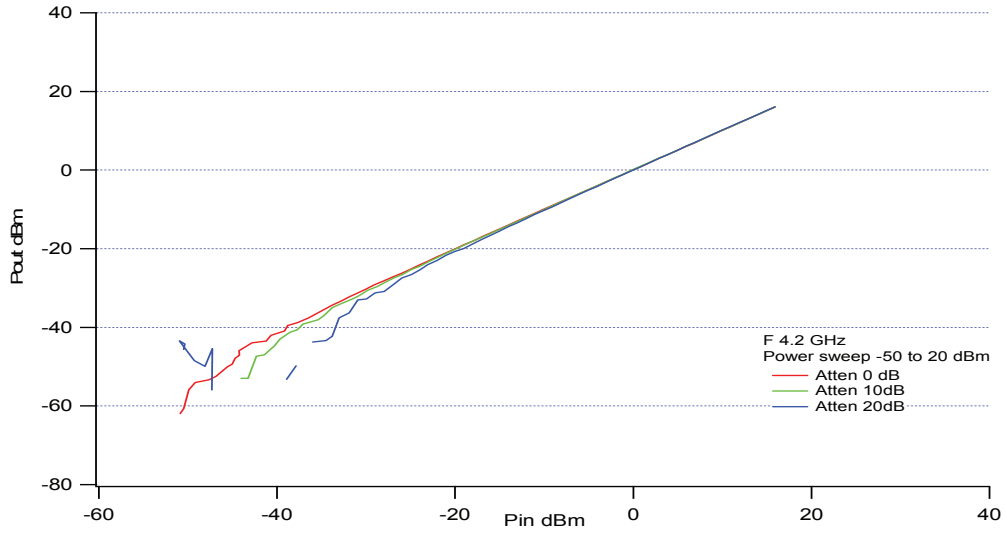

Figure 4.15: CW power sweep from -50 to 20 dBm for a frequency of 4.2 GHz using the 7mm thru standard. The result shows the comparison at the DUT output on for the step attenuator states 0, 10 and 20 dB.

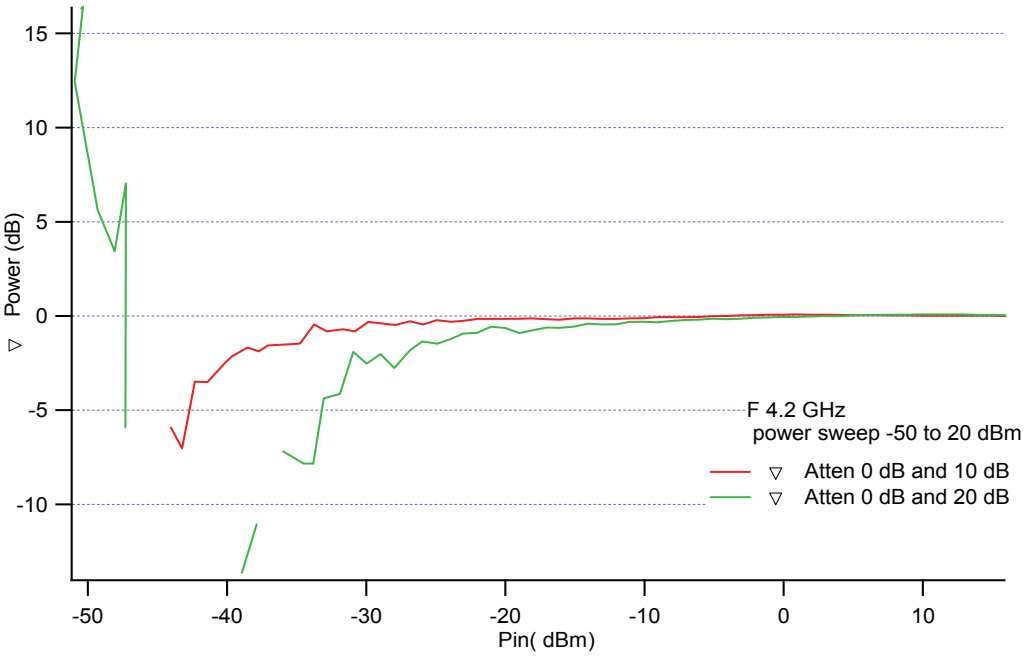

Figure 4.16: CW power sweep from -50 to 20 dBm for a frequency of 4.2 GHz using the 7mm thru standard. The result shows error comparison in term of ∇ Output power between the step attenuator states 0 and 10 dB, and between the step attenuator states 0 and 20dB.

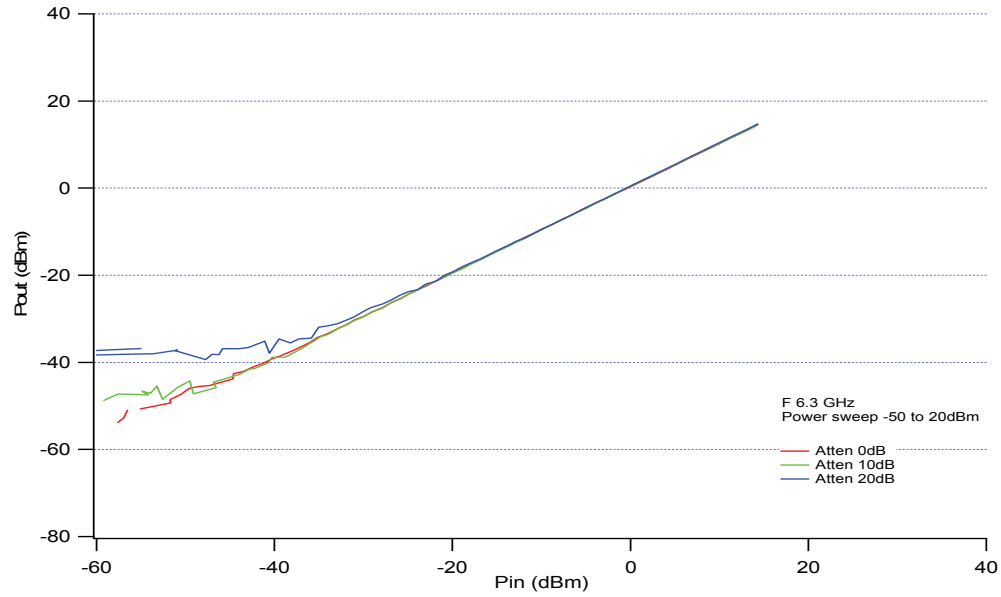

Figure 4.17: CW power sweep from -50 to 20 dBm for a frequency of 6.3 GHz using the 7mm thru standard. The result shows the comparison at the DUT output on for the step attenuator states 0, 10 and 20 dB.

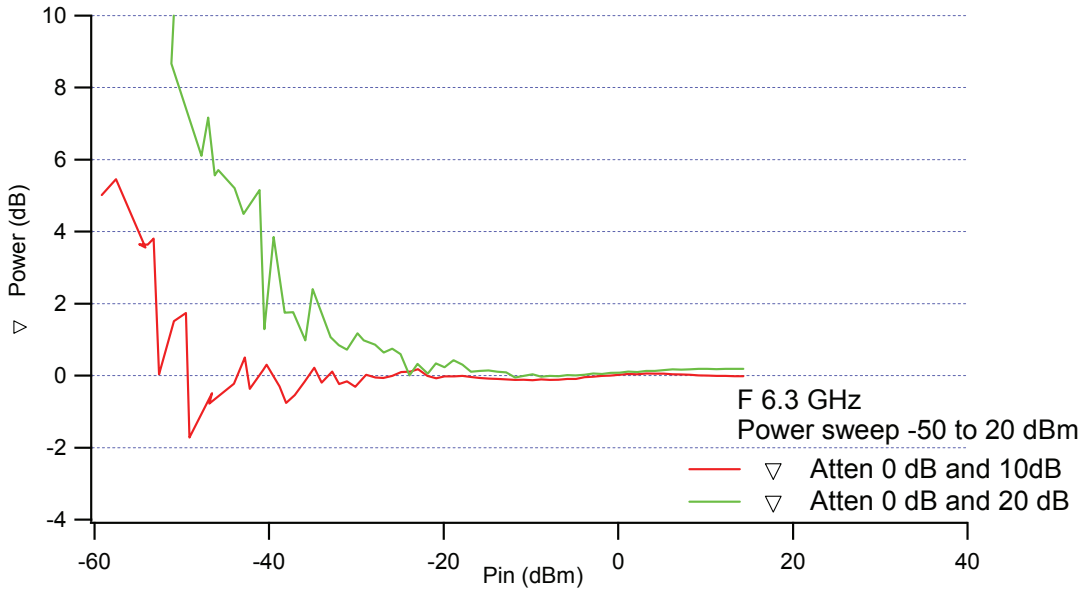

Figure 4.18: CW power sweep from -50 to 20 dBm for a frequency of 6.3 GHz using the 7mm thru standard. The result shows error comparison in term of ∇Output power between the step attenuator states 0 and 10 dB, and between the step attenuator states 0 and 20dB.

4.4.6 Verification of the Results Using a GaN 50W Transistor Device

4.4.6.1 A Comparison of Raw Travelling Wave a2 and b2

The measurement system was performed on a DUT GaN transistor device with a frequency of 2.1 GHz. The GaN was biased by DC power supply Vds 28 V and Vgs 1.5377 V. The measurement system applied the CW power input 30 dBm and the step attenuator is varied according its state from 0dB to 20dB. The resulting comparison of raw travelling waves a and b was observed. It is useful to note that the travelling waves a and b were taken before applying both step attenuator S-parameter model correction and measurement system error coefficient.

Figure 4.19 illustrates the waveform of the travelling waves a2 and b2 in the time domain. The results show the waveform when the step attenuator was transited from 0 dB to 20 dB. It can be seen that the amplitude of travelling waves a2 and b2 decrease according to step attenuator state. The waveform shape does not change as the whole frequency components have been attenuated in proportion. The travelling wave a2 is smaller than b2 due to the DUT being terminated. Figure 4.20 illustrates the travelling wave b2 in frequency domain; it shows the amplitude of fundamental and harmonics. At points A, B, and C the amplitude of fundamental and harmonic have been attenuated equally at 10 dB when the step attenuator state is also at 10 dB. Similarly, when the step attenuator state is 20 dB, the fundamental and harmonic clearly decrease by 20 dB. It is important to consider that when the step attenuator has been used at a high attenuation then it might destroy the harmonic content if its amplitude is very small comparing with fundamental. Moreover, if the harmonic component of the travelling signal falls into the system noise floor then it obviously changes the waveform shape. Consequently, the correction of the travelling signal by step attenuator S-parameter model may then be invalid.

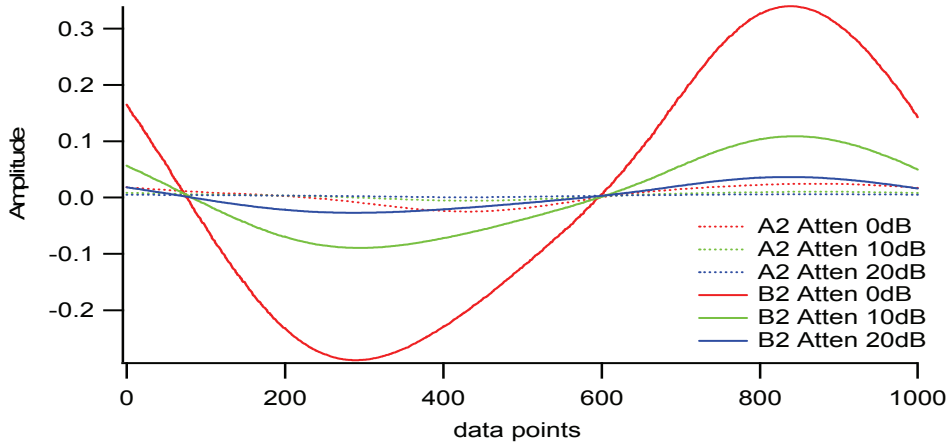

Figure 4.19: Comparison of uncorrected travelling waves b2 and a2 in the time domain with step attenuator states 0dB to 20dB.

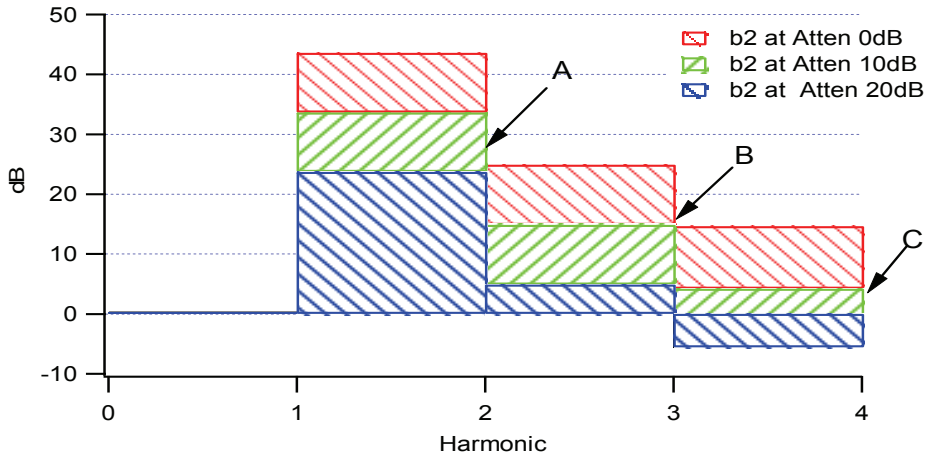

Figure 4.20: Comparison of uncorrected travelling wave b2 in the frequency domain at the DUT output of a GaN transistor device for the step attenuator settings 0dB, 10dB and 20dB.

4.4.6.2 Output Correction Comparison

The measurement system was performed on a GaN transistor device with constant CW power input 30dBm at frequency 2.1 GHz. This transistor was biased at Vds=28 V and Vgs=1.5377 V. The step attenuators were varied along with its state from 0dB to 20dB before transiting back to its original state of 0dB. This enables the measurement system to do repeated measurements. The observation was focused on the comparison of the output reference of DUT in terms of voltage-current output, power output, and gain.

Figures 4.21 and 4.22 depict the comparison output voltage and current waveforms at the output plan of DUT according to the step attenuator state from 0 dB to 20 dB. The measurement of the voltage and current wave were taken from the transformation of travelling wave a and b; both applied an error coefficient and a step attenuator S-parameter model. The DUT was biased into the region where it can generate harmonics in order to maintain validation of the step attenuator S-parameter model over the broadband frequency, as a result the voltage and current waveforms are non-sinusoidal waves. Comparison of the results shows that the waveforms are clearly identical. From this it can be concluded that the step attenuator S-parameter model can correct the travelling waves a and b over the broadband frequency.

A further comparison was conducted in terms of power at the DUT reference plane (as can be seen in Figure 4.23). The output power of DUT at step attenuator state 0dB, 10dB and 20 dB was plotted as measurement number function. Similarly, these output powers were derived from the corrected travelling waves a and b. The repeated measurement of the output power of DUT at step attenuator 0 dB was randomly acquired in a range of 36.81 dBm to 36.84dB. When the step attenuator was at 10 dB and 20 dB the output power was in range 36.83dBm to 36.86 dBm, and 36.84 dBm to 36.87 dBm, respectively. The power difference between step attenuator states is on average 0.02dB. When considering the gain of DUT the difference in the gain between step attenuator states is on average 0.01dB (as can been seen in Figure 4.24). These results provide a good agreement with both voltage and current waveforms.

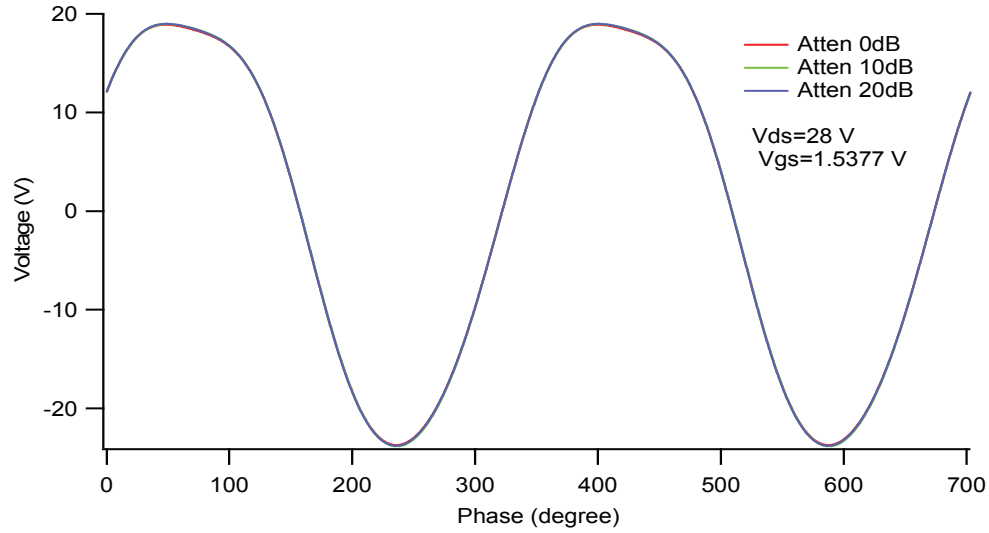

Figure 4.21: Measured output voltage of GaN transistor device.

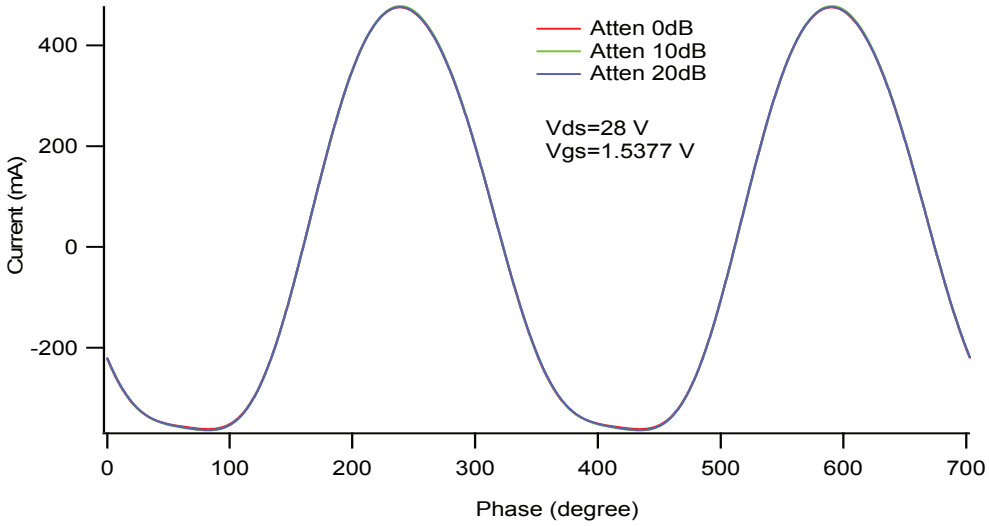

Figure 4.22: Measured output current of GaN transistor *device.*

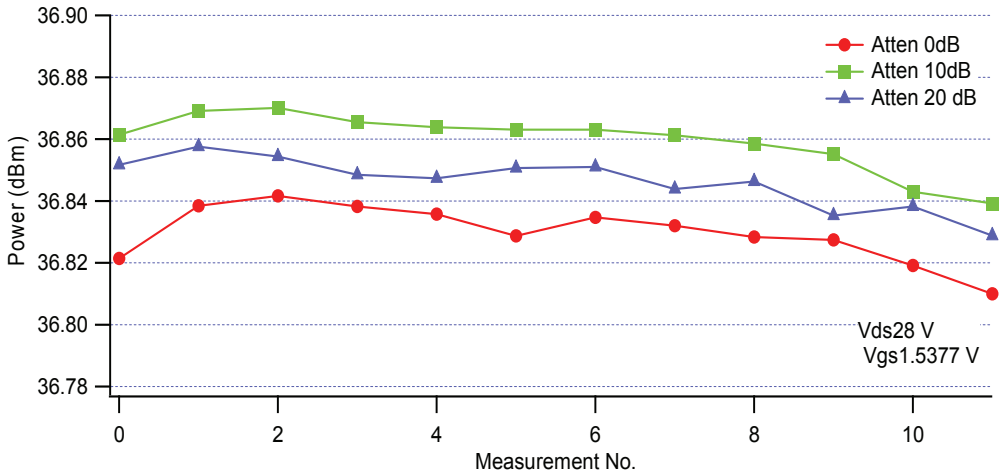

Figure 4.23: Power output comparison between step attenuator settings 0, 10 and 20 dB when measuring a GaN device.

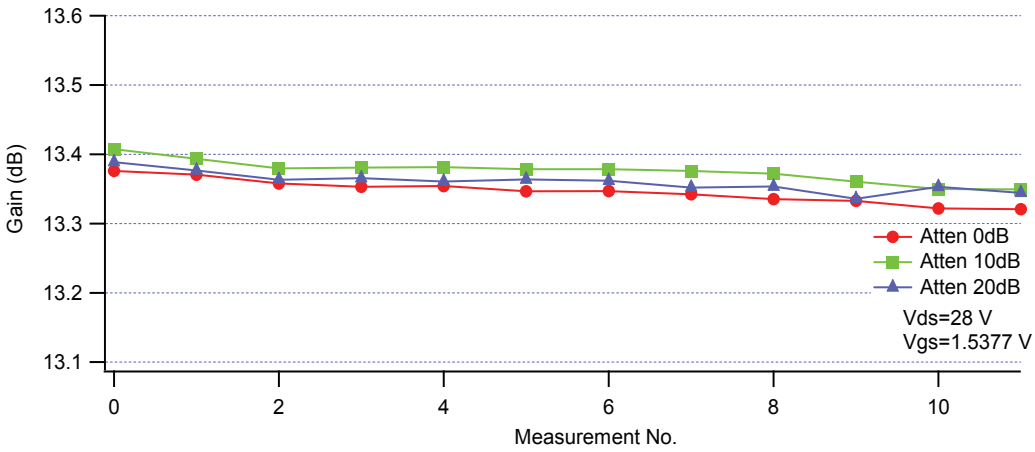

Figure 4.24: Gain comparison between the step attenuator settings 0, 10 and 20 dB when measuring the GaN device.

4.4.6.3 Power Sweep Measurement

The GaN transistor device that was embedded on the test fixture incorporated a cooling system, which was set to 40^{o}C. The GaN was biased by a DC power supplied at Vds= 28 V and Vgs= 1.5372 V. The CW power sweep was performed with a range of -25 dBm to 32 dBm 1dBm/step res. at fundamental frequency 2.1GHz for varying the step attenuators states (from 0dB to 20 dB). To avoid a power amplifier drift effect the power measurements were acquired with the step attenuator set at 0dB, 10dB, and 20dB before the next increased power sweep was performed.

Figure 4.25 illustrates the CW power sweep results at the output of DUT. The results show the common non-linear response characteristics of the transistor device and they show the power spectrum of the fundamental and harmonic. In this demonstration, the 2nd and 3rd harmonic power spectrums were plotted. These power spectrums were transformed from the travelling waves a and b, which was applied for both system error coefficient and step attenuator S-parameter models. From Figure 4.25 it can be seen that the GaN transistor device was not driven to the compression point. Therefore, the fundamental power spectrum increases linearly across the entire sweep. The second harmonic power characteristic is approximately linear on the output power intervals -30dBm to 38 dBm. Similarly, the third power characteristic is approximately linear on the output power intervals -30dBm to 38 dBm. Moreover, there are dip steps on the third harmonic power spectrums as shown in point D, E, and F, giving the corresponding output powers -29 dBm, -19 dBm, and 1dBm, respectively. These dips came from the adjusted internal attenuator of a power sweep Agilent 83623B. The use of a step attenuator S-parameter model correction suffered in the low output power ranges from -60 dBm to -30dBm due to the noise floor. From the harmonic output power spectrum, the noise floor was amplified to -50 dBm and -40dBm by the step attenuator S-parameter models at states of 10dB and 20 dB, respectively. The validation of the S-parameter model was determined from Figure 4.39, giving results that the S-parameter model for the states of 10dB and 20dB are valid from -40 dBm and -30dBm and can be seen at points A, C and B, D, respectively.

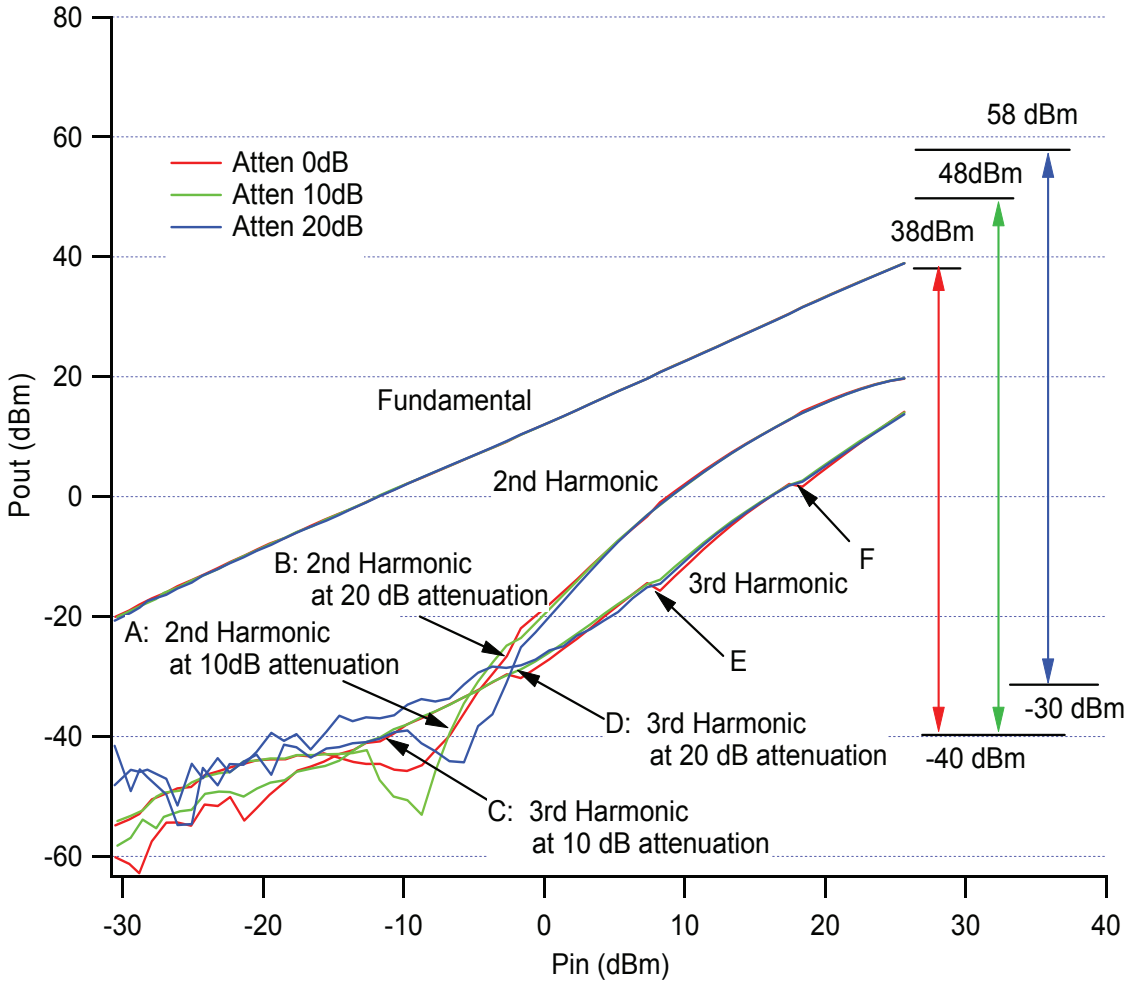

Figure 4.25: Measured CW power transfer characteristic of a GaN transistor, which is attached to a 50Ω load. The fundamental frequency is 2.1 GHz with the first 3 harmonics being measured. Label E and F show a power dip that is sourced by the internal step attenuators of the utilised signal generator.

The maximum save input power for the sampling oscilloscope was determined from the summation of coupling factor of directional coupler (~ 35dB), the insertion loss of the step attenuator (0dB,~10dB,~20dB) and the maximum power input of electrical sampling module in use 80E20 (typically ~3dBm). The maximum power input for the sampling oscilloscope is found to be 35+0+3=38 dB for step attenuator at 0dB, 35+10+3=48dB for step attenuator at 10dB, and 35+20+3=58 dB for step attenuator at 20dB. If the step attenuator acceptable error band is defined at -40dB then by varying the step attenuator state the measurement system has achieved a dynamic range of up to 98 dB. It is important to note that the step attenuator acceptable error for 20 dB state is valid from -30 dB.

4.5 Conclusion

The use of high precision and high repeatability characteristics of step attenuators to extend the dynamic range of high power RF measurement systems has been demonstrated to be an acceptable approach. In order to use the step attenuator S-parameter model, the S-parameter characterisation of step attenuators was performed. The step attenuators characteristics are included as a data sheet. Validation of the step attenuation's repeatability has been achieved for magnitude 0.03 dB and for phase 0.2 degree over the interested frequency band of 45 MHz to 12 GHz.

The four step attenuators were implemented in the measurement system in-between the direction couplers and the sampling oscilloscope. The step attenuator S-parameter model was imported into the measurement software. The measurement system was then calibrated with the step attenuator state set at 0dB. The first validation of measurement system was performed with a 7mm thru standard, which became the DUT. Attenuator states were investigated by performing the CW power sweep at the frequencies 2.1 GHz, 4.2 GHz, and 6.3 GHz, and then comparing the output power spectrum of DUT at each step. Consequently, the correction output power spectrum at step attenuator

settings of 10dB and 20 dB has been achieved. However, the correction step attenuator S-parameter model is invalid whereas the step attenuators suppress the travelling wave a or b into the systems noise floor.

The second validation of the measurement system was performed with a GaN transistor device that was addressed at DUT. The demonstration of the measurement system on the transistor device GaN was successful. The comparison of the voltage and current waveform at the output of DUT are obviously identical. The demonstration also showed that the power error comparison is on average 0.02 dB. The single tone CW power sweep was performed with a fundamental frequency 2.1 GHz. Consequently, the power spectrum comparison has also confirmed a positive result. The second and third harmonic power spectrum comparison has also shown good results. The power sweep spectrum of second and third harmonic exploits the level the system noise floor. However, the demonstration showed a limitation of the step attenuator when used at a high attenuation state because it causes a distortion of the harmonic contents. It is crucial to carefully determine the power harmonic level before deciding a suitable step attenuator state otherwise they could suspend harmonic information and this could introduce error correction via the step attenuators S-parameter model. When defining the error acceptable band comparison 0.01(i.e. at -40dB), the extended dynamic range of measurement system can be increase to 38dB, 48dB, and 58 dB for the step attenuator states of 0 dB, 10 dB and 20 dB, respectively. The whole dynamic range of the measurement system can achieve up to 98 dB.

References

[1] Agilent, Agilent Technologies 33320A/B/G/H 33321 A/B/D/G/H/K 33322A/B/G/H 33323K Step attenuator for OEM & System Use dc to 26.5GHz, 1990, Technical data sheet.

[2] D.J. Williams, "Non-Linear Measurement System and Techniques for RF Power Amplifier Design," Cardiff University, PhD thesis 2003.

[3] D.M. Pozar, *Microwave engineering*, 3rd ed. New York, USA: John Wiley & Son,INC., 2005.

[4] IEE, "Half day Colloquium on Uncertainties made easy," Institution of Electrical,Engineering Savoy Place, London, 1996.

[5] Agilent, Understanding the Fundamental Principles of Vector Network Analysis, 2000, Application note.

[6] Agilent, 3488A switch/control Unit operating ,Configuration Manual, 1995, USA.

[7] Agilent, 8510C Network analyzer System operating and programming manual, 2001, 3rd edit,USA.

[8] WaveMetrics Inc, *IGOR Pro Version 6.0 manual*, 1st ed. Lake Oswego, USA: WaveMetric Inc, 2007.

[9] Agilent, Applying Error Correction to Network Analyzer Measurements, 2002, Application Note AN 1287-3,USA.

[10] Agilent, Specifying Calibration Standards for the Agilent 8510 Network Analyzer, 2004, Application Note 8510-5B.

[11] Agilent, Network Analysis Applying the 8510 TRL Calibration for Non-Coaxial Measurements, 2001, Product Note 8510-8A, USA.

[12] Agilent, 8510C Network Analyzer Key word dictionary, 2001, rev3, USA.

[13] R. Ludwig and P. Bretchko, *RF Circuit Design Theory and Applications*. Upper saddle River NJ, USA: Prentice Hall, 2000.

[14] Yeou-Song Lee, "Testing Dynamic Accuracy of Vector Network Analyzers Using the 40 GHz Step Attenuator," in *ARFTG Conference Digest, 2005. Spring 2005. 65th*, 17 June 2005, pp. 149-158.

[15] A. Chenakin, "2-22 GHz Continuously Variable Attenuator Has Low IMD and Float Response," *High Frequency Electronics*, pp. 16-20, July 2006.

[16] Joo-Gwang Lee, Jeong-Hwan Kim, Jeong-Il Park, and Ung-Taeg Kang, "Uncertainty Evaluation of a Broadband Attenuation Standard," *IEEE Transactions on Instrumentation and Measurement*, vol. 54, no. 2, pp. 705-708, April 2005.

[17] A.G. Morgan, N.M. Ridler, and M.J. Salter, "Generalized Adaptive Calibration Schemes for precision RF Vector Network Analyzer Measurements," *IEEE Transactions on instrumentation and measurement*, vol. 52, no. 4, pp. 1266-1272, 2003.

[18] P. G. Ananasso, "A Low Phase Shift step attenuator Using p-i-n Diodes switches," *IEEE transactions on microwave theory and techniques*, vol. MTT-28, no. 7, pp. 774-776, 1980.

[19] J. Benedikt, R. Gaddi, P. J. Tasker, and M. Goss, "High Power Time-Domain Measurement system with Active Harmonic Load-Pull for High-Efficiency Base-Station Amplier Design," *IEEE Trans. On Microwave Theory and Technique*, vol. 48, pp. 2617-2624, 2000.

[20] Tektronix, 80E01, 80E02, 80E03, 80E04 & 80E06 electrical sampling module, User Manual.

[21] Agilent, Agilent AN 1287-3 Applying Error Correction to Network Analyzer

Measurements, 2002, Application Note.

[22] J. Benedikt, "Evaluation and Measurement Enhancement of the High Frequency Measurement System at the University of Wales College Cardiff," Cardiff University, Cardiff, Thesis 2000.

[23] G.H. Bryant, *Principles of Microwave Measurements*. London, United kingdom: Peter Peregrinus Ltd, 1993.

[24] F.H. Raab et al., "Power amplifiers and transmitters for RF and microwave," *IEEE Transactions on Microwave Theory and Techniques*, vol. 50, no. 3, pp. 814-826, 2002.

[25] J. F. Sevic, "Theory of High-Power Load-Pull Characterization for RF and Microwave Transistors," in *RF AND MICROWAVE CIRCUITS,MEASUREMENTS,AND MODELING*, M. Golio and J. Golio, Eds. New York, U.S.A: CRC press, 2008, ch. 7.

[26] V. Teppati, A. Ferrero, V. Camarchia, A. Neri, and M. Pirola, "Microwave Measurements Part III Advanced non-linear measurements," *IEEE Instrumentation & Measurement Magazine*, vol. 11, no. 6, pp. 17-22, December 2008.

[27] V. Camarchia, V. Teppati, S. Corbellini, and M. Pirola, "Microwave Measurements Part II Non-linear measurements," *IEEE instrumentation & Measurement Magazine*, vol. 10, no. 3, pp. 34-39, June 2007.

[28] NitroNex corporation, AN-009: Bias Sequencing and Temperature compensation for GaN HEMTs, October 2008, Appliction Note.

[29] Nitronex corporation, Gallium Nitride 28V, 50W RF Power Transistor, May 2009, NPTB00050 Datasheet.

Chapter 5

S-parameter Characterisation of Harmonic Bypass Structure (HBS)

Chapter 5 – S-parameter Characterisation of Harmonic Bypass Structure (HBS)

5.1 Introduction

A demonstration of the implementation of step attenuators into a high power RF measurement system has previously shown the validity of the use of a step attenuator S-parameter model (see Chapters 3 and 4).This approach shows the ability of step attenuators to adjust significantly the dynamic range of the measurement system without the need for re-calibration, even if the step attenuation state changes. These advantages mean that the measurement system gains are capable of dynamic range. However, a number of constraints are encountered when using a step attenuator S-parameter approach. For example, sometimes an inappropriate setting of the step attenuator can distort the measured travelling waveforms due to the high attenuation adjustment of the step attenuator. This problem occurs when the measurement system is dealing with the huge difference of magnitude of the frequency components that contains the measured waveforms; for example, by assuming that the measurement system has been used to measure the travelling waveforms which are composed of high amplitude fundamental frequencies and other frequencies at a small amplitude. This assumption is normally generated by the non-linear behaviour of the active device. If the attenuation setting of the step attenuator is high, thereby enabling the measurement system to attenuate the amplitude of fundamental into the dynamic range of the receiver, the other frequencies with small magnitudes (e.g. the harmonic of the measured travelling waveforms), are pressed into the noise floor and lost. Consequently, the harmonic information has been suppressed. In the worst-case scenario, they have been distorted by the noise floor of measurement system.

To avoid this problematic issue a new approach has to found and a new structure

developed, namely a Harmonic Bypass Structure (HBS), which is proposed for a range of solutions. The benefit of this solution is that the new structure simply replaces the step attenuator without the need to change anything else, even the procedure of the measurement software can remain unaltered. The only thing that has to be changed in the measurement software is to impose an HBS S-parameter model instead of a step attenuator S-parameter model. This HBS S-parameter model, as detailed in chapter 3, is directly obtained from S-parameter measurements. Further details are also discussed in chapter 6.

This chapter details the S-parameter characterisation of an HBS, including the conceptual design, an explanation of how to build an HBS, and a simulation of an HBS to observe its behaviour and its S-parameters. Understanding the S-parameters of the HBS is of vital importance to the implementation of the S-parameter model into the high power RF measurement system. However, some limitations were found and these will be explored later in this chapter. This chapter will also explain the HBS simulation, which seeks to improve the HBS so that it can act as a measurement system above its limitations.

5.2 Harmonic Bypass Structure

5.2.1 Design Concept

The HBS has been designed in order to improve the approach of using step attenuators in an RF high power measurement system. The objective is to overcome the problem of harmonics that have been suppressed because the step attenuator model has been used in the RF high power measurement system to characterise the active device (especially on the transistor devices application). Therefore, the design of the HBS has to be able to avoid distorting the harmonic of the measured signal. Consequently, there are two key functions that have to be achieved in this structure: firstly, it needs to be able to control

the attenuation the same as a step attenuator approach would behave; and secondly, it should be able to avoid suppression on a selected frequency band.

Following the concept design, the travelling waveform has to decide if the frequency band is going to avoid suppression or if it is to attenuate its magnitude. When the frequency band has been decided, the next step is to decide the method that will be used to divide these travelling waveforms.

In this research project, the design requirement of the HBS is an operating range over a frequency bandwidth spanning from dc to 20 GHz. The fundamental frequency of interest is about 2,100 MHz, which is most frequently used in commercial RF applications; therefore, the first design bandwidth would cover frequencies up to 2,100MHz (or a bit more) but it would be less than 4,200 MHz as it will then reach the 2nd harmonic. The second design bandwidth would cover from the 2nd harmonic of 4,200 MHz up to 9th harmonic of 18,900 MHz, depending on the application and the designer.

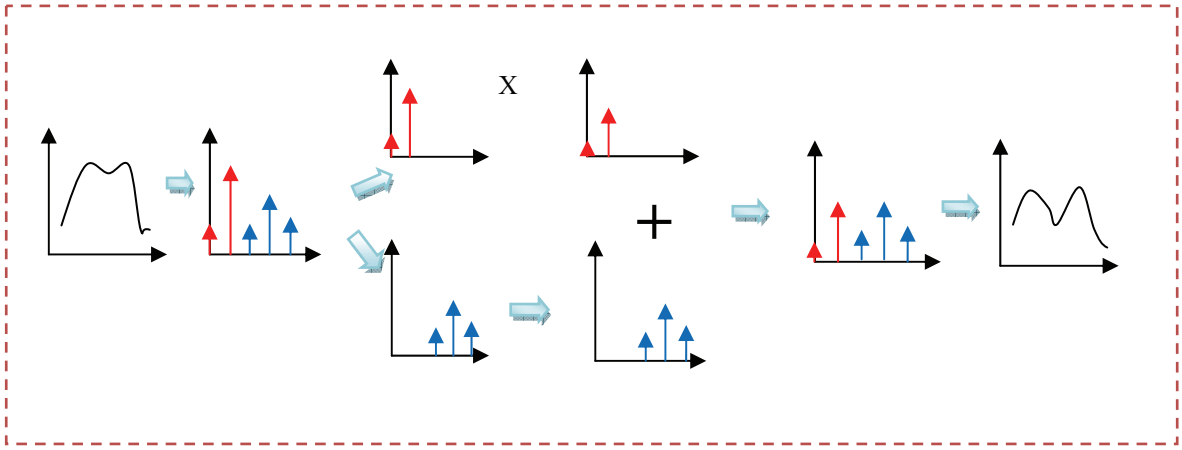

Figure 5.1: A concept diagram of a simplified HBS.

The concept diagram in Figure 5.1 shows the flow from the entrance and exit signal from the HBS. In fact, the HBS works on the time domain, there is no conversion between the time domain and the frequency domain. However, the diagram presents the signal in a frequency domain only as a visual aid to illustrate the concept. Following the diagram, it can be seen that the travelling waveform that contains the dc, fundamental, and its harmonic will separate into two-frequency bandwidths. The first bandwidth contains the dc component, the fundamental and another bandwidth contains the harmonics. The fundamental is almost dominant in the measured travelling waveforms, and so its magnitude is quite high when compared with its harmonics. Consequently, it now has to be attenuated into a form suitable for the receiver. On the other frequency bandwidth path, the bandwidth (which contains harmonics) is kept constant and it is waiting for another bandwidth. Eventually, the two frequency bandwidths are recombined at the output of the HBS. This concept shows that the harmonics leave unchanged through the structure and so is quite unlike the step attenuator approach. Using an HBS avoids the introduction of both suppression and distortion.

5.2.2 Component and Functionality

Choosing the components that are required to build the HBS is challenging because they need to be cost effective, reliable, and easy to build. There are a wide variety of RF and microwave components that are commercially available and a number of manufacturers provide high quality and high specification components; however, if this path alone were to be followed then consumers would quickly find that the costs would rise. Hence, a cost effective compromise solution has to be found which includes component functionality and quality. Consumers have to spend more time considering and eventually make a decision on the required components. Similarly, choosing the components for the HBS takes time and requires more effort to compromise between cost effectiveness and functionality. However, the selection of components for HBS on

this project was based on both the availability of components in the Centre for High Frequency Engineering, and an alternative option based on the use of components that have been sourced externally. Therefore, it is possible to design either alternative HBS circuitry or another configuration that is different from the HBS, as described in the next section (see Figure 5.2).

A step attenuator was chosen for use in this research project because it provides the controllable attenuation that is required in the HBS. Hybrids have been considered as part of the HBS because of their ability to divide and integrate the input signal at the first and final stages. The last component of the HBS that has been considered was the Low Pass Filter (LPF). The interesting function of an LPF is its ability to separate the frequency bandwidth. It also allows the frequency below its cut-off frequency to pass through. The specification of these components is shown in Table 5.1

The HBS has been built to provide the full features that are stated in the design. It consists of three 90^{o} hybrids (which are labelled as H1, H2 and H3), two low pass filters (which are labelled as LPF1 and LPF2), and a programmable attenuator, which have been constructed as shown in Figure 5.2. The HBS is configured as a two-port network. The input port and the output ports are at the input port 1 of the hybrid H1, and the output port is the output port 3 of hybrid H3. The HBS can be divided into three modules. The first, second, and third modules of the HBS are a bandwidth division module, an attenuation control module, and a bandwidth integration module. The bandwidth division module consists of two hybrids that have been bridged together through two low pass filters. Output ports 2 and 3 of hybrid H1 correspond to input port 1 and isolation port 4 of hybrid (H2) respectively. Output port 2 of hybrid H2 is terminated by matching impedance 50 Ω since there is no reflection from this port and because it aims to terminate the signal at this port. The nearby output port 3 of hybrid H2 is connected to a programmable attenuator, which is called the attenuation control module of the HBS. Output isolation port 4 of hybrid H1 of the bandwidth division module is connected to isolation port 4 of hybrid H3. The attenuation control module of the HBS is constructed only of a programmable attenuator that has bridged the

bandwidth division module to the bandwidth integration module. Like the attenuation control module, the bandwidth integration module also consists only of a hybrid H3. The other output port 2 of hybrid H3 is terminated by the matching impedance 50 Ω, and for the same reason as the output port 2 of the hybrid H2 (i.e. it aims to stop the reflection and terminated signals). Finally, the last output port 3 of the hybrid H3 becomes an output of the HBS. Almost all of the connectors in the HBS are 3.5mm; the only exception is the connector in the step attenuator, which is an SMA. Due to the long distances between the isolation port 4 of hybrid H1 and the isolation port 4 of hybrid H3, an RF cable has been used to link the two.

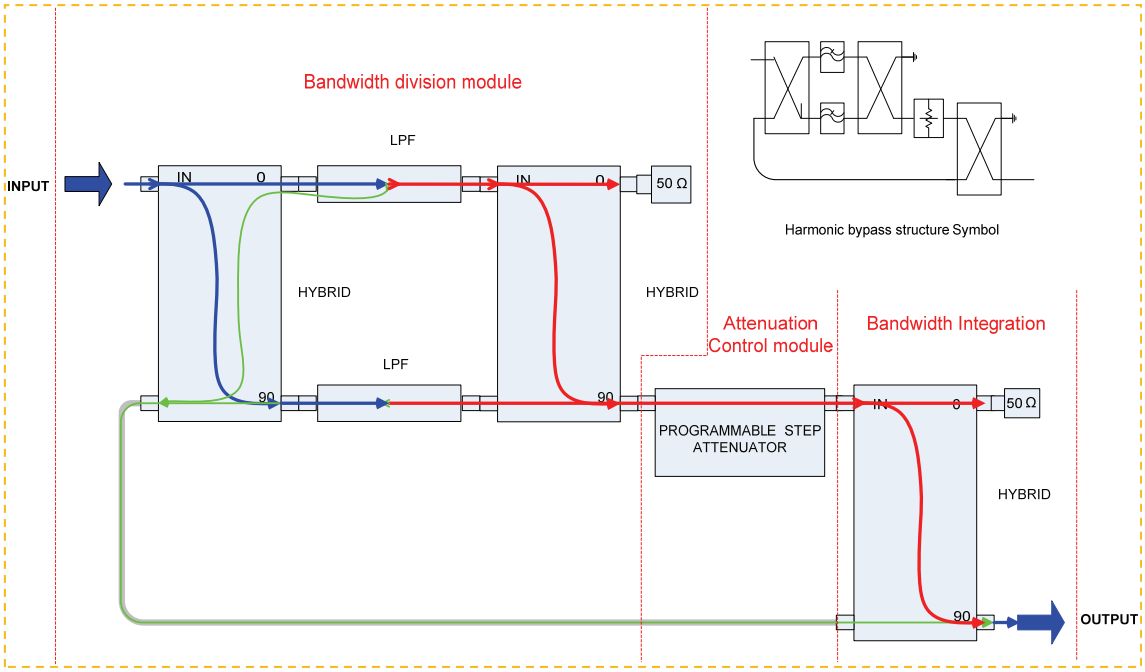

Figure 5.2: HBS configuration .

Figure 5.2 shows the operation of a real HBS configuration. The blue, green, and red solid lines represent the input travelling waveforms, the frequency bandwidth that contain the harmonics, and the frequency bandwidth that contains the fundamental. Input signals entering port 1 of hybrid H1 are evenly divided between ports 2 and 3, with a 90^{o} phase shift between these outputs. Both signal output ports 2 and 3 enter LPF 1 and LPF 2, respectively. At this stage, the original single bandwidth input has been divided into two separated bandwidths: firstly, the frequency bandwidth that contains the fundamental (red line) is filtered through a LPF; and secondly, the reflected signal (green line) from the LPF contains the harmonic. Looking at the concept diagram it can be seen that the bandwidth division in the HBS is achieved by the LPF. In the next stage, both of the LPF output signal waveforms of the fundamental bandwidth enter the input port 1 and isolation port 4 of hybrid H2. Similarly, the signal input (either port 1 or port 4 of hybrid H2) is divided between port 2 and port 3. However, because of the termination of port 2 by 50 Ω impedance, the only interesting signal input is the output

signal port 3. The signals are combined between the coupling signal from post 1 and the transferred signal from post 4. These combination signals are significant only for adding its signal power, the frequency bandwidth remains unchanged. In the next state, the output signal from post 3 of Hybrid H2 enters into the attenuation control module of the HBS where the step attenuator attenuates it. The attenuated signal passes into the last module of HBS by entering at port 1 of hybrid H3. Returning to another path, the reflection signals (i.e. the green line) from both of the LPFs form together at output port 4 of hybrids H1. These reflection signals travel through the RF cable, which is linked to the isolation port 4 of hybrids H3. Finally, the operation of the HBS is present at output port 3 of hybrid H3. Hybrid H3 integrates the whole signal from port 1 and port 3 into output port 3.

Items	Description	Type
1 90^{o} Hybrid	1-18 GHz	KRYTAR Model 1831
2 Low Pass filter (LPF)	1450-3700 MHz	Microlab LA
3 Programmable attenuator	0-70 dB 10 dB/step dc-26.6 GHz	HP 33331H
5 cable	DC-67GHz	GORE

Table 5.1: The HBS's component specifications.

5.3 An ADS Simulation of HBS

The harmonic balance and S-parameter simulations have been conducted in an ADS simulation in order to observe HBS behaviour. Harmonic balance, the first simulation, aims to investigate the functions of HBS so that it is able to function properly according to the design. The harmonic balance simulation describes the wave form signal output from the structure in terms of phase and magnitude. The harmonic balance simulations will provide information about how much is lost in the structure and how much phase has been shifted. They can also show the selected frequency band that has to be attenuated and the frequency band which has been passed through.

Secondly, the S-parameter simulation will be conducted in order to observe the HBS's S-parameter characteristics. It will be used to compare the measured HBS S-parameters that will become the S-parameter model that is going to be used instead of the step attenuator S-parameter model. The HBS S-parameters will also show the adjustable S-parameter characteristics which correspond to the changing attenuation of the step attenuator. The adjustable S-parameter can limit only on the desired frequency bandwidth stressed by the fundamental.

5.3.1 Harmonic Balance Simulation

5.3.1.1 Harmonic Balance Simulation Setting

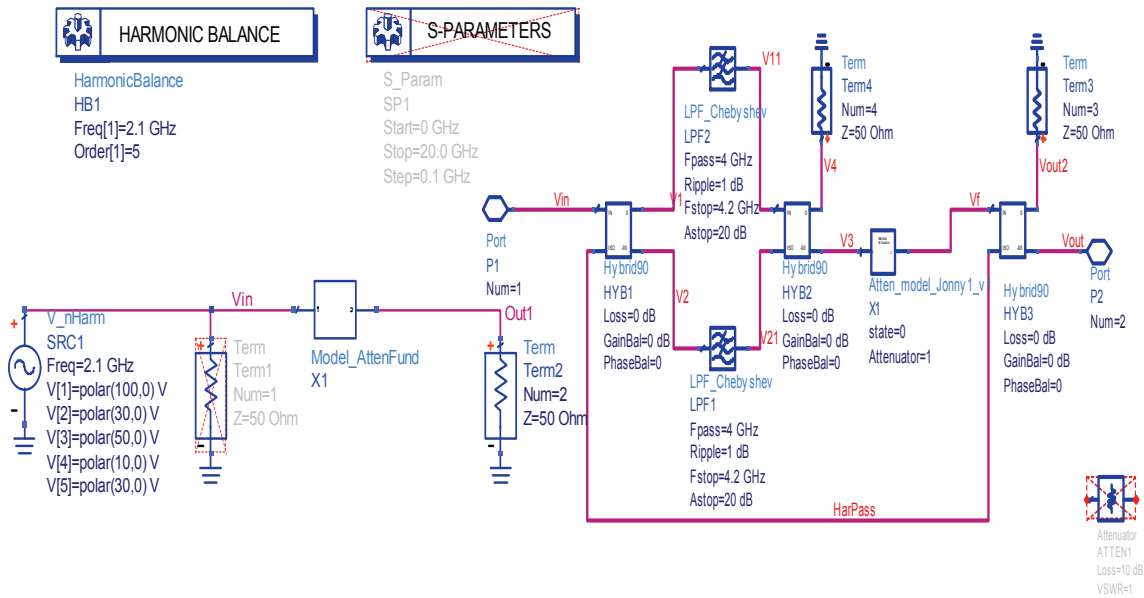

(a) (b)

Figure 5.3: An ADS simulation schematic diagram: (a) Main schematic shows the source voltage input; (b)A schematic diagram of HBS.

Figure 5.3 shows the HBS simulation on CAD tools using ADS simulation software. The 2 port network of the HBS has been implemented in Figure 5.3(b). Ports P1 and P2 are the input port and output port of HBS. Hybrid HYB1, HYB2, and HYB3 are the hybrid H1, H2, and H3, respectively. Output port 2 of hybrid HYB1 and HYB3 are terminated by 50 Ω terminators (labelled Term 3 and Term 4). The voltage monitors have been defined over the connection of each component (the defined voltage monitors are shown in Table 5.1). The analysis has focused on the Vin, HarPass V3, Vf and Vout because these voltage monitor points express important characteristics of the HBS.

The ideal built-in model components in the ADS simulation software are almost all used in the HBS simulation, the only exception is the step attenuator. The step attenuator component model has been built on the user defined S2P data file model Atten_model_Jonny. This model is based on the measured S-parameter data of the step attenuator HP 3331H, which can provide attenuation from 0 dB up 70 dB on 10dB/state. The measured S-parameters provide the full 2 port S-parameter S11, S22, S21, and S22, the frequency bandwidth 45Mz-20GHz, and 201 data point. This data was measured by HP8510. The S-parameter data has been stored in a generic MDIF digital file type. This data can be accessed on a Data Component Access (DAC) ADS simulation tool. The Atten_model_Jonny step attenuator model provides two setting parameters: State and Attenuator. State refers to the attenuator state and the Attenuator refers to the attenuator number.

The harmonic balance simulator has been set up as a single tone in this simulation. The fundamental frequency of interest is 2.100 GHz on 50 Ω environment. The harmonic voltage source has been used in order to simulate the harmonic up to order 5. The arbitrary amplitude voltage source has been set as in the table below.

Name	Name
Vin : input voltage signal port 1 HYB1	V3: output voltage port 3 of HYB2
HarPass : by pass voltage signal	V4: output voltage port 2 of HYB2
V1 : output voltage port 2 of HYB1	Vf : output voltage of attenuator
V11 : output voltage of LPF2	Out1 : output voltage port3 of HYB3
V2 : output voltage port 3 of HYB1	Vout2 :output voltage port 2 of HYB3
V21: output voltage of LPF1	

Table 5.2: Voltage monitors synonyms.

Name	Type	F_1	V(1)	V(2)	V(3)	V(4)	V(5)
V_nharm	Voltage	2.1 GHz	100 V	30 V	50 V	10 V	30 V

Table 5.3: Voltage source.

Name	Type	Loss	GainBal	PhaseBal
HYB1,2,3	Ideal build-in ADS sim.	0 dB	0	0

Table 5.4: 90 Hybrids.

Name	Type	F pass	F stop	A stop	N
LPF1,2	Chebyshev	4GHz	4.2 GHz	20 dB	13

Table 5.5: Low pass filter.

Name	Type	Variable X	Attenuator No
Atten_model_Jonny	User defined P2P s-parameter data.	0,1	1

Table 5.6: Attenuator.

5.3.1.2 Simulation Results

The harmonic balance simulation was performed under two different conditions. The first condition was conducted on the step attenuator set at a value of 0dB and the second was conducted on a step attenuator value of 10dB. The other variables remained unchanged throughout. The observations in this simulation have focused on the voltage as previously defined. These voltages express the behaviour of the HBS.

Investigation of the characteristics of measured waveforms has been easily done in terms of amplitude and phase information while the waveform is present in the time domain; however, they lack frequency information. Fortunately, waveforms in a frequency domain can provide the missing frequency information. Therefore, the results of the HBS simulation are presented in both time domain and frequency domains.

Figures 5.4 and 5.5 illustrate the results of the HBS simulation where the step attenuator setting is 0dB. The input voltage waveforms (Vin) consist of fundamental and harmonic; 2^{nd}, 3^{rd}, 4^{th} and 5^{th} (which is the power component that is shown in Table 5.7).The Vin signal enters the bandwidth division module of the HBS at port 1 of hybrid HYB1. There are two output voltage signals from the first module: firstly, the output port 3 of HYB2; and secondly, the isolation port 4 of HYB1. Figure 5.5 depicts the HarPass voltage and V3 as the output voltage port 3 of HYB2 and output voltage port 4 of HYB1, respectively. These output waveforms show clearly that the bandwidth division module of the HBS is able to divide the input frequency bandwidth.

Control of the attenuation of the HBS has been achieved by the use of a step attenuator, which is shown in the output voltage waveforms at terminal of Atten_model_Jonny step attenuator model as defined V3 and Vf. The amplitude V3 and Vf (Figure 5.5) is identical when the simulator has set the attenuation to be 0dB. There is phase shift between the two that is a result of the characteristics of the step attenuator. Amplitude Vf decreases while the 10 dB attenuation was applied. The amplitude difference between Vf at 0dB and Vf at 10dB is about 9.07 dB, which shows a good agreement,

while the changing of the step attenuator of the HBS is 10dB.

The phase information of the HBS is not an observation aspect because the HBS is only used to control the amplitude of the input signal and, consequently, there is no need to measure what the phases are. Additionally, while the measurement software performs the HBS S-parameter model to compensate the measured signal, it does not need to access the phase information directly; however, if the user is dealing with the HBS's input raw data in the measurement software then the result of simulation in term of phase information could be predicted from the output signal shapes. It is difficult to predict the exact phase shift when the step attenuator is changing its operating state.

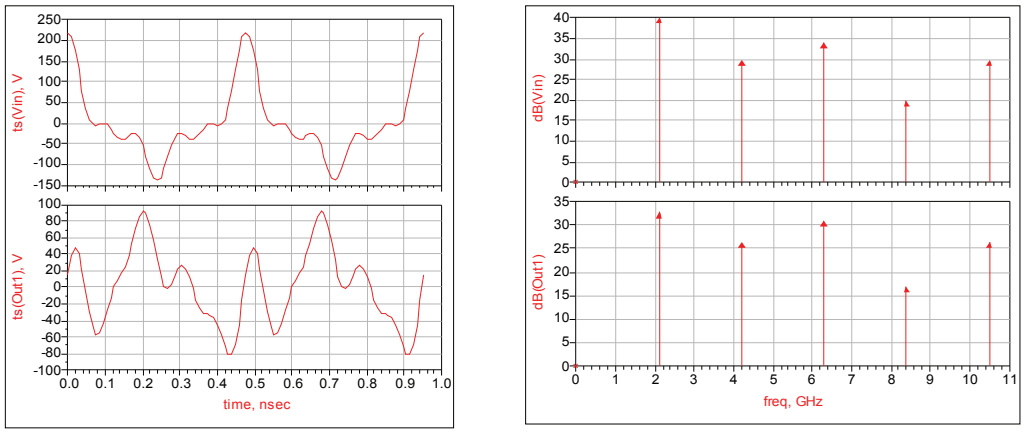

(a) *(b)*

Figure 5.4: Voltage input and output resulting from simulation at step attenuator setting 0dB (Atten_model_jonny state=0), (a) Input and output Voltage waveforms in time domain (b) Input and output voltage magnitude spectrum (dBm).

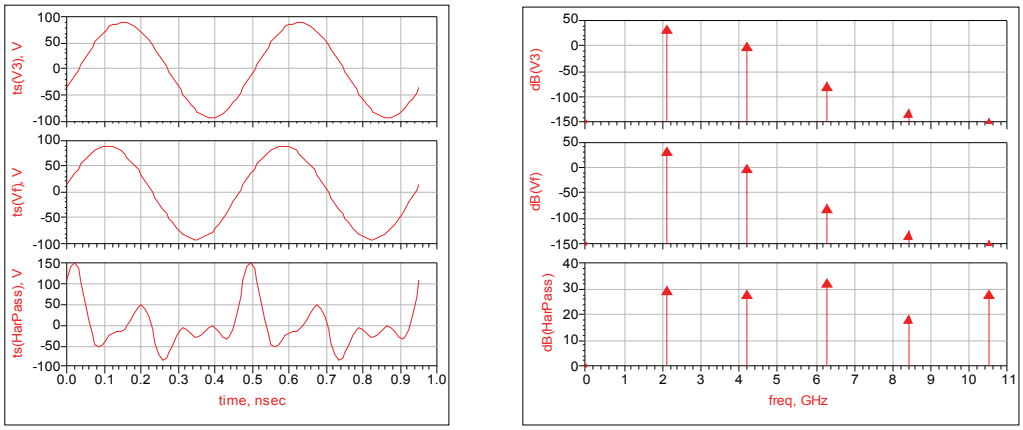

(a) *(b)*

Figure 5.5: Input and harmonic bypass voltages resulting from simulation at step attenuator setting of 0dB (Atten_model_jonny X=1), (a) Input and harmonic bypass voltage waveform in time domain (b) Input and harmonic bypass voltage magnitude spectrum (dBm).

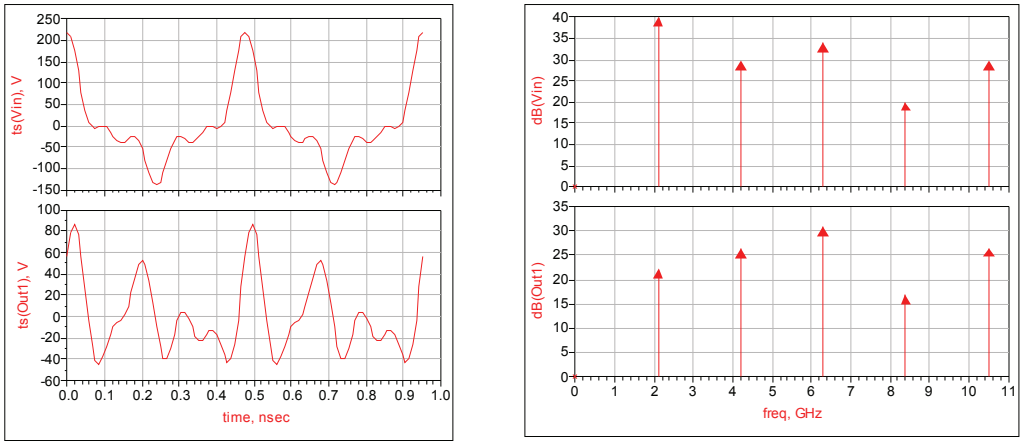

(a) *(b)*

Figure 5.6: Voltage input and output resulting from simulation at step attenuator setting of 10dB (Atten_model_jonny X=1), (a) Input and output Voltage waveform in time domain (b) Input and output voltage magnitude spectrum (dBm).

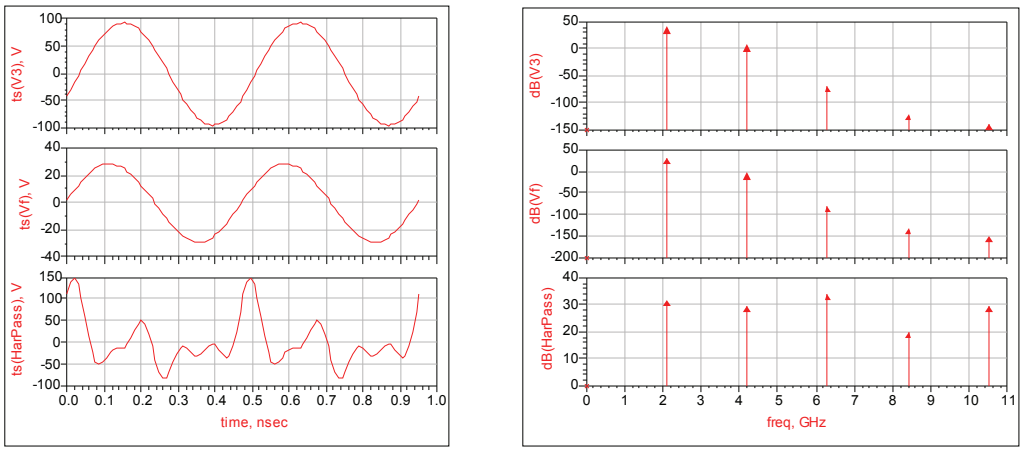

(a) *(b)*

Figure 5.7: Input and harmonic bypass voltages resulting from simulation at step attenuator setting of 10dB (Atten_model_jonny X=1), (a) Input and harmonic bypass voltage waveforms in time domain (b) Input and harmonic bypass voltage magnitude spectrum (dBm).

dB/degrees

freq	Vin	Out1	HarPass	V3	Vf
0.0000 Hz	<-infinity> / 0.000	<-infinity> / 0.000	<-infinity> / 0.000	<-infinity> / 0.000	<-infinity> / 0.000
2.100 GHz	40.000 / 0.000	32.773 / -153.947	31.364 / -24.029	39.243 / -113.677	39.073 / -82.351
4.200 GHz	29.542 / 0.000	26.299 / 6.244	29.524 / 9.568	5.949 / -80.979	5.411 / -15.167
6.300 GHz	33.979 / 0.000	30.969 / -50.708	33.979 / -50.708	-69.721 / -141.949	-70.603 / -43.092
8.400 GHz	20.000 / 0.000	16.990 / -62.875	20.000 / -62.875	-123.400 / -155.794	-123.738 / -21.706
10.50 GHz	29.542 / 0.000	26.532 / -69.002	29.542 / -69.002	-141.299 / -155.851	-142.118 / 0.908

Mag/degrees

freq	Vin	Out1	HarPass	V3	Vf
0.0000 Hz	0.000 / 0.000	0.000 / 0.000	0.000 / 0.000	0.000 / 0.000	0.000 / 0.000
2.100 GHz	100.000 / 0.000	43.517 / -153.947	36.998 / -24.029	91.656 / -113.677	89.880 / -82.351
4.200 GHz	30.000 / 0.000	20.652 / 6.244	29.938 / 9.568	1.984 / -80.979	1.865 / -15.167
6.300 GHz	50.000 / 0.000	35.355 / -50.708	50.000 / -50.708	3.266E-4 / -141.949	2.950E-4 / -43.092
8.400 GHz	10.000 / 0.000	7.071 / -62.875	10.000 / -62.875	6.761E-7 / -155.794	6.503E-7 / -21.706
10.50 GHz	30.000 / 0.000	21.213 / -69.002	30.000 / -69.002	8.611E-8 / -155.851	7.836E-8 / 0.908

Table 5.7: Voltage simulation results for the step attenuator setting 0dB.

dB/degrees

freq	Vin	Out1	HarPass	V3	Vf
0.0000 Hz	<-infinity> / 0.000	<-infinity> / 0.000	<-infinity> / 0.000	<-infinity> / 0.000	<-infinity> / 0.000
2.100 GHz	40.000 / 0.000	22.138 / -74.736	31.384 / -25.395	39.462 / -115.953	29.183 / -86.920
4.200 GHz	29.542 / 0.000	26.425 / 8.579	29.524 / 9.565	5.781 / -81.343	-4.507 / -21.506
6.300 GHz	33.979 / 0.000	30.969 / -50.708	33.979 / -50.708	-69.738 / -141.672	-80.534 / -52.674
8.400 GHz	20.000 / 0.000	16.990 / -62.875	20.000 / -62.875	-123.509 / -155.728	-133.692 / -34.442
10.50 GHz	29.542 / 0.000	26.532 / -69.002	29.542 / -69.002	-141.322 / -157.434	-152.085 / -15.267

Mag/degrees

freq	Vin	Out1	HarPass	V3	Vf
0.0000 Hz	0.000 / 0.000	0.000 / 0.000	0.000 / 0.000	0.000 / 0.000	0.000 / 0.000
2.100 GHz	100.000 / 0.000	12.792 / -74.736	37.087 / -25.395	93.998 / -115.953	28.782 / -86.920
4.200 GHz	30.000 / 0.000	20.954 / 8.579	29.936 / 9.565	1.946 / -81.343	0.595 / -21.506
6.300 GHz	50.000 / 0.000	35.355 / -50.708	50.000 / -50.708	3.259E-4 / -141.672	9.403E-5 / -52.674
8.400 GHz	10.000 / 0.000	7.071 / -62.875	10.000 / -62.875	6.676E-7 / -155.728	2.067E-7 / -34.442
10.50 GHz	30.000 / 0.000	21.213 / -69.002	30.000 / -69.002	8.588E-8 / -157.434	2.487E-8 / -15.267

Table 5.8: Voltage simulation results for the step attenuator setting 10dB.

The appearance of the signal waveforms shapes is clearly different between the input and output port. This deformation is caused from the new mixed amplitude between the fundamental and harmonic. In particular, the significant change is fundamental. Investigation of the output signal of HBS under the different conditions of the step attenuator shows that the degree of deformation in the waveform shape is increasing (as can be seen in Figures 5.4 and 5.6). It is important to note that if the amplitude of the fundamental is less than the amplitude of harmonic then the waveform shape is

extremely different, which has to be taken into account when the HBS is implemented in the measurement system. It is possible to avoid huge deformation in the waveform by ensuring that the amplitude of the fundamental remains above the amplitude of the harmonic.

The insertion loss of the HBS is a crucial aspect of the model. The S-parameter simulation will be used to determine the total insertion loss along with the entire frequency band. Although in the case of the harmonic balance simulation, the individual frequency can easily determine the insertion loss. The results show that when the condition of the step attenuator is 0dB then the insertion loss of fundamental is 7.22 dB and the insertion loss of the harmonic is on average 3 dB (computing from input and output magnitude, see Table 5.7). When the step attenuator is set at 10dB then it is not entirely surprising that the insertion loss increases to 17.86 dB (adding 10dB by step attenuator, see Table 5.8). On the other hand, as expected, the harmonics remain at similar values and the average insertion loss is about 3 dB.

In summary, the HBS simulation on a harmonic balance simulation has shown an achievement of HBS functionality. The frequency bandwidth can be divided at input by the hybrid and the LPF, and they can subsequently re-combine it at the output. The harmonic has been passed through the structure linked between isolation port 4 of HYB1 and HYB3 without distortion. Lastly, the magnitude of the fundamental can be controlled by the step attenuator. The simulation shows that the expected insertion losses of fundamental 2.1GHz and the harmonic are about 7dB and 3dB, respectively; or, almost all the loss caused by the hybrids. The appearance of the output signal waveforms have been changed due to the new combination between the restricted fundamental amplitude and the passed harmonics at the output of the HBS.

5.3.2 S-parameter Simulation

Figure 5.8 shows the HBS ideal S- parameters, this figure presents the S12 or S21 parameter.

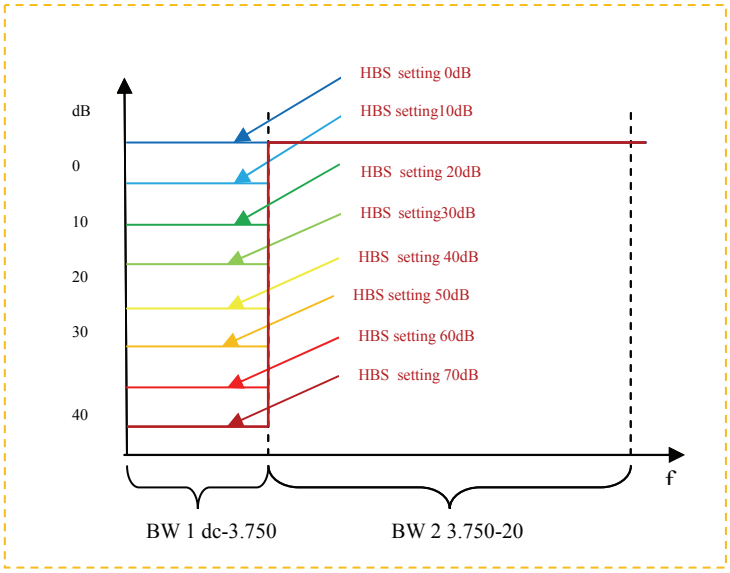

Figure 5.8:Ideal S-parameters for HBS.

The ideal S-parameter; S12 or S21 of lossy HBS on entire bandwidth dc to 20 GHz is shown in Figure 5.8. The desired S12 characteristic is an adjustable boundary from 0dB down to 70 dB along the dc-3.750 GHz, which corresponds to the setting value of the step attenuator. For example, if the setting value of the step attenuator is changed in a sequence of 0dB, 10dB, and 20 dB then S12 should follow the values 0dB, -10dB, and -20 dB, respectively. In the step attenuator HP 33331H, S12 could be able to reach down to - 70 dB in 10 dB steps. S12 is desired to be constant at 0dB along the bandwidth 3.750 -20 GHz. In practice, the insertion loss of the HBS exists as the behaviour of its components.

5.3.2.1 S-parameter Simulation Setting

Figure 5.9 illustrates the HBS schematic diagram for the S-parameter simulator. The HBS component model was re-built in the measured S-parameter data file model, this is a method, which aids the realism of the simulation. The 4 port hybrid S-parameter data was measured by a PNA-X Agilent. The 2 port S-parameter data of the LPFs and step attenuator were measured by a VNA HP8510. Although the LPFs and step attenuator can also be measured by a PNA-X, it was heavily used by the other users of the laboratory and, consequently, the HP8510 has been used instead. The measured S-parameter data of each component will be described later in the measured S-parameter topic.

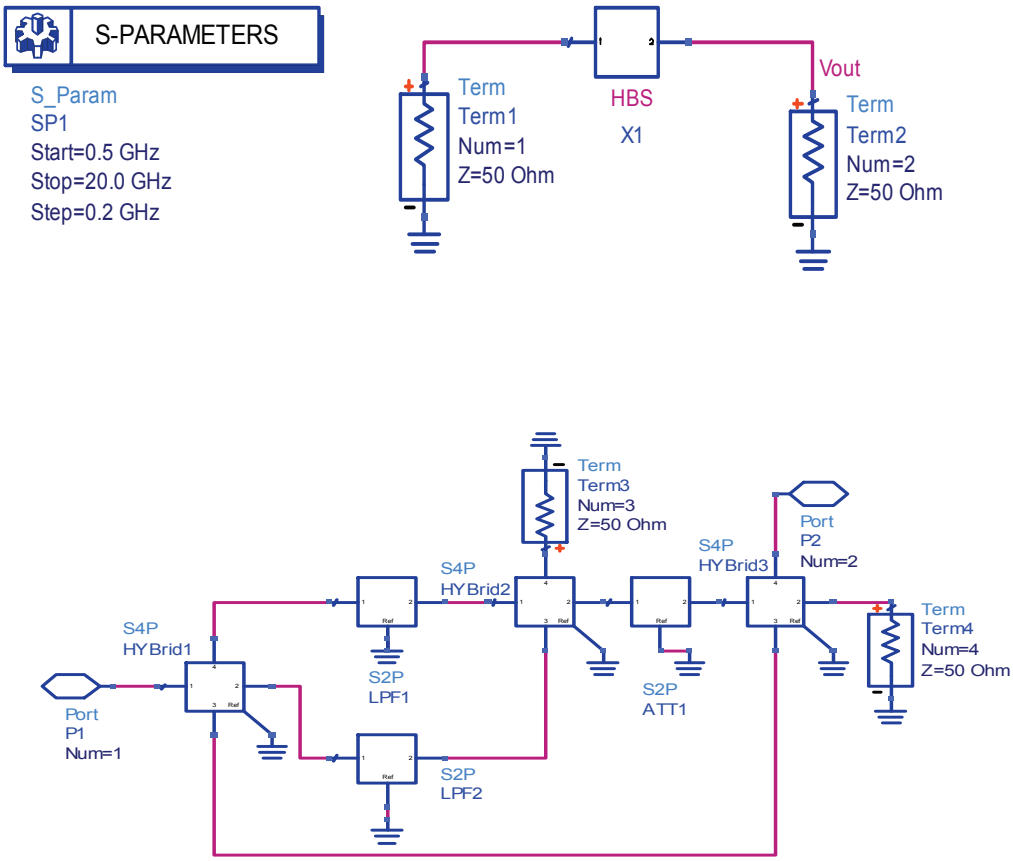

Figure 5.9: HBS schematic for S-parameter simulation (ATT1 is a step attenuator and it used the S-parameters of Hp 33331H serial 474).

The S-parameter simulation was performed over frequencies of 0.5 – 20 GHz at 0.2 GHz resolution steps. The intention was to cover the fundamental frequency at 2.1GHz and spread over the operational bandwidth of the HBS components, which are normally limited by either the hybrids or the LPF at 18GHz in the 50Ω environment. Port 1 and port 2 in the HBS schematic are defined by the input and output ports, respectively. ATT1 varied the attenuation from 0-70 dB in 10 dB steps.

5.3.2.1 S-parameter Simulation Results

Figure 5.10 shows the S-parameters of the HBS. Both S12 and S21 are identical curves. The setting of the step attenuator was 0dB at a starting frequency sweep of 0.5 GHz. S12 increases magnitude from -11dB to 4dB at 1GHz, a point that is the starting operating bandwidth of the hybrid. The curve slightly declines, until at 3.5 GHz the average was -5 dB. The S12 then suddenly drops to almost -25dB at 3.6GHz, after which the S12 rises sharply to -4.8dB at 4.1GHz. It then continues to decline to -8dB at 14 GHz. The S12 curve fluctuates over the frequencies 14 -20 GHz. At the next step attenuator setting of 10 dB the S12, curve increases from -18.5dB to -13.38 dB at 1 GHz. It then continues down to -16.52 dB at 1.9 GHz before starting a few fluctuations. After which it raises to -13.26 dB at 3.6 GHz. Once again, the S12 drops suddenly to -26 dB at 3.7GHz. It then it follows the same pattern as S12 where the step attenuator is set at 0dB. The control settings of the step attenuator are 20dB, 30dB, 40dB, 50dB, 60dB, and 70dB which gives the S12 curve a similar trend along the bandwidth of 0.5 - 3.7 GHz. The S12 drops to a value between -30 and -45dB at 1GHz. It then fluctuates and rises to meet the other S12 curve at 3.7 GHz. The whole S12 of the HBS can be called a likeness over the bandwidth 3.7 GHz to 20 GHz. The reflection of HSB can be defined from the S11 and S22. The overall reflection averages -30dB over the bandwidth of 0.5 – 10 GHz. It slightly increases over the bandwidth 10 -20 GHz at an average -20 dB.

The result S12 shows the insertion loss over the frequency bandwidth of the HBS. The insertion loss is about -4 dB at 1GHz, which decreases to -10dB to 15 dB at 20GHz. The insertion loss is controllable along the bandwidth of 0.5 -3.7 GHz. If it is focused on a fundamental of 2.1 GHz then the insertion losses are 5.1dB, 16.33dB, and 27 dB, which correspond to 0dB, 10dB, and 20 dB of a step attenuator.

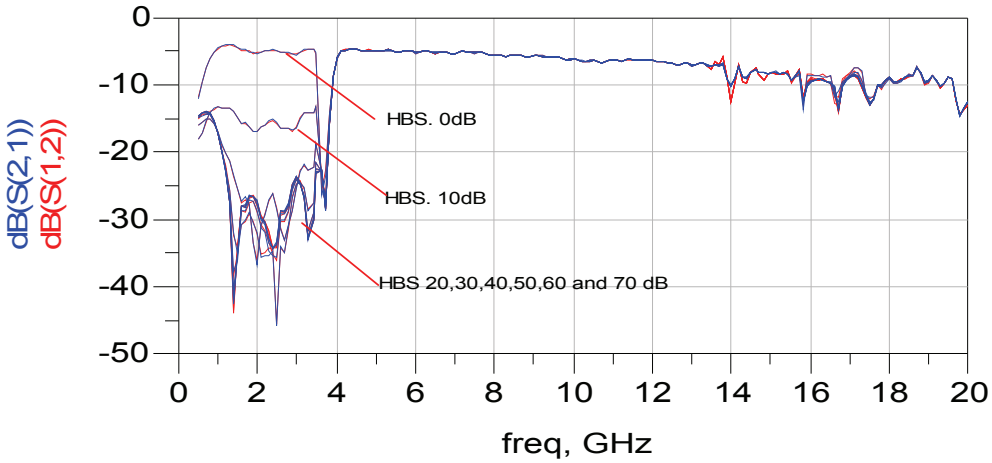

(a) S21,S12 of HBS

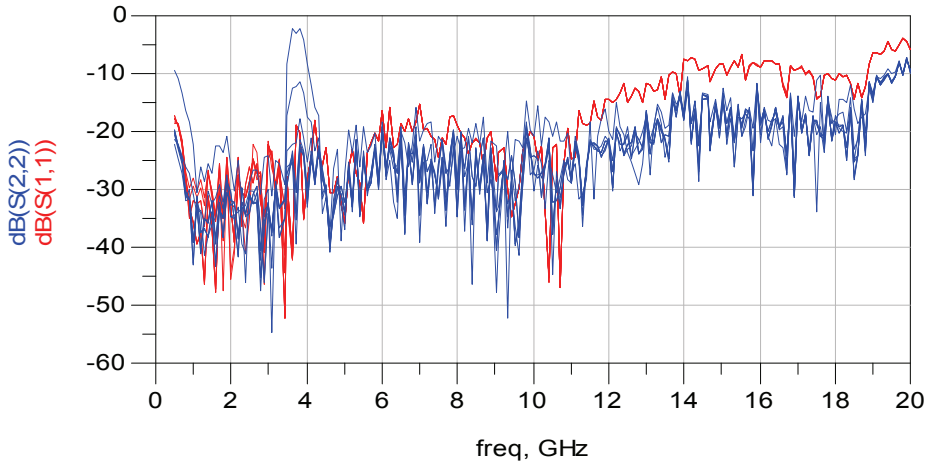

(b) S11, S22 of HBS

Figure 5.10: HSB S-parameter simulation results (the HBS was varied from 0dB to 70 dB 10 dB step resolution).

Although the S12 shows good results over the step attenuator settings of 0dB, 10dB, and 20 dB, the drawback of the HBS is that it cannot reach the requirement of S12 over the step attenuator settings of 30dB, 40dB, 50dB, and 60 dB. The cause of this was found after an investigation of the S-parameter data model of the HBS components and the harmonic balance simulation results, which found that the control S12 could not meet the requirement below -30dB. This is a result of some of the reflection fundamental frequencies that are generated by the LPF that travel through the bypass path which links the isolation port 4 of hybrid H1 and H4 (see Figure 5.2). The reflected signal power of the LPF is related to the control of the attenuation of the HBS. The reflection of the LPF is about -30 dB (S11, see Figure 5.12). If the step attenuator blocks the fundamental below -30 dB then the reflection of the fundamental from LPF is apparently an influence at the HBS's output port.

To overcome the limitations of the HBS, two modified HBS circuits have been investigated with an S-parameter simulation. Figure 5.11 illustrates the modified HBS circuitry. An ideal isolator was installed between an isolation port 4 of hybrid 1 and an isolation port 4 of hybrid 3, thereby enabling the HBS to stop the reflected fundamental from the LPF.

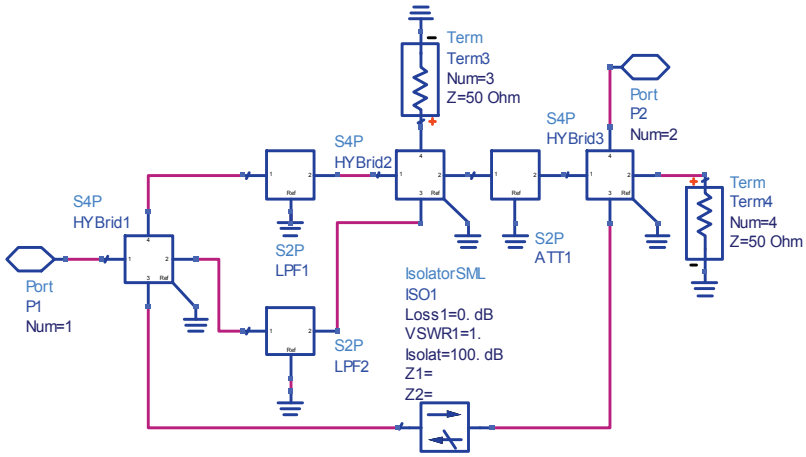

Figure 5.11: Modified HBS - an isolator has been installed between hybrid 1 and hybrid 3.

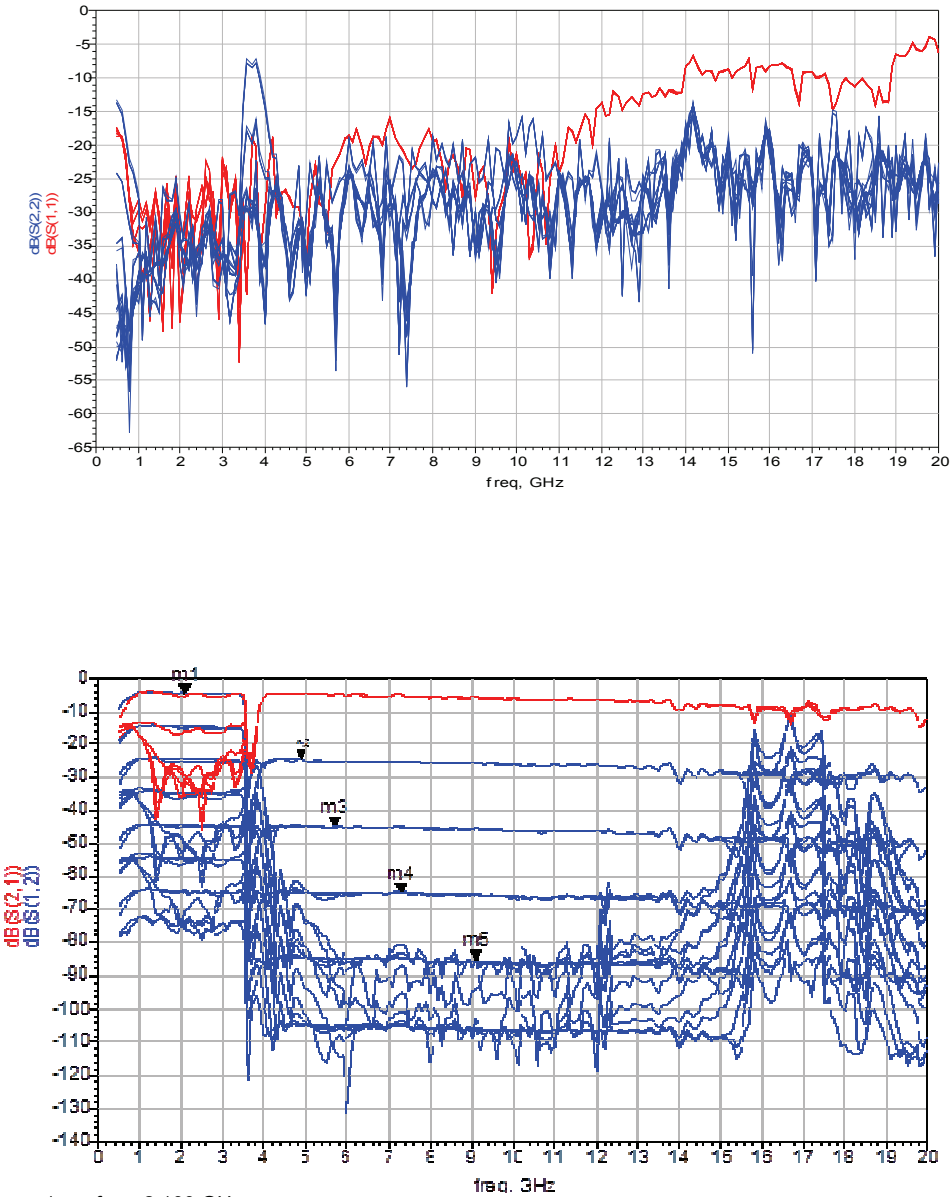

Figure 5.12: HBS S-parameter results - HBS was modified by including an isolator.

Figure 5.12 shows the S-parameter simulation of an HBS-isolator modifier. The S-parameter simulation was performed on a frequency sweep 0.5-20GHz at 0.2 step resolutions, the components remained unchanged. The isolator was varied from 10dB to 100dB in 10dB step resolutions. It is seen that the S21 and S12 characteristic is not a requirement. Although S12 is changed, the S21 is not able to control below -30 dB of the step attenuator; in other words, it keeps the same characteristic.

The second modified HBS is shown in Figure 5.13. Instead of using isolation, the HBS was modified by a High-Pass Filter (HPF). The cut-off frequency passband of the HPF has been set to 4GHz.

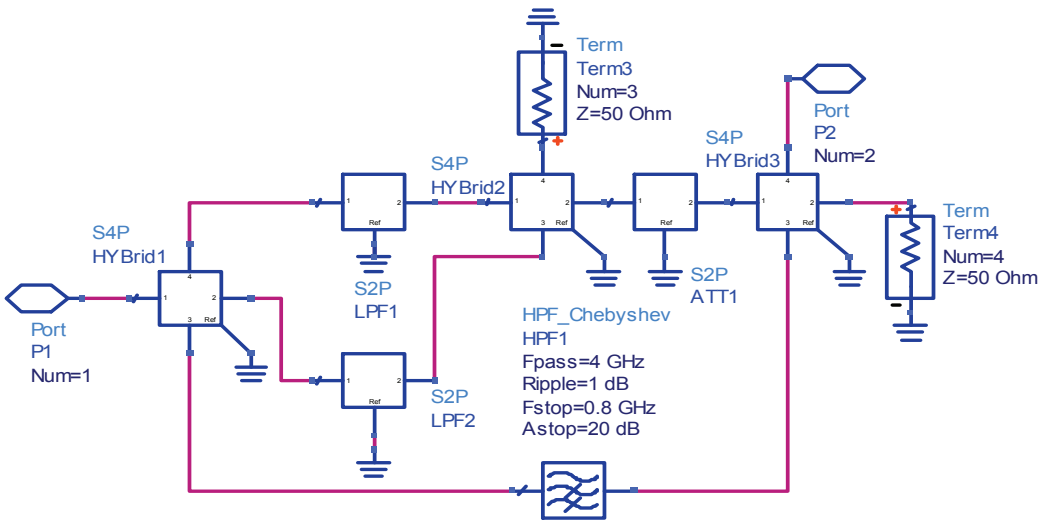

Figure 5.13: A modified HBS - a high pass filter (HPF) has been installed between hybrid 1 and hybrid 3.

The S-parameter simulation on this set-up was performed in same manner (i.e. a frequency sweep of 0.5GHz to 20 GHz with a step attenuator setting of 0-70 dB in 10dB steps). Figure 5.16 depicts the results of this simulation. The results show that the S12 and S21 are identical; they both reach the requirement of the HBS characteristics. The HBS is able to control the S12, while the step attenuator has gone below -30 dB. S12 on the frequency bandwidth 0.5- 4 GHz is well behaved, while the step attenuator is set at 0dB, 10dB, 20dB, and 30dB, and their curve is constant and smooth. Although S12 can reach to 40dB, 50dB, 60dB and 70 dB on this band, their curves are fluctuating and rising to -30 dB at a frequency of 3.7 GHz. It is important to note that the fluctuation curves behave like the reflection passband of an LPF.

On the other hand, S22 and S11 are quite high when compared with S11 and S22 of the HBS without HPF. S22's curve tracks from -5 dB, declines to -10 dB at 4GHz, and then suddenly drops to -30dB at 4.5 GHz. In contrast, S11 behaves opposite to and is unlike S22, its curve is average at -30dB at frequency band 0.5-3.7 GHz, after which it rises shapely to -10 dB at 4 GHz. This characteristic of both S11 and S22 is caused by both the LPF and the HPF.

In summary, the S-parameter results show that the HBS provides the S-parameter characteristic as required up to 30 dB. Although the HBS can provide control of S12 on 0.5-3.7 GHz at a frequency band of up to 70 dB, they have to modify the structure by adding an HPF that takes place between port 4 of hybrid 1 and port 4 hybrids. An HPF is used in the HBS with the aim of blocking the reflected fundamental frequency from the LPF, which influences the output port of the HBS. The response of the S-parameter curve is greatly influenced from the LPF or HPF. Therefore, when implementing the HBS the specification of the LPF has to avoid the undesirable output signal at the output port of the HBS.

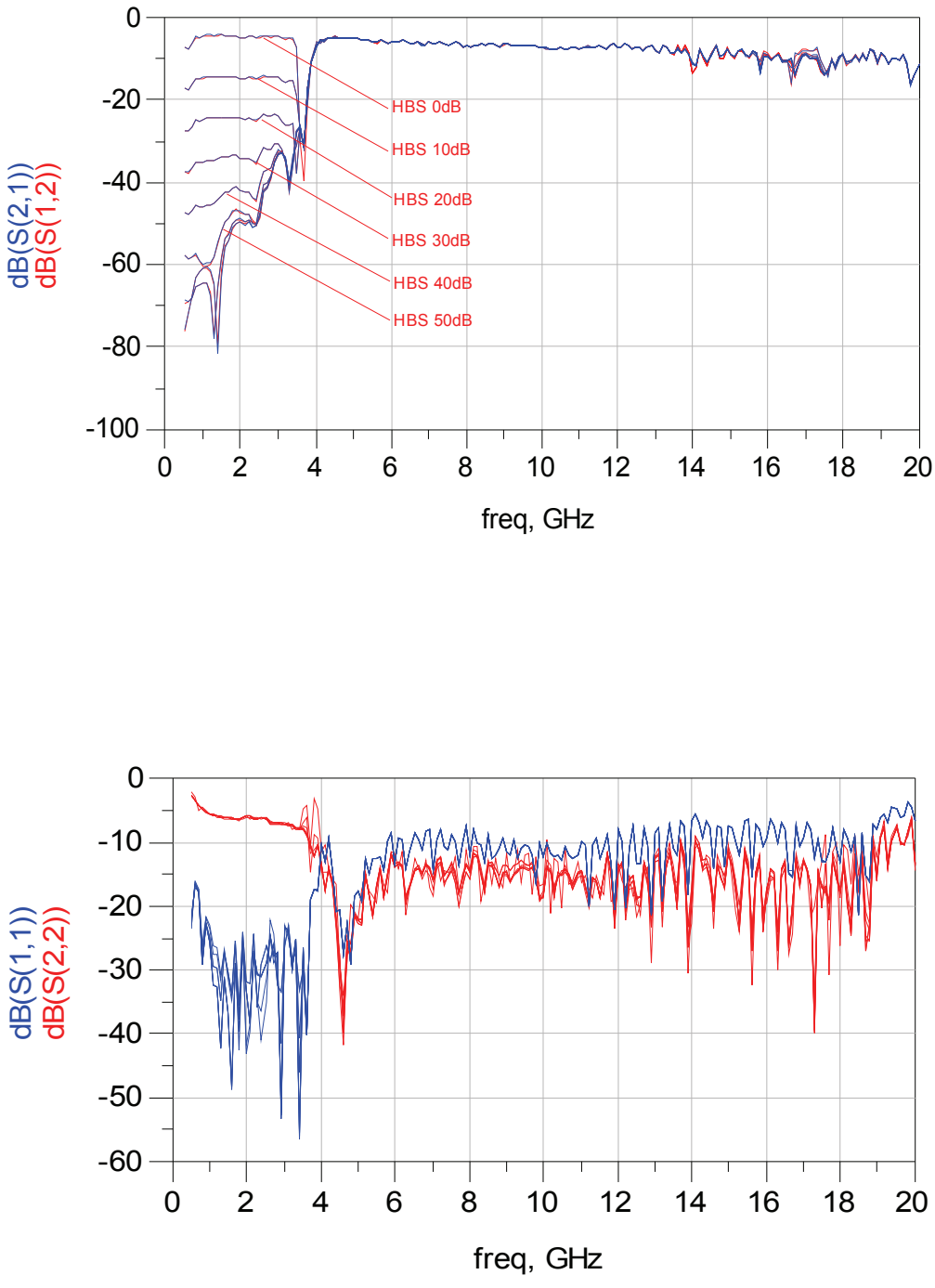

Figure 5.14: HBS S-parameter results (the HBS was modified by including a HPF).

5.4 S-parameter Characterisation of the HBS

Usually an S-parameter characterisation of RF or microwave networks is used to investigate the behaviour of interested or designed networks. The S-parameter characterisation is achieved by a Vector Network Analyser (VNA). In this section, the S-parameter of the HBS and its components was measured by VNA HP8510 and PNA-X Network Analyser Agilent N5242A. The following results show the S-parameter of each component; confirming its qualification such as gain flatness, insertion loss, frequency bandwidth range.

5.4.1 Calibration and Measurement

The 2 full port SOLT (short, open, load and through) was used to calibrate the VNA HP8510 with the 3.5 mm Agilent standard. The frequency band spans from 45MHz to 20 GHz with 801 data points. Some HBS components were measured by a 4 port PNA-X, the calibration was done on an electronic calibration module with a 3.5mm connector. The frequency band setting on PNA-X spans from 0.5- 20GHz, with 3,200 data points.

The measurement configuration of HBS for HP8510 is similar to the measurement configuration of the step attenuator that was described earlier in Chapter 3. The measurement process is the same as that used for the step attenuator measurement, with repeated measurement of 20 samples along with the step attenuator settings that varied from 0 dB to 70dB. Because the step attenuator is part of the HBS, it has to measure the S-parameter over its operating range of 0dB-70dB. In association with the computer controller and HP8510, the S-parameter was processed and was stored in an IGOR binary file that is easy to analyse and to proceed the S-parameter model.

5.4.2 Results and Discussion

Figures 5.17, 5.18, and 5.19 have shown the S-parameter characterisation of each component of the HBS. The hybrid was characterised by PNA-X because it can measure a 4 port network. The LPF and step attenuator were characterised by HP8510. The S-parameter characteristic of each component shows a good agreement to its specification (see Appendix B).In the hybrid the insertion loss is a flat 3 dB over a valid frequency of 1-18 GHz, reflection is an average of -30dB. In the LPF, the insertion loss is 0dB over the passband 1.350-3.750 GHz, while rejection reaches 80dB in a frequency band of 8-14 GHz. The LPF has to be careful while it operates up to 16GHz to 20 GHz because the rejection is decreased to 10 dB and a ripple of 0dB to 20 dB. The reflection of the LPF ripples between -20 dB to 40 dB on passband. The step attenuator shows good behaviour over the control attenuation 0dB-30 dB; however, there is some distortion while the attenuation is between 40dB-70 dB, especially at a high frequency of 18-20 GHz. The reflection is satisfied below -30 dB.

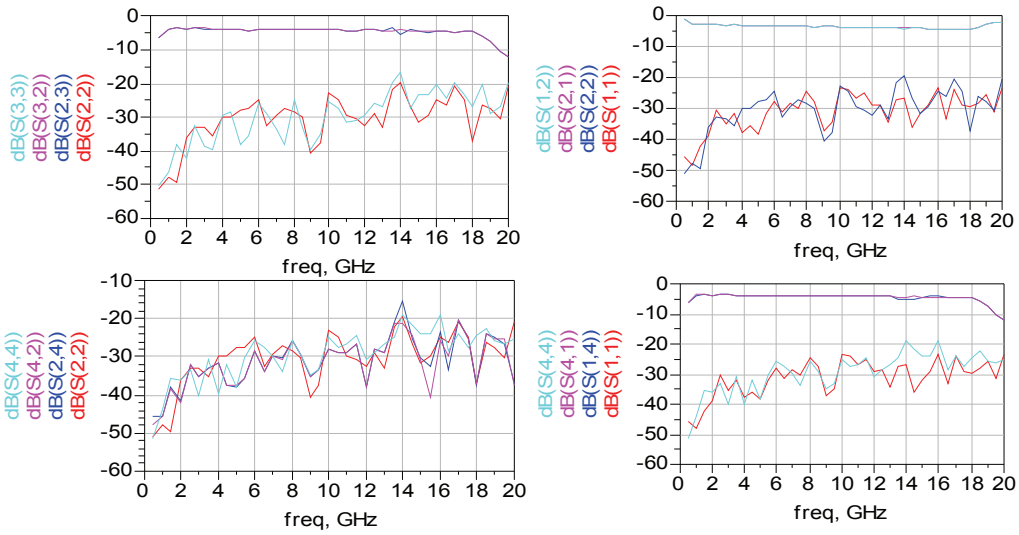

Figure 5.15: 4 ports S-parameter characterization of the 90^{o} hybrid (measured by PNA-X Network Analyser Agilent N5242A).

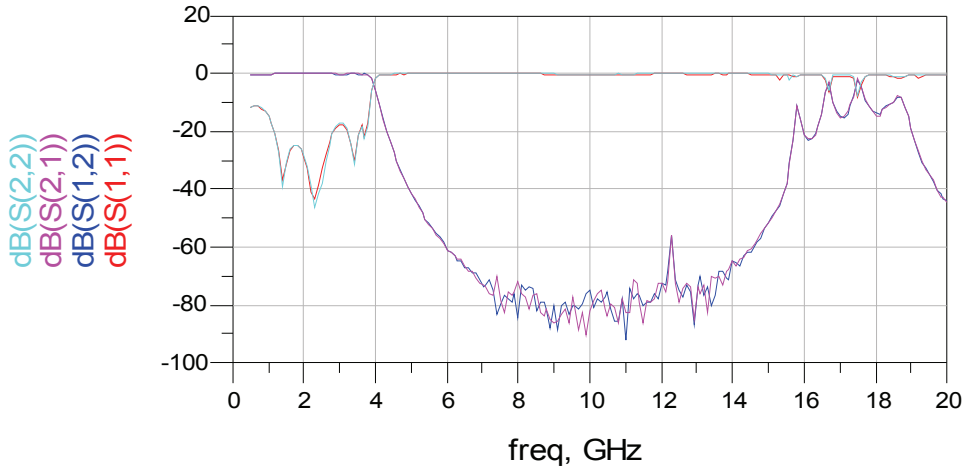

Figure 5.16: 2 ports S-parameter characterisation of the LPF (measured by VNA HP8510).

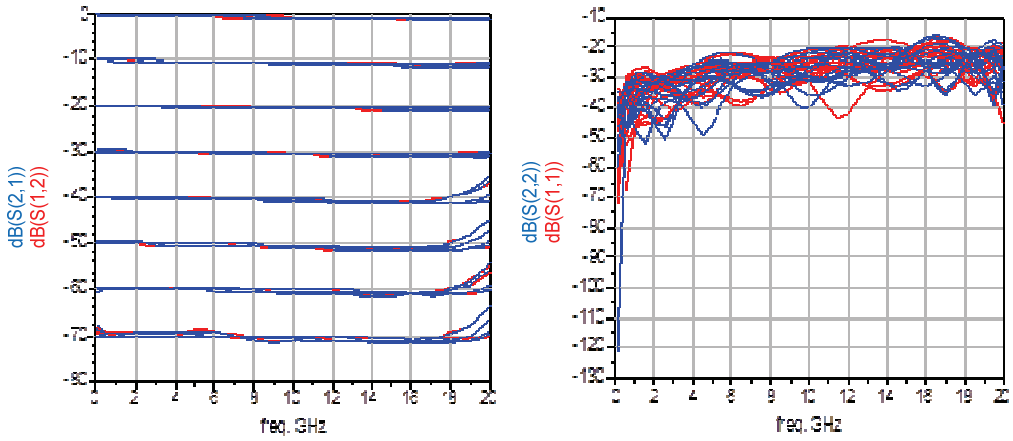

Figure 5.17: 2 ports S-parameter characterisation of the step attenuator (measured by VNA HP8510).

Figures 5.18, 5.19, and 5.20 show the results of the S-parameter characterisation of the HBS. It is obvious that the HBS has achieved the S-parameter requirements up to 30 dB of the step attenuator control. This limitation is caused from the reflection of the fundamental from the LPF. The insertion loss in the HBS is about 5 dB and it increases to 10 dB along the frequency bandwidth of 1GHz to 20 GHz. There are two interesting feature of S12 or S21. Firstly, on the bandwidth 1GHz to 3.7 GHz, the measured S12 or S21 curve is found to fluctuate more than the simulation results (as can be seen in Figure 5.21). Most fluctuation occurs when the step attenuator is set at 20dB or 30 dB, which is caused by the behaviour of the LPF. Secondly, fluctuation also exists on the bandwidth 14-20 GHz. This result is similarly derived from the behaviour of the LPF with its rejection lower than 20dB. In other words, the LPF provides good operation only up to 14 GHz. On the other hand, the S11 and S22 have been found to agree with the simulation, both S11or S22 curves drop in boundary -20 to -30dB.

In brief, the HBS can provide a good operational bandwidth of 1-14 GHz and can control the attenuator on a fundamental of up to 30 dB. Moreover, the S-parameter is unique to each HBS. Although the appearance of the HBS is similar, the plotted lines are slightly different depending on the unique characteristics of each component; for example, Figures 5.20 and 5.22 show different S22 characteristics due to the difference of the step attenuator. In cases where S21 or S12 is significant in the HBS S-parameter model then generally the difference of the plotted line is about 0.1-0.3 dB. Therefore, the unique characteristics of the HBS have to be treated carefully in the S-parameter model because it is significant in terms of the accuracy of the measurement systems.

Figure 5.21 illustrates the S-parameter comparison between the measured S-parameters and the simulated S-parameters. It can be seen from this comparison that the simulated S12 is less than the measured S12 along the bandwidth of 4.0GHz to 16 GHz; because of this, the insertion loss of the cable that links hybrid H1 and hybrid H3 can be assumed to have no loss.

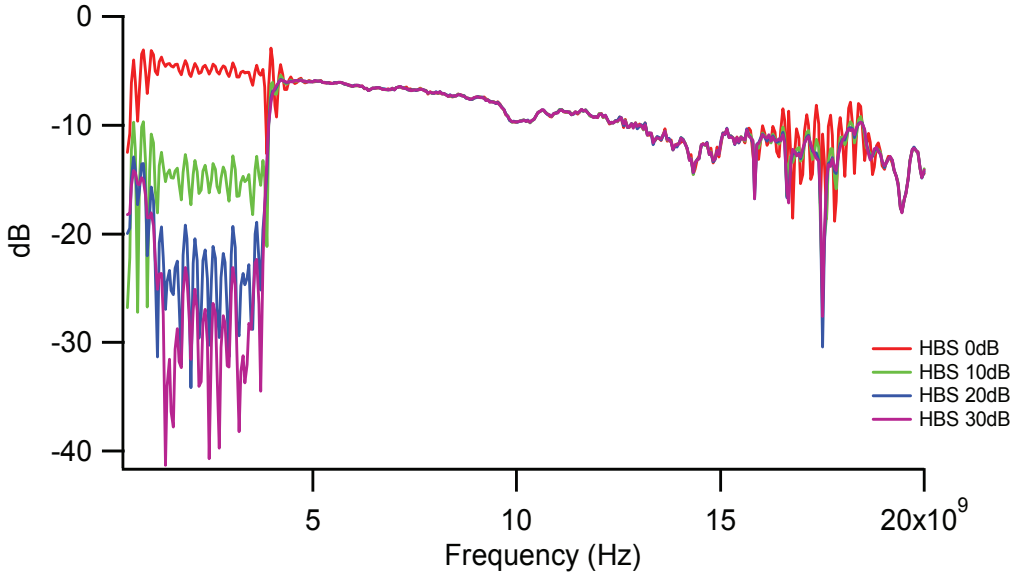

(a) S12 of HBS

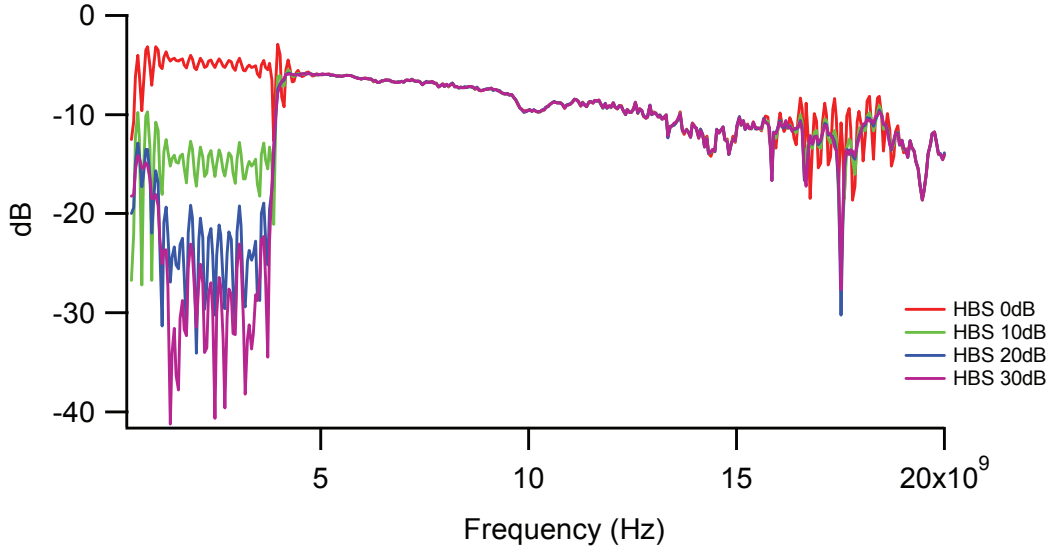

(b) S21 of HBS

Figure 5.18: S-parameter characterisation of HBS (based on step attenuator serial 839) These S –parameters were measured by PNA-X Network analyser Agilent N5242A. (a) S12 (b) S21.

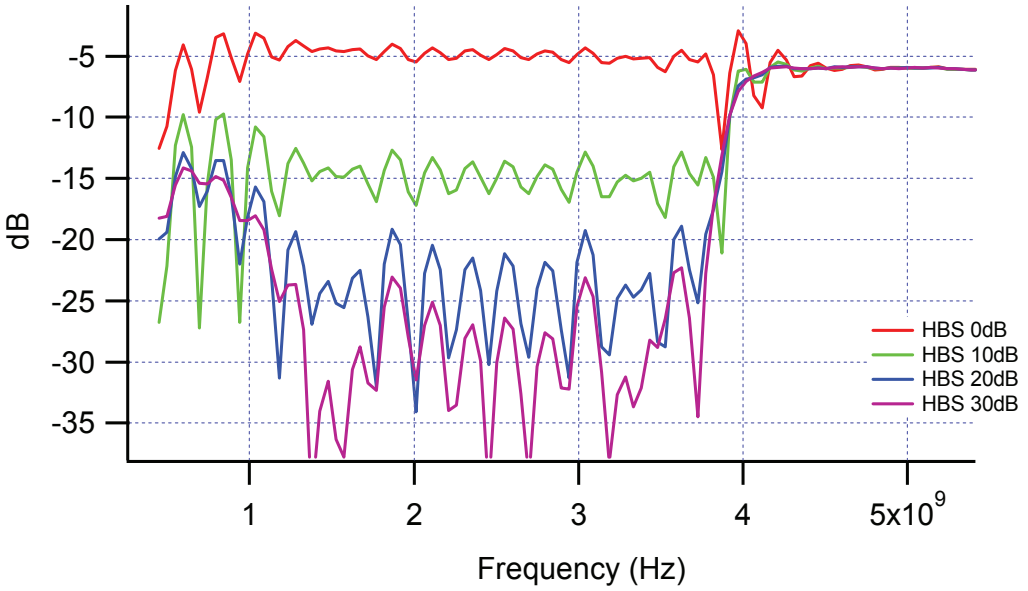

(a) S12 of HBS

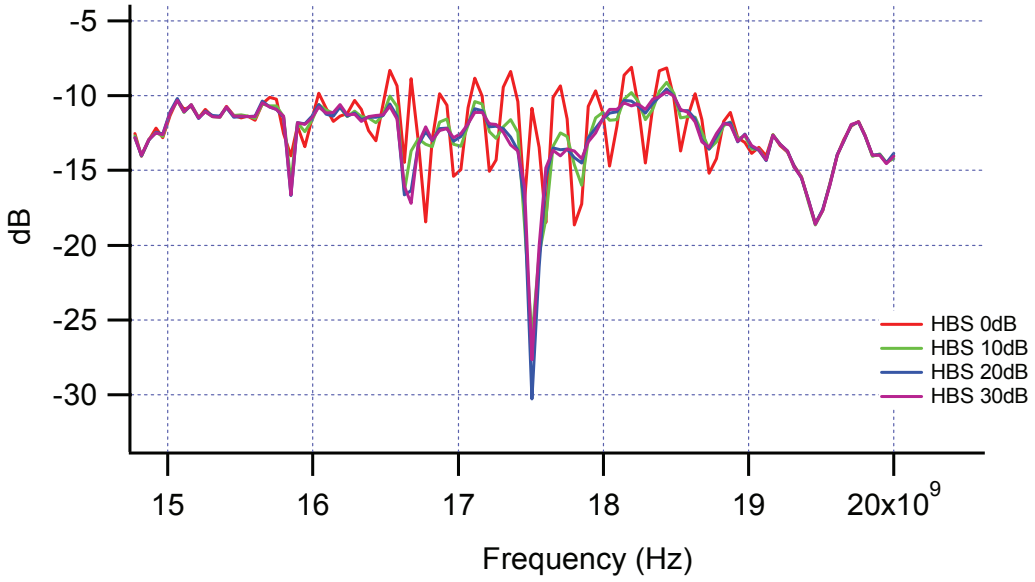

(b) S12 of HBS

Figure 5.19: HBS S12 present in the interested frequency range (a) 0-5 GHz (b) 14 -20 GHz. Two bandwidth ranges show the fluctuation curve of S12 (the HBS is based on step attenuator serial 839).

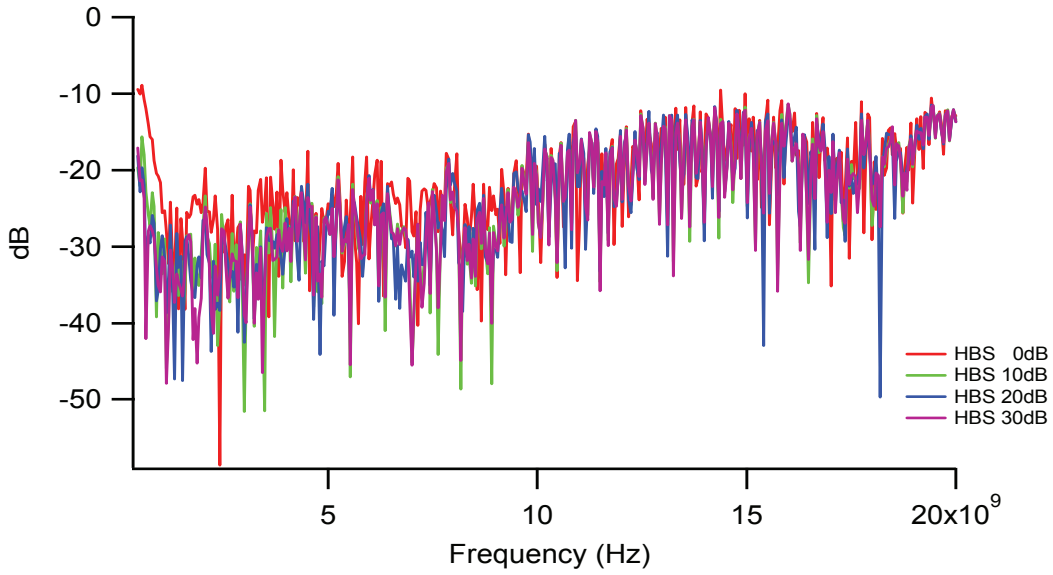

(a) S22 of HBS

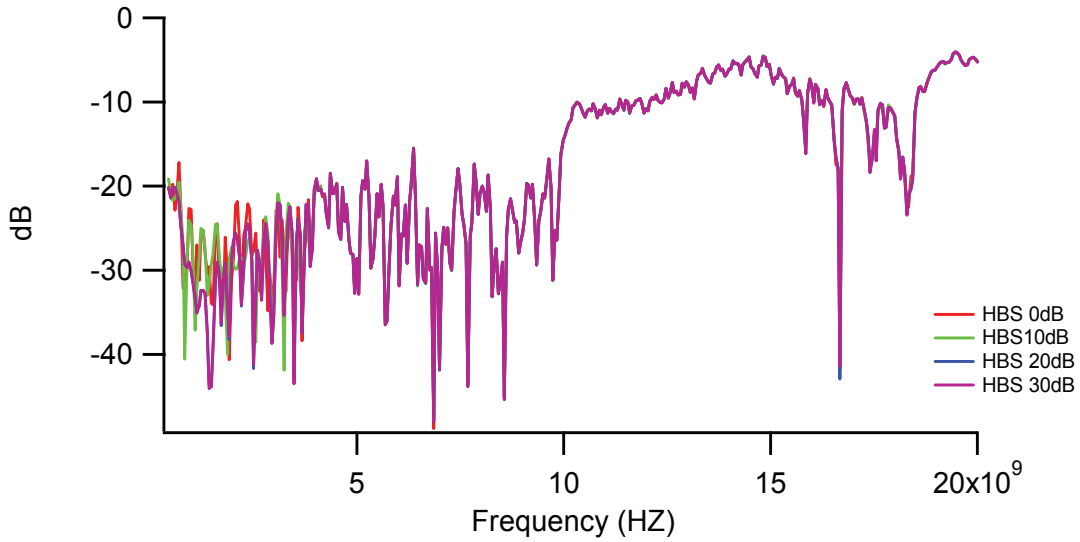

(b) S11 of HBS

Figure 5.20: An S-parameter characterisation of HBS (based on step attenuator serial 839). These S-parameters were measured by PNA-X Network Analyser Agilent N5242A. (a) S22 (b) S11.

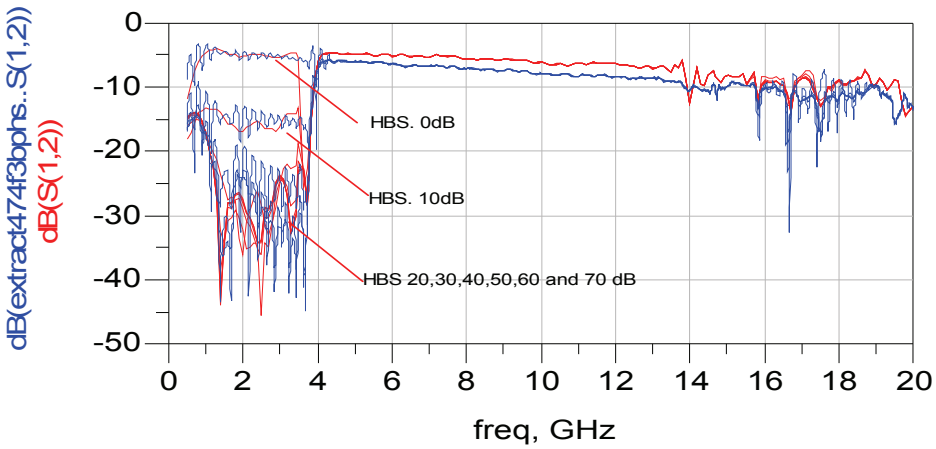

(a)

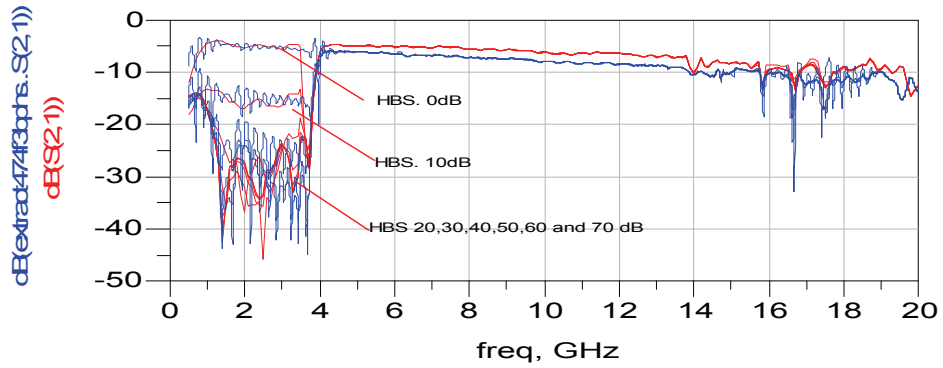

(b)

Figure 5.21: A comparison between HBS S-parameter and HBS measured S-parameter (a) S12 (b) S21 (based on the step attenuator serial 474).

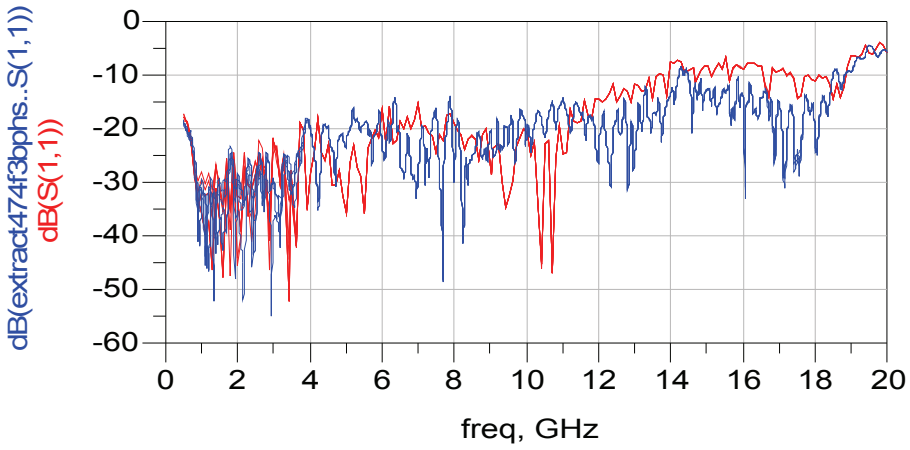

(a)

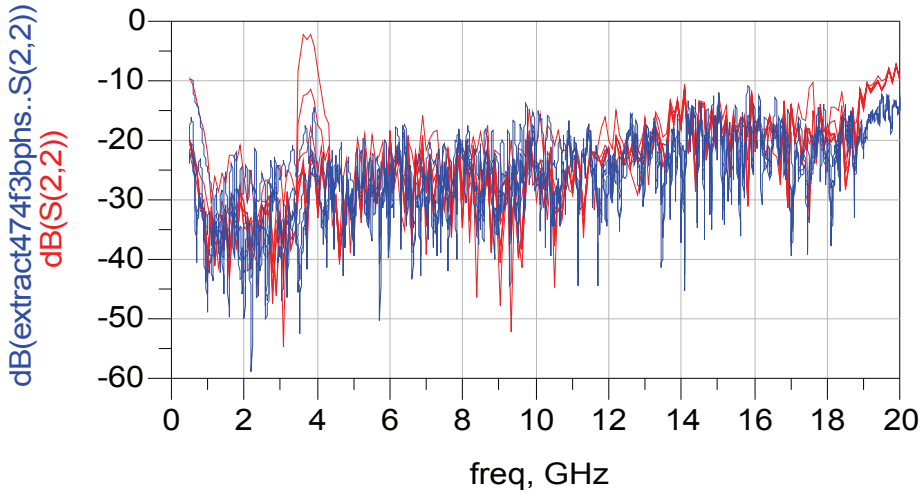

(b)

Figure 5.22: A comparison between HBS S-parameter and HBS measured S-parameter (a) S11(b) S22 (base on the step attenuator serial 474).

5.5 Conclusion

A characterisation of the HBS S-parameter has been achieved in this chapter. The functionality of the HBS has been verified on an ADS simulation. The harmonic balance simulation confirms that the signal input can be divided into two frequency bandwidths, the HBS can avoid harmonic distortion, and the fundamental has been attenuated successful by the step attenuator. The S-parameter simulation shows the S-parameter data of the HBS, which informs our understanding of the behaviour of the HBS. The drawback of the use of a HBS has been found to be its limitation when blocking the fundamental in between the isolation port 4 of hybrids H1 and H4, which is intended to link together only the harmonics. Although a solution has been found by inserting the HPF to filter out the frequency band below the harmonic, the solution has not been implemented due to the existing HBS that is still suitable in the current measurement system. The HBS S-parameter data has shown good agreement between the simulated S-parameter data and the measured S-parameter data. The measured S-parameter data of the HBS will proceed in the S-parameter model and will be stored in the IGOR binary format. The next chapter will demonstrate the HBS in a practical measurement system.

References

[1] D.M. Pozar, *Microwave engineering*, 3rd ed. New York, USA: John Wiley & Son,INC., 2005.

[2] Agilent, 8510C Network analyzer System operating and programming manual, 2001, 3rd edit,USA.

[3] Agilent, Agilent Technologies 33320A/B/G/H 33321 A/B/D/G/H/K 33322A/B/G/H 33323K Step attenuator for OEM & System Use dc to 26.5GHz, 1990, Technical data sheet.

[4] Agilent, Agilent AN 1287-3 Applying Error Correction to Network Analyzer Measurements, 2002, Application Note.

[5] Agilent, Specifying Calibration Standards for the Agilent 8510 Network Analyzer, 2004, Application Note 8510-5B.

[6] Agilent, Understanding the Fundamental Principles of Vector Network Analysis, 2000, Application note.

[7] WaveMetrics Inc, *IGOR Pro Version 6.0 manual*, 1st ed. Lake Oswego, USA: WaveMetric Inc, 2007.

Chapter 6
Improving Dynamic Range with an Harmonic Bypass Structure

Chapter 6 - Improving Dynamic Range with an Harmonic Bypass Structure

6.1 Introduction

A demonstration of the use of step attenuators to extend the measurement system dynamic range appeared in Chapter 4. Although the use of a step attenuator can extend the dynamic range, the measurement system has been found to suffer a constraint in the harmonic content while inappropriate attenuation is switching in. This event can occur if the measurement system is used to characterise high power amplifier devices with high gain. Chapter 5 introduced the HBS. It was found to be possible to use a HBS to overcome the problematic issues that are experienced by the measurement system. The HBS provides the specific attenuated frequency that is the fundamental frequency while allowing the other harmonic frequency bands to pass through. Therefore, the S-parameter characterisation of the HBS that is used to compose the HBS S-parameter model has been accomplished.

This chapter will give a demonstration of an extended dynamic range in RF measurement systems using an HBS, which has been implemented instead of a step attenuator. An HBS extends the dynamic range of the measurement system while overcoming the harmonic distortion issue. Similarly, the approach of using an S-parameter model to compensate the measured signal was also used in the HBS approach. This chapter will discuss a number of topics that are associated with the measurement configuration, including the software configuration, the calibration method with TRM short, and the measurement procedure.

6.2 Measurement System Configuration

6.2.1 System Configuration

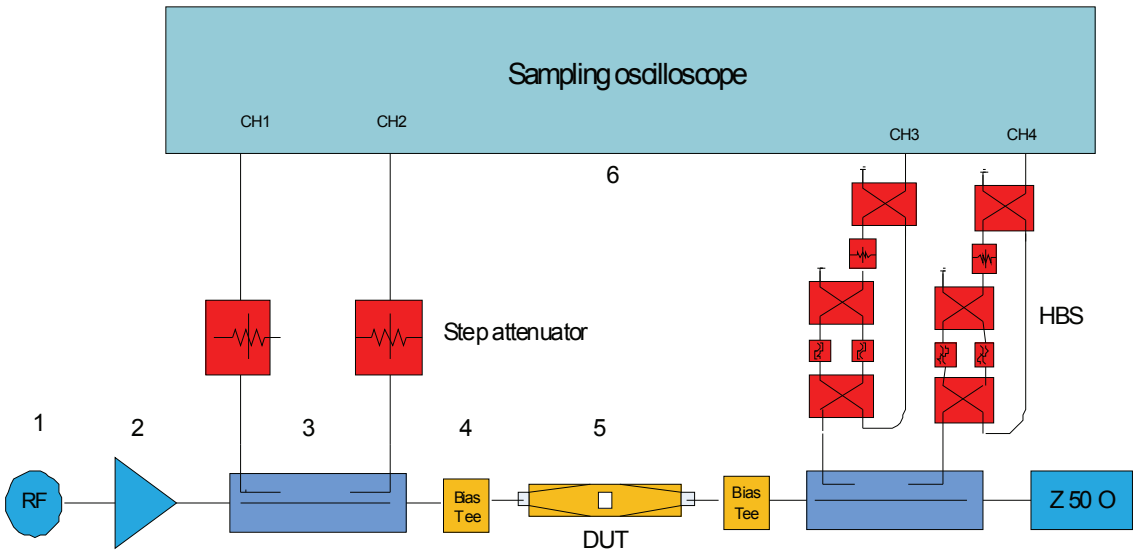

Figure 6.1: A simplified schematic diagram utilising HBS within the measurement system.

The high power RF measurement system that is given in [1] was used in this demonstration. This measurement system is based on a four channel sampling oscilloscope with an harmonic load pull capability. Figure 6.1 shows the simplified measurement system. In fact, a number of RF switches are installed in the measurement system that enable it to diversify the signal source to the input or output of the measurement plan; thereby, connecting the other parts of measurement system (such as the harmonic load pull, the source pull system, or the external power amplifier which enables the RF sweeper source to reach the desired power). However, the important parts of the demonstration have focused on the HBS, which takes place between the direction coupler and the sampling oscilloscope. This HBS deals with the measured

incident and reflected travelling wave from the DUT at the output of the measurement plan. It is important to note that only two sets of HBS are installed in the output of the measurement plan because of the issue of cost. Two step attenuators are installed on the input measurement plan, which are acting on the incident and reflected travelling wave from the input measurement plane. The other setting parts of the measurement system are:

1. *RF Sweeper* - This sweeper is used as a CW source for this measurement system. An Agilent 83623B sweeper was used in the demonstration, providing a frequency range from 10MHz to 20GHz (maximum output 20dBm).
2. *Narrow Band Power Amplifier* - This amplifier is used to amplify the signal power from the RF sweeper. In the demonstration, the operating band was 2.110GHz to 2.170 GHz, providing a gain of up to 40 dB (maximum output power 51dBm).
3. *Directional Coupler* - A four port directional coupler is used. This is able to capture the incident and reflected signal separately, providing a coupling factor of 35dB with broadband frequency.
4. *Bias Tee* - Two 90^{o} hybrids are joined together as a back to back configuration to form the bias tee that provides the external DC power supply to the DUT.
5. *DUT* – The DUT in this set up is an extensive transistor device GaN model NPTB00050, providing a maximum average output of power at 3dB, gain compression (typically 50 W), and which is optimised for broadband operation from dc-4.0 GHz (more detail in Appendix B). The GaN transistor is mounted in a test fixture with a 50 Ω matching line transformer. The test fixture incorporates a temperature regulator, which consists of a cooling and heating system with a USB computer interface that is controlled by the NI Labview application software. The demonstration can take an advantage of this test fixture so that it can neglect temperature as a factor of the transistor device.
6. *Sampling Oscilloscope* – In the demonstration, the sampling oscilloscope was a Tektronix CSA8000 with 80E02 sampling module.

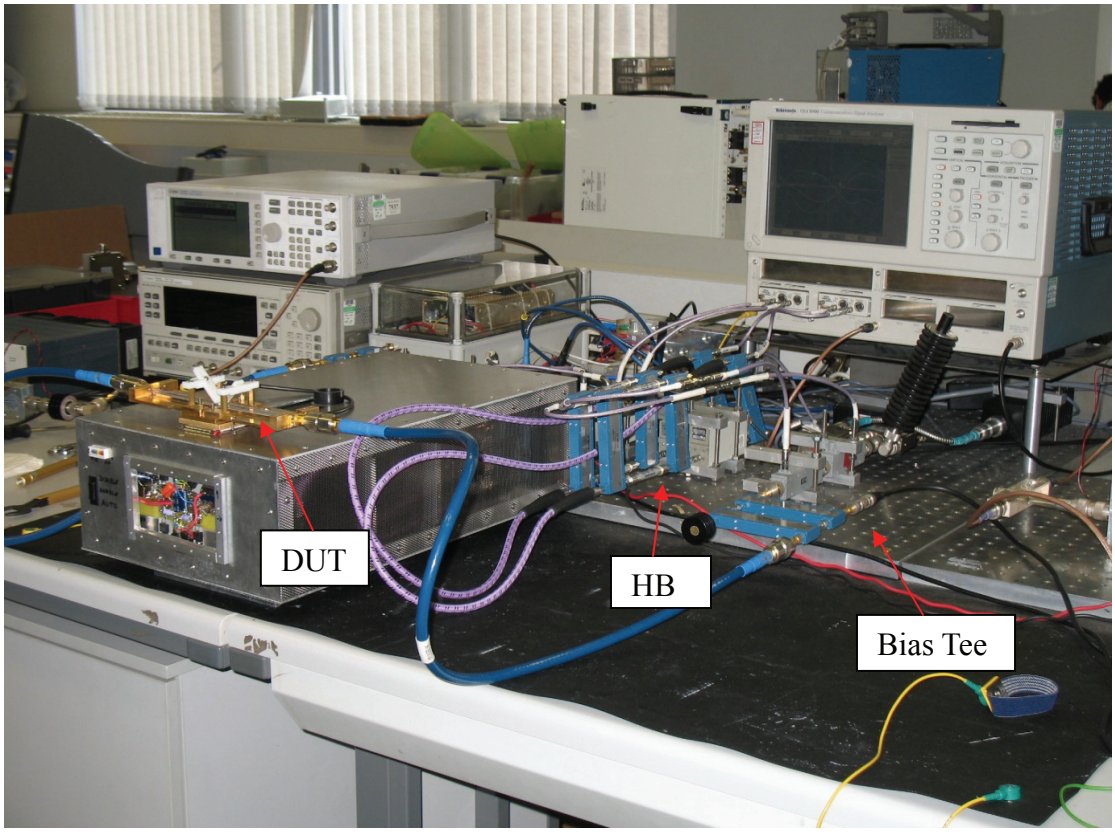

Figure 6.2: The practical realisation of a measurement system that employs HBS.

6.2.2 Measurement Software Configuration

The modification of the measurement software for implementing the S-parameter model was discussed earlier in Chapter 3. These modifications provide an extensive utility tool to embed new S-parameter models into the measurement software, which helps the user to import the new S-parameters of newly inserted devices more easily. Basically, four S-parameter models are imposed in the measurement software, corresponding to four measured travelling waves, which are: a1and b1 at input of DUT; and, a2 and b2 wave at output of DUT. However, as can be seen in Figure 6.1, only two new HBS S-parameter models are replaced. This happened because there were only two HBS units at the output of the DUT. The two-step attenuators on the input DUT side remain the

same as in the demonstration in Chapter 4. Therefore, the two-step attenuator S-parameter models were unchanged.

The measurement system can extend the dynamic range. The measurement system accuracy depends on a number of factors amongst which is the accurate S-parameter model. An S-parameter model is given in Equation (1), which rewrites the equation from Chapter 3 for convenience. The variables in this equation can be categorised into two groups: the first are the four S-parameters of the HBS, and the second are the reflection coefficients Γ_S and Γ_L looking into a directional coupler and a sampling oscilloscope, respectively. These variables have a huge impact on the accuracy of the S-parameter model and they consequently impact on the correction of the measured travelling wave a and b from the DUT. Special care has to be taken while the first group of variables are measured and modelled (as in Equation (1)) because an early attempt at a measurement demonstration has shown that the accuracy impact of the measurement system depends on the S-parameter's data more than the Γ_S and Γ_L. In practice, the factors that have to be seriously considered while the HBS S-parameters as modelled are: the unique S-parameter data of each HBS, the huge dynamic ripple pattern of the HBS on the passband 0.5GHz to 3.700 GHz, and the reflection coefficient Γ_S and Γ_L (due to changing either the RF cables or the connectors).

$$a0 = \left[\frac{1-S22\Gamma_L}{S21} - \frac{\Gamma_S\Gamma_L S12S21}{S21(1-S11\Gamma_S)}\right] a'0 \qquad (1)$$

As discussed in Chapter 5, the S-parameter characterisation of the HBS has shown that each of the HBS S-parameter data is unique. Although their patterns are similar, the exact line curves are significantly different in terms of 0.3 to a few decibels, depending on the frequency. It is, therefore, enough to produce the error if a specific HBS S-parameter is used for all. It is important to stress that each of the HBS S-parameters have to be measured and implemented in its S-parameter model in the correct place.

Generally speaking, in the measurement procedure the compensation of the travelling waves a and b has been achieved by either the HSB or the step attenuator S-parameter model. These measurement procedures prepare the S-parameter by interpolating the whole measured S-parameter, including the Γ_S and Γ_L to the desired frequency or, in other words, the measured frequency. This interpolation is accurate only if the measured S-parameter can present precisely its values along with enough frequency resolution. As exhibited in Figure 6.3, the interpolation error exists because of the lack of a measured signal resolution. This problem also occurs in the HBS S-parameter model. The HBS S-parameter was modelled from the S-parameters that were taken from VNA HP8510 in the early stages of the demonstration. This provided a frequency resolution of up to 801 data points, even though it was not enough to represent the extreme dynamics of the HBS S-parameter on the frequency bandwidth 0.5GHz to 3.700 GHz. A high performance PNA-X was used to overcome this problem, which provided sufficiently dense data points.

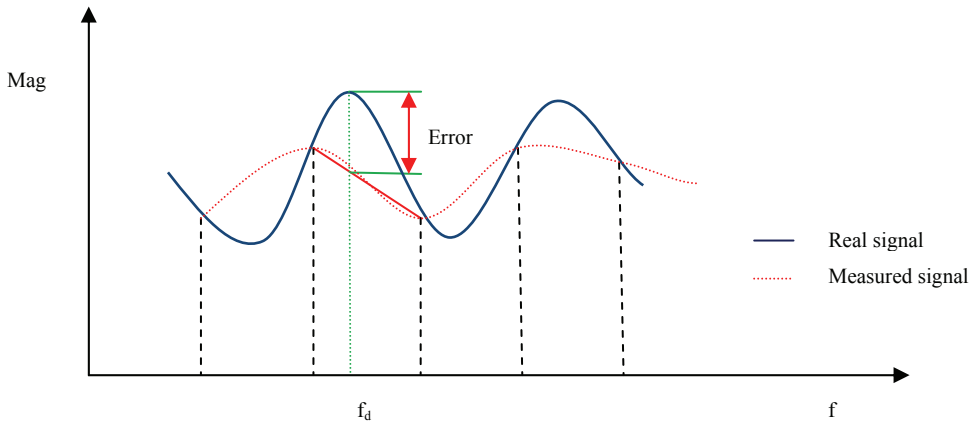

Figure 6.3: Interpolation errors due to the limited frequency grid resolution of the measured signal.

Although Γ_S and Γ_L of the reflection coefficient are not significantly different when they are replaced by new RF cables or connectors, their re-measurement is still necessary while the measurement accuracy comparison of the HBS is between 0dB and 10 dB, or

below 0.01 dB. In fact, the reflection coefficients from both the directional coupler and the sampling oscilloscope are definitely unchanged while the HBS was used instead of step attenuators. To minimise the errors from the Γ_S and Γ_L, the implementation of the HBS into the system should either use 3.5mm type connectors or be designed as precision devices with good repeatability.

For the above reasons, the HBS S-parameter models that were used in this demonstration were unique. The S-parameter data which were taken from the Agilent PNA-X Network Analyser Agilent N5242A (with a frequency span of 0.5 -20 GHz, and resolution data point of 160,001) can significant represent the highly dynamic ripple pattern of the HBS behaviour on the frequency band of 0.5GHz to 3.7 GHz. In addition, these HBS S-parameter models were modelled into the full S-parameter model by using the Polynomial data fit function approach (as described in Chapter 3). The procedure process is similar when using the step attenuator model.

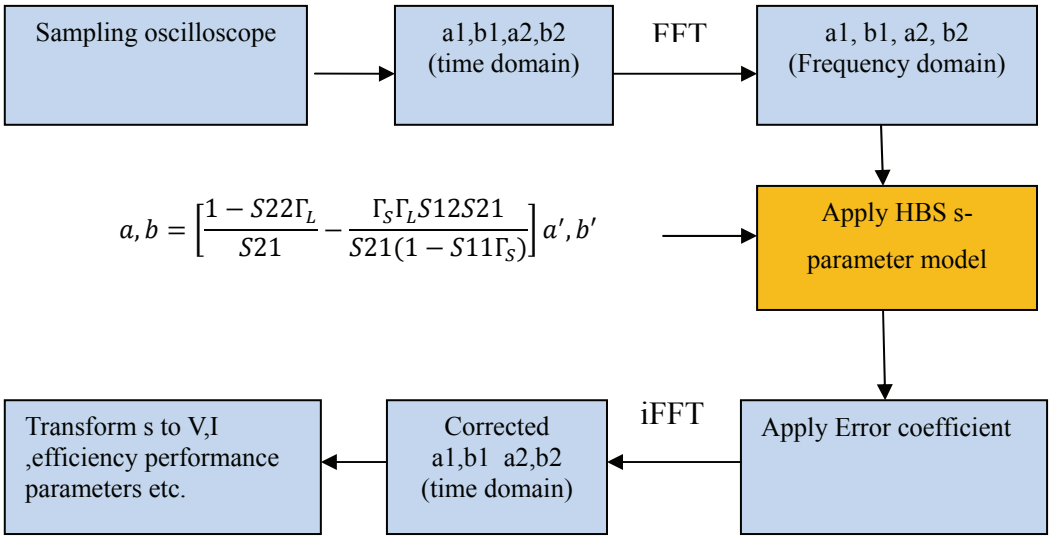

Figure 6.4: A simplified schematic diagram of the measurement software configuration for HBS.

6.3 System Calibration

The measurement system calibration was followed by the calibration procedure, which is explained in [1]. The objective of the calibration requires the researcher to obtain the error coefficients that describe the imperfection of the test set resulting from attenuation losses, and delay and impedance mismatches, which is a function with frequency. Generally, the calibration procedure initially performs the small signal S-parameter with the aim of computing the error coefficients of the test set. An additional calibration, called an absolute calibration, is then performed. The result of these calibration procedures is that the measurement system is able to obtain the absolute power and phase of the travelling wave. There are a number of calibration methods that are able to provide this function in the measurement software, such as SLOT (Short, Load, Open, Thru) and TRM (Thru, Reflect Match). These calibration methods have different trade-offs, and so choosing which to use is dependent on the requirements of the user.

In this research project the modification of the measurement software does not involve a calibration procedure (including error coefficients), the only requirement is the defined calibration state of the HBS (or step attenuator) which was defined at the HBS (or step attenuator) set at 0dB. This information is particularly important with regard to the correction of the travelling waves a and b before they are applied by the error coefficient.

In this demonstration system, the calibration procedures are performed using small signal S-parameter calibration on TRM- short APC 7mm using the Agilent standard, with the frequency grid 2.1GHz to 7.7 GHz at 0.7 GHz step resolution. This frequency bandwidth covers the fundamental 2.1 GHz and goes up to the 3rd harmonic. The sampling oscilloscope was set on average 1024 and the data point sampling was 1024. Calibration at low frequencies used the SOLT with the Agilent 3.5 standard cal kit. For the absolute calibration the power setting was 7.4 dBm, the intention was to reach a power output of nearly 3 dB at sampling oscilloscope ch2.

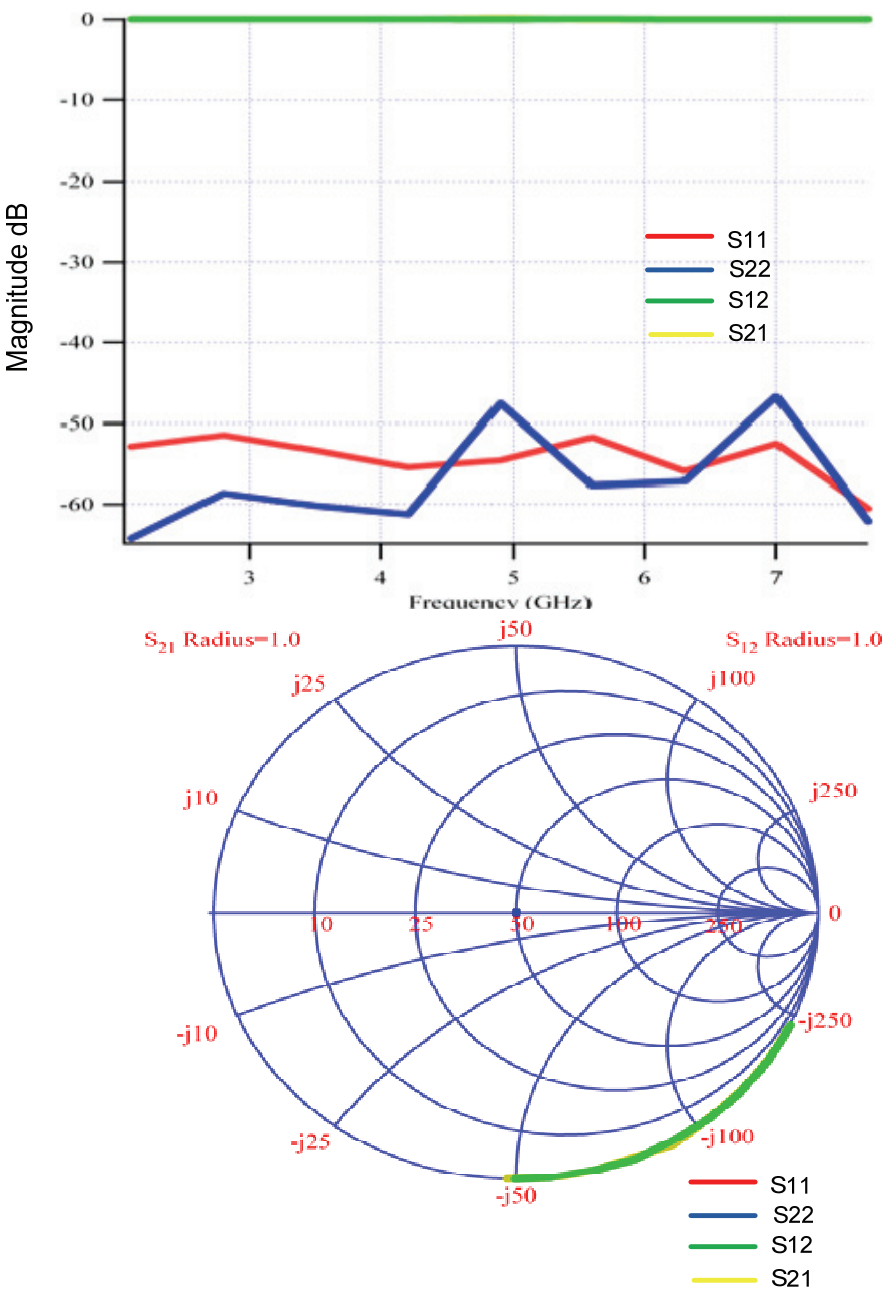

Figure 6.5: Log chart and Smith chart of S-parameter measurements on a thru 7mm standard verifying the small signal S-parameter calibration of HBS.

6.4 Measurement Procedure for utilising the HBS approach

The first part of the demonstration was conducted on a passive device. The linearity response of the passive device is the element that is most required in this demonstration because it enables the measurement system to be investigated easily at each individual frequency of interest, on condition that the HBS is varied. Therefore, a thru 7mm Agilent standard that provides a linearity response on the broadband dc-18 GHz and which provides good repeatability has been used in the first pass of this demonstration. The objective of the first part of the demonstration is to investigate the HBS S-parameter model correction and its extended measurement system dynamic range. The measurement procedure starting from the single tone CW power sweep was performed at a fundamental frequency 2.1GHz with powers from -50 dBm to 44 dBm and 1dB step for attenuator values of 0dB, 10dB, and 20 dB. A CW power sweep was also performed on the 2^{nd} and 3^{rd} harmonic frequencies.

The second part of the demonstration was conducted on the active device. The objective was to investigate the non-linearity response from the active device in comparison with the varying HBS, which was set at 0dB, 10dB, and 20dB. A GaN 50W transistor device was used, it was biased at 28 Vdc, and the quiescent current was set constant at 1029 mA, where this bias point of the GaN would provide the non-linear behaviour resulting in the comparison of a non-linear region under observation. The measurement procedure started from the CW 30 dBm and was applied to the DUT. The voltage and current time domain waveforms were then measured in respect to the HBS at 0dB and 10dB. A CW power sweep was next performed to investigate non-linear response from the GaN, corresponding to HBS 0dB, 10dB, and 20 dB.

6.5 Demonstration Results

As acknowledged earlier, the measurement system is modified by implementing a HBS, which is located between the directional coupler and the sampling oscilloscope. The assumption is that the measurement system was calibrated and was absolutely valid when the HBS was set at 0dB. For this reason, the measurement system has treated the HBS as being set at 0dB or, in other words, as acting as a fixed attenuator for the calibration state. Additionally, the measurement software has also treated the HBS S-parameter model which is equal to unity because of the equivalence between S_m (i.e. the S-parameter model at the measurement state) and S_{cal} (i.e. the S-parameter model at the calibration state) at HBS 0dB. Thus, when the calibration is set at HBS 0dB the measurement system can assume that it is the same as its traditional configuration and, therefore, it behaves like a regular measurement system. Consequently, the discussion of the results is going to focus on the comparison between the HBS 0dB and either HBS 10dB or 20dB.

6.5.1 Verification of the Results using a 7mm thru Standard

Figure 6.6 illustrates the CW power sweep results with fundamental 2.1 GHz over power -50 dBm to 40 dBm, on the condition HBS 0dB, 10dB, and 20 dB. The power sweep results at the HBS calibration state 0dB show the linearity response curve over the power -50dBm to 40dBm. The response curve of HBS 10dB fluctuates over the HBS 0dB response curve on a power sweep of between -50 dBm to -30 dBm before their track line eventually approaches the HBS 0dB curve. Similarly, the response curve of HBS 20 dB behaves the same as the HBS 10 dB; however, there is more fluctuation along with a bit more power sweep interval (from -50dBm to 20 dBm). This result has been shown in Figure 6.7 in terms of a power difference comparison with HBS 0 dB. When the HBS is set at 10dB the power difference is in an error boundary of -2dBm to 2dBm, they then decline to zero. If the error band acceptability is set to be 0.01 dB then

the HBS 10dB response curve reaches the acceptable point power sweep input at -30 dBm. When the HBS is set at 20dB then the response curve reaches the acceptable error band at a power sweep input of 18 dBm.

Figure 6.8 and Figure 6.10 similarly depict the CW power sweep results with a harmonic frequency of both 4.2 GHz and 6.3 GHz, and Figure 6.9 and Figure 6.11 show the power differences between a HBS of 0dB and 10dB of a harmonic of 4.2 GHz and 6.3 GHz. The CW power sweep has been done up to 20 dBm because the RF power sweeper has swept the output power directly even though the DUT without a power amplifier can be provided only on the narrow band of 2.1GHz. The results show the same behaviour as the fundamental but its fluctuation value of HBS at 10dB and 20dB is less than the fundamental. Moreover, the error comparison of HBS at 10dB and 20dB is quite similar in contact with the fundamental; the error comparison of the HBS at 20dB is more than an error comparison of HBS 10dB. When the CW power sweep is achieved with a frequency of 4.2 GHz then both error bands of HBS 10dB and 20dB reach the error acceptability band of 0.01 at RF power sweep input ~ 38 dBm. When the CW power sweep is conducted with a frequency of 6.3 GHz then they also reach the error acceptable band 0.01dB at RF power sweep input ~38 dBm.

These results can be used to discuss the causes that come from the characteristics of the HBS. Performing HBS at 10 dB and 20 dB has attenuated the amplitude of the fundamental frequency to hit the noise floor of the measurement system. In this case, the noise floor is defined as the noise of the sampling oscilloscope. The specification [2] of the sampling oscilloscope Tektronix CSA8000 shows that it incorporates with 80E02 sampling module, the maximum input voltage is (Dc+ peak AC) 3.0V, and the random noise is displayed typically at 400μVrms. The effective system noise floor was found to be about ~ -57.95 dBm in a 50Ω environment. Hence, if performing HBS 10 dB with a power sweep input of -50dBm then the power input of the travelling wave at the input of the sampling oscilloscope can be measured as -64 dBm (calculating from the power input -50 dBm subtracted by -14 dBm of insertion loss of HBS at 10 dB setting). It was found that a HBS of 10dB was below the system noise floor of the measurement

system. The suitable power input while using the HBS should more than -43dBm and -33 dBm (the insertion loss of the HBS at 20dB is about 24 dB) to the HBS 10dB and 20 dB, respectively.

A further significant characteristic of the HBS is that the harmonic frequencies are not forced to hit the floor because the HBS is performing the setting 10dB and 20 dB. Consequently, these results show that the error of the HBS at 10dB and at 20dB is similar. In fact, by observing the response curves of HBS 0dB at harmonic 4.2GHz and 6.3 GHz it has been shown that the linearity response curve starts from the power input -40 dBm. It can consequently be inferred that the actual system noise floor occurs at -40 dBm. Returning to the result of fundamental, it was found that if the system noise floor is replaced by -40 dBm instead of -57 dBm then the re-calculation result of the suitable power input for HBS 10 dB and 20 dB shows a good agreement with the error band acceptable of HBS 10 dB and 20 dB.

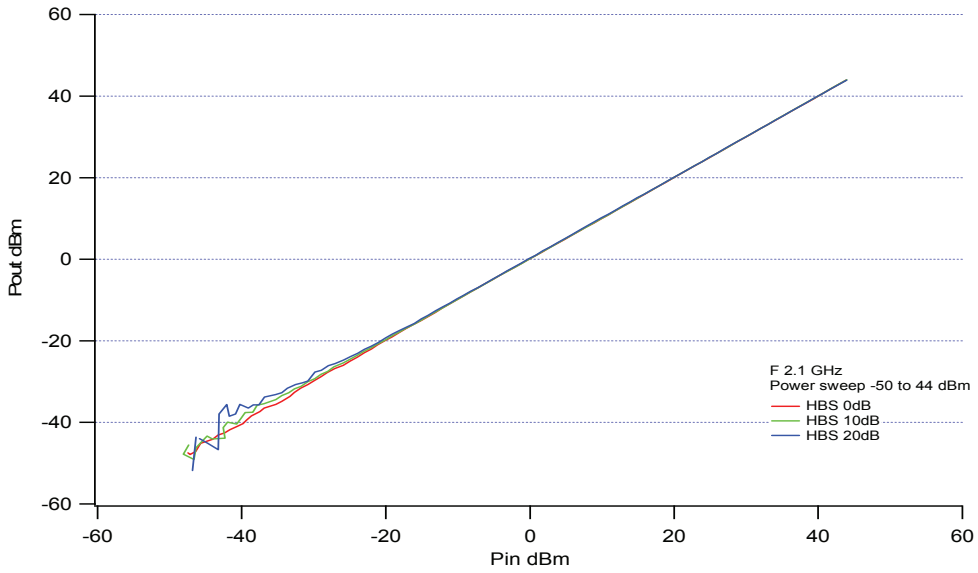

Figure 6.6: CW power sweep from -50 dBm to 44 dBm for a frequency of 2.1 GHz using the 7mm thru standard. The result shows the comparison at the DUT output on for the HBS setting 0 dB, 10 dB, and 20 dB.

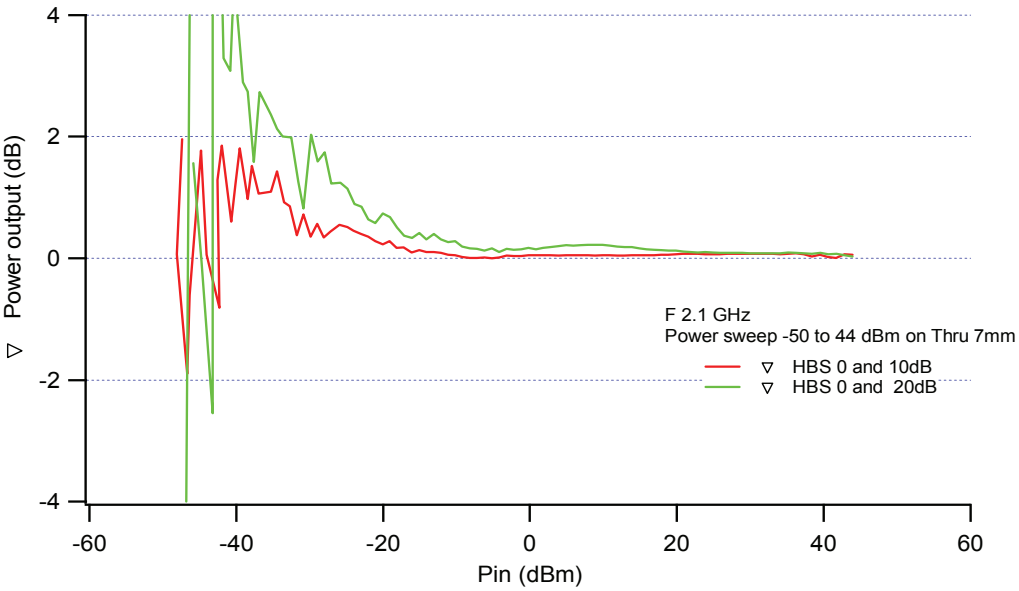

Figure 6.7: CW power sweep from -50 to 44 dBm for a frequency of 2.1 GHz using the 7mm thru standard. The result shows the error comparison in term of∇ Output power between the HBS setting 0 dB and 10 dB and between the HBS setting 0dB and 20dB.

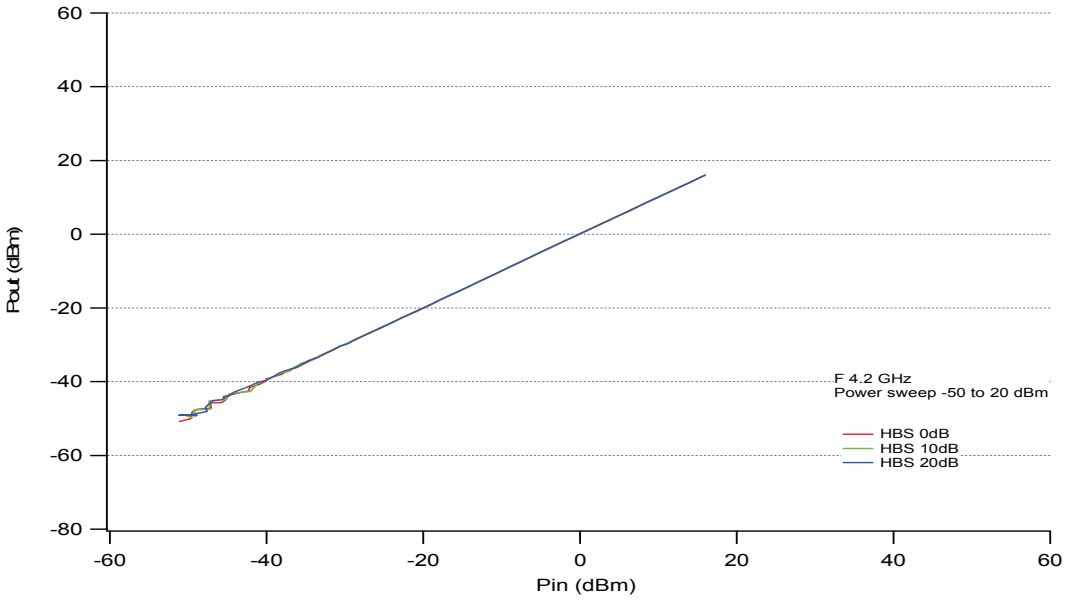

Figure 6.8: CW power sweep from -50 to 20 dBm for a frequency of 4.2 GHz using the 7mm thru standard. The result shows the comparison at the DUT output on for the HBS setting 0dB, 10dB, and 20 dB.

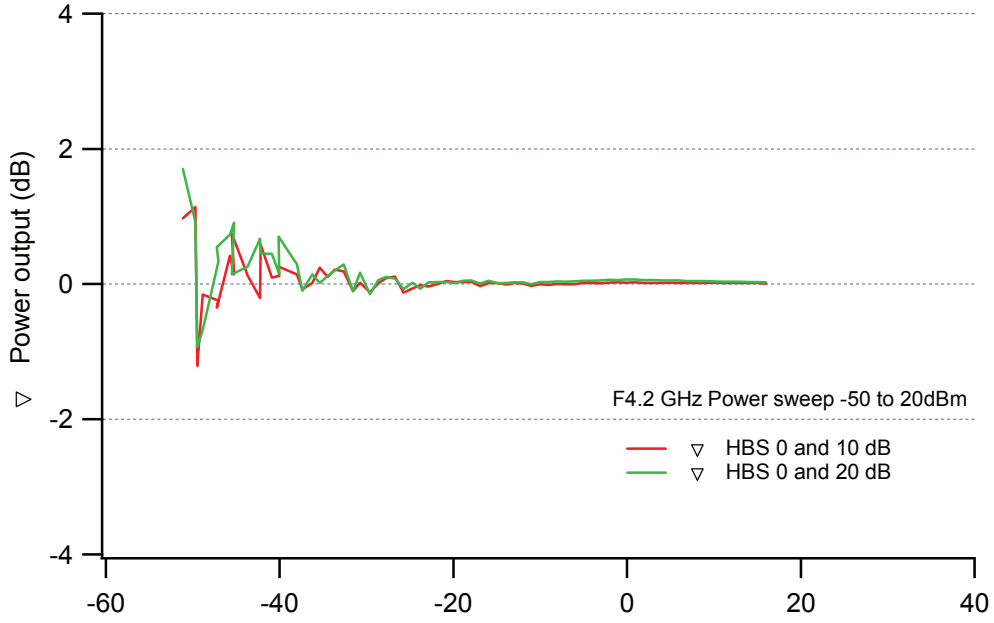

Figure 6.9: CW power sweep from -50 to 20 dBm for a frequency of 4.2 GHz using the 7mm thru standard. The result shows error comparison in term of ∇Output power between the HBS setting 0dB and 10 dB, and between the HBS setting 0dB and 20dB.

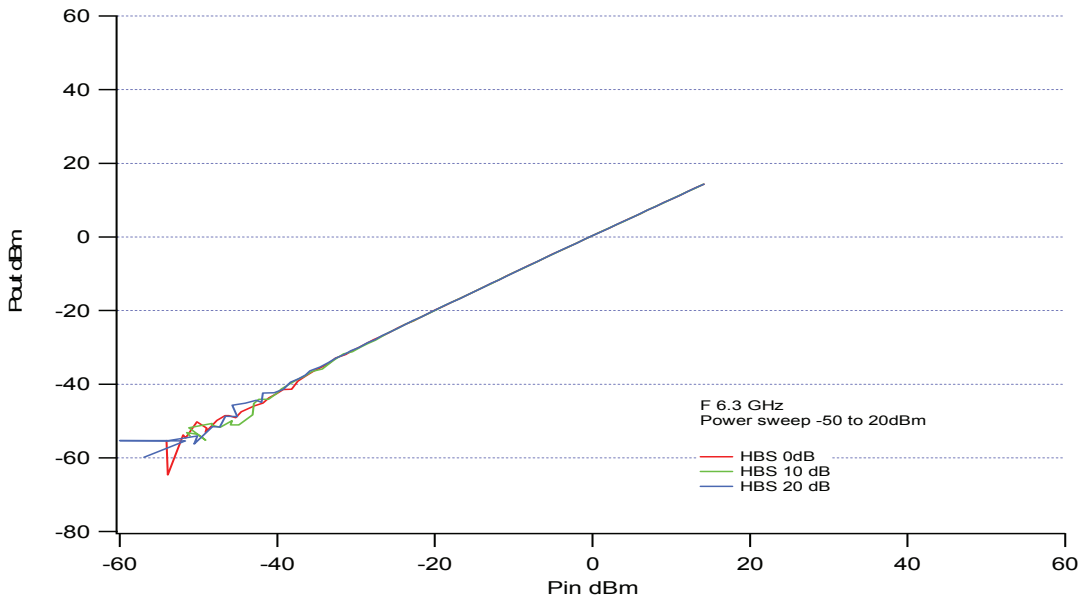

Figure 6.10: CW power sweep from -50 to 20 dBm for a frequency of 6.3 GHz using the 7mm thru standard. The result shows the comparison at the DUT output on for the HBS setting 0dB, 10dB and 20 dB.

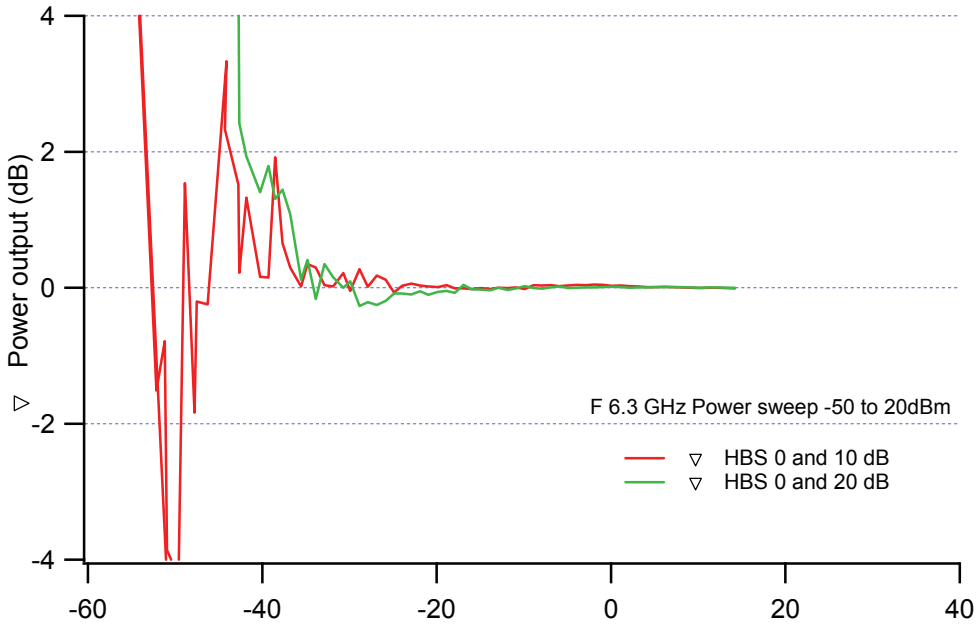

Figure 6.11: CW power sweep from -50 to 20 dBm for a frequency of 6.3 GHz using the 7mm thru standard. The result shows error comparison in term of ∇ Output power between the HBS setting 0dB and 10 dB, and between the HBS setting 0dB and 20dB.

6.5.2 Verification of the Results using a GaN 50W Transistor Device

6.5.2.1 A Comparison of Raw Travelling Wave a2 and b2

Basically, all four travelling waves (a1, b1, a2, b2) at the DUT reference planes are measured by a sampling oscilloscope. It is possible to apply classical calibration algorithms once the time samples are transformed into frequency domain via a Fast Fourier Transform (FFT). Then, an inverse FFT transforms the waveform back to the time-domain. Finally, the travelling waves are transformed to desired parameters (such as Voltage-current waveforms and performance parameter).

Figures 6.12 and 6.13 shows the travelling waves a2, b2 at the output reference plane of DUT transistor GaN device. The measurement system was performed on the single tone CW 30dBm with bias condition Vds=28 V and Ids =1029 mA. At this bias condition, the GaN generated a non-linear output, which aids observation of the demonstrated comparison of a varied HBS setting. The travelling waves a2 and b2 were taken before they were applied to the HBS S-parameter model correction and the classical error coefficient. They show the actual travelling waveform that has gone through the HBS. Since the GaN was mounted in a test fixture that provides a load 50Ω transformer matching impedances, the reflection a2 is very small in comparison to travelling wave b2. In order to increase the dynamic range of the measurement system the HBS was performed from setting 0 dB to 10 dB and, consequently, the travelling waves a2 and b2 are smaller. By comparing between the HBS settings, the b2 characteristic is found to be obviously different in terms of magnitude and distorted waveform shape. The distortion of the b2 waveform is greater due to a decrease of the fundamental. On the other hand, Figure 6.13 has shown the comparison of b2 in the frequency domain. Point A on this graph shows that the fundamental magnitude is 10 dB smaller in contrast with points B and C; the second and third harmonic magnitudes are quite similar with 1 dB difference

or less. All investigations of the raw travelling waves have led to the conclusion that the HBS behaves as required, it is found to provide the attenuation of the fundamental and, in the meantime, it preserves the harmonic content.

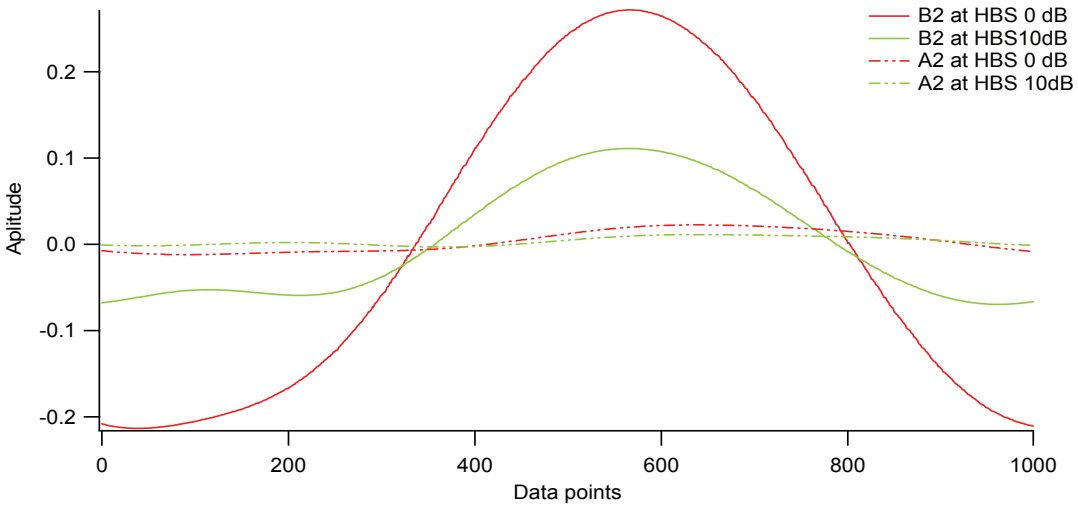

Figure 6.12: Comparison of uncorrected travelling waves b2 and a2 in the time domain with harmonic bypass structure setting 0dB and 10dB.

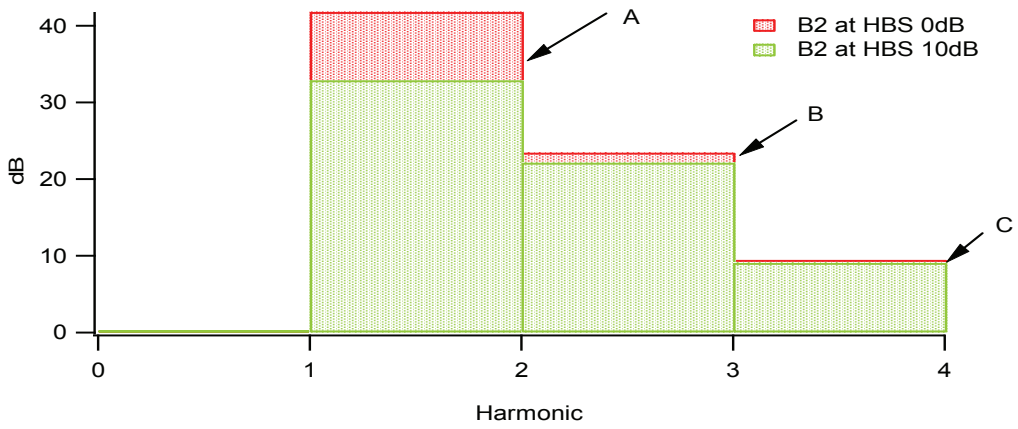

Figure 6.13: Comparison of uncorrected travelling wave b2 in the frequency domain at the DUT output of a GaN transistor device using the HBS setting 0dB and 10dB. This figure shows the selected frequency (fundamental) has been attenuated and the other frequencies (2^{nd} and 3^{rd} harmonics) have been passed through the harmonic bypass structure.

6.5.2.2 Output Correction Comparison

The repeated measurement output of DUT was performed on twelve samples over the HBS 0dB and 10dB. The measurement procedure sequence was switched between HBS 0dB and 10dB over the twelve cycles. The bias condition remained the same as the previous section at Vds=28V Ids=1029 mA. The observation was focused on a comparison of the output reference of DUT in voltage-current output, and power output and gain.

Figures 6.14 and 6.15 depict the voltage and current waveform output of the GaN. These output voltage and current waveforms were transformed from travelling wave a2 and b2, which had been applied in both the HBS S-parameter models and error coefficient. The voltage and current waveforms comparison show that the amplitude and phase of waveforms is identical. It was found above that the travelling waves a and b contain the harmonic, and this has led to the conclusion that the HBS S-parameter model is able to correct the travelling wave on the non-linear measurement.

Figures 6.16 and 6.17 depict the power output and gain comparison, respectively. Repeated measurements have shown that the power output is randomly acquired in the narrow interval of 38.950dBm to 38.965 dBm at HBS 0dB. By comparing these results point by point with HBS at 10 dB, the difference of the power output is found to be less than 0.01 dBm, and this is a good agreement with the voltage and current waveform. The gain comparison between HBS 0dB and 10dB presents the same result, the error between them is found to be less than 0.01 dB.

In summary, repeated measurement of an HBS comparison on 0 dB and 10 dB confirms that the HBS S-parameter model has a good repeatability. It also confirms that accuracy has been met on the demonstration, with power comparison acceptable at 0.01dBm or less.

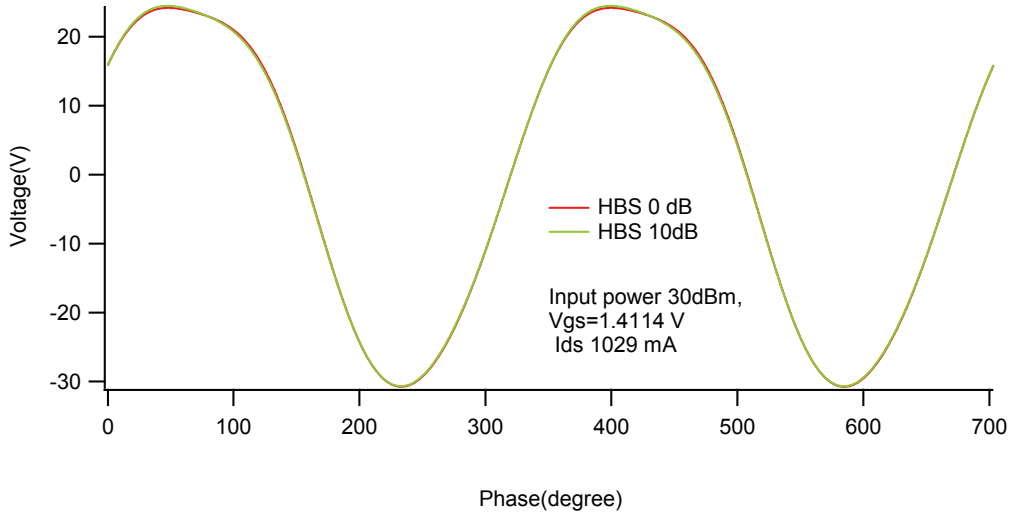

Figure 6.14: Measured output voltage of GaN transistor device

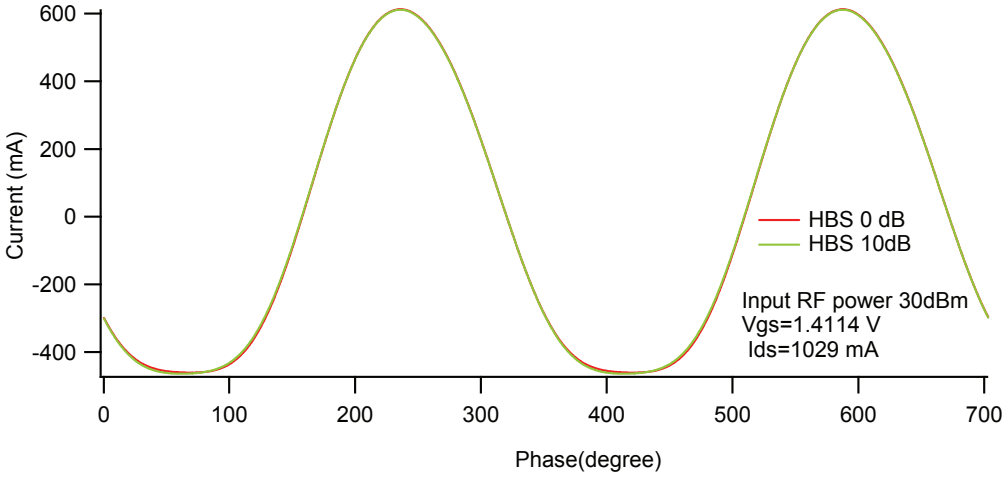

Figure 6.15: Measured output current of GaN transistor device.

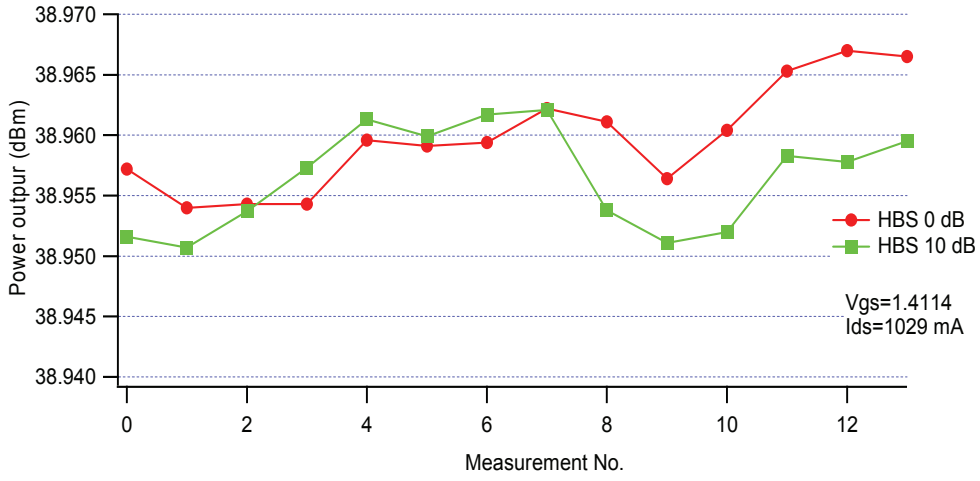

Figure 6.16: Power output comparison between the HBS settings 0dB and 10 dB when measuring a GaN device.

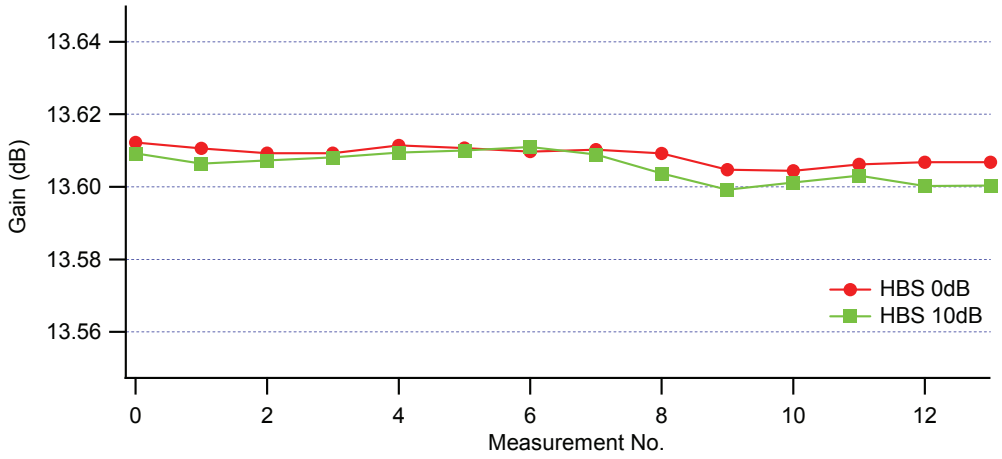

Figure 6.17: Gain comparison between the HBS settings 0dB and 10 dB when measuring the GaN device.

6.5.2.2 Power Sweep Measurement

A single tone CW power sweep was performed on the DUT, a GaN transistor device with a fundamental frequency of 2.1 GHz in a 50Ω environment. The GaN transistor was biased on the condition Vds=28 V and Vgs=1.5377 V. The power sweep range was set to be suitable with the measurement system dynamic range with respect to the HBS setting. They were -25 dBm to 36dBm 1 dBm/step res. for HBS 0dB, -25 dBm to 42 dBm 1dBm/step res. for HBS 10dB and 20 dB. To avoid a power amplifier drift affect, the power measurements were acquired according to HBS 0dB, 10dB, and 20dB before the next increased power sweep was performed. The text fixture incorporates a temperature control that keeps the transistor temperature constant throughout the power sweep; the temperature was set at 40^{o}C.

Figure 6.18 shows the output power spectrum obtained over the swept input power. The graph shows the common response of the characteristics of the GaN transistor device. The 1dB compression point was determined giving 34.19 dBm for the input power. The fundamental output power increases linearly to the compression point 34.19 dBm. The second harmonic power increase was approximately linear to saturating at the power input 27.21 dBm. It then decreases to a minimum point in the magnitude of the second harmonic at power input 32.22dBm, resulting in a power output of 13.92 dBm. The third harmonic power also increases approximate linearity to the saturation point at the power input 33.2 dBm. There is a small step appearing in third harmonic power at power input ~0 dBm, ~10 dBm, and ~20dBm due to the switching of attenuators of the power sweep (i.e. Agilent 83623B).

When comparing the power spectrum according to the HBS setting (as can been seen in Figure 6.18) it was found that the fundamental power spectrums are clearly identical.

The second harmonic spectrum is in the noise flow at power output -60dBm, until the power input reaches -20dBm above which it is starts to increases linearly. The second harmonic spectrums are still significantly different in periods of power input -20 dBm to -14 dBm, matched with power output -60 dBm to -40 dBm. After the power output reaches -40 dBm the spectrum power moves closer together. In the third harmonic, the spectrum power at HBS 0dB follows the second harmonic in the output period of -60 dBm to -40 dBm, after which it separates and increases its own curve. The third harmonic spectrums for HBS 10 dB and 20 dB appear to leave the noise floor at the power input -15 dBm, after which they increase linearly. This characteristic of the power harmonic spectrums shows that, in contrast to step attenuators, a HBS is clearly an improvement in preventing the harmonic to the noise floor. The harmonic content can emerge from system noise flow while the power output is about -30 dBm.

The maximum power input at the sampling oscilloscope was determined from the summation of the coupling factors of the directional coupler (~ 35dB), insertion losses of the HBS (~4dB, ~14dB, ~24dB), and the maximum power inputs of electrical sampling 80E20 (typically ~3dBm). As a result, the maximum power input for the sampling oscilloscope is: 35+4+3=42 dBm for HBS 0dB; 35+14+3=52dBm for HBS 10dB; and, 35+24+3=62 dBm for HBS 20dB. If the HBS acceptable error band is defined at -40dBm then the measurement system has achieved the dynamic range up to 102 dB by varying the HBS.

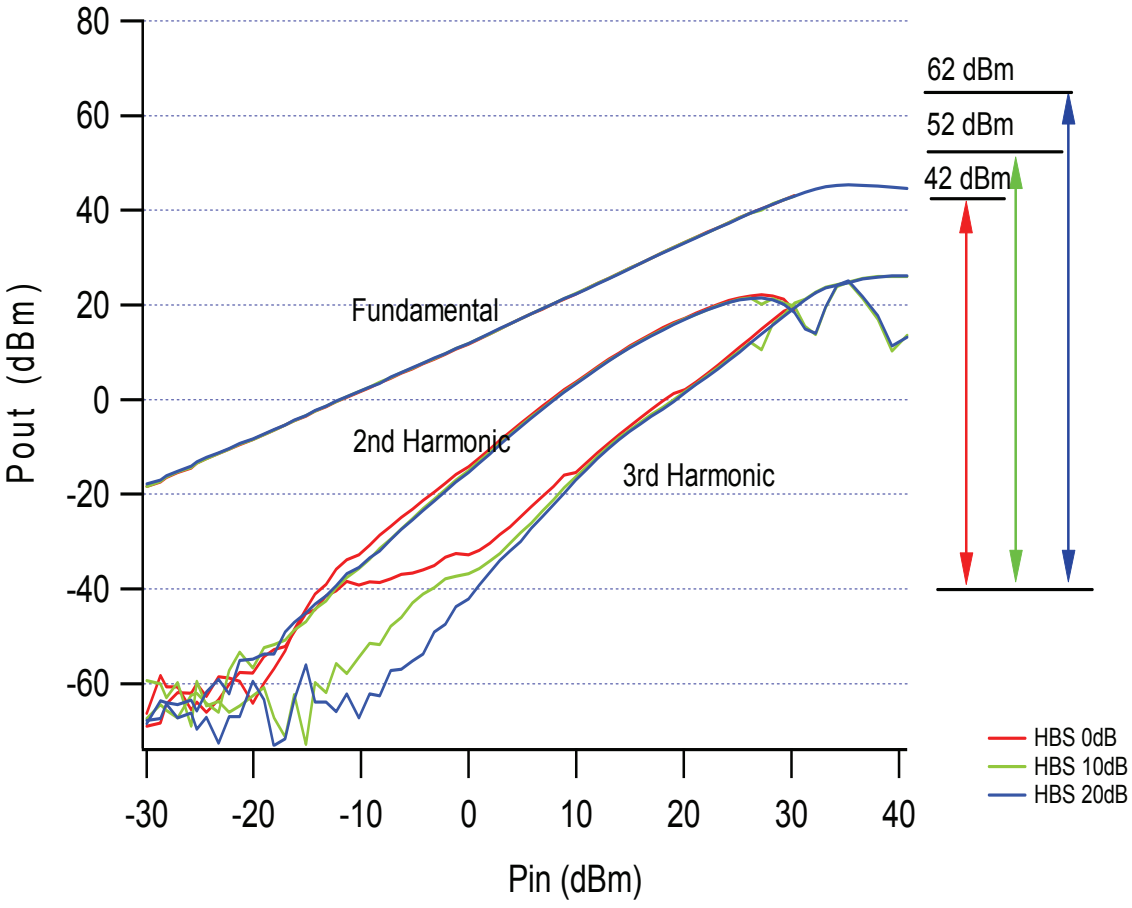

Figure 6.18: Measured CW power transfer characteristic of a GaN transistor, which is attached to a 50Ω load. The fundamental frequency is 2.1 GHz with the first 3 harmonics being measured.

6.5.2.3 Error Sources in the Measurement System

This section will detail the definition of the error sources that were found while demonstrating the measurement system as it implemented the S-parameter model. It will also detail the definition of the error sources that were found when the measurement system was launched for the first time. The definition of the error sources in this section will cover only those error sources that came from the use of the S-parameter model for an HBS implementation, it will not cover the traditional errors that commonly arise in measurement systems (e.g. systematic errors from directional imperfections in the couplers, mismatch errors from the adapters and cables, cross-talk, coaxial configuration switches losses, and mismatches). These traditional errors can be overcome through the use of an appropriate calibration technique. Although some of the error sources in this section were discussed in the measurement software configuration topic (such as errors arising from the Γ_S and Γ_L), the extended explanations are represented in terms of the measurement results errors.

Figure 6.19 illustrates the measurement result on the thru 7 mm standard. This result shows an error comparison at the output of DUT that comes from the low resolution of the HBS S-parameter. Figure 6.19 (b) shows that the voltage output waveform comparisons are absolutely different, the voltage amplitude is increasing while the HBS is set to 10 dB and 20 dB and the phase is dramatically shifting away. Meanwhile, Figure 6.19 (d) shows agreement in terms of power comparison, the power difference is more than 1 dBm. This is a symptom of an S-parameter error, which can come from the low resolution of the S-parameter, the implementation of a wrong S-parameter, or it has been caused by the unique S-parameter that has been used. If the indication error comparison is more than 1 dB then these S-parameter issues will have to be addressed.

Figure 6.20 illustrates the measurement result on the thru 7mm standard. This result shows the error comparison at the output of DUT which comes from the reflection coefficient Γ_L looking into the sampling oscilloscope Ch4, which was composed in the S-parameter model. Figure 6.20 illustrates the voltage output waveform comparison and shows a small difference in phase shift, while the amplitude is the same at each HBS setting. The symptom can be identified from the waveform shape close to its peak. Figure 6.20 (d) shows that the power comparison is usually 0.4dB to 0.8dB different. Hence, if the measurement systems comparison shows a small phase difference with equal amplitude then the reflection coefficient Γ_S and Γ_L will have to be taken into account.

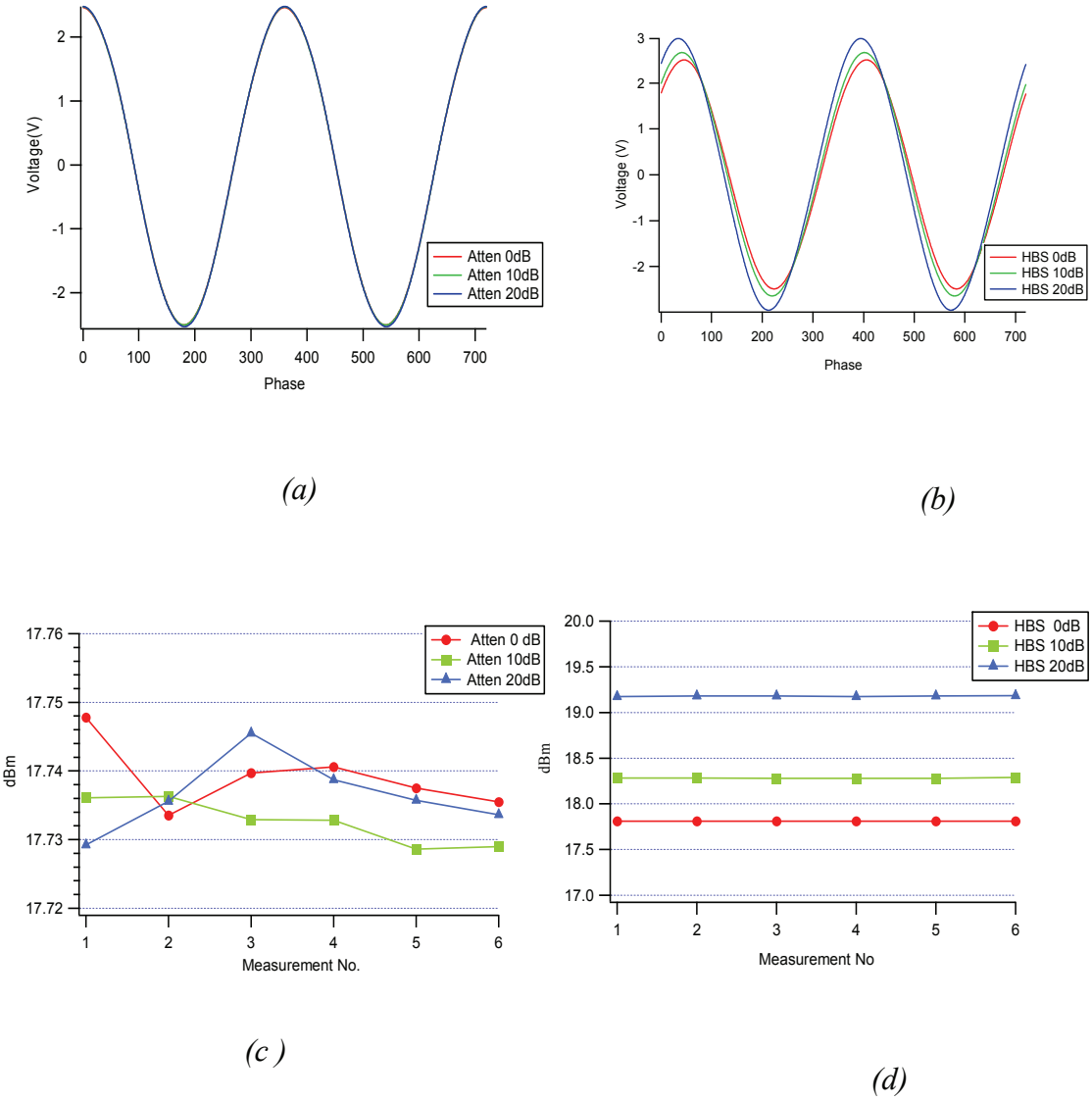

Figure 6.19: Measurement results using the 7mm thru standard showing the errors resulting from the low resolution frequency grid of the S-parameters. (a) RF input voltage on the input plane of DUT by using step attenuator; (b) RF output voltage on the output plane of DUT by using HBS; (c) Power input comparison at the input plane of DUT; and, (d) Power output comparison on out plane of DUT. As can be seen the problem occurs only on the HBS.

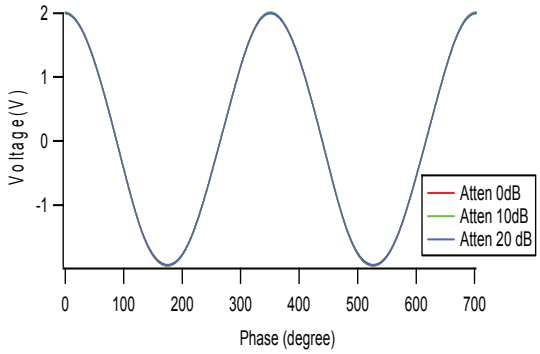

(a)

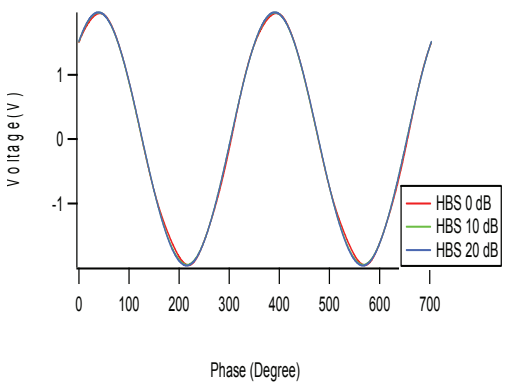

(b)

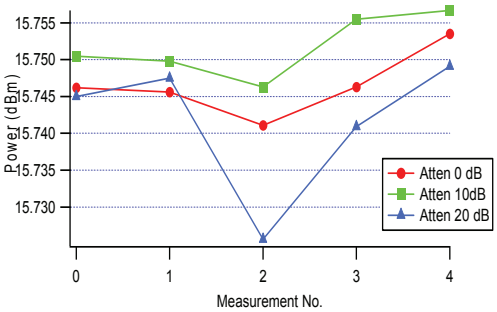

(c)

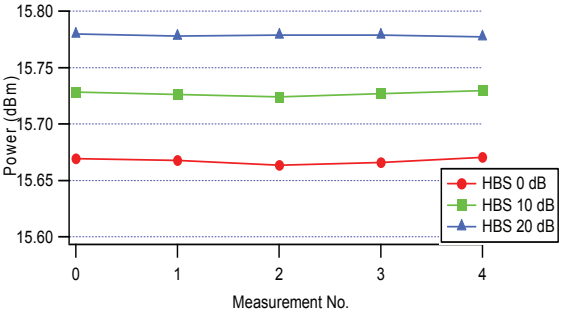

(d)

Figure 6.20: Measurement results using the 7mm thru standard showing the errors resulting from reflection coefficient Γ_S and Γ_L . (a) RF input voltage on the input plane of DUT by using step attenuator; (b) RF output voltage on the output plane of DUT by using HBS; (c) Power input comparison at the input plane of DUT; and, (d) Power output comparison on out plane of DUT. As can be seen the problem occurs only on the HBS.

Figure 6.21 depicts the measurement results of the GaN due to the error from the distortion of travelling waves a2 and b2. Figure 6.21 (a) shows what happens when the HBS was changed to 10 dB or 20 dB. It can be seen from this that the travelling wave b2 reduced in magnitude as the waveform was changed. The distortion of travelling wave b2 is identified at points A and B on the graph, this distortion happens because the decrease of the fundamental amplitude is not proportional with the harmonic. At point A on Figure 6.21 (b) the fundamental can be seen to be close to the second harmonic, while Figure 6.21 (a) shows where the waveforms have dramatically changed. Figure 6.21 (c) shows the correction voltage waveforms at the output of DUT, the key point here is that the amplitude is greater at HBS 20dB and there is a small shift in phase. When comparing the power output it was found that the power diverted from the HBS 0dB and 10dB in terms of 0.8 dB. To avoid correction errors, it is recommended that the fundamental first be determined, after which the appropriate HBS setting should be selected. It is further recommended that the fundamental not be attenuated below its harmonic content.

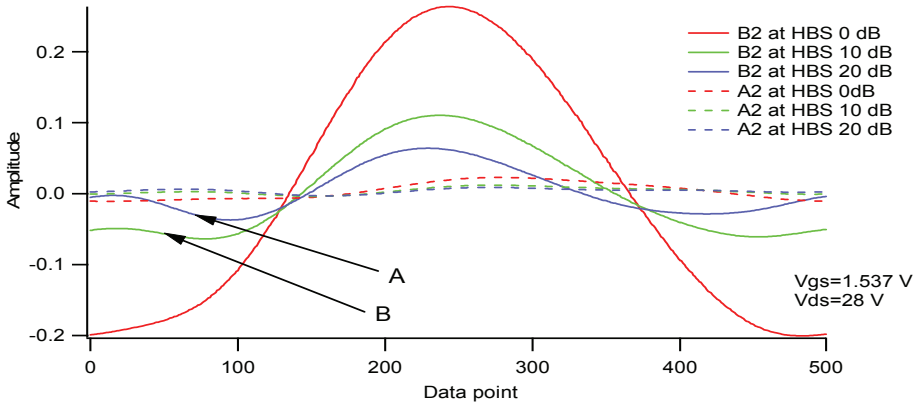
B2 at HBS 0 dB
B2 at HBS 10 dB
B2 at HBS 20 dB
A2 at HBS 0dB
A2 at HBS 10 dB
A2 at HBS 20 dB
Amplitude
0.2
0.1
0.0
-0.1
-0.2
A
B
Vgs=1.537 V
Vds=28 V
0
100
200
300
400
500
Data point

(a)

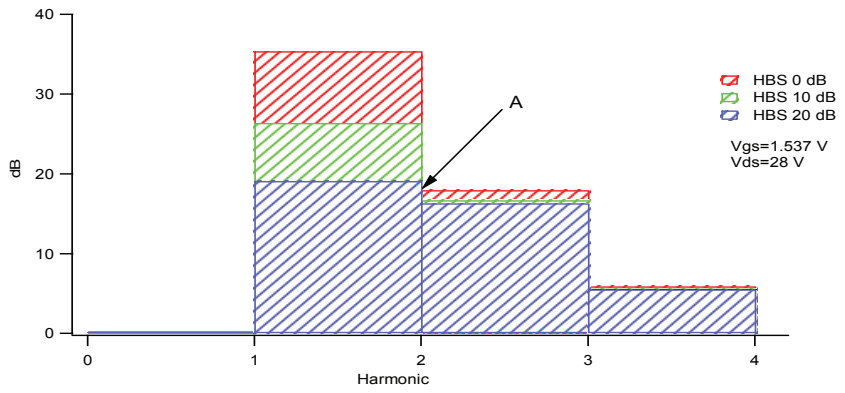
40
30
20
10
0
dB
A
HBS 0 dB
HBS 10 dB
HBS 20 dB
Vgs=1.537 V
Vds=28 V
0
1
2
3
4
Harmonic

(b)

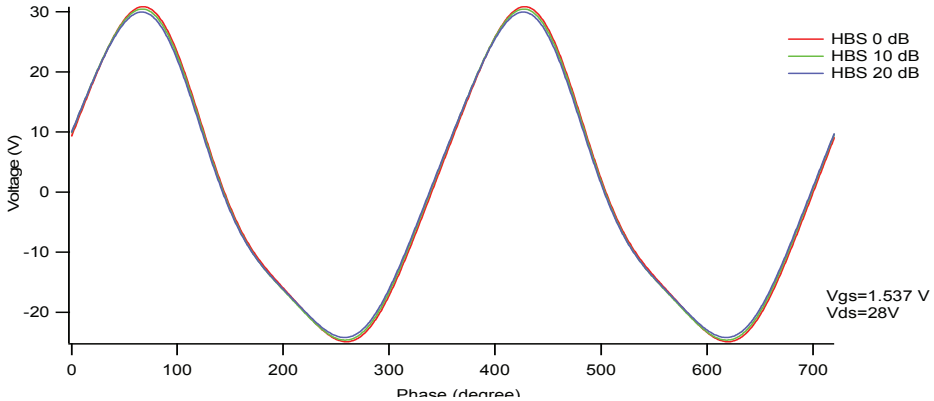

(c)

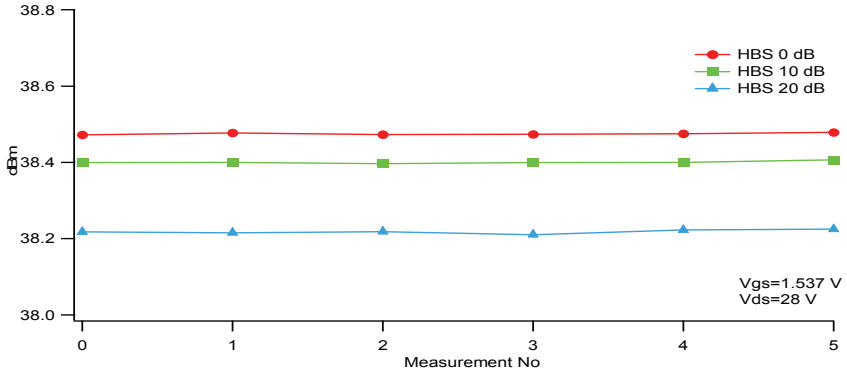

(d)

Figure 6.21 Measurement results when using a GaN device due to the errors generated from the distortion of the travelling waves a2 or b2: (a) travelling wave a2 and b2 comparison on GaN using HBS; (b) travelling wave b2 comparison on GaN using HBS; (c) output voltage comparison on HBS; and, (d) Power output comparison on out plane of DUT.

6.6 Conclusion

This implementation of an HBS instead of a step attenuator in order to demonstrate the extension of the dynamic range of a high power RF measurement system has shown that it can easily be used to overcome the problematic issue of harmonic distortion. However, the difficult high dynamic issue of the HBS S-parameter in the frequency bandwidth 0.5GHz to 3.700 GHz has to be taken into account in order to use the HBS S-parameter model because it can lead to measurement errors. Therefore, a high performance VNA should be used to characterise the HBS S-parameter. Following these qualifications, the demonstration of the measurement system on the transistor device GaN was successfully completed. The comparison of the voltage and current waveform at the output are found to be identical and the power error comparison is less than 0.01 dB. A single tone CW power sweep was performed with a fundamental frequency of 2.1 GHz; subsequently, the power spectrum comparison has also confirmed a positive result. The second and third harmonic power spectrum comparison has shown good results. The power sweep spectrum of the second and third harmonic exploits the level of the system noise floor. It confirms that the HBS does not suspend the harmonic contents. If defining the error acceptable band comparison of 0.01dB at -40dB, then the extended dynamic range of measurement system can be reached to 42dBm, 52dBm and 62 dBm for HBS 0 dB, 10 dB and 20 dB. Finally, the dynamic range of the measurement system has been achieved that reaches 102 dB when considering the fundamental frequency alone and extend to 120 dB when taking the harmonic content into account.

References

[1] D.J. Williams, "Non-Linear Measurement System and Techniques for RF Power Amplifier Design," Cardiff University, PhD thesis 2003.

[2] Tektronix, 80E01, 80E02, 80E03, 80E04 & 80E06 electrical sampling module, User Manual.

[3] Agilent, 8510C Network analyzer System operating and programming manual, 2001, 3rd edit,USA.

[4] Agilent, Agilent AN 1287-3 Applying Error Correction to Network Analyzer Measurements, 2002, Application Note.

[5] Agilent, Agilent Technologies 33320A/B/G/H 33321 A/B/D/G/H/K 33322A/B/G/H 33323K Step attenuator for OEM & System Use dc to 26.5GHz, 1990, Technical data sheet.

[6] J. Benedikt, "Evaluation and Measurement Enhancement of the High Frequency Measurement System at the University of Wales College Cardiff," Cardiff University, Cardiff, Thesis 2000.

[7] G.H. Bryant, *Principles of Microwave Measurements*. London, United kingdom: Peter Peregrinus Ltd, 1993.

[8] F.H. Raab et al., "Power amplifiers and transmitters for RF and microwave," *IEEE Transactions on Microwave Theory and Techniques*, vol. 50, no. 3, pp. 814-826, 2002.

[9] WaveMetrics Inc, *IGOR Pro Version 6.0 manual*, 1st ed. Lake Oswego, USA: WaveMetric Inc, 2007.

[10] J. F. Sevic, "Theory of High-Power Load-Pull Characterization for RF and Microwave Transistors," in *RF AND MICROWAVE CIRCUITS,MEASUREMENTS,AND MODELING*, M. Golio and J. Golio, Eds. New York, U.S.A: CRC press, 2008, ch. 7.

[11] D.M. Pozar, *Microwave engineering*, 3rd ed. New York, USA: John Wiley & Son,INC., 2005.

[12] V. Teppati, A. Ferrero, V. Camarchia, A. Neri, and M. Pirola, "Microwave Measurements Part III Advanced non-linear measurements," *IEEE Instrumentation & Measurement Magazine*, vol. 11, no. 6, pp. 17-22, December 2008.

[13] V. Camarchia, V. Teppati, S. Corbellini, and M. Pirola, "Microwave Measurements Part II Non-linear measurements," *IEEE instrumentation & Measurement Magazine*, vol. 10, no. 3, pp. 34-39, June 2007.

[14] NitroNex corporation, AN-009: Bias Sequencing and Temperature compensation for GaN HEMTs, October 2008, Appliction Note.

[15] Nitronex corporation, Gallium Nitride 28V, 50W RF Power Transistor, May 2009, NPTB00050 Datasheet.

Chapter 7

An Investigation of Harmonic Range Using HBS

Chapter 7: An Investigation of Harmonic Range Using HBS

7.1 Introduction

Information about harmonic content is crucial for the characterisation of non-linear devices (e.g. in PA design). Hence, the development of a large signal non-linear waveform measurement system is of interest to both the researcher and the design engineer of non-linear devices. However, the signal conditioning part, which is connected between the test set and receiver in the configuration of large signal non-linear waveform measurement, is difficult to develop because of the distortion of small harmonic signals. This issue arises from the signal conditioning part, which consists of fixed attenuators.

Chapters 4 to 6 have shown the implementation of a step attenuator and HBS, which has improved the dynamic range of the RF measurement system. Although the implementation of a step attenuator in the measurement system can possibly distort the integrity of the harmonic content, the use of a HBS can overcome these issues (as described in Chapter 5). In short, the incident and reflected measured waves that are obtained by the directional coupler are put into the HBS before being detected by the receiver (i.e. the sampling oscilloscope). The HBS selects the fundamental frequency for attenuation and passes the harmonic frequencies through the structure itself. In contrast to a step attenuator, the harmonic frequencies can be easily suppressed into the noise floor of receivers with a HBS, while the high attenuation of step attenuators is present in the signal path between the directional coupler and the receivers.

This chapter describes how a HBS is implemented in the RF measurement system at the input measurement plane. The aim here is to demonstrate the improvement that a HBS provides because it is able to pass through the harmonic content without introducing distortion while extending the dynamic range. The demonstration will show that the 2nd source harmonic impedance can be controlled anywhere on the smith chart

independently of HBS attenuation settings at 0 dB and 10 dB states.

7.2 Measurement System Configuration

7.2.1 System Configuration

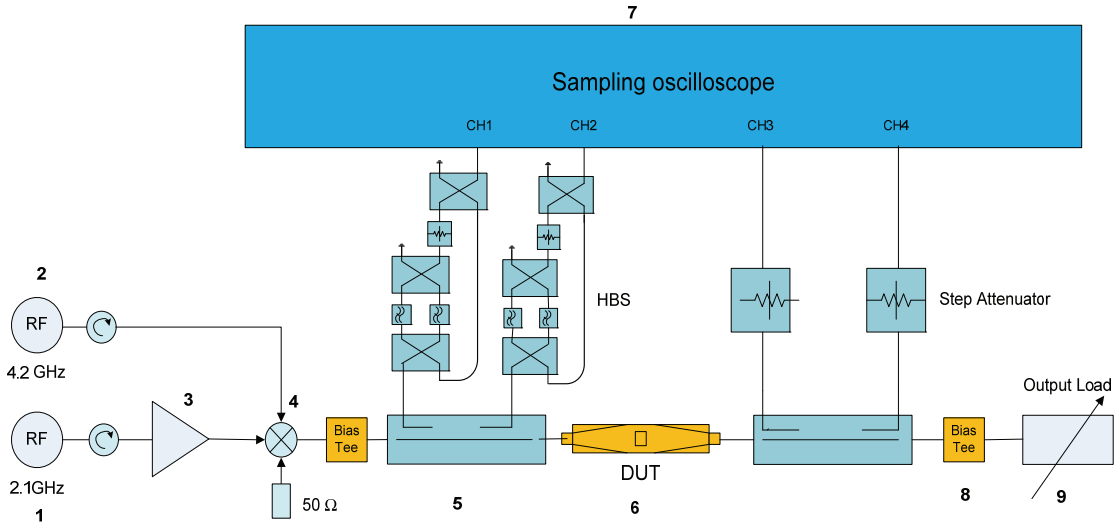

Figure 7.1: A simplified schematic diagram of RF measurement system.

The configuration of the high power RF measurement system, which is shown in Figure 7.1, is similar to the measurement system that was described in Chapter 6. There are, however, a few significant differences in the signal excitation sources, the adjustable output load, and the location of the HBS. The second harmonic signal source is combined with the fundamental signal source by triplexers, which provide the combined signal for exciting the DUT. The crucial parts of the demonstration have focused on the HBS that takes place between the direction coupler and the sampling oscilloscope, which deals with the measured incident and reflected travelling wave from the DUT at the input of the measurement plane. Meanwhile, there are two step attenuators which have been installed on the output measurement plane that act on the incident and reflected travelling wave from the output measurement plane. The other setting parts of the measurement system are:

1. RF Sweeper - An Agilent 83623B sweeper providing a frequency range from 10MHz to 20GHz (maximum output 20dBm).This sweeper is used as an CW source for this measurement system;

2. RF Signals Generator - An Agilent N5182A MXG vector signal generator provides a frequency range from 100 kHz to 6 GHz, a resolution of 0.01Hz, and a phase offset 0.1^{o} increment. This signal generator is used to generate the second harmonic source at 4.2 GHz.

3. Narrow Band Power Amplifier - The operating band of this narrow band power amplifier is 2.110 to 2.170 GHz, providing a gain of up to 40 dB (maximum output power 51dBm). This amplifier is used to amplify the signal power from the RF sweeper;

4. Triplexers - This provides a frequency range at port 1 of 2.1 to 2.2 GHz, at port2 of 4.2 to 4.2 GHz, and at port 3 of 6.3 to 6.6 GHz. In this measurement setup, port 3 was terminated by 50 Ω.

5. Directional Coupler - This is a four port directional coupler that is able to capture the incident and reflected signal separately, providing a coupling factor of 35dB with broadband frequency;

6. DUT - This is an extensive transistor device GaN Gee model CGH 40025, providing a maximum average output of power at 3dB, a gain compression (typically of 25W), and which is optimised for broadband operation from dc -4.0 GHz. The GaN transistor is mounted in a test fixture and it is cooled by a fan;

7. *Sampling Oscilloscope* - Tektronix CSA8000 with 80E02 sampling module;
8. *Bias Tee* - These are made up of two 90^{o} hybrids joined together in a back to back configuration, they provide the external DC power supply to the DUT; and,
9. *Mechanical tuner load.*

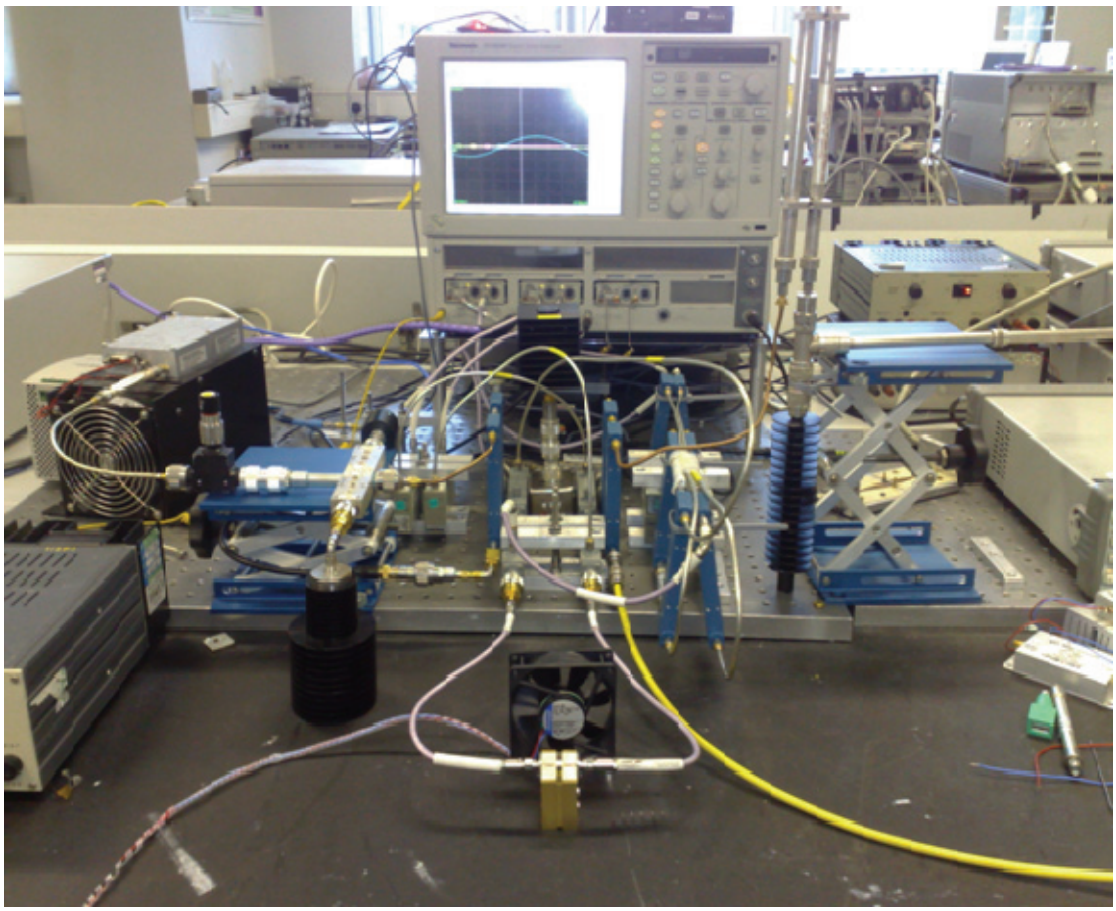

Figure 7.2: Measurement system utilised for the investigation of the resulting harmonic dynamic range when using HBS.

7.2.2 Measurement Software Configuration

The software configuration is the same as that which is detailed in Chapter 6. The equation for compensation of incident and reflection measured waveforms are identical, as re-stated below in Equation (1), while the correction procedure is re-stated below in Figure 7.3.

$$a0 = \left[\frac{1-S22\Gamma_L}{S21} - \frac{\Gamma_S\Gamma_L S12S21}{S21(1-S11\Gamma_S)}\right] a'0 \qquad (1)$$

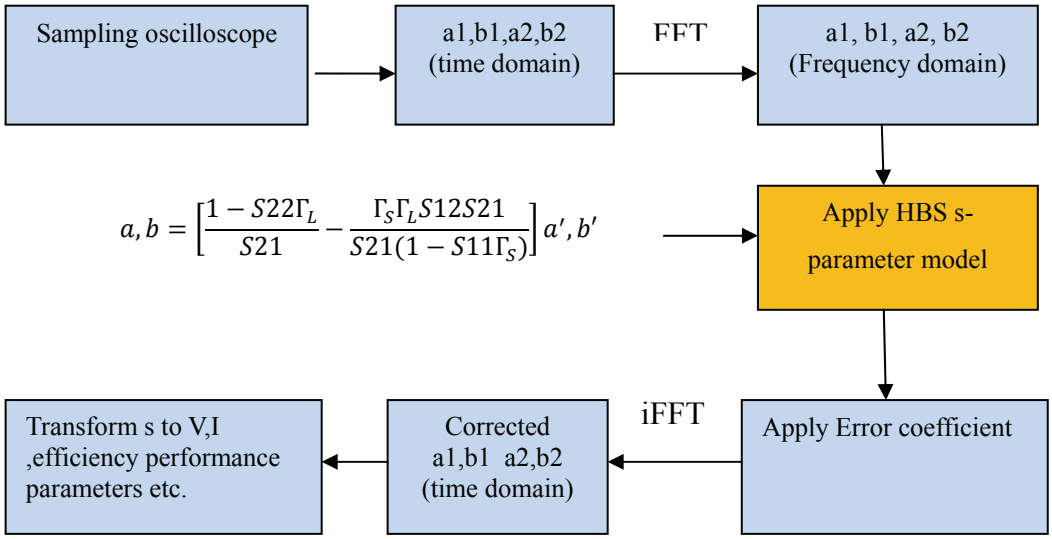

Figure 7.3: A simplified schematic diagram of the measurement software configuration for the HBS.

An Agilent PNA-X Network Analyser N5242A (with a frequency span of 0.5 -20 GHz and a resolution data point of 160,001) was found in this demonstration to cope much better with the highly dynamic ripple pattern of the HBS behaviour on the frequency band of 0.5-3.7 GHz. It is possible to move the ripple pattern of the HBS apart from fundamental frequency by changing the length of a link bypass cable, which changes the phases of the harmonic bypass waveform. Therefore, the ripple of the fundamental frequency has been decreased by the combined signal waveforms at the output of the HBS. In addition, these HBS S-Parameter models were modelled into the full S-Parameter model by using the Polynomial data fit function approach (as described in Chapter 3); the procedure process is similar when using the step attenuator model.

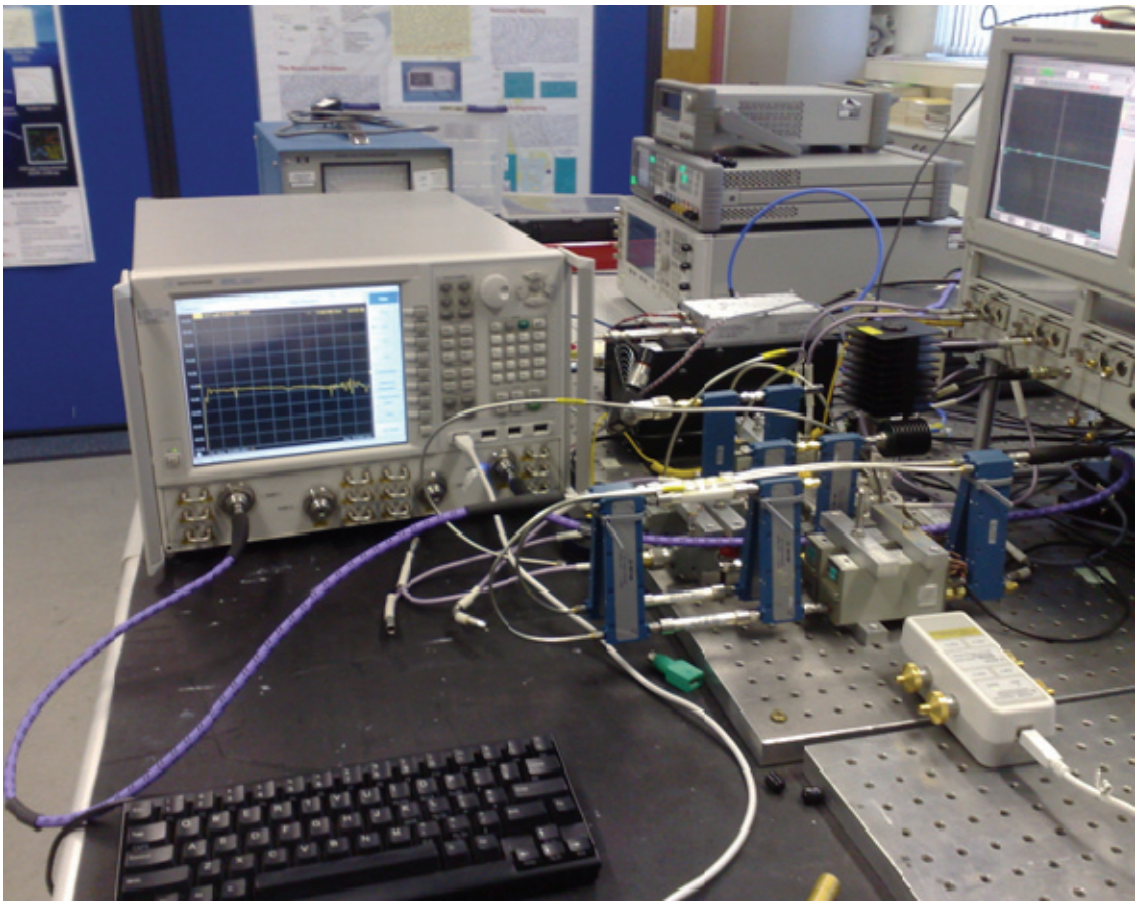

Figure 7.4 Implementation of HBS S-parameters into the measurement software by PNA-X Network analyser.

7.3 System Calibration

A full calibration was conducted on this measurement system, which includes the small signal S-parameter calibration, and power meter and phase calibration. The calibration procedure followed the same calibrations that were used in Chapter 6. The calibration of this measurement system was conducted at the HBS and step attenuators setting state 0dB.

In this demonstration system the calibration procedures are performed using small signal S-Parameter calibration on TRM- short 3.5 mm using the Maury standard, with a frequency grid of 2.1-11.9 GHz at 0.7 GHz step resolution. This frequency bandwidth covers the fundamental 2.1 GHz and goes up to the 5^{th} harmonic. The sampling oscilloscope is set on average 1024 and the data point sampling is 1024. Calibration at low frequencies uses the SOLT with the Agilent 3.5 standard calibration kit. For absolute calibration the power setting was 7.0 dBm, the intention was to reach a power output of nearly 3 dB at sampling oscilloscope ch2.

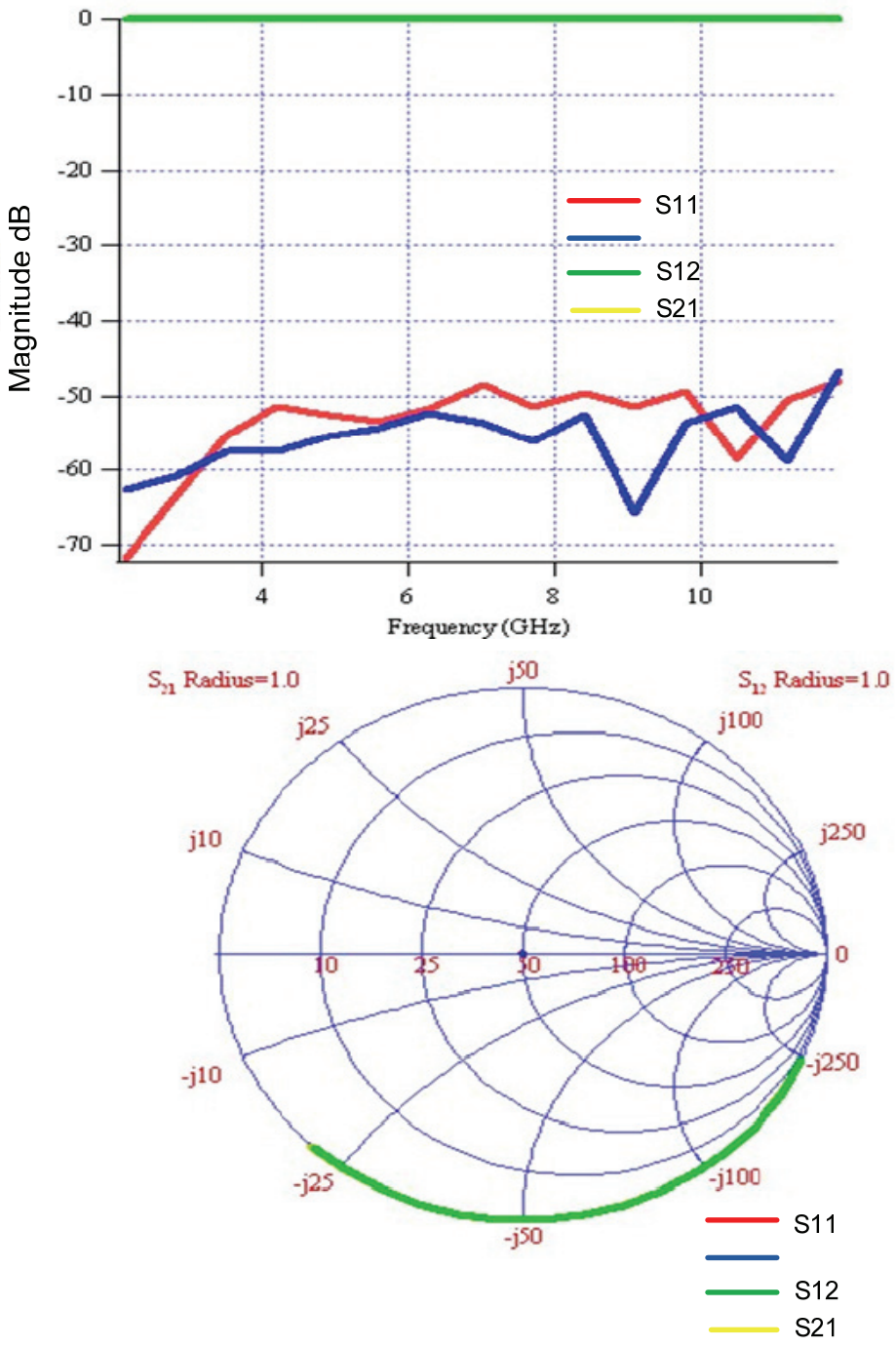

Figure 7.5: Log chart and Smith chart of S-parameter measurements on a thru 3.5mm standard verifying the small signal S-Parameter calibration for HBS.

7.4 Measurement Procedure demonstrating the harmonic range when using the HBS

The basic verification of the calibration is done on the thru standard once the calibration has been completed. The verification procedure that is used is similar to that used in Chapter 6. The measured waveforms are compared between a HBS 0dB calibration state and HBS 10dB and they show good results. The thru verifications have also been done with each frequency (i.e. fundamental 2.1 GHz, 2^{nd} and 3^{rd} harmonic frequencies).

A GaN Gee model CGH 40025 (25 W) is placed as a DUT in this demonstration. The GaN device biased the DC power through bias tees; the bias point was set at Vg=-3.10 V, Vds=28V, and Ids=203 mA.

The fundamental frequency CW source signal excitation applies to DUT at 2.1 GHz, where the power output setting is at 32 dBm. The mechanical manual tuning of the output impedance was proceeded to reach the maximum possible output.

In order to move the 2^{nd} harmonic source impedances, the second signal source of 4.2GHz is varied according to the sequential choice of 2^{nd} input signal magnitude (i.e. at -20, -10, -5, 0, 1, 2, 3 and 7dBm). This increase of 2^{nd} signal magnitudes allows the 2^{nd} impedance loci to be expanded from the centre of the Smith chart. In the same manner, the varying phase was performed between 180^{o} to -180^{o} at a resolution of 10^{o}/step. The result was that the 2^{nd} input harmonic impedance was circulated around the Smith chart while the amplitude is maintained at a constant level.

The experiment was conducted on the compared loci of the 2^{nd} input impedances, while the HBS setting was present between HBS 0dB and HBS 10dB. To perform this task, the Gee GaN was biased and CW signal was applied on the conditions that are described above. After confirming the maximum possible output power, the 2^{nd} signal was injected into the DUT though the triplexers. The procedure started with injecting the 2^{nd} signal with the power level set at -20dBm. The varying phase of the 2^{nd} signal

was then performed at a resolution grid of 10^{o}/step. The HBS was switched between 0dB and 10dB by the measurement software at each state of the changing phase. Both input and output signal from the DUT was instantaneously taken into the measurement software. The process was repeatedly performed by increasing the power of the injected 2^{nd} signal until it reached the required power setting at 7dBm. The results of these experiments will be discussed in the next section.

7.5 Demonstration Results

In order to show an improvement of the harmonic dynamic range, the results of the demonstration from Chapters 4 and 6 have been plotted on the same graph (as shown below in Figure 7.6). Although the two demonstration environments are unlikely to be identical due to the measurement configuration, the result clearly shows an improvement of the harmonic dynamic range. By using a HBS approach; the harmonic can be detected above -60dBm. This is in contrast to the step attenuator approach, which shows a curve until the power output level reaches -40 dBm. This result demonstrates that the HBS approach does not suppress the harmonic content as much as the step attenuator approach does.

To investigate this point further, the HBS was installed in the input side of measurement plane. The aim of this is to investigate the effect on harmonic content easily by applying a controlled 2nd harmonic generator as the input excitation source.

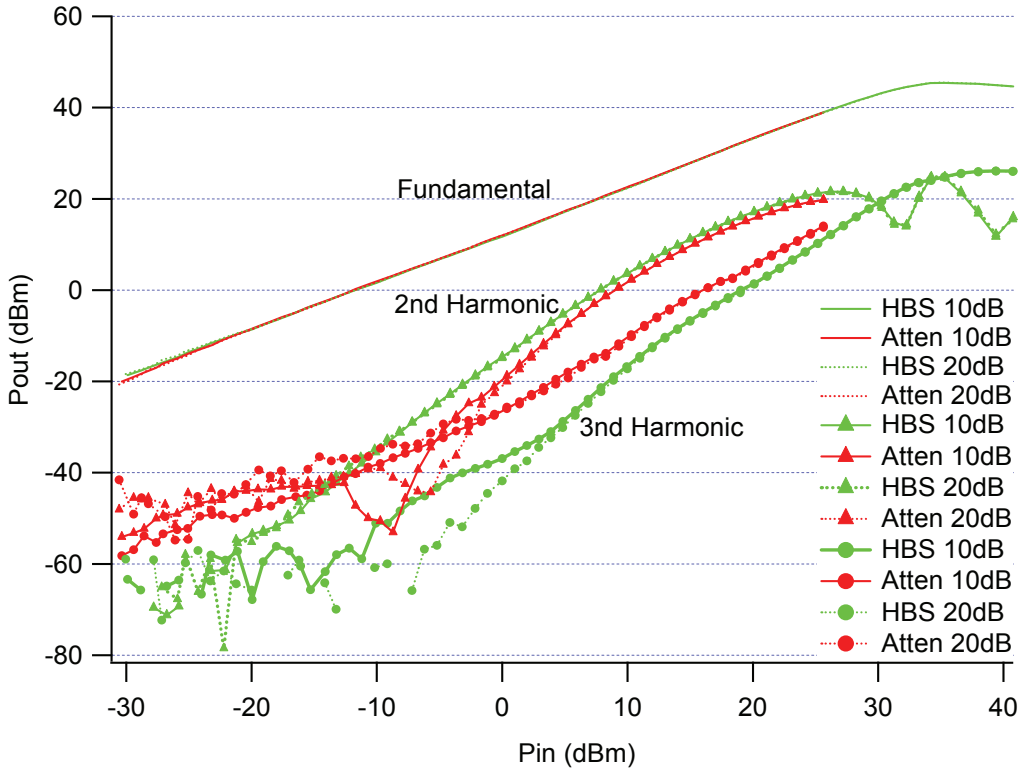

Figure 7.6: GaN power sweep comparisons between Step attenuator approach and HBS approach (including the results from Chapters 4 and 6).

Figures 7.7 and 7.8 illustrate the results of a comparison of the loci of 2nd input source impedance between HBS 0dB state and HBS 10dB when this measurement procedure is followed. The harmonic content can be explored through the loci of harmonic impedance. This experiment was focused on 2nd impedances that can be used to indirectly investigate the magnitude and phase of the harmonic content.

The results in Figure 7.7 below show the implementation of a loci circle of 2nd harmonic

impedances according to its magnitude and phase. The inside circle is the impedance locus circle of the -20dBm 2nd harmonic signal input. The other circle is the expanding relation to its magnitude at -10, -5, 0, 1, 2, and 3dBm. At the same magnitude, the locus became a track circle by varying the phase of the 2nd harmonic input signal. When doing the investigation, the comparison of impedance due to HBS state between 0dB and 10dB clearly shows the same loci on the Smith chart. This is caused by the HBS, which can properly pass harmonic content through its structure.

These results can be explained by using the characteristic curves of the HBS's S-parameter model. This shows that its S21 or S12 are identical in frequency beyond the cut-off frequency of the LPF. Therefore, it can be predicted that the 2nd harmonic impedances are not influenced by the HBS state. Therefore, these impedances do track an identical locus on the Smith chart. This demonstrates that the HBS does not suppress the harmonic content and this links it to the improvement of the dynamic range of harmonic while the HBS is in a varying state.

In conclusion, the results of this experiment show that the HBS approach can improve the harmonic range. The 2nd harmonic impedance locus has been found to follow the same track between the setting of HBS 0 dB and 10 dB, which is a good result.

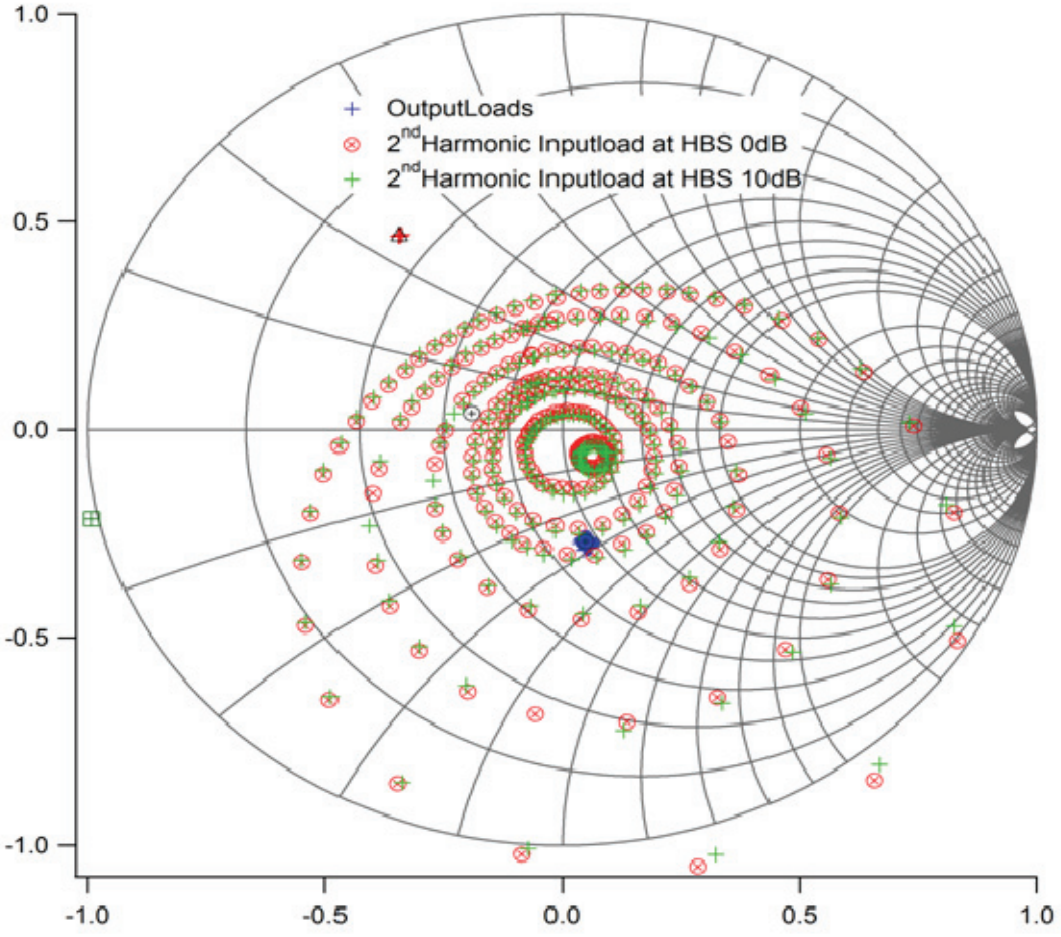

Figure 7.7: A comparison of loci of 2nd input source impedance between HBS 0dB state and HBS 10dB.

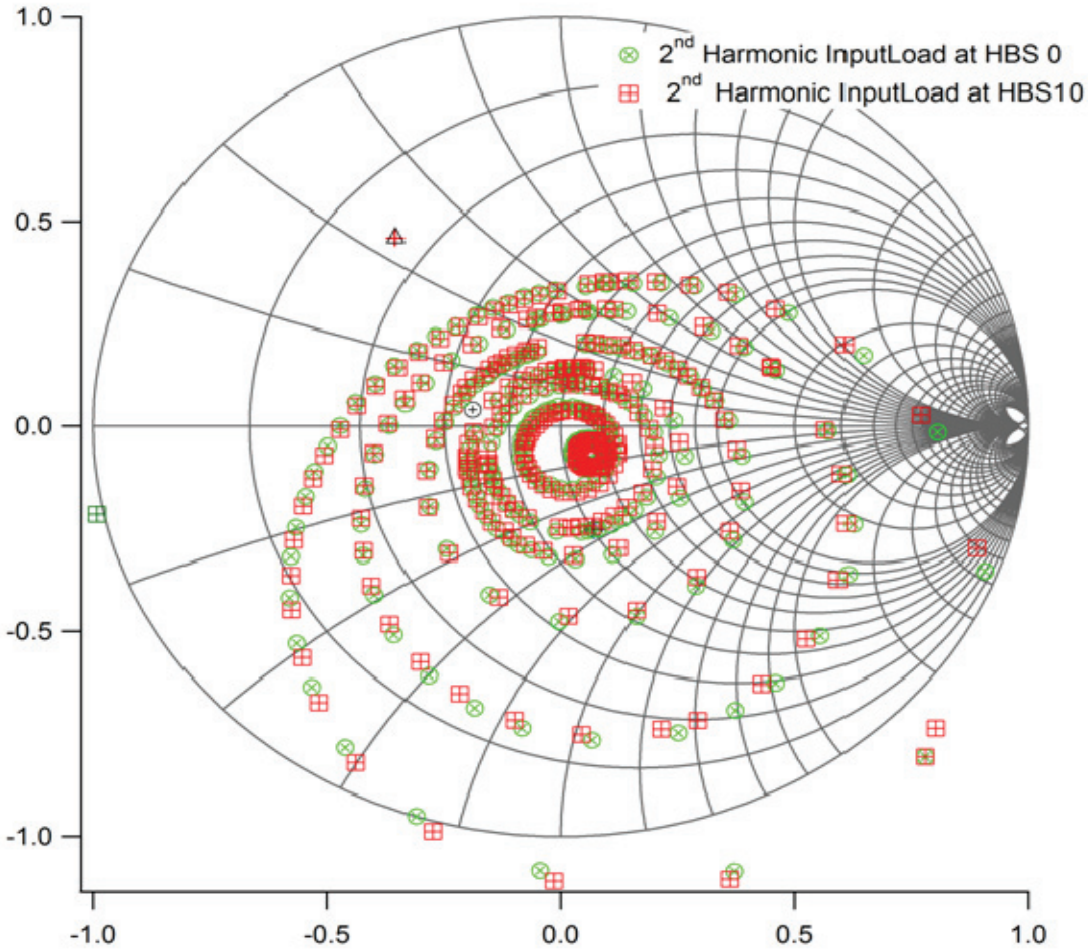

Figure 7.8: A comparison of loci of 2nd input source impedance between HBS 0dB state and HBS 10dB; including the interpolation errors within the HBS's S-parameter model (it is important to note that the error is increasing if the measured frequency is in the cut off frequency of LPF).

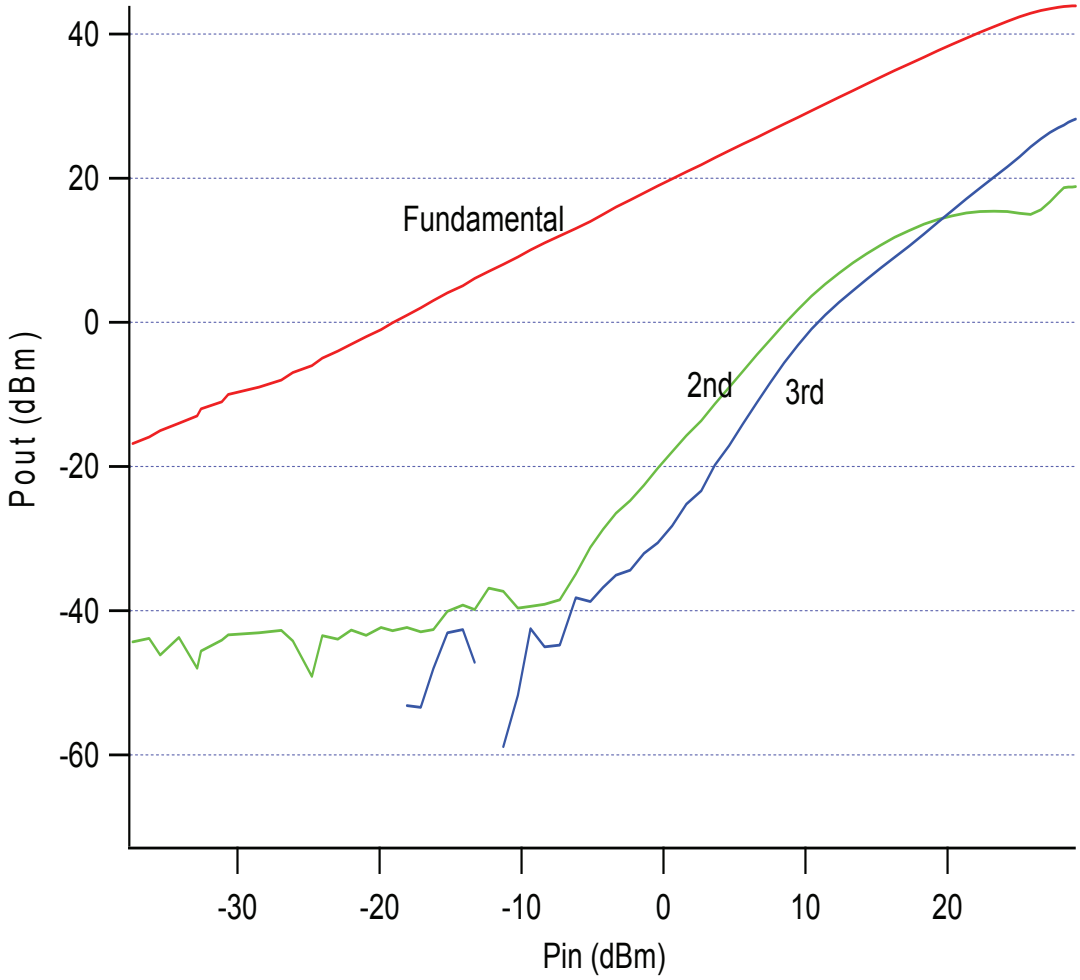

Figure 7.9: A CW power sweep on GaN CGN 40025 at fundamental 2.1 GHz bias with a point Vg -3.10 V, Vds 28V (the power sweep was performed to validate that the configuration measurement system on GaN CGN 40025 was working properly).

7.6 Conclusions

This chapter has described the results of an investigation of harmonic range using HBS. The investigation was conducted in the measurement of a GaN device. The measurement system was arranged with HBS at the input side of the DUT reference plane, which involved the forward and reflected signal from the DUT. The 2^{nd} harmonic source was combined with the CW fundamental frequency source, which allows the measurement systems to investigate the input 2^{nd} harmonic impedances on an Smith chart. Consequently, the 2^{nd} harmonic impedance loci were compared between the HBS state at 0 dB and 10 dB. This comparison aimed to show the improvement of dynamic range of a harmonic frequency (i.e. the HBS should not suppress the harmonic range according to the variance of the HBS state). The results showed that the HBS approach has achieved the expected improvement.

References

[1] Z. Aboush et al., "High power active harmonic load-pull system for characterization of high power 100-watt transistors," in *Microwave Conference, 2005 European*, 4-6 Oct. 2005, p. 4 pp.

[2] Z. Aboush, J. Lees, J. Benedikt, and P.J. Tasker, "Active Harmonic Load-Pull System for Characterizing Highly Mismatched High Power Transistors," in *Microwave Symposium Digest, 2005 IEEE MTT-S International*, 12-17 June 2005, p. 4 pp.

[3] J. Benedikt, "Evaluation and Measurement Enhancement of the High Frequency Measurement System at the University of Wales College Cardiff," Cardiff University, Cardiff, Thesis 2000.

[4] J. Benedikt, R. Gaddi, P. J. Tasker, and M. Goss, "High Power Time-Domain Measurement system with Active Harmonic Load-Pull for High-Efficiency Base-Station Amplier Design," *IEEE Trans. On Microwave Theory and Technique*, vol. 48, pp. 2617-2624, 2000.

[5] D.J. Williams, "Non-Linear Measurement System and Techniques for RF Power Amplifier Design," Cardiff University, PhD thesis 2003.

[6] T. Williams, J. Benedikt, and P. J. Tasker, "Experimental Evaluation of an Active Envelope Load Pull Architecture for High Speed Device Characterization," in *Microwave Symposium Digest, 2005 IEEE MTT-S International*, 12-17 June 2005, pp. 1509-1511.

Chapter 8

Conclusions and Suggestions for Further Work

Chapter 8 - Conclusions and Suggestions for Further Work

8.1 Conclusion

The motivation of this thesis was to develop a high power RF measurement system. For many years the Centre of High Frequency Engineering, Cardiff University has been developing high power RF measurement systems, which are essential in the characterisation of a DUT in real and large signal excitation environments. Although many RF applications have been designed and they have had a number of advantages, conveniences, and reliabilities, there are still many challenging issues that need to be addressed in this field (e.g. the extension of dynamic range).

This research project has been able to make two contributions to our understanding of high power RF measurement systems. Firstly, the implementation of a step attenuator incorporated with its S-parameter model in the measurement system is able to extend the dynamic range. Secondly, the improvement of the step attenuator approach by using an HBS is able to extend the dynamic range of the measurement systems without introducing distortion of measured harmonic content.

To achieve these tasks, the existing RF measurement system software has to modify some script procedures in order to allow the system to control the step attenuator and/or HBS. This modification required the correction of the measured incident and reflected waveforms of the DUT, which was followed by applying the error coefficient of the measurement system. The measurement results were then processed for display.

The correction of measured waveform has been achieved by applying the step attenuator's (or HBS's) S-parameter model to compensate the raw measured incident or reflected waves. These S-parameter models were derived from full, two port, small signal S-parameters. This includes the influence of the impedance mismatch that appeared in terms of reflection coefficients. These reflection coefficients can be

obtained from either a directional coupler and receiver or a sampling oscilloscope. The reduced form of the S-parameter model can be measured by ignoring the impedance mismatch assumption. Consequently, in this study, the S-parameter model has no reflection coefficient and the final model is in terms of S21 alone. This is a simple form and it is easy to implement, although it has less accurate. Consequently, the choice of model has to carefully consider on applications.

In order to implement the S-parameter model, the full two ports S-parameter data of either step attenuator or HBS have to be imported into the measurement system software, where these data are produced in a useful electronic format. This has been done with statistical data processing, such as polynomial function fit. Consequently, the measurement software would provide the available frequencies grid, amplitude and phase of the S-parameters data. It is essential to access the setting state data of either the step attenuator or the HBS when forming an S-parameter model. The reflection coefficient of both directional couplers and receiver sampling oscilloscope has been similarly managed.

The accuracy of the new implementation measurement system is influenced by the accuracy of the high-resolution data point of the S-parameter model. To reach acceptance accuracy, either a high efficiency VNA or PNA was used to determine the S-parameters. Although the step attenuator's model can be modelled by using a VNA HP8510 at 801points, the HBS's S-parameters model needs more dense data points to cope with its characteristic ripple curves, especially at the fundamental frequency.

The high precision and high repeatability approach of the step attenuator to extend dynamic range of high power RF measurement systems has been demonstrated in this study. It has achieved a good success on the measurement of the GaN transistor device. In order to use the step attenuator S-parameter model, the S-parameter characterisation of the step attenuators was performed. Consequently, the step attenuator characteristics are included as a data sheet. The validation of step attenuation's repeatability has been achieved for magnitude 0.03 dB and for phase 0.2 degree over the interested frequency

band 45 MHz to 12 GHz.

Four step attenuators were implemented in the measurement system. They take place between the direction couplers and sampling oscilloscope. The step attenuator S-parameter model was imported into the measurement software. The measurement system was then calibrated with the step attenuator state at 0dB. The first validation of the measurement system was performed with a 7mm thru standard, which became a DUT. By performing the CW power sweep at frequency 2.1 GHz, 4.2 GHz and 6.3 GHz, it was possible to compare the output power spectrum of the DUT at each step attenuator state. Consequently, the corrected output power spectrum for step attenuator value 10 and 20 dB has been successfully achieved. However, this compensation for step attenuator is invalid in case the attenuation is sufficiently large to push the travelling waves a or b, which are detected at the receivers, into the system's noise floor.

Additionally, the second validation of the measurement system was performed with a GaN transistor device, which was utilised as an nonlinear DUT. The demonstration of the measurement system on the transistor device GaN was successful. The comparison of the voltage and current waveform at the output of DUT are obviously identical. In addition, it shows that the power error comparison is an average of 0.02 dB. It was further demonstrated that the single tone CW power sweep was performed with fundamental frequency 2.1 GHz. Consequently, the power spectrum comparison has also confirmed a positive result. The second and third harmonic power spectrum comparison has also shown the good results. The power sweep spectrum of second and third harmonic exploits the level of the system noise floor. It shows a limitation of the step attenuator when being used at the high attenuation state since it causes a distortion of harmonic contents. It is critical to determine the power harmonic level before deciding a suitable step attenuator state; otherwise, they could suspend harmonic information and introduce the error correction via the step attenuator S-parameter model. If the error acceptable band comparison is defined at 0.01dB and -40dB then the extended maximum power level of the measurement system at the fundamental frequency can be increased to 38 dBm, 48 dBm, and 58dBm for step attenuator state of

0dB, 10dB, and 20dB, respectively. The whole dynamic range of measurement system can reach value up to 98 dB.

Furthermore, the HBS was implemented to improve the harmonic dynamic range that was suppressed by the step attenuator. The solution was found in designing a new structure that is able to bypass the harmonic from the step attenuator. This has been achieved by using filters and 90^{o} hybrids. Two 90^{o} hybrids were connected together in a back-back configuration. This configuration allows a diversion of the harmonic signal through an isolation port without passing a step attenuator. The third functionality of the 90^{o} hybrid is the recombination of the harmonic signal and an attenuated fundamental. An attenuated fundamental comes from the step attenuation, where it is connected between the second and third 90^{o} hybrid.

The demonstration of a HBS in the measurement system has been done on the measurement of a transistor GaN, the results of this demonstration show good success. The work of the HBS demonstration followed a similar step attenuator approach. Meanwhile, the HBS S-parameter characterisation has been achieved. The functionality of the HBS has been verified on an ADS simulation. A harmonic balance simulation confirms that: the signal input can be divided into two frequency bandwidths; the HBS can avoid harmonic distortion while the fundamental spectrum has been attenuated successfully by the step attenuator. An S-parameter simulation shows the S-parameter data of the HBS, which helps to understand the behaviour of the HBS. The drawback of an HBS has been found to be its limitation of blocking the fundamental in between the isolation port 4 of hybrids H1 and H3, which are linked together only for harmonics. Although a solution has found by inserting a HPF to stop the frequency band below the harmonic, the solution is not implemented in this study because the existing HBS are still suitable in the current measurement system. The HBS S-parameter data has shown good agreement between simulated S-parameter data and the measured S-parameter data. The measured S-parameter data of HBS will proceed in the form of the S-parameter model and the data are stored in the IGOR binary format.

The implementation of an HBS instead of step attenuator in the demonstration of the extension of the dynamic range of a high power RF measurement system has clearly shown that it has overcome the distortion of harmonic issue. In order to use the HBS S-parameter model, the high dynamic problem issue of HBS S-parameter in frequency bandwidth 0.5-3.700 GHz has to be taken into account because it clearly leads to a measurement error. Therefore, the high performance of a VNA should be used to characterise the HBS S-parameter. Additionally, the demonstration of the measurement system on the transistor device GaN was successful. The comparison of the voltage and current waveform at the output are obviously identical. It also shows that the power error comparison is less than 0.01 dB. It further demonstrated that the single tone CW power sweep was performed with fundamental frequency of 2.1 GHz. Consequently, the power spectrum comparison has also confirmed a positive result. The second and third harmonic power spectrum comparison has shown good results. The power sweep spectrum of the second and third harmonic exploits the level of the system noise floor, and the results indicate that the HBS does not suppress the harmonic contents. If the error acceptable band comparison is defined as 0.01dB, then the extended maximum save power level of the measurement system reaches 42 dBm, 52 dBm and 62 dBm for HBS 0 dB, 10 dB and 20 dB, respectively. The whole dynamic range of the measurement system can achieve up to 102 dB when considering the fundamental frequency alone and extend to 120 dB when taking the harmonic content into account.

8.2 Suggestions for Further Work

8.2.1 A Fully Automated Independent Step Attenuator Control Switch

At present, the IGOR script procedure of the measurement system software defaults to independent setting control switch circuits of the step attenuator on the input side and output side, it does not provide for the individual control of the step attenuator. This

control method has a disadvantage while it is dealing with different amplitudes of measured signal. In fact, the incident and reflected waveforms exits from DUT are quite different in terms of amplitude, which depends on the mismatch load condition or on the setting environment (e.g. source pull or load pull operation). Basically, the reflected waveforms are smaller than the incident waveforms. In practice, the measurement system could give the individual receiver dynamic range for the incident and reflected signal by taking advantage of the HBS approach. To take advantage of this, the controlling circuit should respond correctly according to the amplitude of the waveforms.

It is possible to design an external detected electronic circuit that can determine the amplitude of the incident and reflected signal from the DUT. The detected electronic circuit should be placed between the directional coupler and the HBS, where it can capture the incident or reflected signal before reaching the HBS. The detected circuit should then send the detected information to measurement software for processing. Consequently, the command signal will be sent to the step attenuators, which consist of the HBS, for switching. This procedure will provide an individual control HBS that will cope with the incident and reflected waveform more accurately and more realisably.

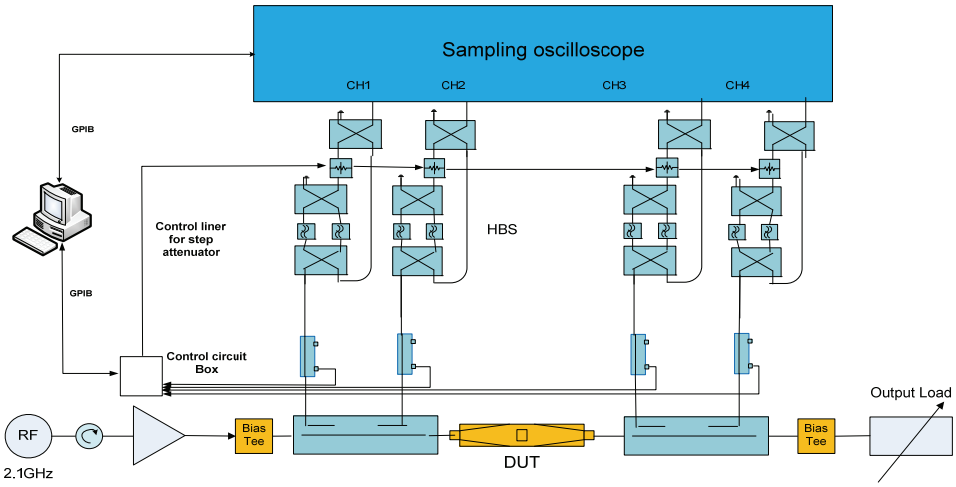

Figure 8.1: Suggestion for an independent control switch for an HBS in an RF measurement system.

8.2.2 New Improvements for a HBS

The simulation of an HBS in Chapter 5 shows that the attenuation controllable band can reach the only 30 dB in the design of an HBS with step attenuator HP 33321, although in practice this step attenuator model provided attenuation up to 70dB. An investigation of the simulation results shows that this is caused from the leakage of the signal from the fundamental band while the step attenuator presents an attenuation of more than 30 dB. The leakage signal can then pass through the bypass path of HBS. As a result, the combination of leakage signal and output signal leads to an uncontrollable band of fundamental frequency below 30dB. The simulation suggests that this issue can overcome by using blocked leakage signal devices (e.g. a high pass filter or a band pass filter). This can provide the block signal at the desired frequency and it can also bypass the high frequency.

To prove this assumption in a practical task, it is advised that further research should implement the HF into the HBS. The new structure has been then characterised and its S-parameter model built by using a VNA or PNA. The simulation indicates that the practical S-parameter could provide more attenuation in a controllable band below 30 dB. For example, it could reach 70dB by using the step attenuator model HP 33321. The S-parameter characteristic curve could be smoother than older HBS's S-parameter. In particular, it could reduce the ripple of the S-parameters model in fundamental band due to the blocking of leakage signals.

If the new HBS is implemented in the measurement system, then the demonstration will show the ability of the measurement system in terms of gaining more control dynamic range, accuracy, and realisation.

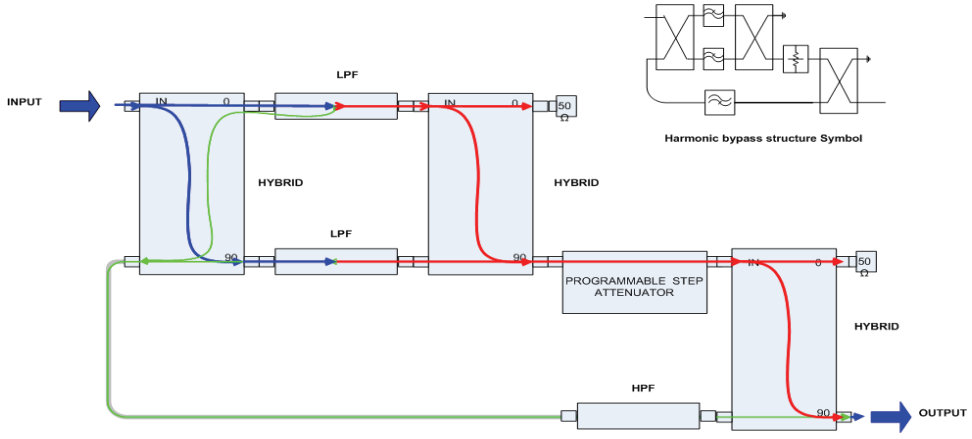

Figure 8.2: A suggested improvement of the HBS by adding an HPF in to the structure.

8.2.3 Further Implementation of the HBS Approach in a Multi-tone Measurement System

The implementation of an HBS in this present study has only focused on a high power CW measurement system. It is recommended that further work should be done on the implementation of an HBS in a multi-tone RF measurement system. Figure 8.3 illustrates a possible configuration of this set up, where the HBS is located in between the directional couplers and the duplex RF-IF devices. The other configurations are followed as is usual in a multi-tone setup.

Additional work needs to be done on modification of the script procedure software for a multi-tone measurement system. These modifications would allow the measurement software to access the HBS's S-parameter model for correction of the measured incident and reflected waveforms, as it does in single tone CW measurement systems.

If this suggested measurement system were implemented, then the intensive observation should focus on the integrity of multi-tone waveforms that are exiting from the HBS. This observation would determine the opportunity to correct the measured incident and

reflected waveforms by using the HBS's S-parameter model.

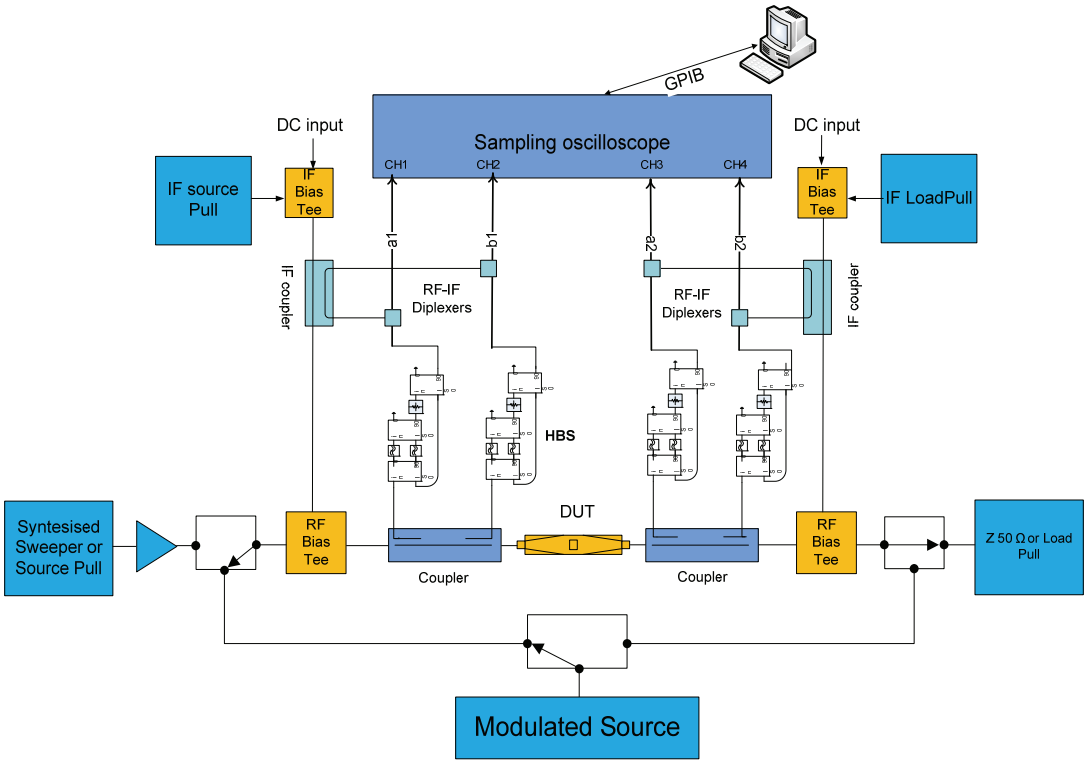

Figure 8.3: A suggested implementation of an HBS in a multi-tone RF measurement system.

References

[1] Z. Aboush et al., "High power active harmonic load-pull system for characterization of high power 100-watt transistors," in *Microwave Conference, 2005 European*, 4-6 Oct. 2005, p. 4 pp.

[2] J. Benedikt, "Evaluation and Measurement Enhancement of the High Frequency Measurement System at the University of Wales College Cardiff," Cardiff University, Cardiff, Thesis 2000.

[3] P.J. Tasker, "Practical Waveform Engineering," *IEEE microwave magazine*, vol. 10, no. 7, pp. 65-76, December 2009.

[4] P.J. Tasker, "RF Waveform Measurement and Engineering," in *Compound Semiconductor Integrated Circuit Symposium, 2009. CISC 2009. Annual IEEE*, Greensboro, NC, 11-14 Oct. 2009, pp. 1-4.

[5] D.J. Williams, "Non-Linear Measurement System and Techniques for RF Power Amplifier Design," Cardiff University, PhD thesis 2003.

Appendix A:

Modified Measurement Software Control.

Appendix A: Modified Measurement Software Control

The ConVarAtten.ipf is an IGOR procedure file which contains script functions source code. It has been embed in main RF measurement software which enhances the software capabilities. It provides three main functions, they are:

(1) Switching step attenuators and/or HBS;

(2) Preparing Step attenuator's and/or HBS's S-parameter model suitable for setting state; and,

(3) Appling the S-parameter model to raw travelling waves.

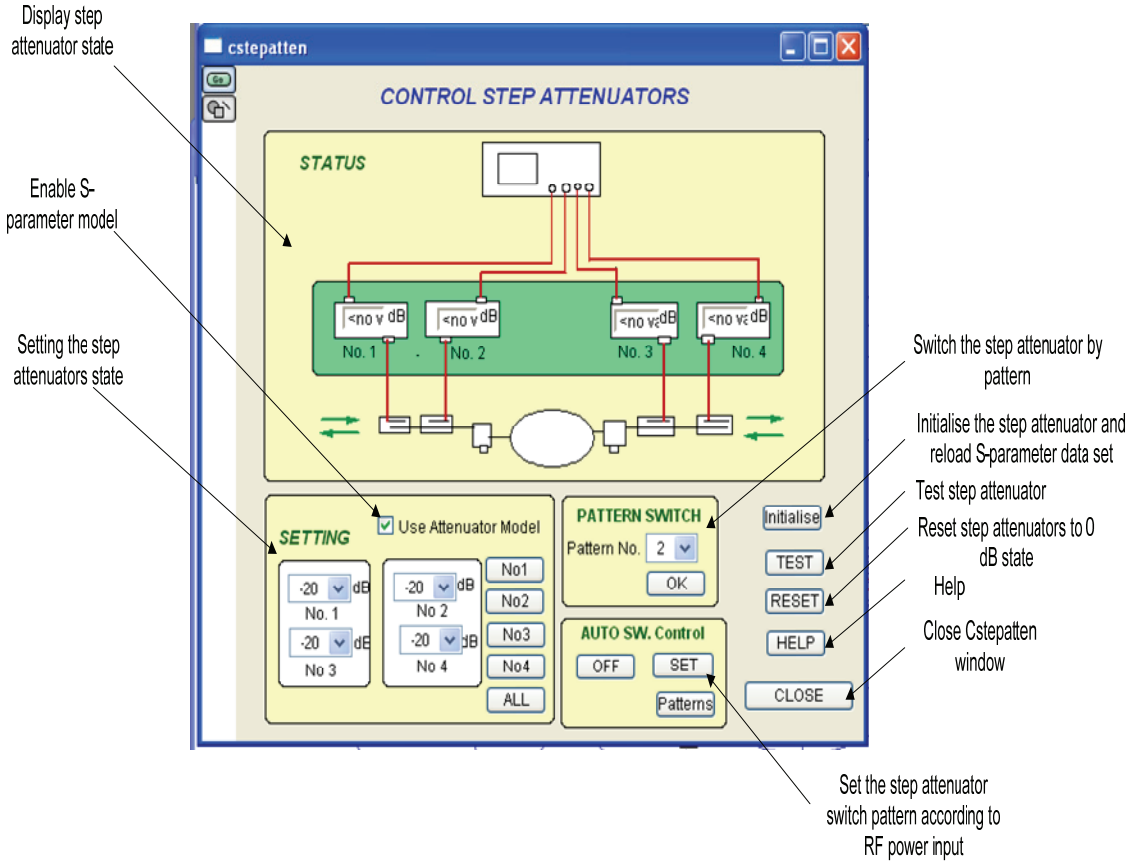

Figure A.1:Main step attenuator control panel.

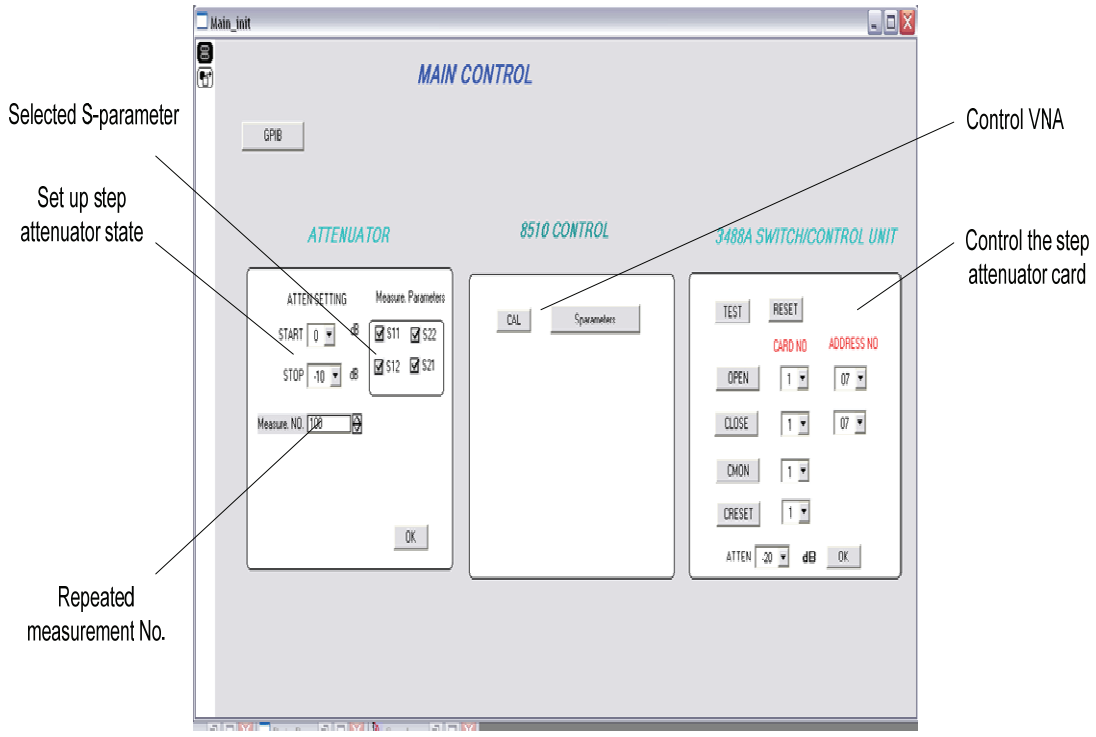

Figure A.2: Control panel for characterization of both step attenuator and HBS by using a VNA HP8510

Table A.1: Function name in ConAtten.ipf procedure file.

Function name	Description
Cstepsinit()	- set global variable - load S-parameter - Switch attenuator to default state.
Csteps(ctrlName):ButtonControl	Main control button function
AUTO_StepAtten(ctrlName) : ButtonControl	It uses to control automatically the step attenuators.
VarStepPatCon(ctrlName):ButtonControl	It uses to set the step attenuator state partern.
ReadVarStepStatus()	Read the step attenuator states.
SetStepAtten()	Set the step attenuator state. It's used with TestSWstepAtten() function.
PatternSwitch(PatNo)	Read out the pattern switch of step attenuator for display
enablePatternNO(PatNo)	Enable step attenuator state partern.
VarStepUpdatedisplay()	Update the step attenuator state variables.
VarStepdefault()	Set default of the step attenuator state
Mcontrol_stepAtten()	Centre control of step attenuator state
control_StepAtten(V_dB,AttenNO)	Switch the step attenuator state - Send command to GPIB
openAtten(AttenNo)	Switch the step attenuator state to 0dB
CstepDisplayUpdate(V_dB,AttenNO)	-update the variable
CstepDisplayReset(AttenNO)	Reset the variable and display on control panel

Function name	Description
TestSWstepAtten()	Test switching the step attenuator
HotswitchAtten()	Automatic control the step attenuator according to RF power input
SetVarPowAtten(ctrlName,varNum,varStr, varName) : SetVariableControl	Set the RF power input level corresponding to step attenuator state.
CorrectDataAtten(Ch)	Correct the travelling wave a0, b0,a3 and b3 using the simple S-parameter model
CorrectStepAtten(freq_Attenlist_tem , Step_status, StepNo)	Interpolate the S21 for correctionDataAtten(ch)
CorrectS21Cal(freq_Attenlist_tem , Step_status,StepNo)	Prepare the S21 data at calibration state. This function is designed for Measurement software version.
CorrectDataAttenFull_S_OSC(Ch,counter)	Correct the travelling wave a0, b0,a3 and b3 using the full S-parameter model. This function is designed for the calibration software version.
CorrectDataAttenFull_S_Meas(Ch_port)	Correct the travelling wave a0, b0,a3 and b3 using the full S-parameter model. This function is designed for the Measurement software version
CorrectS21Cal_OSC(freq_Attenlist_tem , Step_status,StepNo,Counter, HarmonicAtten)	Prepare the S21 data at calibration state. This function is designed for calibration software version.
CorrectFull_S_Cal_OSC(freq_Attenlist_tem , Step_status,StepNo,Counter, HarmonicAtten)	Compute the full s-parameter model at defined step attenuator calibration state. This function is designed for Calibration software version

Function name	Description
CorrectFull_S_Cal_Meas(freq_Attenlist_tem , Step_status,StepNo)	Compute the full s-parameter model at defined step attenuator calibration state. This function is designed for Measurement software version
CorrectStepAtten_OSC(freq_Attenlist_tem , Step_status, StepNo,Counter, HarmonicAtten)	Compute the full s-parameter model at defined step attenuator measurement state. This function is designed for Calibration software version.
CorrectStepAttenFull_S_Meas(freq_Attenlist_tem , Step_status, StepNo)	Compute the full s-parameter model at defined step attenuator measurement state. This function is designed for Measurement software version

Appendix B

Hardware and devices data sheet

Appendix B Hardware and devices data sheets

B.1 NPTB00050 data sheet Gallium Nitride 28V

NPTB00050 Datasheet

NITRONEX CORPORATION

Gallium Nitride 28V, 50W RF Power Transistor

Built using the SIGANTIC® NRF1 process - A proprietary GaN-on-Silicon technology

FEATURES

- Optimized for broadband operation from DC - 4000MHz
- 50W P_{3dB} CW narrowband power
- 25W P_{3dB} CW broadband power from 500-1000MHz
- Characterized for operation up to 32V
- 100% RF tested
- Thermally enhanced industry standard package
- High reliability gold metallization process
- Lead-free and RoHS compliant
- Subject to EAR99 export control

Broadband 50 Watt, 28 Volt GaN HEMT

RoHS

RF Specifications (CW): V_{DS} = 28V, I_{DQ} = 450mA, Frequency = 3000MHz, T_C = 25°C, Measured in Nitronex Test Fixture

Symbol	Parameter	Min	Typ	Max	Units
P_{3dB}	Average Output Power at 3dB Gain Compression	45	50	-	W
P_{1dB}	Average Output Power at 1dB Gain Compression	33	38	-	W
G_{SS}	Small Signal Gain	10.5	11.5	-	dB
η	Peak Drain Efficiency at $P_{OUT} = P_{3dB}$	55	60	-	%
Ψ	Output mismatch stress, VSWR = 7:1, all phase angles, $P_{OUT} = P_{1dB}$	No Performance Degradation After Test			

Typical OFDM Performance: V_{DS} = 28V, I_{DQ} = 300mA, Single carrier OFDM waveform 64-QAM 3/4, 8 burst, continuous frame data, 10MHz channel bandwidth. Peak/Avg = 10.3dB @ 0.01% probability on CCDF. Frequency = 2400 to 2600MHz. $P_{OUT,AVG}$ = 6W, T_C=25°C.

Symbol	Parameter	Typ	Units
G_P	Power Gain	12.0	dB
η	Drain Efficiency	23	%
EVM	Error Vector Magnitude	2.0	%

DC Specifications: T_C = 25°C

Symbol	Parameter	Min	Typ	Max	Units
Off Characteristics					
V_{BDS}	Drain-Source Breakdown Voltage (V_{GS} = -8V, I_D = 16mA)	100	-	-	V
I_{DLK}	Drain-Source Leakage Current (V_{GS} = -8V, V_{DS} = 60V)	-	0.1	16	mA
On Characteristics					
V_T	Gate Threshold Voltage (V_{DS} = 28V, I_D = 16mA)	-2.3	-1.8	-1.3	V
V_{GSQ}	Gate Quiescent Voltage (V_{DS} = 28V, I_D = 450mA)	-2.0	-1.5	-1.0	V
R_{ON}	On Resistance (V_{GS} = 2V, I_D = 120mA)	-	0.25	0.40	Ω
I_D	Drain Current (V_{DS} = 7V pulsed, 300µs pulse width, 0.2% duty cycle, V_{GS} = 2V)	9.2	9.8	-	A

Absolute Maximum Ratings: Not simultaneous, T_C = 25°C unless otherwise noted

Symbol	Parameter	Max	Units
V_{DS}	Drain-Source Voltage	100	V
V_{GS}	Gate-Source Voltage	-10 to 3	V
I_G	Gate Current	80	mA
P_T	Total Device Power Dissipation (Derated above 25°C)	55	W
θ_{JC}	Thermal Resistance (Junction-to-Case)	3.2	°C/W
T_{STG}	Storage Temperature Range	-65 to 150	°C
T_J	Operating Junction Temperature	200	°C
HBM	Human Body Model ESD Rating (per JESD22-A114)	1B (>500V)	
MM	Machine Model ESD Rating (per JESD22-A115)	M2 (>100V)	

Load-Pull Data, Reference Plane at Device Leads

V_{DS}=28V, I_{DQ}=450mA, T_A=25°C unless otherwise noted

Table 1: Optimum Source and Load Impedances for CW Gain, Drain Efficiency, and Output Power Performance

Frequency (MHz)	Z_S (Ω)	Z_L (Ω)	P_{SAT} (W)	Gain (dB)	Drain Efficiency @ P_{SAT} (%)
2000	3.2 - j3.5	4.8 - j2.5	50	15.0	65
2400	3.1 - j7.5	5.0 - j3.5	50	13.8	62
2500	3.1 - j8.4	5.2 - j3.6	50	13.8	62
2600	3.2 - j9.4	5.3 - j3.7	50	13.5	61
2700	3.7 - j11.0	5.2 - j4.9	50	13.1	60
3000	4.4 - j13.0	5.2 - j5.3	50	13.0	60

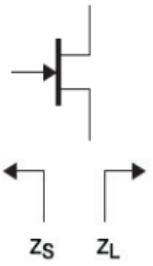

Z_S is the source impedance presented to the device.
Z_L is the load impedance presented to the device.

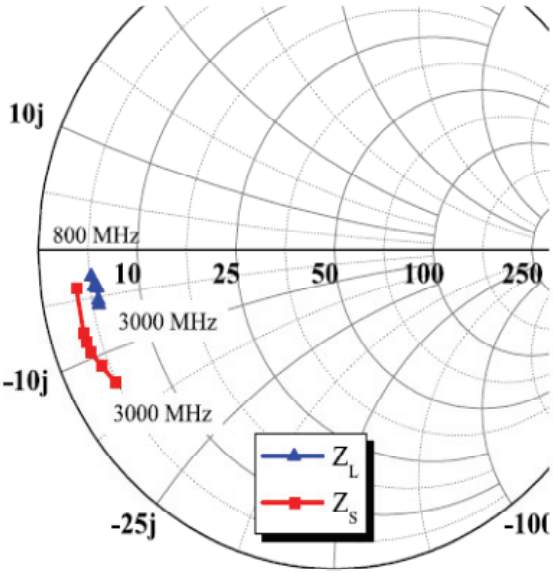

Figure 1 - Optimal Impedances for CW Performance, V_{DS} = 28V, I_{DQ} = 450mA

Load-Pull Data, Reference Plane at Device Leads

V_{DS}=28V, I_{DQ}=450mA, T_A=25°C unless otherwise noted.

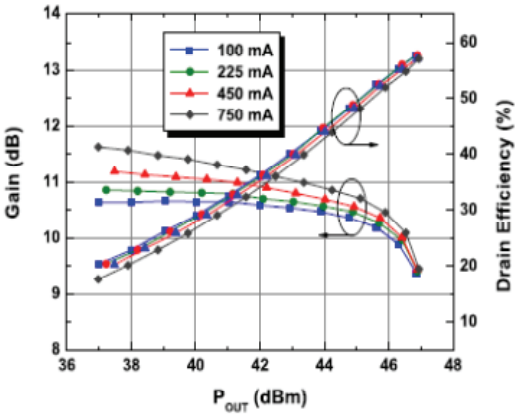

Figure 2 - Typical CW Performance vs. I_{DQ}
V_{DS} = 28V, 3000MHz

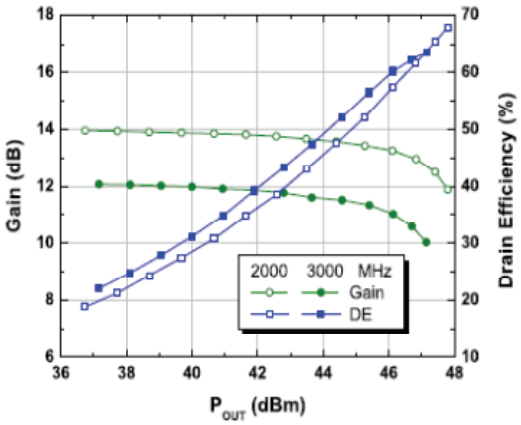

Figure 3 - Typical CW Performance
V_{DS} = 28V, I_{DQ} = 450mA

Typical Device Characteristics

V_{DS}=28V, I_{DQ}=450mA, T_A=25°C unless otherwise noted.

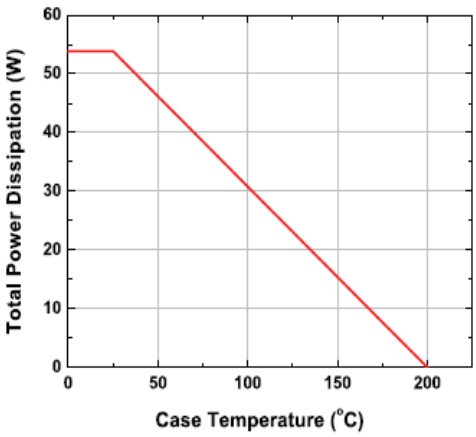

Figure 4 - Power Derating Curve

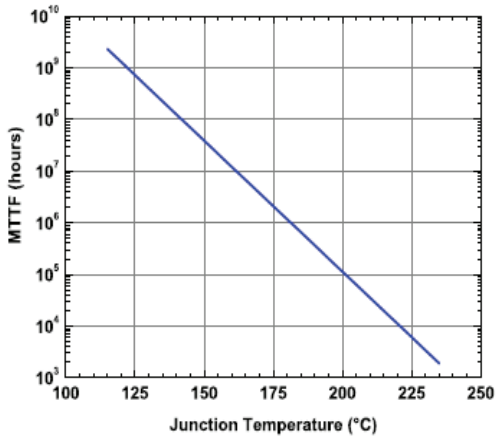

Figure 5 - MTTF of NRF1 Devices as a Function of Junction Temperature

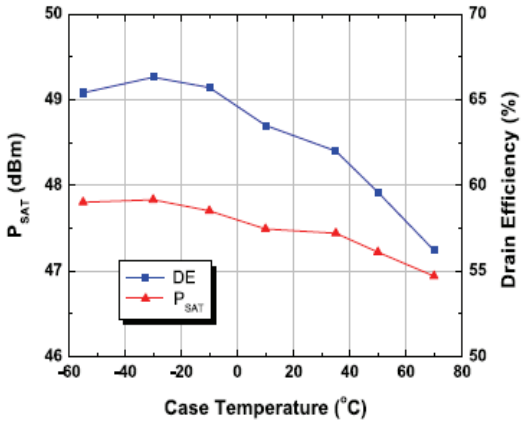

Figure 6 - Typical CW Performance vs. Temperature in Nitronex Test Fixture,
V_{DS} = 28V, I_{DQ} = 450 mA, 3000MHz

B.2 CREE CGH40025 RF Power GaN HEMT

CGH40025

25 W, RF Power GaN HEMT

Cree's CGH40025 is an unmatched, gallium nitride (GaN) high electron mobility transistor (HEMT). The CGH40025, operating from a 28 volt rail, offers a general purpose, broadband solution to a variety of RF and microwave applications. GaN HEMTs offer high efficiency, high gain and wide bandwidth capabilities making the CGH40025 ideal for linear and compressed amplifier circuits. The transistor is available in a screw-down, flange package and solder-down, pill packages.

Package Type: 440196 and 440166
PN: CGH40025P and CGH40025F

FEATURES

- Up to 6 GHz Operation
- 15 dB Small Signal Gain at 2.0 GHz
- 13 dB Small Signal Gain at 4.0 GHz
- 30 W typical P_{SAT}
- 62 % Efficiency at P_{SAT}
- 28 V Operation

APPLICATIONS

- 2-Way Private Radio
- Broadband Amplifiers
- Cellular Infrastructure
- Test Instrumentation
- Class A, AB, Linear amplifiers suitable for OFDM, W-CDMA, EDGE, CDMA waveforms

RoHS COMPLIANT

Rev 3.2 – July 2011

Large Signal Models Available for SiC & GaN

Absolute Maximum Ratings (not simultaneous) at 25°C Case Temperature

Parameter	Symbol	Rating	Units
Drain-Source Voltage	V_{DSS}	84	Volts
Gate-to-Source Voltage	V_{GS}	-10, +2	Volts
Storage Temperature	T_{STG}	-65, +150	°C
Operating Junction Temperature	T_J	225	°C
Maximum Forward Gate Current	I_{GMAX}	7.0	mA
Soldering Temperature[1]	T_S	245	°C
Screw Torque	τ	60	in-oz
Thermal Resistance, Junction to Case[2]	$R_{\theta JC}$	4.8	°C/W
Case Operating Temperature[2,3]	T_C	-40, +150	°C

Note:
[1] Refer to the Application Note on soldering at www.cree.com/products/wireless_appnotes.asp
[2] Measured for the CGH40025F at P_{DISS} = 28 W.
[3] See also, the Power Dissipation De-rating Curve on Page 6.

Electrical Characteristics (T_C = 25°C)

Characteristics	Symbol	Min.	Typ.	Max.	Units	Conditions
DC Characteristics[1]						
Gate Threshold Voltage	$V_{GS(th)}$	-3.8	-3.3	-2.3	V_{DC}	V_{DS} = 10 V, I_D = 7.2 mA
Gate Quiescent Voltage	$V_{GS(Q)}$	–	-3.0	–	V_{DC}	V_{DS} = 28 V, I_D = 250 mA
Saturated Drain Current	I_{DS}	5.8	7.0	–	A	V_{DS} = 6.0 V, V_{GS} = 2.0 V
Drain-Source Breakdown Voltage	V_{BR}	120	–	–	V_{DC}	V_{GS} = -8 V, I_D = 7.2 mA
RF Characteristics[2] (T_C = 25°C, F_0 = 3.7 GHz unless otherwise noted)						
Small Signal Gain	G_{SS}	12	13	–	dB	V_{DD} = 28 V, I_{DQ} = 250 mA
Power Output[3]	P_{SAT}	20	30	–	W	V_{DD} = 28 V, I_{DQ} = 250 mA
Drain Efficiency[4]	η	55	62	–	%	V_{DD} = 28 V, I_{DQ} = 250 mA, P_{SAT}
Output Mismatch Stress	VSWR	–	–	10 : 1	Ψ	No damage at all phase angles, V_{DD} = 28 V, I_{DQ} = 250 mA, P_{OUT} = 25 W CW
Dynamic Characteristics						
Input Capacitance	C_{GS}	–	9.0	–	pF	V_{DS} = 28 V, V_{gs} = -8 V, f = 1 MHz
Output Capacitance	C_{DS}	–	2.6	–	pF	V_{DS} = 28 V, V_{gs} = -8 V, f = 1 MHz
Feedback Capacitance	C_{GD}	–	0.4	–	pF	V_{DS} = 28 V, V_{gs} = -8 V, f = 1 MHz

Notes:
[1] Measured on wafer prior to packaging.
[2] Measured in CGH40025-TB.
[3] P_{SAT} is defined as I_G = 0.72 mA.
[4] Drain Efficiency = P_{OUT} / P_{DC}

Cree, Inc.
4600 Silicon Drive
Durham, NC 27703
USA Tel: +1.919.313.5300
Fax: +1.919.869.2733
www.cree.com/wireless

Typical Performance

Small Signal Gain and Return Loss vs Frequency of the CGH40025F in the CGH40025-TB

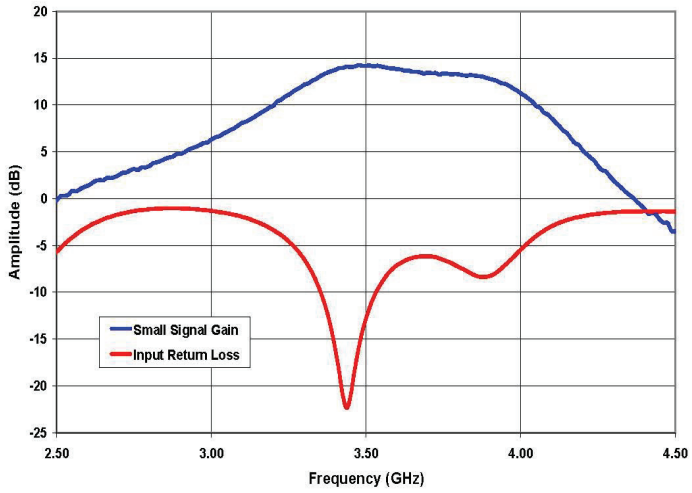

P_{SAT}, Gain, and Drain Efficiency vs Frequency of the CGH40025F in the CGH40025-TB
V_{DD} = 28 V, I_{DQ} = 250 mA

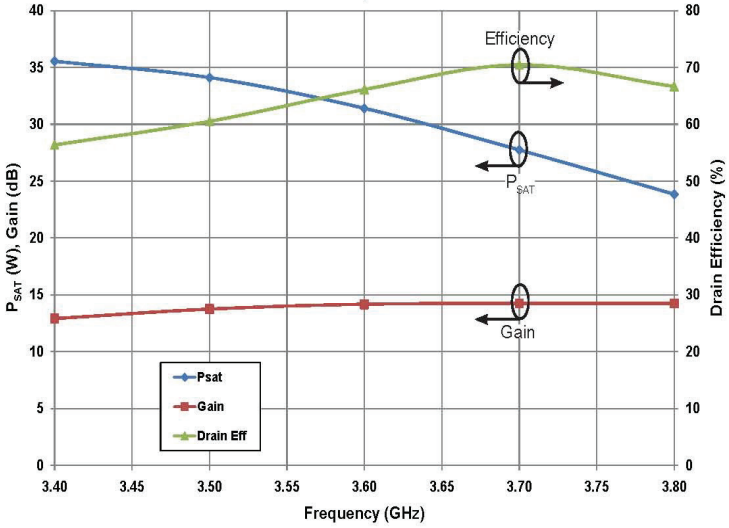

Cree, Inc.
4600 Silicon Drive
Durham, NC 27703
USA Tel: +1.919.313.5300
Fax: +1.919.869.2733
www.cree.com/wireless

Typical Performance

Swept CW Data of CGH40025 vs. Output Power with Source and Load Impedances Optimized for P_{SAT} Power in CGH40025-TB
V_{DD} = 28 V, I_{DQ} = 250 mA, Freq = 3.7 GHz

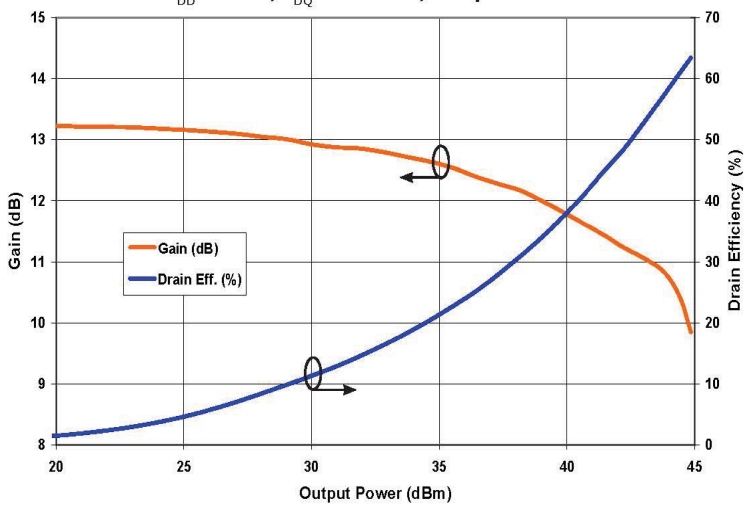

Maximum Available Gain and K Factor of the CGH40025
V_{DD} = 28 V, I_{DQ} = 250 mA

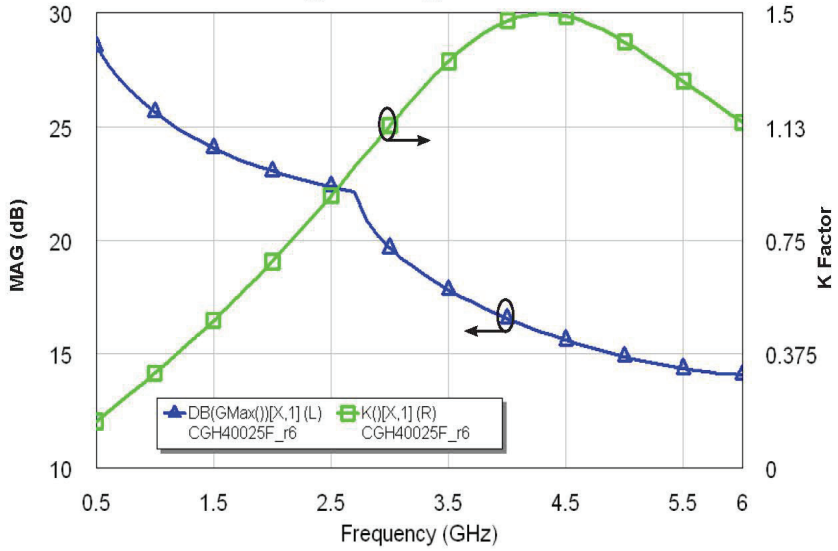

Cree, Inc.
4600 Silicon Drive
Durham, NC 27703
USA Tel: +1.919.313.5300
Fax: +1.919.869.2733
www.cree.com/wireless

Typical Noise Performance

Simulated Minimum Noise Figure and Noise Resistance vs Frequency of the CGH40025F
V_{DD} = 28 V, I_{DQ} = 250 mA

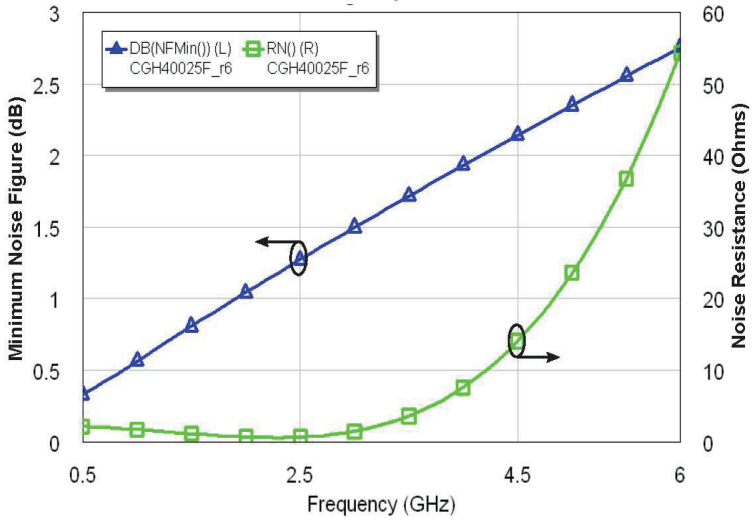

Electrostatic Discharge (ESD) Classifications

Parameter	Symbol	Class	Test Methodology
Human Body Model	HBM	1A > 250 V	JEDEC JESD22 A114-D
Charge Device Model	CDM	1 < 200 V	JEDEC JESD22 C101-C

Cree, Inc.
4600 Silicon Drive
Durham, NC 27703
USA Tel: +1.919.313.5300
Fax: +1.919.869.2733
www.cree.com/wireless

Source and Load Impedances

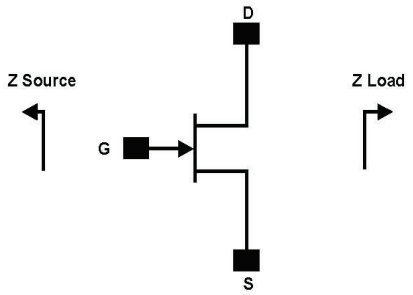

Frequency (MHz)	Z Source	Z Load
500	7.75 + j15.5	20 + j5.2
1000	3.11 + j5.72	17 + j6.66
1500	2.86 + j1.63	16.8 + j3.2
2500	2.4 - j3.52	8.02 + j4.32
3500	1.31 - j7.3	5.85 - j0.51

Note 1. V_{DD} = 28V, I_{DQ} = 250mA in the 440166 package.
Note 2. Optimized for power gain, P_{SAT} and PAE.
Note 3. When using this device at low frequency, series resistors should be used to maintain amplifier stability.

CGH40025 Power Dissipation De-rating Curve

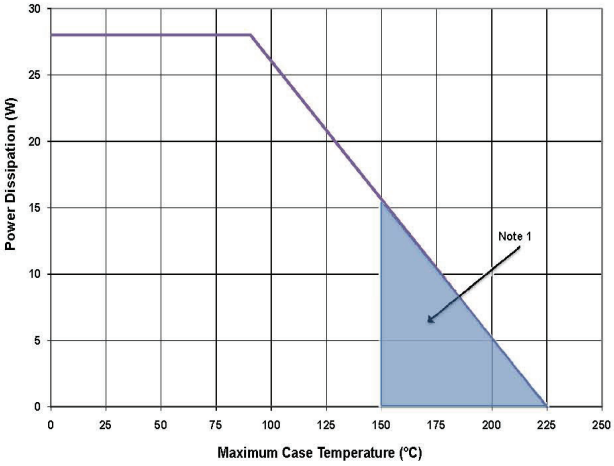

Note 1. Area exceeds Maximum Case Operating Temperature (See Page 2).

Cree, Inc.
4600 Silicon Drive
Durham, NC 27703
USA Tel: +1.919.313.5300
Fax: +1.919.869.2733
www.cree.com/wireless

B.3 Step Attenuator Data Sheet

HEWLETT PACKARD

STEP ATTENUATORS

FOR OEM & SYSTEM USE
dc to 26.5 GHz

models
HP 33320A/B/G/H
HP 33321A/B/D/G/H/K
HP 33322A/B/G/H
HP 33323K

TECHNICAL DATA 1 MAY 1990

Features:

- Broadband Frequency Coverage (dc-4 GHz, dc-18 GHz, and dc-26.5 GHz)
- Optional Calibration Data
- 0 to 11 dB, 70 dB, 90 dB, 110 dB
- 1 dB Steps, 10 dB Steps
- High Accuracy (±2% of dB reading to 18 GHz Typical)
- High Repeatability (0.01 dB to 18.0 GHz Typical)
- Manual and Programmable Models
- Environmentally Rugged; Small Size; Low Cost; Long Life

General Description

This family of HP step attenuators represents the state-of-the-art in attenuator design. These attenuators offer an unprecedented combination of broadband accuracy, high repeatability, small size, rapid switching, and low cost. They are particularly well suited for controlling the signal levels of microwave sweepers, spectrum analyzers, network analyzers, receivers, and automatic and special test equipment. These attenuators have proven extremely reliable inside Hewlett-Packard's microwave instrumentation as well as a wide variety of other applications. For bench use applications, models HP 8494, HP 8495 and HP 8496 are available in manual and programmable versions. Bench models include a base and the manual model has an indicator dial.

Each attenuator is composed of three or four attenuation sections connected in cascade. Each section (Figure 1) consists of a precision thin-film attenuation card, a lossless thru line, and a ganged pair of contacts that switch the attenuation card in or out. This combination results in high accuracy and exceptional repeatability.

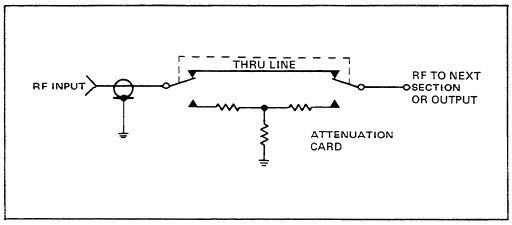

Figure 1. Schematic of Single Attenuator Section.

High Repeatability

Excellent repeatability (typically 0.01 dB to 18 GHz and 0.05 dB to 26.5 GHz for up to five million cycles) has been achieved by employing edge-line design for the transmission line.[1] This construction requires that only the center conductor be switched, thus eliminating the high friction contacts characteristic of turret type attenuators. The resulting benefits are long life and highly repeatable performance.

Reliable Performance

Each unit is tested over its operating frequency range by a computer-controlled HP Automatic Network Analyzer to insure consistent accurate measurements, traceable to the National Institute of Standards and Technology. This measurement system brings standards lab accuracy to production testing and assures that each attenuator meets specifications over the entire frequency range. Calibration data can be provided on request.

[1]HP Journal Article, May 1974, p. 21.

Broadband Accuracy and Low SWR

High accuracy (typical ±2% of the dB reading to 18 GHz and ±4% of the dB reading to 26.5 GHz) and low SWR are achieved through the use of miniature thin-film attenuation cards composed of high stability tantalum resistive film on a sapphire substrate. This thin-film technique permits the construction of circuits which are truly distributed and without stray reactances, even at very high microwave frequencies. These precision cards and the cascaded section design provide high step-to-step accuracy, typically better than ±1 dB to 18 GHz and ±2 dB to 26.5 GHz for a 10-dB step and ±0.2 dB for a 1-dB step.

Figures 2 and 3 show the typical performance of the step attenuators as tested on a computer-controlled HP Automatic Network Analyzer. This typical data represents a mean sampling of current production and is given to provide useful applications information. Special selections can be made on request.

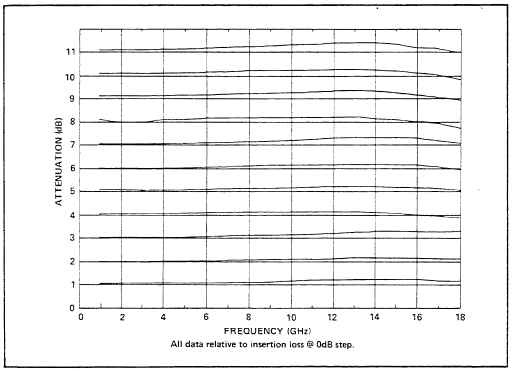

Figure 2. HP 33320B/H Typical Accuracy as Measured on an HP Automatic Network Analyzer.

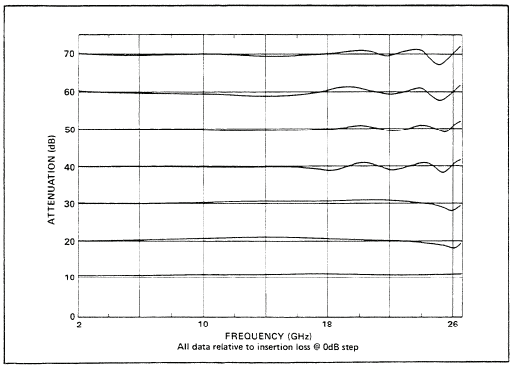

Figure 3. HP 33321 Typical Accuracy as Measured on an HP Automatic Network Analyzer (Band H models operate to 18 GHz, D and K models operate to 26.5 GHz).

Product Information

3.5 mm Connector

The HP 33321D/K and HP 33323K step attenuators use the 3.5 mm connector[2] which is compatible with the industry standard SMA but is more rugged and offers improved repeatability over hundreds of connections. Use of this connection extends the frequency range to 26.5 GHz.

Environmentally Rugged

HP 33320 Series Attenuators have undergone a very extensive environmental qualification program and have been tested at the extremes of temperature, shock, vibration, and humidity and have proven to be extremely reliable. A summary of the environmental data is given on the specifications page.

[2]"A High Performance 3.5 mm Connector to 34 GHz," Microwave Journal, July 1976. Also, IEEE Transaction on MTT, December 1976, Volume MTT-24 Number 12, page 995.

Small Size

The small size of these attenuators is an important feature for applications where space is critical. When panel mounted, the manual versions take less than 1.5 square inches of panel area. Since the programmable models are only slightly larger than the manual versions and have the same RF performance, the designer gets more flexibility in providing manual and programmable models of instruments without major redesign.

Low Cost

Utilizing state-of-the-art manufacturing processes, including numerically controlled machining, thin-film deposition, and computer controlled testing, this family of attenuators offers a significant technical contribution at a low cost to the user. In addition, OEM quantity discounts are offered.

Programmable Model Information

Positive Latching Solenoids

In the programmable models, solenoids are used to switch the attenuation card of each section into and out of the circuit. Once switched, the solenoids are held in place by strong permanent magnets able to withstand shocks over 10 G's. Thus, power can be removed without affecting the status of the attenuator sections.

Rapid Switching

Use of miniature solenoids has resulted in more than a two-to-one improvement in switching speed over previous models. The 20 millisecond maximum switching time includes contact settling and is a significant advantage for automatic testing, and other applications where speed is of prime importance.

Low Heat Dissipation

A unique design feature of these attenuators is that the solenoids automatically disconnect after switching. Current is drawn for approximately eight milliseconds during a switching operation, after which internal relay contacts open the solenoid circuit, and current is not drawn again until another switching operation is performed. This automatic turnoff feature greatly simplifies the driver circuit design (Figure 5) and minimizes the amount of heat dissipated by the solenoids, often a critical concern. For example, in an application with 60 switchings a minute, the average power dissipated is less than 0.03 watts.

HP-IB Attenuator/Switch Driver

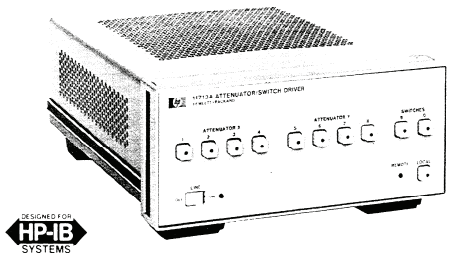

Employing programmable HP step attenuators and switches in an automatic test system becomes an easy task when the HP 11713A Attenuator/Switch Driver is specified into the system.

The HP 11713A has all of the necessary features to provide HP-IB control of up to two programmable attenuators of the HP 33320 Series, and concurrently up to two electromechanical switches (e.g., HP 8671B or HP 33311 series).

The HP 11713A includes an integral power supply (with short circuit protection) that can simultaneously provide 125 milliamps at 24 volts to all contacts for control of the attenuators and switches, so no external power supply is needed. Each HP 11713A is provided with two (2) plug-in drive cables for the programmable attenuators to simplify connection to the driver.

The HP 11713A also features convenient front panel keys so the user can manually activate the individual attenuation sections and switches when in the "local" mode. Switching time for the drivers is less than 10 milliseconds.

Optional Calibration Data for HP 33320 Series Step Attenuators

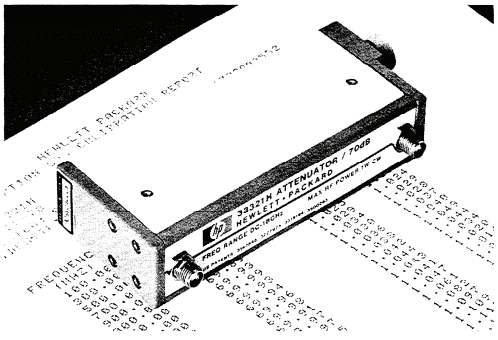

Use of calibration data (i.e. accurate, recorded data of a device's characteristics) has always been an effective means of reducing measurement uncertainty at RF and microwave frequencies. Now, however, use of calibration data is experiencing rapid growth in test systems because inexpensive calibration data is available. Another key reason for this trend is that automated test systems can easily store and manipulate extensive amounts of the calibration data.

There are three primary uses for optional test data:

1. Accuracy Enhancement

Step attenuators have long been used as reference standards in the measurement of gain, attenuation, and receiver sensitivity. Since the accuracy specifications include margins for frequency response and unit-to-unit variations, calibration data can improve overall measurement uncertainty. In many cases, this improves the reference attenuator's accuracy by 60 percent or more.

2. Test System Verification

Calibration data has an important use in ensuring that a test system is operating properly. As a final step in the verification procedures of the automatic systems by Hewlett-Packard to test microwave devices, a previously calibrated attenuator is tested and compared to the stored data. If the differences are within the system measurement uncertainty, proper operation of the test system is ensured.

3. Implementing Calibration Data in a Computer Program

To integrate the calibration data into an automated measurement program, first set up variables in the computer program that will be loaded with the data. Then measurements can be made at the calibration frequencies after which the calibration data is recalled and used to adjust the measured data or calculate measurement uncertainties.

Data is available on HP 33320 Series Step Attenuators as Option 890 and is generated from measurements made by an Automatic Network Analyzer. Option 890 provides a tabulated list of attenuation and SWRs for each step at 14 to 72 frequencies (see Table 1). Measurements through 50 dB are directly traceable to NIST standards and feature very low measurement uncertainties (see Tables 2 and 3). Step attenuator data provided from 60 dB to 110 dB is generated by combining the measured data of the individual attenuation sections (e.g. adding the data for the 10, 20, and 40 dB sections to get the 70 dB step data). Option 890 data is available when the attenuators are first purchased and recalibrations are available.

Table 1. HP 33320 Series Calibration Frequencies

Model	Calibration Frequencies
33320A/G 33321A/G 33322A/G	200 to 4000 MHz every 200 MHz (20 frequencies)
35320B/H 33321B/H 33322B/H	200 to 18000 MHz every 200 MHz (90 frequencies)
33321D/K 33323K	1500 to 26500 MHz every 250 MHz (101 frequencies)

Table 2. HP 33320 Series SWR Data Uncertainty

Connector Type	Frequency Range (GHz)	SWR Data Uncertainty	
		Measured SWR 1.0 to 1.35	Measured SWR 1.35 to 1.86
Female SMA	dc to 8.0	±0.054	±0.088
	8.0 to 12.4	±0.077	±0.132
	12.4 to 18.0	±0.122	±0.206
Female APC-3.5	18 to 26.5	±0.045	±0.067

Table 3. HP 33320 Series Attenuation Data Uncertainties

Attenuation (db)	Attenuation Data Uncertainty (dB)				
	0.1 to 2.0 GHz	2 to 6 GHz	6 to 12.4 GHz	12.4 to 18.0 GHz	18.0 to 26.5 GHz
0/0-4	±0.07	±0.06	±0.06	±0.11	±0.3
5-8	±0.07	±0.07	±0.07	±0.11	—
10/9-11	±0.08	±0.07	±0.07	±0.12	±0.2
20	±0.09	±0.08	±0.08	±0.13	±0.2
30	±0.12	±0.11	±0.11	±0.15	±0.24
40	±0.15	±0.14	±0.14	±0.21	±0.28
50	±0.23	±0.23	±0.23	±0.34	±0.54
60	±0.50*	±0.48*	±0.90*	±0.90*	±1.00*
70	±0.50*	±0.50*	±0.90*	±0.90*	±1.75*
80	±0.50*	±0.50*	±0.90*	±0.90*	±1.80*
90	±0.50*	±0.50*	±0.90*	±0.90*	±1.95*
100	±0.90*	±0.90*	±1.80*	±1.80*	—
110	±0.90*	±0.90*	±1.80*	±1.80*	—

*For step attenuator data from 60 to 110 dB the uncertainties noted represent 99.7% probability values.

Attenuation Section Switching

Figure 4 shows one attenuator section schematic. Each attenuation section utilizes one solenoid with dual coil windings, one coil to switch in the attenuation card (e.g. 10 dB) and one coil to switch in the thru line (0 dB).

With a positive voltage applied to the common pin, the state (attenuation card or 0 dB) of a particular section is determined by connecting its attenuation card pin or thru line pin to a negative voltage or ground. Table 4 defines the pin assignments and the pin configurations are shown on page 8.

As a section is switched, the internal contacts of the activated coil open, thus shutting off current flow. At the same time, the internal contacts for the other coil close so that it can be activated when desired. Figure 5 shows a section that has been switched to the attenuation card position (note the closed thru line coil contact). The switching is "break-before-make" type, thus a momentary interruption of the RF signal occurs at switching.

Although all sections can be switched simultaneously, the attenuator driver must not allow both pins of the same section (e.g. Section 1, pins 5 and 6) to be activated concurrently, or else that section would cycle rapidly. All terminals are "floating", so bipolar or unipolar power supplies can be used.

Typical Driver Circuit

Figure 5 shows an economical TTL compatible driver circuit for a single attenuation section utilizing an IC relay driver and an inverter. A TTL "HI" input to the driver switches in the attenuation card, while a "LO" will activate the thru line for that section. This provides a complementary driver for the section which assures that only one solenoid of the pair is activated at a time. Diode protection is required to protect the IC from the solenoid voltage flyback.

Switch position can be indicated remotely by utilizing the open and closed states of the internal coil contacts. The shaded areas of Figure 5 display two indicator circuits, one providing a TTL output and one that activates an LED. These circuits will output a TTL 'HI' (LED lamp 'ON') if the attenuation card is in the RF circuit, and will output a TTL 'LO' (LED) lamp 'OFF') if the thru line is in the RF circuit. Since current is drawn through the coil for these circuits, inadvertent switching is prevented by limiting the current to 5 mA.

Hewlett-Packard assumes no responsibility for the use of any circuits described herein and makes no representation or warranties, express or implied, that such circuits are free from patent infringement.

Table 4. Solenoid pin and color code assignment guide.

Section	Section 1		Section 2		Section 3		Section 4	
Solenoid Coil[1]	Thru Line	Atten. Card	Thru Line	Atten. Card	Thru Line	Atten. Card	Thru Line	Atten. Card
Cable Wire Color Code[1]	PUR	YEL	BLK	GRN	ORN	BLU	BRN	WHT
Connector Plug Pin Number[2]	5	6	7	8	9	10	11	12
Opt.008/016 Ribbon Wire Color Code	BLK	WHT	BLU	ORN	VIO	RED	GRN	YEL
Flat Pack Plug Pin Number[3]	13	2	11	5	3	9	4	10
33320G/H(11dB)	0 dB	1 dB	0 dB	2 dB	0 dB	4 dB	0 dB	4 dB
33321G/H(70dB)	0 dB	10 dB	0 dB	20 dB	0 dB	40 dB	*	*
33321K[4](70dB)	0 dB	10 dB	0 dB	20 dB	0 dB	20 dB	0 dB	20 dB
33323K[4](90dB)	0 dB	10 dB	0 dB	20 dB	0 dB	30 dB	0 dB	30 dB
33322G/H(110dB)	0 dB	10 dB	0 dB	20 dB	0 dB	40 dB	0 dB	40 dB

*Not Used
[1]Five-foot cable and mating plug assembly provided.
[2]Pin 1 (red wire) is common for all coils. Pins 2, 3 and 4 are not used on all models. See connector pin diagram in Figure 7, page 8.
[3]Pin 6 (brown wire) is common for all coils. Pins 1, 7, 8, 12, and 14 are not used.
[4]See page 6 for recommended switching sequence for the 33321/23K. Also see Figure 8, page 8.

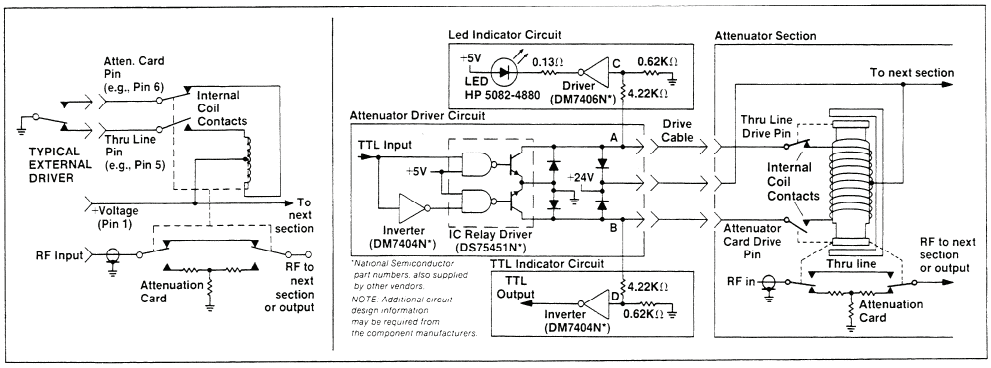

Figure 4. Section electrical diagram.

Figure 5. Driver and indicator circuits for one section of an HP 33320, 1, 2, 3, G/H/K

Specifications

Specifications describe the instrument's warranted performance. Supplemental characteristics are intended to provide information useful in applying the instrument by giving typical, but non-warranted, performance parameters. These are denoted as "typical", "nominal", or "approximate".

Electrical

Attenuation Accuracy (± dB Referenced from 0-dB Setting):

HP Models 33320A/B/G/H (11 dB max*)											
Frequency Range	Attenuator Setting (dB)										
	1	2	3	4	5	6	7	8	9	10	11
dc-4 GHz (A,G only)	0.2	0.2	0.3	0.3	0.3	0.3	0.4	0.4	0.4	0.4	0.5
dc-12.4 GHz (B,H only)	0.3	0.3	0.4	0.4	0.5	0.5	0.6	0.6	0.6	0.6	0.7
12.4-18.0 GHz (B,H only)	0.7	0.7	0.7	0.7	0.7	0.8	0.8	0.8	0.8	0.9	0.9
*Typical step-to-step accuracy is ± 0.2 dB to 18 GHz											

HP Model Numbers	33321A/B/G/H (70 dB max*)										
	33322A/B/G/H (110 dB max*)										
Frequency Range	Attenuator Setting (dB)										
	10	20	30	40	50	60	70	80	90	100	110
dc-4 /GHz (A,G only)	0.2	0.4	0.5	0.7	0.8	1.0	1.2	1.3	1.5	1.6	1.8
dc-12.4 GHz (B,H only)	0.5	0.7	0.9	1.2	1.5	1.8	2.1	2.4	2.7	3.0	3.3
12.4-18.0 GHz (B,H only)	0.6	0.8	1.2	1.6	2.0	2.4	2.8	3.2	3.6	4.0	4.4
*Typical step-to-step accuracy is ± 1 dB to 18 GHz.											

HP Model Numbers	33321D/K (70dB max*)								
	33323K (90 dB max*)								
Frequency Range	Attenuation Setting (dB)								
	10	20	30	40	50	60	70	80	90
dc-6.0 GHz	0.3	0.5	0.6	0.7	0.8	1.0	1.1	1.1	1.2
6.0-12.4 GHz	0.4	0.5	0.7	0.9	1.0	1.3	1.5	1.6	1.7
12.4-18.0 GHz	0.5	0.6	0.8	1.1	1.2	1.4	1.7	1.8	2.1
18.0-26.5 GHz	0.7	0.8	1.0	1.5	1.6	1.9	2.3	2.5	2.8
*Typical step-to-step accuracy is ± 0.6 dB to 18 GHz ± 0.9 to 2.65 GHz.									

To insure warranted specifications for the HP 33321K, and HP 33323K, the following combination of sections is recommended.

Attenuation (dB)	10	20	30	40	50	60	70	80	90
HP 33321K	1	4	1, 4	2, 4	1,2,4	2,3,4	1,2 3,4	—	—
HP 33323K	1	2	4	1, 4	2, 4	3, 4	1,3,4	2,3,4	1, 2 3, 4

SWR (Characteristic Impedance: 50 ohms)

HP Model	Frequency (GHz)				
	dc-4	4-8	8-12.4	12.4-18	18-26.5
33320A/G 33322A/G	1.5 1.5	— —	— —	— —	— —
33320B/H 33322B/H	1.5 1.5	1.5 1.5	1.6 1.6	1.9 1.9	— —
33321A/G	1.35	—	—	—	—
33321B/H	1.35	1.35	1.5	1.7	—
	dc-6	dc-12.4			
33321D/K 33323K	1.25 1.25	1.45 1.45		1.6 1.6	1.8 1.8

Attenuation Temperature Coefficient: Less than 0.0001 dB/dB/°C.

Power Sensitivity: 0.001 dB/watt.

RF Input Power (max.): 1 watt average, 100 watts peak (10 μs pulse width).

Life, Minimum: 5 million cycles per section.[1]

Repeatability: 0.01 dB, typical to 18 GHz, 0.05 dB, typical to 26.5 GHz.

Insertion Loss (0 dB position, f is frequency in GHz):

HP 33320A/B/G/H: (0.6 + 0.09 x f) dB

HP 33321A/B/G/H: (0.4 + 0.07 x f) dB

HP 33321D/K/: (0.4 + 0.09 x f)dB

HP 33322A/B/G/H: (0.6 + 0.09 x f)dB

HP 33323K: (0.4 + 0.09 x f) dB

[1]A cycle is defined as switching from the thru-line position to the attenuation card and back to the thru-line position or vice versa.

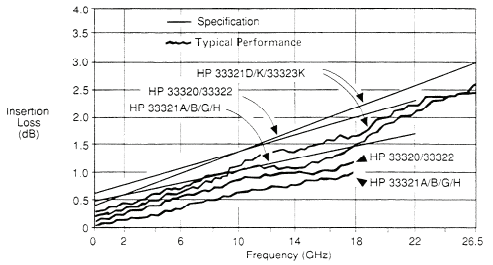

Environmental Capabilities*

Temperature, Operating: -20° to +75°C.
Temperature, Non-Operating: -55°C to +85°C.
Altitude, Operating: 15,000 ft.
Altitude, Non-operating: 50,000 ft.
Humidity: Cycling 5 days, 40°C at 95% RH with condensation.
Shock, Operating: 10 g's, 6 ms, on six sides, three blows.
Shock, Non-operating: 500 g's, 1.8 ms, in 6 directions.
Vibration, Operating: 5 g's, 34–2000 Hz (for all models except the HP 33321D/K); 0.015 inches DA, 5-55 Hz (for the 33321D/K only).
EMC: radiated interference is within the requirements of MIL-STD-461 method RE02, VDE 0871 and CISPR Publication II.

*Additional environmental data provided on request.

Mechanical

Mounting Position: Any.
Net Weight:
HP 33321 / **HP 33323**: A/B: 198 grams (7 oz); G/H: 227 grams (8 oz); D: 255 grams (9 oz); K: 284 grams (10 oz).
HP 33320 / **HP 33322**: A/B: 255 grams (9 oz); G/H 284 grams (10 oz).

RF Connectors: SMA female for HP 33320/1/2 A/B/G/H. APC-3.5 female (SMA compatible) for HP 33321D/K & HP 33323K.

Programmable Models (G, H, K)

Switching Speed: Max. 20 msec including settling time.

Solenoids	Coil Voltage	Switching Current*	Nominal Coil Impedance
Standard (G, H, and K models)	24V (20 - 30V)	125 mA (@ 24V)	190Ω (65 mh)
Option 011 (G & H models plus HP33323K)	5V (4 - 7V)	300 mA (@ 5V)	17Ω (5.5 mh)

*Current per section; appoximately 8 msec duration before internal contacts open the coil circuit.

Accessory provided (except Option 008 & 016)
Solenoid drive plug on 5-foot cable included with programmable models. (Replacement plug and cable assembly available as HP Part Number 8120-2178.)

Step Attenuator Selection Guide

To order, basic model number and suffix letter must be specified. The basic model number defines the step size and maximum attenuation value. HP 33320 (1-dB step, 11-dB max.) HP 33321 (10-dB step, 70-dB max.), HP 33322 (10-dB step, 110-dB max.), HP 33323 (10-dB step, 90 dB max.). The suffix letter denotes frequency range and switching mode (manual or programmable); A, B, and D denote dc — 4 GHz, dc — 18 GHz, and dc —26.5 GHz respectively for the manual models; G, H, and K denote dc — 4 GHz, dc —18 GHz, and dc — 26.5 GHz respectively for the programmable models. Standard coils are 24 volt, Option 011 specifies 5 volt.

Attenuation Step Size	Attenuation Range	Frequency Range	Switching Mode (Manual or Programmable)	HP Basic Model Number
1 dB	0–11 dB	dc–4 GHz	MAN.	33320A
			PROG.	33320G
		dc–18 GHz	MAN.	33320B
			PROG.	33320H
10 dB	0–70 dB	dc–4 GHz	MAN.	33321A
			PROG.	33321G
		dc–18 GHz	MAN.	33321B
			PROG.	33321H
		dc–26.5 GHz	MAN.	33321D
			PROG.	33321K
	0–90 dB	dc–26.5 GHz	PROG.	33323K
	0–110 dB	dc–4 GHz	MAN.	33322A
			PROG.	33322G
		dc–18 GHz	MAN.	33322B
			PROG.	33322H

Ordering Information

Specify basic model number and suffix, per the table above.

Option 008: 8 inch (20.3 cm) ribbon cable with 14 pin flat pack male connector. (See back page.)

Option 016: 16 inch (40.6 cm) ribbon cable with 14 pin flat pack male connector (see back page.)

Option 011: 5 volt solenoid operation.

Option 890: Calibration data:
4 GHz models: 20 frequencies
18 GHz models: 90 frequencies
26.5 GHz models: 101 frequencies

B.4 Hybrid coupler

KRYTAR

MODEL 1831

1-18 GHz 90° HYBRID COUPLER

SPECIFICATIONS

FREQUENCY RANGE	1-18 GHz
COUPLING	3 dB
AMPLITUDE IMBALANCE	± 0.5 dB
PHASE IMBALANCE *	± 10 Degrees
ISOLATION	> 17 dB
MAXIMUM VSWR	1.35
INSERTION LOSS	< 2.0 dB
POWER RATING	
Average	20 W
Peak	3 KW
STANDARD CONNECTORS	SMA Female
Optional: N Female	
WEIGHT (ounces)	
SMA Female Connectors	5.2
N Female Connectors	7.7
OPERATING TEMPERATURE	-54° to +85° C

* Units with a tighter phase imbalance specification can be supplied.

DIMENSIONS

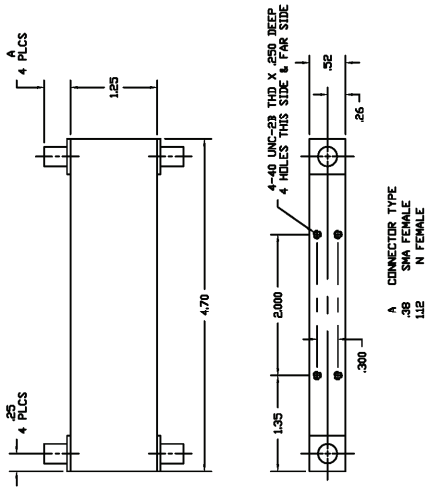

KRYTAR
1288 Anvilwood Ave. • Sunnyvale, CA 94089 • (408) 734-5999 • FAX: (408) 734-3017
Toll Free 1 (877) 734-5999 • www.krytar.com

8/05

Appendix C

Experiment reports

Appendix C Experiment Reports

Appendix C.1 . 1st technical report of Increasing the dynamic range in High power RF measurement system by using step attenuator

TARGET
TOP AMPLIFIER RESEARCH GROUPS
IN A EUROPEAN TEAM

WP 1.3.2: LAB EXTENSION

TARGET Technical Report - Increasing the dynamic range in High power RF Measurement by using step attenuators

Date	2006-11-22
Author	Jonathan Lees, Nilaped Russamee
Crganisation	Cardiff University
Version	0.1
Document ID	TARGET-20061114-132-CAS-0_1
Dissemination	WP 1.3.2 participants

Abstract

There is no doubt that time-domain load-pull measurement systems giving access to the voltage and current waveforms present at the input and output terminals of a device represent powerful tools in modern PA design. They allow for example the observation of dynamic load-line and transfer characteristic behaviour, along with the ability to actively synthesise complex harmonic impedance environments. When these systems are used in high power applications however, a dynamic range problem exists: whilst measurements involve the customisation of the microwave test-set in order to observe significant forward and reverse power levels, the broadband nature of the measurement system and the difficulty in achieving significant, very broad-band power amplification forces the calibration to be conducted at much lower power levels.
Cne solution to this dynamic range problem is to use programmable step attenuators within the calibrated path. This overcomes the difficulties presented by large signal calibration, generally increase measurement dynamic range, and introduces additional flexibility into

microwave measurement at high power levels. This report discusses the value of this implementation, presents measurement results and discusses future work.

1 Introduction

A number of measurement systems have been developed at Cardiff University over recent years that are all based upon a common theme of waveform measurement and active harmonic load-pull [18]. The most recent of these include modulated envelope and IF load-pull systems, and a high-power harmonic load-pull system employing broad-band impedance transformers, which is capable of operating at fundamental power levels in excess of 100W, and over a bandwidth of 1 to 12.5 GHz. This system has been demonstrated through the extensive characterisation of various 100W LDMOS devices, enabling measurement and characterisation under optimum harmonic load conditions [19].

The increasing need to actively load-pull and measure these very high power devices presents new and challenging demands for load-pull measurement systems. One example is the need to achieve and manipulate the necessary dynamic range for accurate high and low-power measurement without impacting overall measurement accuracy.

It is usually the case, and indeed a necessity that the microwave test-set architecture, once calibration remains unchanged for the measurement phase. The obvious approach of using fixed, broad-band attenuators effectively fixes the measurement dynamic range, and this results in the problem that the system is unable to measure small signals when using large attenuation values, and similarly cannot measuring large signals when using small attenuation values.

Another related problem surrounds the final stage of calibration of these systems, which involves attaching one of the calibrated measurement ports directly to a calibrated power meter. This absolute power calibration step involves using a calibration 'thru' as the DUT, and driving the system with sufficient power in order to obtain measurable signal levels from the attenuated directional couplers. This results in the coupled power being up to 60 dB smaller than the thru power, so there is a significant risk of overdriving the calibrated power meter, in this case a Hewlett Packard Microwave Transition analyser (MTA).

The proposed solution involves the introduction of highly characterised, high-quality step attenuators within the measurement path. These attenuators are situated between the directional couplers and the MTA, with measured attenuator s-parameter data used to correct measured voltage travelling waves in advance of software processing within the measurement system itself.

2 S-Parameters measurement

The first step in this exercise was to characterise each step attenuator, in each attenuation state. These measurements were extremely important in deciding firstly if this approach was a realistic option, and secondly to collect the necessary s-parameter data with which to correct the measured data once the stepped attenuators were included in the High Power measurement system. A PC controlled, automated s-parameter measurement system was used to collect the s-parameter measurement data using HP 8510 Vector Network Analyser (VNA). Automation was critical due to the need to switch the attenuators between states, and also due to the large number of measurements necessary to assess switching repeatability.

2.1 Measurement configuration

Figure 2.1 shows the automated measurement system comprising a PC, the VNA, a HP-3488A switch control unit and associated cabling. The control unit is used to select the required step attenuator state, and control of all instrumentation is achieved using a GPIB interface and the IGOR software environment.
The Step Attenuators used are of type HP-33321H, and are selectable between 0-70 dB in 10dB steps. A more detailed specification of these attenuators is provided in references [4-7].

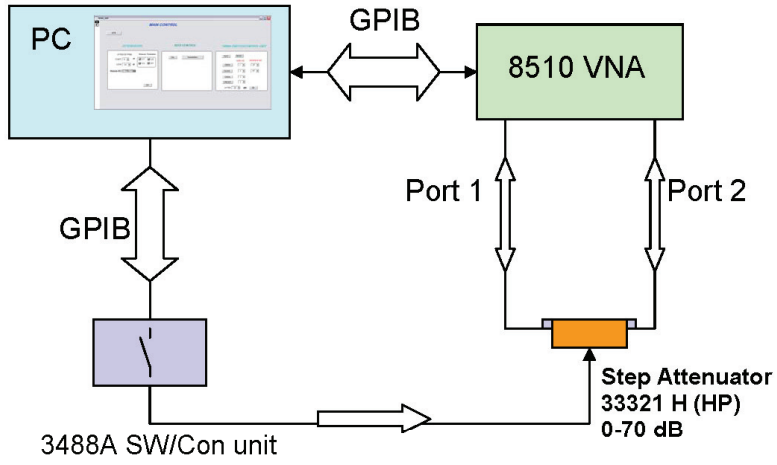

Figure 2.1: Automated Computer measures S-parameter of the step attenuator.

2.2 Measurement procedure and data processing

As stated, the measurement process is automated, and is summarised below:

1 – Perform full 3.5mm coaxial, 2-port Calibration of the HP 8510.
2 - Connect the step attenuator HP 33321H, and to the HP8510 VNA

3 - Launch the Igor software and establish communication

4 - Establish measurement options and start the measurement.

For the characterisation phase, 100 separate 201-point s-parameter measurements were conducted for each attenuation state, for each attenuator and over a bandwidth of 45 MHz to 20 GHz. This was repeated for each of the two attenuators used and resulted in a large amount of data. Following each measurement, all s-parameter data is saved in Igor binary format ready for post-processing. The resulting s-parameter data was then analysed in order to assess switch repeatability, and later averaged. The final step of this process involved converting the averaged s-parameter data into Polar form, and curve-fit magnitude and the unwrapped phase separately using high-order polynomial functions. This process is outlined in Table-1 and Figures 2.4 and 2.5 below.

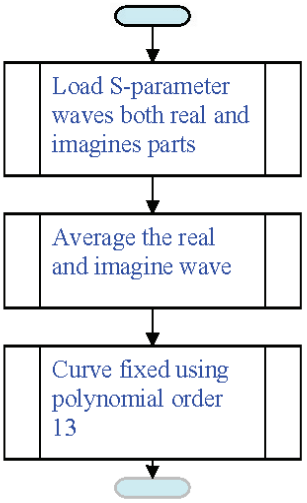

- 100 sample 201point each, frequency 45 MHz- 20 GHz
- A representative S-parameter 201 points , frequency 45 MHz - 20 GHz
- S-parameter waves modelled 201 points frequency 45 MHz- 20 GHz

Table-1: S-parameter modelling process

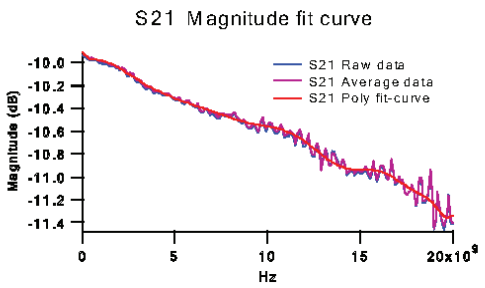

Figure 2.4: s21 magnitude for all measurements, averaged s21 magnitude, and polynomial fit

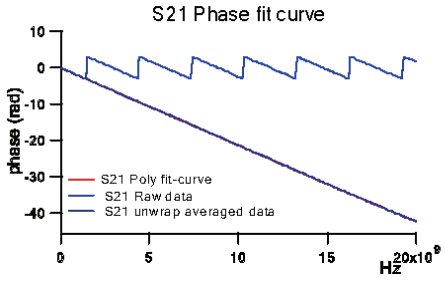

Figure 2.5: s21 phase for all measurements, averaged s21 phase, and polynomial fit

2.3 Assessing repeatability

It was critically important to gain a complete understanding of the attenuator's performance, not only in absolute terms in comparison to the data sheet (see table-2), but also in terms of repeatability. The need to statistically assess repeatability of the attenuator cannot be overstated, and this was done by measuring the ability of the attenuator to transit between all attenuation states, and return to a given state whilst observing the change in the original measured s-parameter data.

Frequency range: DC to 18 GHz.
Attenuation range: 0 to 70 dB, 10 dB steps
Insertion loss at 0 db: 0.4 dB + 0.07 dB/GHz.
Maximum SWR: 1.35 to 8 GHz. , 1.5 to 12.4 GHz., 1.7 to 18 GHz.
Repeatability life: 0.03 dB maximum, 5 million cycles per section.

Table -2 Specification of step attenuator type HP 33321H

Figures 2.4 to 2.8 show that a repeatability of 0.03dB 1SD is achieved over the frequency range of interest from 0 to 12 GHz, for the first four attenuator states of 0, 10, 20 and 30 dB. Similarly a phase repeatability of 0.2° 1SD is achieved over the same frequency range and attenuator states. These figures are well within the usual measurement accuracy of the system.

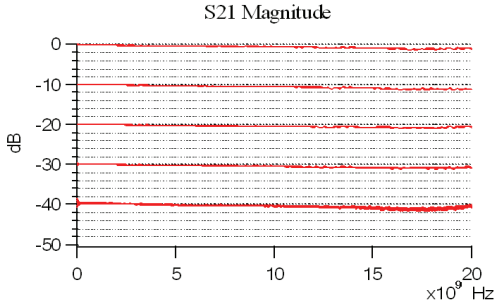

Figure2.4: s21 Magnitude vs. Frequency 45 MHz-20GHz, for states 0dB to 40 dB

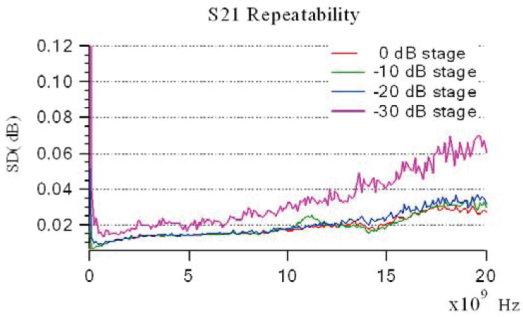

Figure2.5: Standard deviation of magnitude vs. Frequency , for states 0dB to 30 dB

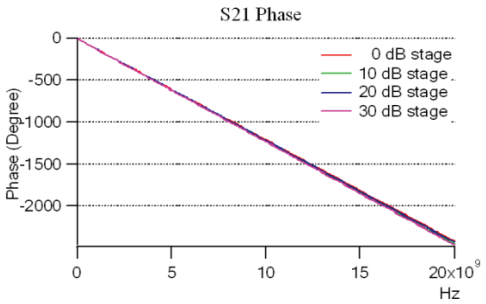

Figure2.5: s21 Phase vs. Frequency 45 MHz-20GHz, for states 0dB to 30 dB

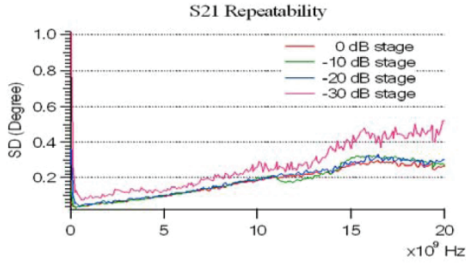

Figure2.6: Standard deviation of phase vs. Frequency , for states 0dB to 30 dB

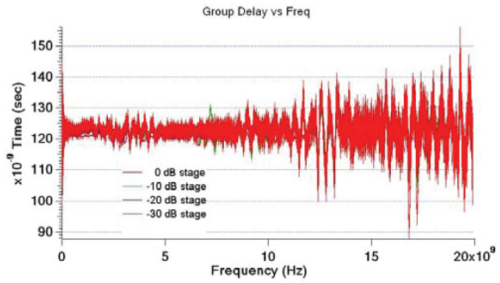

Figure 2.7: Group delay vs. Frequency 45 MHz-20GHz, for states 0dB to 20 dB

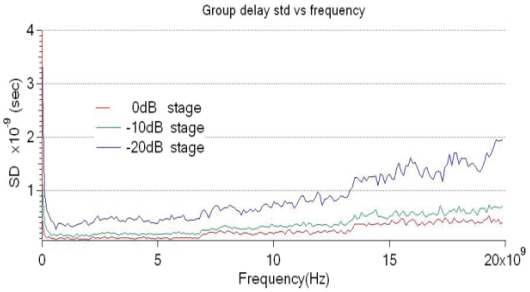

Figure2.8: Standard deviation of Group delay vs. frequency 45 MHz-20GHz, for states 0dB to 20 dB

3 Systems configuration

Figure 3.1 shows a simplified block diagram of waveform measurement system, with the step attenuators inserted between MTA ports and the switches that multiplex a and b signals into the two channel MTA receiver. All instrumentation is computer controlled using the Wavemetrics IGOR software environment and through a GPIB interface.

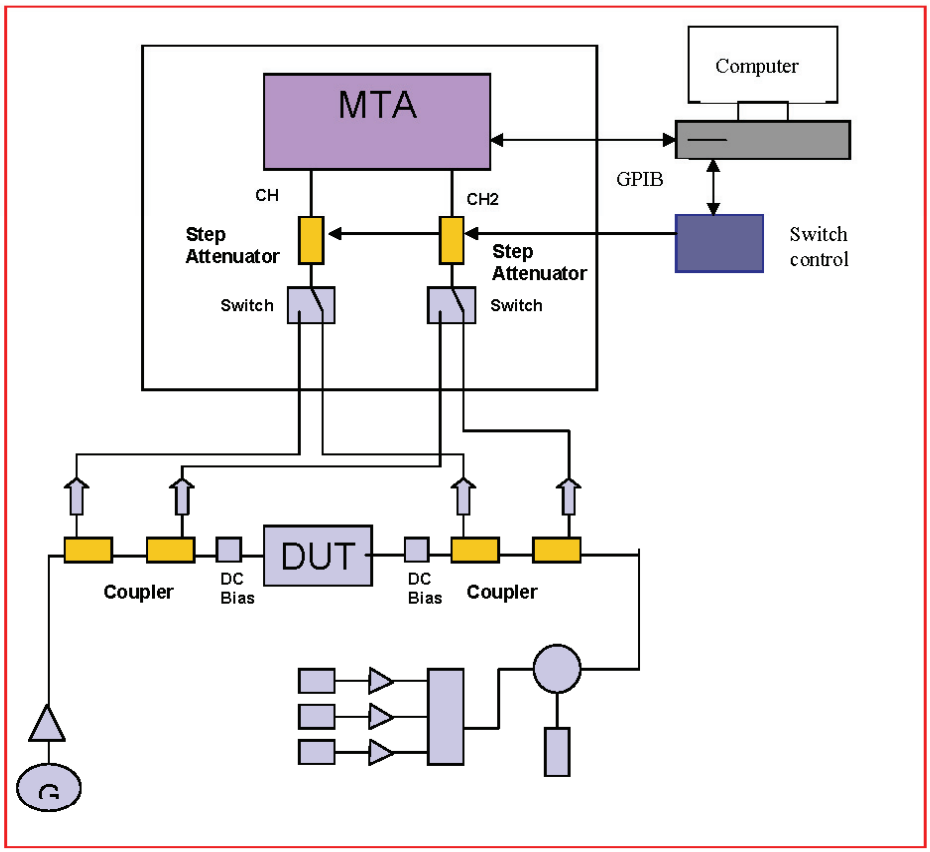

Figure 3.1: RF measurement configuration shows step attenuators which are connected into MTA ports.

The general measurement process can be considered as starting with calibration of the system, and for this stage the step attenuators are both set to their 0 dB states. Following calibration, the DUT is inserted and measurements commence in the usual manner. In-between measurements, the step attenuators are manually switched to the most suitable step level, and the software takes the appropriate action and effectively adjusts the measured a and b voltage waveforms to compensate for the presence of the attenuator.

3.1 Correction procedure

The simple procedure presented in figure 3.2 illustrates how the presence of the attenuator is managed within the measurement software. The first chart shows the original procedure, where the second shows how the correction fits-into this process.

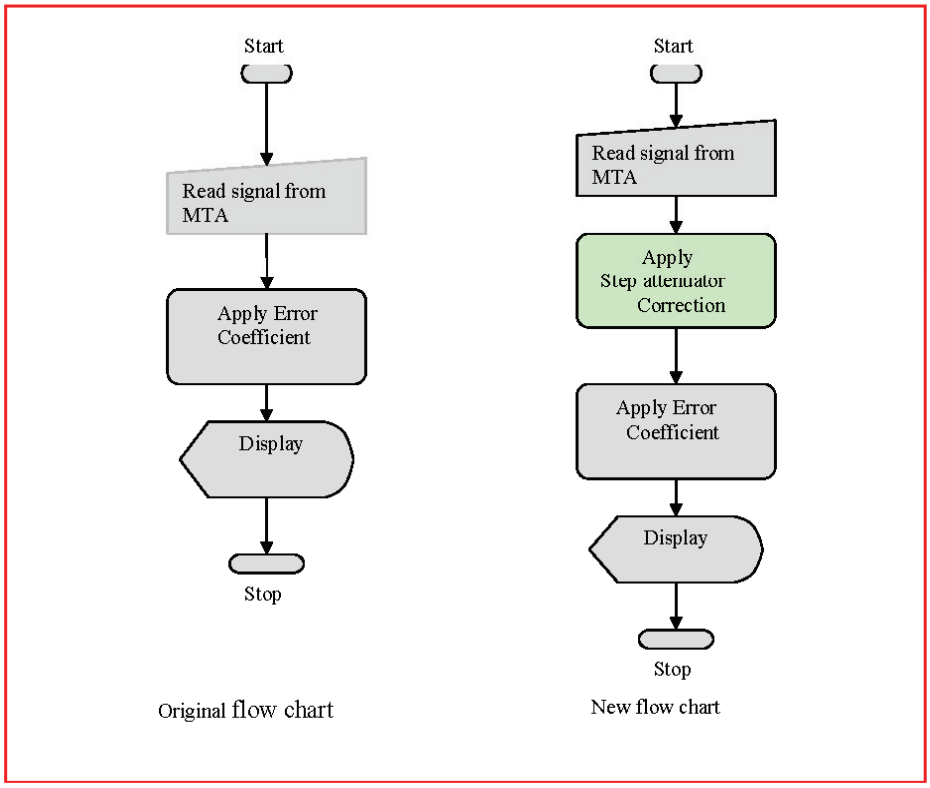

Figure 3.2: show the procedure of corrected data in measurement system.

The step attenuator correction is modelled using the measured s-parameters and the approach discussed in previous sections, and is applied to the measured a0, b0, a3 and b3 voltage waveforms. As the system is calibrated with the attenuators in 0dB states, it is important to realise that the behaviour of the attenuators in the 0dB states will be accounted for in the usual calibration. When switching the attenuators to other states, the 0dB states of both attenuators form a reference. It is therefore the differences between the 0dB states and the selected attenuator state that is used to derive the applied correction.

3.2 Verification through measurement

Initially, the approach has been verified by measuring large-signal excitation, a thru standard in place of an active DUT and comparing the measured waveforms when using different attenuator states. Two s-parameter based correction approaches have been used and are compared and are shown in Figures 3.3 to 3.10.

The first approach uses simple averaged s-parameters, whereas the second uses a polynomial fit, as described earlier in this report. Although comparisons using fundamental sinusoids are useful, they do not test the broadband performance of the system. In order to test over bandwidth, the microwave signal source was driven into compression such that it's output stage saturated, generating harmonically rich, non-sinusoidal waveforms.

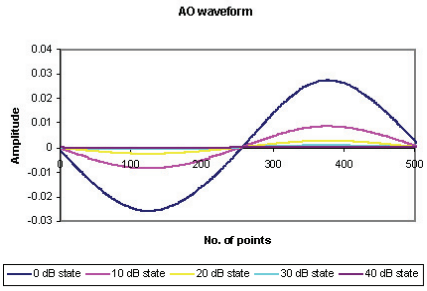

Figure 3.3: Actual a0 voltage waveform incident at the MTA corresponding with five step attenuator stages

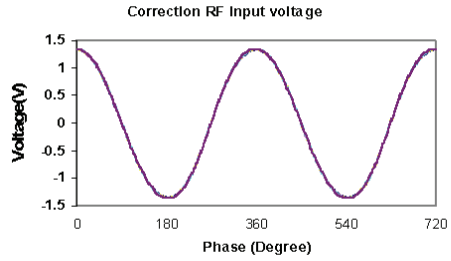

*Figure 3.4: System calculated RF input voltage waveform corresponding to all step attenuator stages using **average** s-parameter correction*

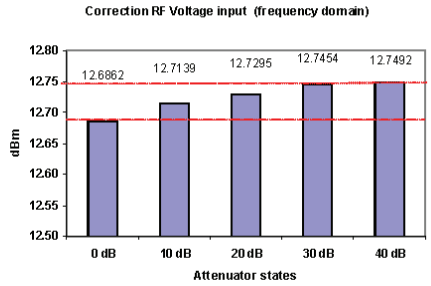

*Figure 3.5: Calculated RF input fundamental voltage magnitude spread when using the **average** s-parameter model.*

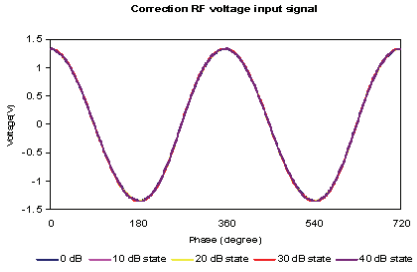

*Figure 3.6: System calculated RF input voltage waveform corresponding to all step attenuator stages using **polynomial** s-parameter correction*

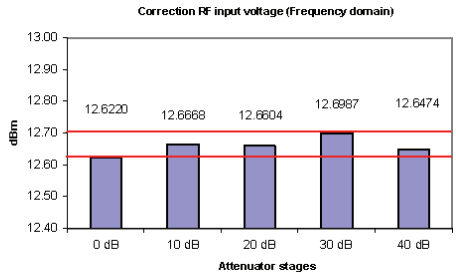

*Figure 3.7: Calculated RF input fundamental voltage magnitude spread when using the **polynomial** s-parameter model.*

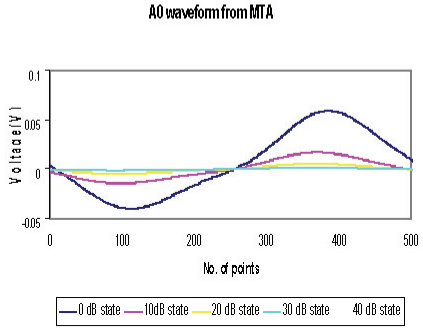

Figure 3.8: Actual a0 distorted voltage waveform incident at the MTA corresponding with five step attenuator stages

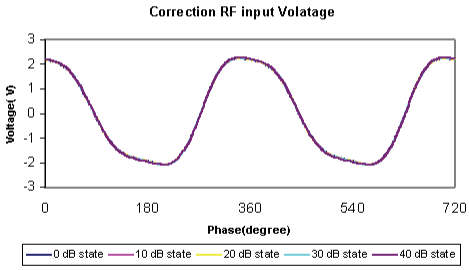

*Figure3.9: System calculated RF input voltage waveform corresponding to all step attenuator stages using **average** s-parameter correction – distorted waveform*

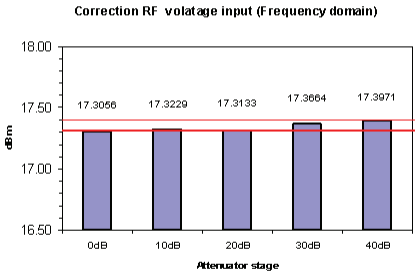

*Figure 3.10: Calculated RF input fundamental voltage magnitude spread using the **polynomial** s-parameter model – distorted waveform.*

4 Conclusions and future work

A solution to the problem of measurement system dynamic range has been proposed that involves the introduction of highly characterised, high-quality step attenuators within the measurement path, between the directional couplers and the MTA. Comprehensive characterisation has shown that it is possible to employ measured attenuator s-parameters to generate models with which to accurately correct measured voltage travelling waves in advance of software processing within the measurement system itself. Two correction methods have been explored; the first using simple averaging of measured s21, and the second employing a polynomial fit to the averaged data, with similar results.
These results indicate that the various attenuation states are highly repeatable, with measured s21 magnitude and phase varying by no more than 0.03dB and 0.2° (1SD) respectively over a switching sequence of at least 100 cycles per state, and over frequency range of 0 to12GHz.
Future work includes developing the system to allow automatic range control of the attenuators. Great care must be exercised when applying auto-ranging in high power measurement systems however due to the significant potential of instrument damage.

5 Acknowledgement

Research reported here was performed in the context of the network TARGET– "Top Amplifier Research Groups in a European Team" and supported by the Information Society Technologies Programme of the EU under contract IST-1-507893-NOE, www.target-org.net

6 References

[1] Pozar, D.M. (2005), *Microwave engineering*, 3rd ed., USA, John Wiley &Son,

[2] IEE. (1996), *Half day Colloquium on Uncertainties made easy*, London, Institution of Electrical, Engineering Savoy Place.

[3] Agilent. (2000), "Understanding the Fundamental Principles of Vector Network Analysis", Application note, USA

[4] Agilent. (1995), *" 3488A Switch/Control Unit Operating, Programming, Configuration Manual"*, USA

[5]. Agilent (2001), *"8510C Network Analyzer System operating and programming manual"* edit 3, USA

[6] Agilent. (1990), *Agilent Technologies 33320A/B/G/H 33321 A/B/D/G/H/K 33322A/B/G/H 33323K Step attenuators for OEM & System Use dc to 26.5 GHz*, Technical data sheet, USA

[7] WaveMetrics Inc, (2004), *"IGOR Pro Verson5.0 manual"*, Lake Oswego, USA

[8] Agilent (2002), "*Applying Error Correction to Network Analyzer Measurements*", Application Note AN 1287-3, USA

[9] Agilent (2004) , *Specifying Calibration Standards for the Agilent 8510 Network Analyzer*, Application Note 8510-5B, USA

[10] Agilent. (2001), *Network Analysis Applying the 8510 TRL Calibration for Non-Coaxial Measurements*, Product Note 8510-8A, USA

[11] Agilent (2001), *"8510C Network Analyzer Key word dictionary"* ,rev.3, USA

[12] Ludwig R. and Bretchko P.(2000), *RF Circuit Design Theory and Applications* , Prentice Hall,Upper saddle River,NJ.

[13] Lee, Yeoy-song (2005), *Testing Dynamic Accuracy of Vector Network Analyzers Using the 40 GHz Step Attenuator*, 65th ARFTG Microwave Measurements, Conference Digest 2005-Millimetre-wave Application, p159-168

[14] A. Chenakin and AP.S "Paul" Khanna phase Matrix (2006), *Inc, "2-22 GHz Continuously Variable Attenuator Has Low IMD and Float Response"* , High Frequency Electronics, pp16-20

[15] Kim, Jeong-Hwan, Park, Jeong-Il; Kang and Ung-Taeg (2005) *"Uncertainty Evaluation Of a Broadband Attenuation Standard"*, IEEE Transactions on Instrumentation and Measurement, v 54, n 2, April, p 705-708.

[16] Andrew G. Morgan, Nick M. Ridler, and Martin J. Salter(2003), *"Generalized Adaptive Calibration Schemes for precision RF Vector Network Analyzer Measurements"*, IEEE Transactions on instrumentation and measurement, Vol. 52, No.4 , pp1266-1272

[17] Pulvio G. Ananasso(1980), " *A Low Phase Shift Step Attenuator Using p-i-n Diodes Switches"*, IEEE transactions on microwave theory and techniques, Vol. MTT-28, No 7, pp774-776

[18] Johannes Benedikt, Roberto Gaddi, Paul J. Tasker, and Martin Goss(2000), *" High Power Time-Domain Measurement System with Active Harmonic Load-Pull for High-Efficiency Base-Stationn Amplifier Design"*, IEEE Trans. On Microwave theory and Techniques, Vol 48, NO. pp 2617-2624

[19] Z. Aboush, J. Lees, J. Benedikt, and P. J. Tasker, "Active Harmonic Load-Pull System for Characterization of Highly Mismatched High Power Transistors," presented at IEEE MTT-S, Long Beach, CA, 2005.

Appendix C.2 2nd technical report of Increase the dynamic range in High power RF measurement system by using step attenuators

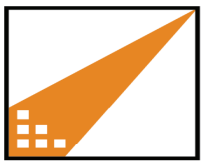

T A R G E T
TOP AMPLIFIER RESEARCH GROUPS
IN A EUROPEAN TEAM

WP 1.3.2: LAB EXTENSION

TARGET Technical Report - Increasing the dynamic range in High power RF Measurement by using step attenuators

Date	2007-07-30
Author	Jonathan Lees, Nilaped Russamee
Organisation	Cardiff University
Version	0.1
Document ID	TARGET-20070730-132-CAS-0_1
Dissemination	WP 1.3.2 participants

Abstract

This report is a summary of the work performed by Cardiff University (partner-ID 5) in the framework of TARGET Work Package 1.3.2 - *Lab Extension*. The main activity reported covers extending non-linear measurement system dynamic range through the use of high-quality, high-repeatability step-attenuators. In addition, Cardiff has participated in a Mini Round Robin exercise with the University of Vigo, where three non-linear waveform measurement systems have been compared through measurement and comparison of waveforms collected fro an on-wafer InGaP HBT device under near identical bias and drive conditions. This systems were specifically MTA, sampling scope and LSNA based, and the measurements were carried out with particular emphasis placed on recreation or 'emulation' of input and output harmonic impedances through the use of active and passive load-pull. In order to prevent duplication, the collaborative findings of this exercise are included within the final report produced by the University of Vigo [20], and are not discussed in any detail here.

EU FP6 Project TARGET IST-1-507893-NOE

1 Introduction

There is no doubt that time-domain load-pull measurement systems that provide access to the voltage and current waveforms present at the input and output terminals of a device represent an extremely powerful tool in modern PA design. Such tools allow for example the observation of key device characteristics such as the knee-walk-out phenomena associated with GaN devices, device memory investigations, dynamic load-line and transfer characteristic behaviour, model creation and verification, along with the ability to actively synthesise complex harmonic impedance environments.
When these systems are used in high-power applications however, a number of dynamic-range problems present themselves. Firstly, high-power measurements involve the modification of the 'conventional' low-power microwave test-set in order to accommodate significant forward and reverse power levels. The broadband nature of the measurement system coupled with the difficulty and expense in achieving significant, very broad-band power amplifiers forces the calibration to be conducted at much lower power levels.
One solution to this dynamic range problem is to use highly repeatable programmable step attenuators within the calibrated path. This approach, if properly implemented overcomes most of the difficulties presented by large signal calibration, and can be used to generally increase measurement dynamic range, introducing additional flexibility into microwave measurement at high power levels which is especially useful for example when measuring very high gain devices where a significant power difference can exist between the input and output of a device.
This report discusses the value of this implementation, presents measurement results and discusses future work.

A number of measurement systems have been developed at Cardiff University over recent years that are all based upon a common theme of waveform measurement and engineering through active harmonic load-pull [18]. The most recent of these systems include modulated envelope and IF load-pull systems, and a high-power harmonic load-pull system employing broad-band impedance transformers, that is capable of operating at fundamental power levels in excess of 100W, and over a bandwidth of 1 to 12.5 GHz. This system has been demonstrated through the extensive characterisation of various 100W LDMOS devices, enabling measurement and characterisation under optimum harmonic load conditions [19].

The increasing need to actively load-pull and measure very high power, high gain devices presents new and challenging demands for load-pull measurement systems. One example is the need to achieve and manipulate the necessary dynamic range for accurate high and low-power measurement without impacting overall measurement accuracy.

It is usually the case, and indeed a necessity that the microwave test-set architecture, once calibrated remains physically unchanged for the measurement phase. The obvious and current approach of using fixed, broad-band attenuators effectively fixes the measurement dynamic range, and this results in a problem where the system is unable to measure small signals when large attenuation values are used. Similarly, the calibrated system cannot measuring large signals when using small attenuation values.

Another related problem surrounds the final stage, or what will be termed here, the 'large-signal' calibration of these systems. This involves attaching one of the small-signal calibrated measurement ports directly to a calibrated power meter. This 'absolute' power calibration step

involves using a 'thru' connection as the DUT, and driving the system with sufficient power in order to obtain measurable relationship between coupled and thru signal levels, from the attenuated directional couplers and the calibrated port respectively. For high-power measurements, this can easily result in the coupled power being up to 60 dB smaller than the thru power, so there is a significant risk of overdriving the calibrated receiver being used as the power meter.

The proposed solution involves the introduction of highly characterised, highly repeatable, high-quality step attenuators inserted within the calibration path. These attenuators are situated between the directional couplers and the calibrated receiver, with the measured attenuator s-parameter data used to correct measured voltage travelling waves in advance of software processing within the measurement system itself.

2 Attenuator Characterisation

The first step in this exercise was to characterise each step attenuator, in each attenuation state. These measurements were extremely important in deciding firstly if this approach was a realistic option, and secondly to collect the necessary s-parameter data with which to correct the measured data once the stepped attenuators were included in the High Power measurement system. A PC controlled, automated s-parameter measurement system was used to collect the necessary measurement data using HP 8510 Vector Network Analyser (VNA). Automation was critical due to the need to switch the attenuators between states, and also due to the large size of measurement dataset that was necessary to assess switching repeatability.

2.1 Measurement configuration

Figure-1 shows the automated measurement system comprising a PC, the VNA, a HP-3488A switch control unit and associated cabling. The control unit is used to select the required step attenuator state, and control of all instrumentation is achieved using a GPIB interface and the IGOR software environment.
The Step Attenuators used are of type HP-33321H, and are selectable between 0-70 dB in 10dB steps. A more detailed specification of these attenuators is provided in references [4-7].

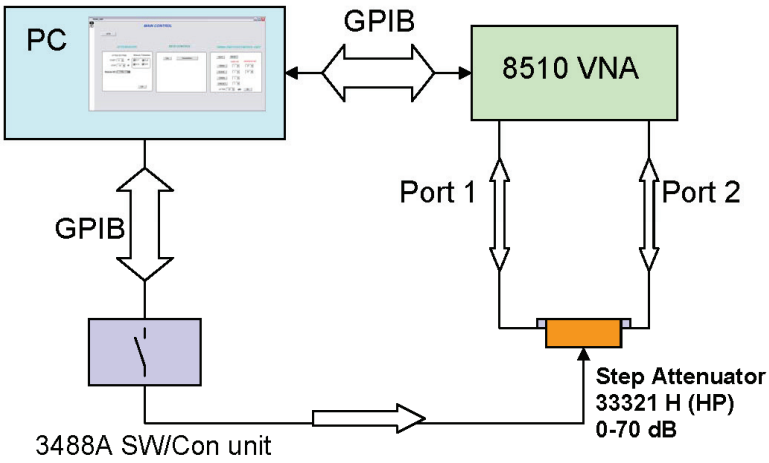

Figure 1: Automated Computer measures S-parameter of the step attenuator.

2.2 Measurement procedure and data processing

As stated, the measurement process is automated, and is summarised below:

1 - Perform full two-port 3.5mm, 2-port Calibration of the HP 8510.
2 - Connect the step attenuator HP 33321H to the switch unit and the HP8510 VNA
3 - Launch the Igor software environment and establish communication
4 - Establish measurement options and start the measurement.

For the characterisation phase, 100 separate 201-point s-parameter measurements were conducted for each attenuation state, for each attenuator and over a bandwidth of 45 MHz to 20 GHz. This was repeated for each of the attenuators used and resulted in a significant amount of data. Following each measurement, all s-parameter data was saved in IGOR binary format ready for post-processing. The resulting s-parameter data was then analysed in order to assess switch repeatability. The final step of this process involved converting the averaged s-parameter data into Polar form, and curve-fitting magnitude and the unwrapped phase separately using high-order polynomial functions. This process is outlined in Table-1 and Figures 2 and 3 below.

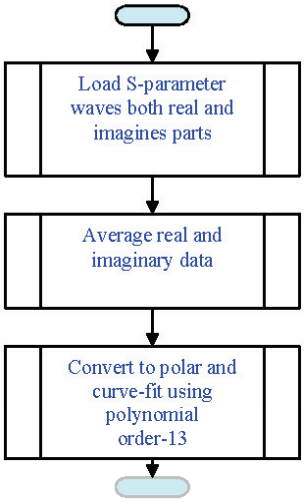

- 100 sample 201point each, frequency 45 MHz- 20 GHz
- Representative s-parameters 201 points , frequency 45 MHz -20 GHz
- S-parameters modelled 201 points frequency 45 MHz- 20 GHz

Table-1: S-parameter modelling process

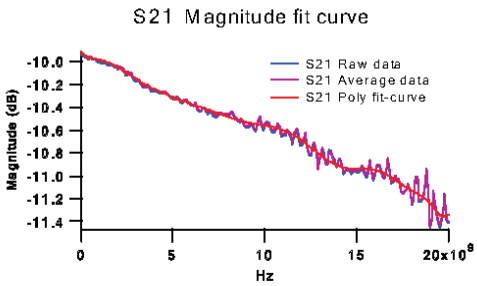

Figure 2: All s21(mag) data – raw, averaged and polynomial fit

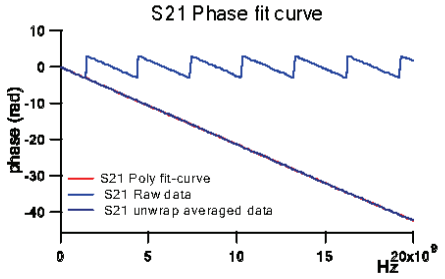

Figure 3: All s21(phase) data – raw, averaged and polynomial fit

2.3 Assessing repeatability

It was critically important to gain a complete understanding of the attenuator's performance, not only in absolute terms in comparison to the data sheet (see table-2), but also in terms of repeatability. The need to statistically assess repeatability of the attenuator cannot be overstated, and this was done by measuring the ability of the attenuator to transit between all attenuation states, and return to a given state whilst observing the change in the original measured s-parameter data.

Frequency range: DC to 18 GHz.
Attenuation range: 0 to 70 dB, 10 dB steps
Insertion loss at 0 db: 0.4 dB + 0.07 dB/GHz.
Maximum SWR: 1.35 to 8 GHz. , 1.5 to 12.4 GHz., 1.7 to 18 GHz.
Repeatability life: 0.03 dB maximum, 5 million cycles per section.

Table -2 Specification of step attenuator type HP 33321H

Figures 4 to 9 show that a repeatability of 0.03dB 1SD is achieved over the frequency range of interest from 0 to 12 GHz, for the first four attenuator states of 0, 10, 20 and 30 dB. Similarly a phase repeatability of 0.2° 1SD is achieved over the same frequency range and attenuator states. These figures are well within the usual measurement accuracy of the system.

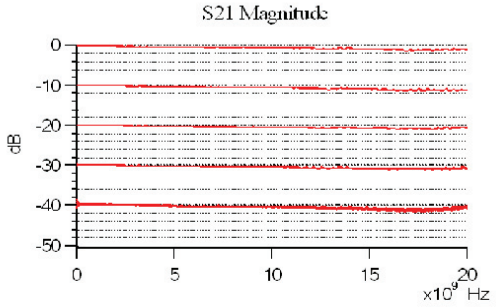

Figure-4: s21 Magnitude vs. Frequency 45 MHz-20GHz, for states 0dB to 40 dB

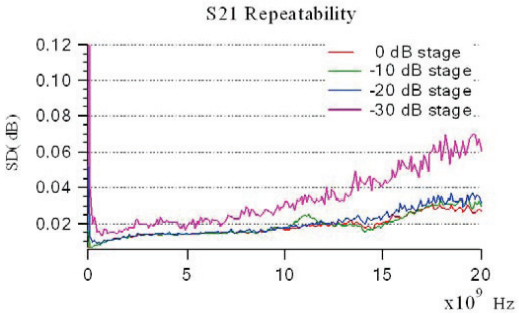

Figure-5: Standard deviation of magnitude vs. Frequency , for states 0dB to 30 dB

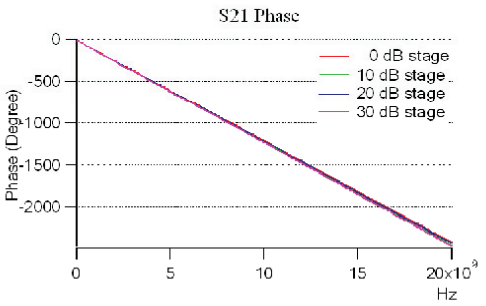

Figure-6: s21 Phase vs. Frequency 45 MHz-20GHz, for states 0dB to 30 dB

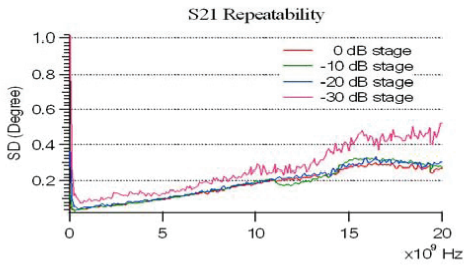

Figure-7: Standard deviation of phase vs. Frequency , for states 0dB to 30 dB

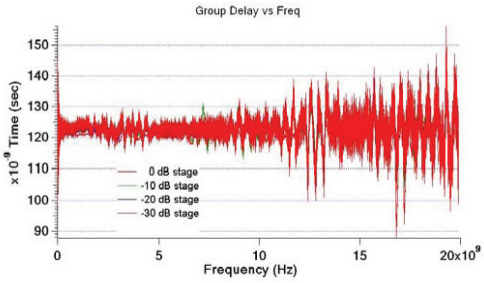

Figure-8 Group delay vs. Frequency 45 MHz-20GHz, for states 0dB to 20 dB

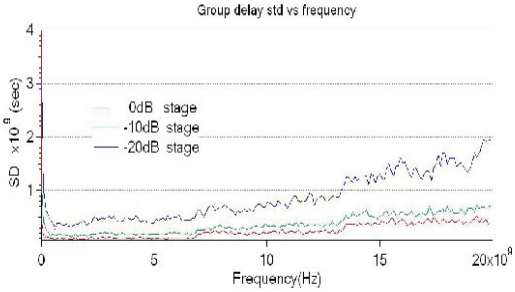

Figure-9: Standard deviation of Group delay vs. frequency 45 MHz-20GHz, for states 0dB to 20 dB

3 Correction approach

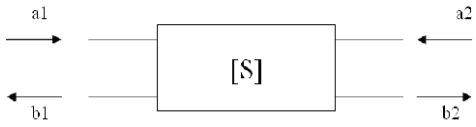

$$\begin{Bmatrix} b_1 \\ b_2 \end{Bmatrix} = \begin{bmatrix} S_{11} & S_{12} \\ S_{21} & S_{22} \end{bmatrix} \begin{Bmatrix} a_1 \\ a_2 \end{Bmatrix}$$

Fig-10 s-parameter formulation

Using the above definition, the step attenuator can be represented within the measurement system by the previously discussed measured s-parameters that accurately describe behaviour, as shown in Fig-11a. If the impedance environment surrounding the step attenuator can be assumed to be constant throughout its range of operation, that is, if Γ_R and Γ_C remain very close to 50Ω for all attenuator states and for all passive values of Γ_{in}, the signal flow representation can be simplified to that shown in fig-11b. Assuming that this is the case, the relationship between the measured traveling wave quantities a_{0a} and a_{0b} and the coupled quantities a_{1a} and a_{1b} can be rewrite in terms of S_{21} alone, as show below.

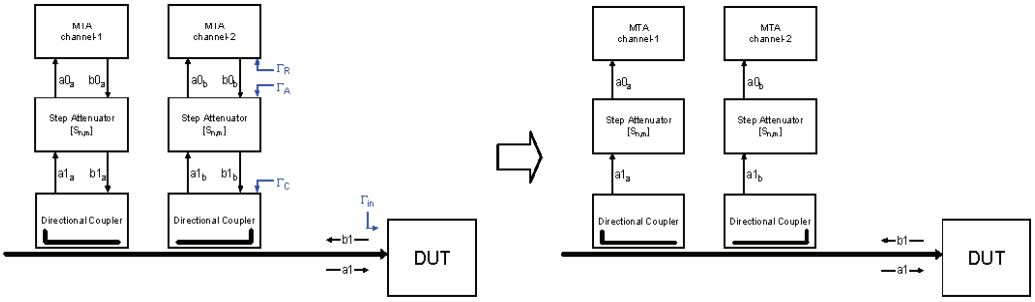

Fig-11a *Fig-11b*

measurement configuration and error model simplification

Generally, and from fig-10,

$$S_{21} = \frac{b_2}{a_1} \rightarrow a_1 = \frac{b_2}{S_{21}}$$

Eqn-1

And re-writing in the form of the measurement architecture illustrated in fig-11b above,

$$S_{21} = \frac{a_{0a}}{a_{1a}} \rightarrow a_{1a} = \frac{a_{0a}}{S_{21}}$$

Eqn-2

From equation-2, the simple correction of travelling wave a_1 can be achieved by measuring the quantity b_2 (or a_{0a} if referring to fig-11b),and knowing the transmission properties of the attenuator for the state it is in. In the actual measurement setting, and as the calibration would have been conducted with the attenuators in some defined reference state, the relative s-parameters must be used instead the absolute s-parameters, as shown in equation-3.

$$a_{1a} = \frac{a_{0a} \cdot S_{21\_cal}}{S_{21\_set}}$$

Eqn-3

Where S_{21_cal} refers to measured S_{21} of step attenuators at calibration state, and S_{21_set} refers to the step attenuators at measurement state.

It must be stressed that the assumptions that allow this simplified approach must be considered carefully. This is only here due to the high low coupling factors of the directional couplers used (35 dB) combined with additional in-line attenuation (6dB). If the same approach was to be used in a lower power system, then it is likely that the full error model built from all the measured s-parameters, would need to be devised and applied.

4 Systems configuration

Figure 3.1 shows a simplified block diagram of waveform measurement system, with the step attenuators inserted between MTA ports and the switches that multiplex a and b signals into the two channel MTA receiver. All instrumentation is computer controlled using the Wavemetrics IGOR software environment and through a GPIB interface.

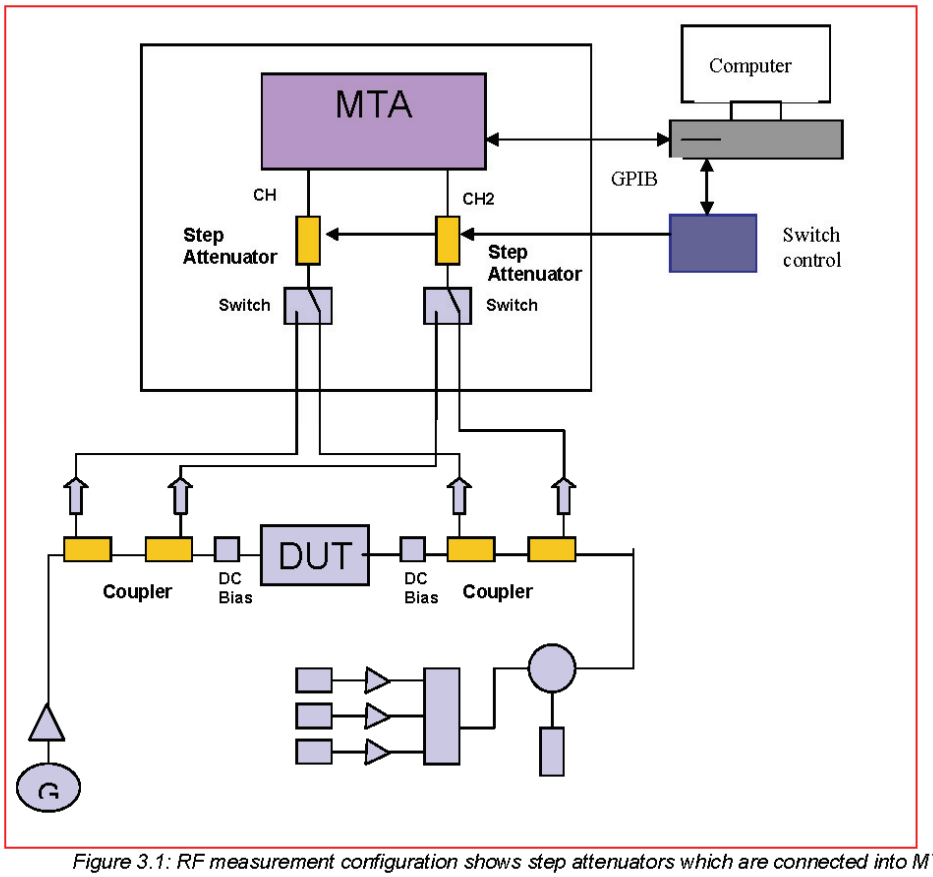

Figure 3.1: RF measurement configuration shows step attenuators which are connected into MTA ports.

The general measurement process can be considered as starting with calibration of the system, and for this stage the step attenuators are both set to their 0 dB states. Following calibration, the DUT is inserted and measurements commence in the usual manner. In-between measurements, the step attenuators are manually switched to the most suitable step level, and the software takes the appropriate action and effectively adjusts the measured a and b voltage waveforms to compensate for the presence of the attenuator.

4.1 Correction procedure

The simple procedure presented in figure 3.2 illustrates how the presence of the attenuator is managed within the measurement software. The first chart shows the original procedure, where the second shows how the correction fits-into this process.

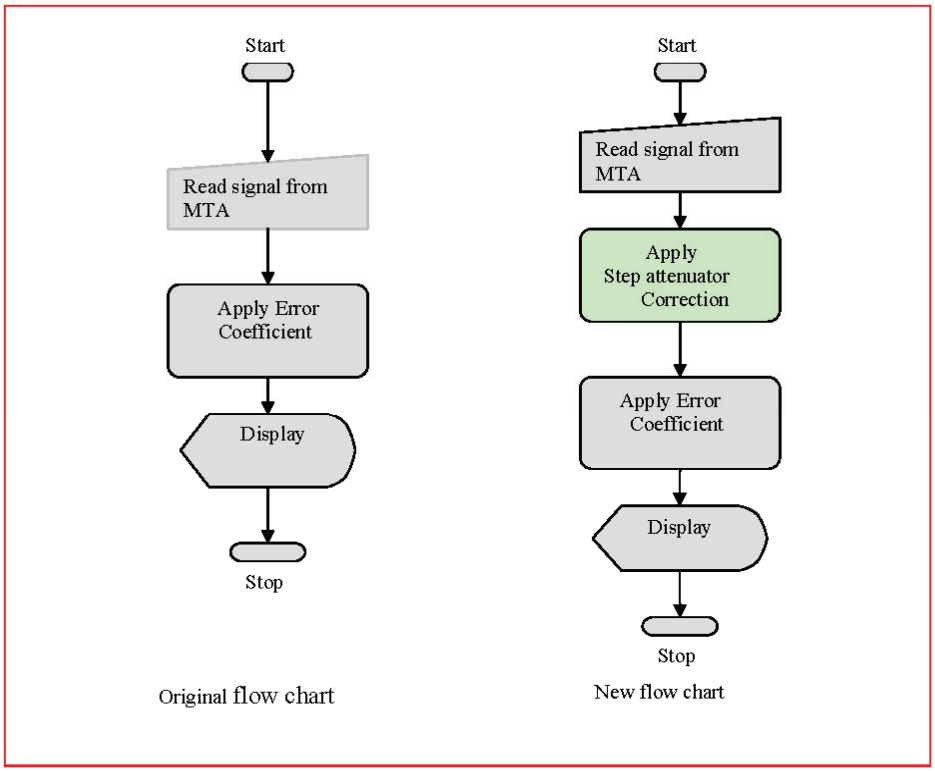

Figure 3.2: show the procedure of corrected data in measurement system.

The step attenuator correction is modelled using the measured s-parameters and the approach discussed in previous sections, and is applied to the a0, b0, a3 and b3 voltage waveforms measured at the receiver reference plane. The system is calibrated with all the attenuators in 0dB states, and it is important to remember that the behaviour of the attenuators in the 0dB states will be accounted for by the usual 'reference' calibration. It is therefore the differences between the measured 0dB states and the selected attenuator state that is used to derive the applied correction.
Although the usual calibration is usually conducted with all attenuators in their nominal 0 dB state, the calibration software allows other states to be used, as show figure 4.3 and 4.4. The calibration software records the calibration state of the attenuators in a file containing all the necessary error coefficient information, that is later used by the measurements software environment.

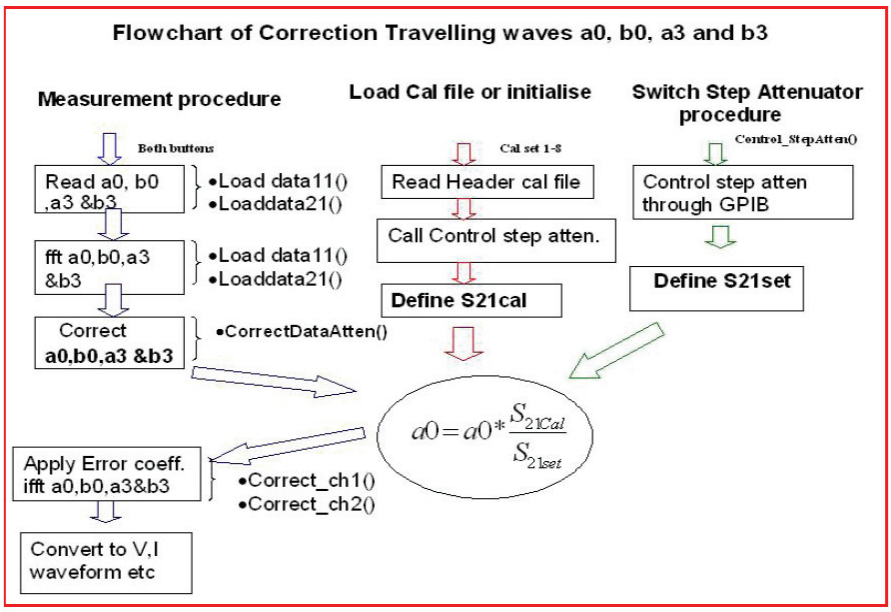
Flowchart of Correction Travelling waves a0, b0, a3 and b3
Measurement procedure
Load Cal file or initialise
Switch Step Attenuator procedure
Both buttons
Cal set 1-8
Control_StepAtten()
Read a0, b0 ,a3 &b3
•Load data11()
•Loaddata21()
Read Header cal file
Control step atten through GPIB
fft a0,b0,a3 &b3
•Load data11()
•Loaddata21()
Call Control step atten.
Define S21set
Correct a0,b0,a3 &b3
•CorrectDataAtten()
Define S21cal
$a0 = a0 * \frac{S_{21Cal}}{S_{21set}}$
Apply Error coeff. ifft a0,b0,a3&b3
•Correct_ch1()
•Correct_ch2()
Convert to V,I waveform etc

4.2 Verification through measurement

Initially, the approach has been verified by measuring large-signal excitation, a thru standard in place of an active DUT and comparing the measured waveforms when using different attenuator states.

In all cases, a polynomial fit has been used to model the measured, averages s-parameters as described earlier in this report. Although comparisons using fundamental sinusoids are useful, they do not test the broadband performance of the system. In order to test over bandwidth, the microwave signal source was later driven into compression such that it's output stage saturated, generating harmonically rich, non-sinusoidal waveforms for comparison.

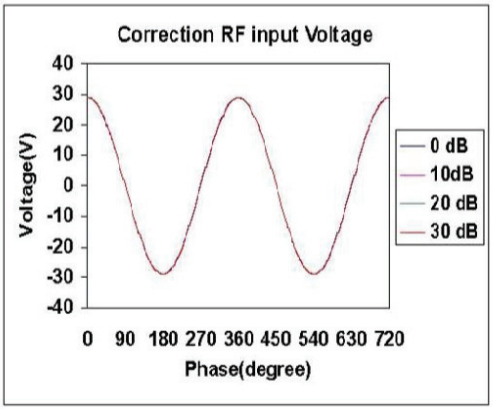

*Figure4:6: System calculated RF **input** voltage waveform corresponding to all step attenuator stages using **polynomial** s-parameter correction*

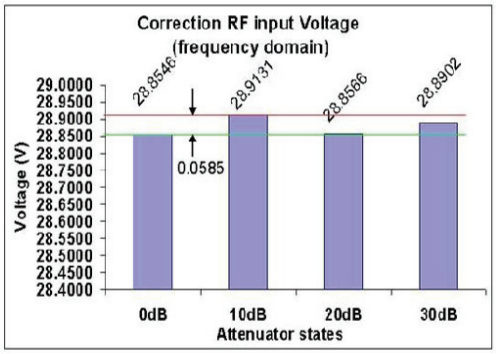

*Figure 4.7: Calculated RF **input** fundamental voltage magnitude spread when using the **polynomial** s-parameter model.*

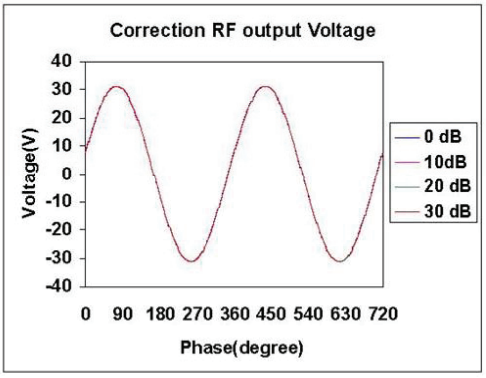

*Figure 4.8: System calculated RF **output** voltage waveform corresponding to all step attenuator stages using **polynomial** s-parameter correction*

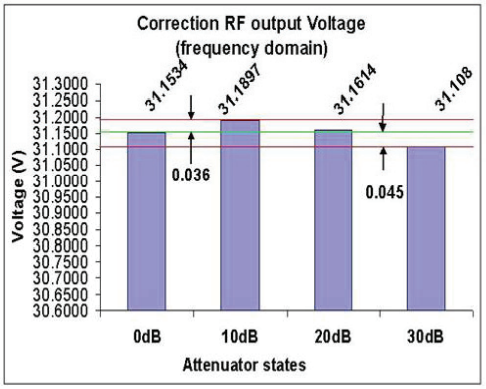

*Figure 4.9: Calculated RF **output** fundamental voltage magnitude spread when using the **polynomail** s-parameter model.*

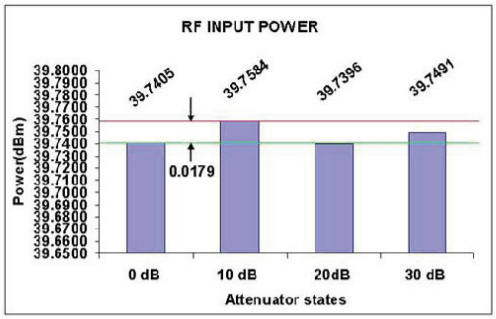

*Figure 4.10: Calculated RF **input** power magnitude spread when using the **polynomial** s-parameter model. using **polynomial** s-parameter correction*

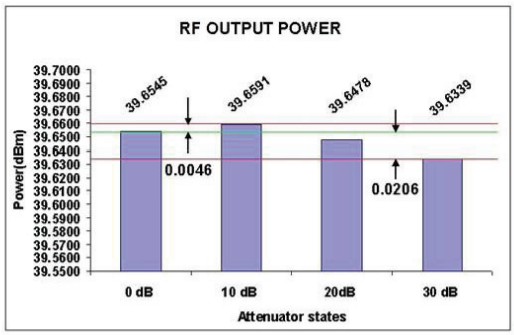

*Figure 4.11: Calculated RF **output** power magnitude spread when using the **polynomial** s-parameter model.*

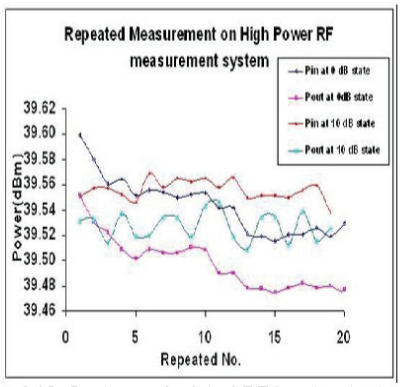

Figure4.12: System calculated RF input-output power repeated measurement over the 0dB and 10dB step attenuator's states.

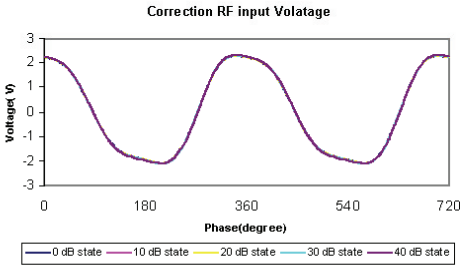

Figure3.9: System calculated RF input voltage waveform corresponding to all step attenuator stages – distorted waveform

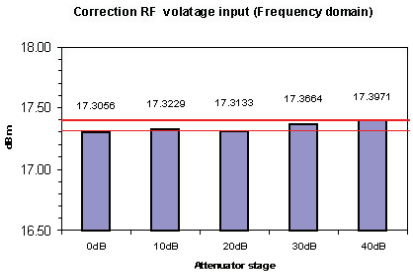

*Figure 3.10: Calculated RF input fundamental voltage magnitude spread using the **polynomial** s-parameter model – distorted waveform.*

5 Conclusions and future work

A solution to the problem of measurement system dynamic range has been proposed that involves the introduction of highly characterised, high-quality step attenuators within the measurement path, between the directional couplers and, in this case an MTA microwave receiver. Comprehensive characterisation has shown that it is possible to employ measured attenuator s-parameters to generate models with which to accurately correct measured voltage travelling waves in advance of software processing within the measurement system itself. Two correction methods have been explored; the first using simple averaging of measured s21, and the second employing a polynomial fit to the averaged data, with similar results.

These results indicate that the various attenuation states are highly repeatable, with measured s21 magnitude and phase varying by no more than 0.03dB and 0.2° (1SD) respectively over a switching sequence of at least 100 cycles per state, and over frequency range of 0 to12GHz.

Future work includes developing the system to allow automatic range control of the attenuators. Great care must be exercised when applying auto-ranging in high power measurement systems however due to the significant potential of instrument damage.

6 Acknowledgement

Research reported here was performed in the context of the network TARGET– "Top Amplifier Research Groups in a European Team" and supported by the Information Society Technologies Programme of the EU under contract IST-1-507893-NOE, www.target-org.net

7 References

[1] Pozar, D.M. (2005), *Microwave engineering*, 3rd ed., USA, John Wiley &Son,

[2] IEE. (1996), *Half day Colloquium on Uncertainties made easy*, London, Institution of Electrical, Engineering Savoy Place.

[3] Agilent. (2000), "Understanding the Fundamental Principles of Vector Network Analysis", Application note, USA

[4] Agilent. (1995), *" 3488A Switch/Control Unit Operating, Programming, Configuration Manual"*, USA

[5]. Agilent (2001), *"8510C Network Analyzer System operating and programming manual"* edit 3, USA

[6] Agilent. (1990), *Agilent Technologies 33320A/B/G/H 33321 A/B/D/G/H/K 33322A/B/G/H 33323K Step attenuators for OEM & System Use dc to 26.5 GHz*, Technical data sheet, USA

[7] WaveMetrics Inc, (2004), *"IGOR Pro Verson5.0 manual"*, Lake Oswego, USA

[8] Agilent (2002), "*Applying Error Correction to Network Analyzer Measurements*", Application Note AN 1287-3, USA

[9] Agilent (2004) , *Specifying Calibration Standards for the Agilent 8510 Network Analyzer*, Application Note 8510-5B, USA

[10] Agilent. (2001), *Network Analysis Applying the 8510 TRL Calibration for Non-Coaxial Measurements*, Product Note 8510-8A, USA

[11] Agilent (2001), *"8510C Network Analyzer Key word dictionary"* ,rev.3, USA

[12] Ludwig R. and Bretchko P.(2000), *RF Circuit Design Theory and Applications* , Prentice Hall,Upper saddle River,NJ.

[13] Lee, Yeoy-song (2005), *Testing Dynamic Accuracy of Vector Network Analyzers Using the 40 GHz Step Attenuator*, 65th ARFTG Microwave Measurements, Conference Digest 2005-Millimetre-wave Application, p159-168

[14] A. Chenakin and AP.S "Paul" Khanna phase Matrix (2006), *Inc, "2-22 GHz Continuously Variable Attenuator Has Low IMD and Float Response"* , High Frequency Electronics, pp16-20

[15] Kim, Jeong-Hwan, Park, Jeong-Il; Kang and Ung-Taeg (2005) *"Uncertainty Evaluation*

Of a Broadband Attenuation Standard", IEEE Transactions on Instrumentation and Measurement, v 54, n 2, April, p 705-708.

[16] Andrew G. Morgan, Nick M. Ridler, and Martin J. Salter(2003), *"Generalized Adaptive Calibration Schemes for precision RF Vector Network Analyzer Measurements"*, IEEE Transactions on instrumentation and measurement, Vol. 52, No.4 , pp1266-1272

[17] Pulvio G. Ananasso(1980), " *A Low Phase Shift Step Attenuator Using p-i-n Diodes Switches"*, IEEE transactions on microwave theory and techniques, Vol. MTT-28, No 7, pp774-776

[18] Johannes Benedikt, Roberto Gaddi, Paul J. Tasker, and Martin Goss(2000), *" High Power Time-Domain Measurement System with Active Harmonic Load-Pull for High-Efficiency Base-Stationn Ampliier Design"*, IEEE Trans. On Microwave theory and Techniques, Vol 48, NO. pp 2617-2624

[19] Z. Aboush, J. Lees, J. Benedikt, and P. J. Tasker, "*Active Harmonic Load-Pull System for Characterization of Highly Mismatched High Power Transistors*" presented at IEEE MTT-S, Long Beach, CA, 2005.

[20] Mónica Fernández Barciela, Orentino Mojón Ojea, Alejandro Rodriguez-Testera, "TARGET-20070630-132-UVIGO41-0_1" Universidad de Vigo (ID 41) TARGET NoE report, 2007.